Harri Nieminen

POWER-TO-METHANOL VIA MEMBRANE CONTACTOR-BASED CO_2 CAPTURE AND LOW-TEMPERATURE CHEMICAL SYNTHESIS

ACTA UNIVERSITATIS LAPPEENRANTAENSIS 930

Harri Nieminen

POWER-TO-METHANOL VIA MEMBRANE CONTACTOR-BASED CO_2 CAPTURE AND LOW-TEMPERATURE CHEMICAL SYNTHESIS

Dissertation for the degree of Doctor of Science (Technology) to be presented with due permission for public examination and criticism in the Auditorium 2310 at Lappeenranta-Lahti University of Technology LUT, Lappeenranta, Finland on the 4th of December, 2020, at noon.

Acta Universitatis
Lappeenrantaensis 930

Supervisors Professor Tuomas Koiranen
LUT School of Engineering Science
Lappeenranta-Lahti University of Technology LUT
Finland

Docent Arto Laari
LUT School of Engineering Science
Lappeenranta-Lahti University of Technology LUT
Finland

Reviewers Professor Liyan Deng
Department of Chemical Engineering
Norwegian University of Science and Technology
Norway

D.Sc. (Tech.) Pekka Simell
Thermochemical Conversions
VTT Technical Research Centre of Finland
Finland

Opponent Professor Riitta Keiski
Department of Environmental and Chemical Engineering
University of Oulu
Finland

ISBN 978-952-335-578-1
ISBN 978-952-335-579-8 (PDF)
ISSN-L 1456-4491
ISSN 1456-4491

Lappeenranta-Lahti University of Technology LUT
LUT University Press 2020

Abstract

Harri Nieminen
Power-to-methanol via membrane contactor-based CO_2 capture and low-temperature methanol synthesis
Lappeenranta 2020
180 pages
Acta Universitatis Lappeenrantaensis 930
Diss. Lappeenranta-Lahti University of Technology LUT
ISBN 978-952-335-578-1, ISBN 978-952-335-579-8 (PDF), ISSN-L 1456-4491, ISSN 1456-4491

In the power-to-methanol concept, methanol acts as a platform chemical facilitating the integration of renewable electricity and captured CO_2 into the fuel and chemical value chains, helping to substitute fossil resources and mitigate CO_2 emissions. To reduce equipment sizes and costs in renewable energy-based methanol production, intensified approaches to CO_2 capture and CO_2-based methanol synthesis were investigated. These approaches consisted of absorption-based CO_2 capture using membrane contactors and low-temperature CO_2 hydrogenation to methanol using co-catalytic alcoholic solvents.

Mass transfer performance of a continuously operated membrane contactor-based CO_2 capture unit was studied. The effects of key operating parameters were investigated, and established mass transfer models were applied to characterize the chemical absorption process and to identify limiting mass transfer resistances. CO_2 fluxes and values of overall mass transfer coefficient were comparable to literature data. The steady-state absorption rate was found to be limited by desorption of CO_2 from the loaded absorbent solution. Ineffective desorption also resulted in high specific energy requirement for CO_2 capture.

Liquid-phase methanol synthesis in alcoholic solvents facilitates the hydrogenation of CO_2 to methanol at reduced, thermodynamically favourable temperatures compared to conventional methanol synthesis processes. Experimental investigations on this process pursued increased methanol productivity by combining heterogeneous catalysts in a cascade catalytic system, and by continuous removal of by-product water using a molecular sieve adsorbent. Both approaches resulted in improved methanol productivity, with a more significant improvement found with use of the water-selective absorbent.

The feasibility of the low-temperature methanol synthesis process was studied by means of a techno-economic analysis and compared to a gas-phase CO_2 hydrogenation process. The use of different alcoholic solvents was considered. The alcoholic solvent in the liquid-phase processes was found to lead to energy- and cost intensive separation. As a result, the methanol production cost was higher compared to conventional gas-phase process. Electrolytic hydrogen constituted the largest fraction of the overall cost in all processes.

Keywords: Carbon capture and utilization, CO_2 capture, CO_2 hydrogenation, methanol synthesis, membrane contactor

Acknowledgements

This work was carried out at Lappeenranta-Lahti University of Technology LUT over the period of 2017–2020. The work was done in the department of Computational and Process Engineering of LUT School of Engineering Science (LENS), in co-operation with LUT School of Energy Systems (LES) under the REFLEX research platform.

I wish to thank my supervisors, Professor Tuomas Koiranen and Docent Arto Laari, for making this work possible. I would also like to acknowledge Professor Jero Ahola, D.Sc. (Tech) Vesa Ruuskanen, et al. at LES/REFLEX; and the reviewers of this manuscript, Professor Liyuan Deng from Norwegian University of Science and Technology and D.Sc. (Tech) Pekka Simell from VTT. I am also thankful to the people at LENS analytical and support services for their assistance, and fellow researchers of the Computational and Process Engineering and Separation Science research groups for making time on campus enjoyable.

Finally, special thanks to Noora for the love, care, and support.

Harri Nieminen
November 2020
Lappeenranta, Finland

Contents

List of publications

This dissertation is based on the following papers. The rights have been granted by publishers to include the papers in dissertation.

I. H. Nieminen, L. Järvinen, V. Ruuskanen, A. Laari, T. Koiranen and J. Ahola, ”Insights into a membrane contactor based demonstration unit for CO_2 capture,” *Sep. Purif. Technol.*, vol 231, 115951, 2020.

II. H. Nieminen, L. Järvinen, V. Ruuskanen, A. Laari, T. Koiranen and J. Ahola, ”Mass transfer characteristics of a continuously operated hollow-fiber membrane contactor and stripper unit for CO_2 capture,” *Int. J. Greenhouse Gas Control*, vol 98, 103063, 2020

III. H. Nieminen, G. Givirovskiy, A. Laari and T. Koiranen, ”Alcohol promoted methanol synthesis enhanced by adsorption of water and dual catalysts,” *J. CO_2 Util.*, vol 24, pp. 180–189, 2018.

IV. H. Nieminen, A. Laari and T. Koiranen, ”CO_2 Hydrogenation to Methanol by a Liquid-Phase Process with Alcoholic Solvents: A Techno-Economic Analysis,” *Processes*, vol 7, 405, 2019.

Author's contribution

I am the principal author and investigator in publications I–IV.

Contribution in Publications I–III: design and implementation of the experimental apparatus, planning and carrying out experimental work, supervision of experimental work carried out by M.Sc. students and trainees, analysis and presentation of results, writing of manuscripts.

Contribution in Publication IV: process modelling and analysis, presentation of results, writing of manuscript.

Nomenclature

Latin alphabet

A	membrane surface area	m^2
C	concentration	mol/m^3
c_p	heat capacity	J/(kg K)
D	diffusivity	m^2/s
d	diameter	m
E	enhancement factor	-
e	specific energy	J/mol
H	Henry's law constant	$mol/(m^3\ Pa)$
l	length	m
K	overall mass transfer coefficient	m/s
K	equilibrium constant	-
k	mass transfer coefficient	m/s
k	reaction rate constant, 2^{nd} order reaction	$m^3/(mol\ s)$
M	molar mass	kg/mol
m	gas-liquid partition coefficient	-
N	flux	$mol/(m^2\ s)$
n	number of membrane fibres	-
$\dot{n}$	molar flow rate	mol/s
P	duty/power	W
p	pressure	Pa
Q	volumetric flow rate	m^3/s
q	exponent (infinite enhancement factor)	-
R	ideal gas constant	J/(K mol)
r	reaction rate	$mol/(m^3\ s)$
S	stoichiometric number	-
T	temperature	K
v	velocity	m/s
w	equivalent work	J/kg
X	membrane wetting ratio	-
y	reaction order, CO_2	-
Z	membrane constant	-
z	reaction order, absorbent	-

Greek alphabet

(Note: This is listing usable Greek symbols in alphabetical order including names of symbols. The first line shows the correct formatting of the entries.)

α	CO_2 loading	mol/mol
β	empirical constant (Wilson plot)	-
γ	Reynolds number exponent	-

ΔC_{lm}	logarithmic average concentration	-
ΔH	reaction enthalpy	kJ/mol
ΔT	temperature difference	K
δ	membrane thickness	m
ε	membrane porosity	-
ζ	Schmidt number exponent	-
η	efficiency	%
θ	contact angle	°
κ	heat capacity ratio	-
ν	kinematic viscosity	m^2/s
ρ	density	kg/m^3
σ	surface tension	N/m
τ	membrane tortuosity	-
υ	stoichiometric coefficient	-

Dimensionless numbers

Gz	Graetz number
Ha	Hatta number
Re	Reynolds number
Sc	Schmidt number
Sh	Sherwood number

Superscripts

*	equilibrium

Subscripts

A	amino acid salt
a	absorbent
abs	absorption
app	approach (temperature)
b	base
c	contactor
chem	chemical
comp	compressor
cond	condensing
e	electricity
des	desorption
g	gas
g,b	gas bulk
g,m	gas-membrane interface
h	hydraulic (diameter)
i	inside

in	inlet
l	liquid
l,b	liquid bulk
lean	lean absorbent
l,m	liquid-membrane interface
K	Knudsen (diffusivity)
m	membrane
max	maximum
n	inert gas
nw	non-wetted
o	outside
out	outlet
p	membrane pore
phy	physical
rich	rich absorbent
t	thermal
vp	vacuum pump
w	wetted
y	reaction order, CO_2
z	reaction order, absorbent
1	forward reaction
-1	reverse reaction
∞	infinite (enhancement factor)

Abbreviations

AMP	2-Amino-2-methylpropan-1-ol
BECCS	bioenergy with carbon capture and storage
DAC	direct air capture
DACCS	direct air carbon capture and storage
DEA	diethanolamine
DFT	density functional theory
DMC	dimethyl carbonate
DME	dimethyl ether
CCS	carbon capture and storage
EDA	ethylenediamine
EDS	energy-dispersive X-ray spectroscopy
FID	flame ionization detector
IEA	International Energy Agency
IR	infrared
IGCC	integrated gasification combined cycle
IRENA	International Renewable Energy Agency
ISBL	inside battery limits
LCOE	levelized cost of electricity

MEA	monoethanolamine
MDEA	methyldiethanolamine
MTBE	methyl tert-butyl ether
MTO	methanol-to-olefins
MTG	methanol-to-gasoline
NET	negative emission technology
NPV	net present value
NTP	normal temperature and pressure
OSBL	outside battery limits
PEM	proton exchange membrane
PE	polyethylene
PEEK	polyether ether ketone
PDMS	polydimethylsiloxane
PES	polyether sulfone
PP	polypropylene
PTFE	polytetrafluoroethylene
PTMSP	poly(1-(trimethylsilyl)-1-propyne
PVDF	polyvinylidene
PZ	piperazine
RITE	Research Institute of Innovative Technology for the Earth
RWGS	reverse water-gas shift reaction
SEM	scanning electron microscope
SNG	substitute natural gas
SOE	solid oxide electrolyser
SRK	Soave-Redlich-Kwong equation of state
TCD	thermal conductivity detector
TETA	triethylenetetramine
WSG	water-gas shift reaction
XRD	X-ray powder diffraction

1 Introduction

Anthropogenic emissions of carbon dioxide (CO_2) and other greenhouse gases have led to climatic change characterised by increasing global average temperatures [1]. The cumulative CO_2 emissions from human activities have led to the disturbance of the natural carbon cycle between the atmosphere, land and oceans, resulting in the increase of atmospheric CO_2 concentration. The majority of anthropogenic CO_2 emissions originate from the combustion of fossil fuels in the energy, transportation and industrial sectors, with major emissions also originating from agriculture, forestry and other land use changes [1]. With increasing population and expanding global economy, the demand for primary energy is expected to increase, and fossil fuels are expected to continue to dominate the primary energy supply [2]. As such, CO_2 emissions are expected to further increase in the coming decades.

As a result of 255 Gt of cumulative increase in the atmospheric carbon content during the period of 1870–2018, the CO_2 concentration has increased from 277 ppm in the pre-industrial era to over 400 ppm today [3]. Further increase is driven by continuous anthropogenic emissions of 40 Gt CO_2 per year. The use of fossil fuels contributes to 81% of this annual CO_2 flux into the atmosphere, with the rest caused by land use changes. Owing to the radiative forcing effect of CO_2 and other greenhouse gases [4] – that is, the absorption of re-emitted solar infrared radiation – the increased atmospheric CO_2 concentration has resulted in the observed warming of the global climate. Significant negative effects have followed, including sea level rise and increased occurrences of extreme weather events such as droughts, flooding and tropical storms.

Strategies for limiting these negative climatic effects include both limiting the rate of future emissions (mitigation) and the prospect of negative emission technologies (NETs) aiming to directly reduce the atmospheric CO_2 concentration [5]. Key elements of mitigation include the reduction in primary energy demand by means of improved energy efficiency and behavioural changes and the decarbonisation of electricity generation. Decarbonisation can be achieved by switching to renewable electricity sources, the share of which is constantly increasing but is still small compared with fossil sources [2].

The cost of renewable energy has been steadily decreasing in recent years. Figure 1.1 presents the global weighted average levelised cost of electricity (LCOE), including both capital and operating costs, for completed renewable electricity projects based on solar photovoltaic (PV), onshore wind and offshore wind during 2010–2018. For instance, the LCOE for onshore wind projects has decreased by 25% from 2010 to 2018; for PV projects, the decrease has been 76% [6]. With continuous decreases in cost, renewable electricity projects are already expected to be more competitive than new investments in fossil electricity in 2020. At the same time, investments in renewable electricity are undercutting the operating costs of the existing coal-fired power plants; this has already led to the significant decommissioning of coal-fired plants. With further decreases in cost, a significant increase in the share of renewables is expected, and 100% renewable

scenarios based on the complete substitution of fossil electricity by 2050 are currently being discussed [7].

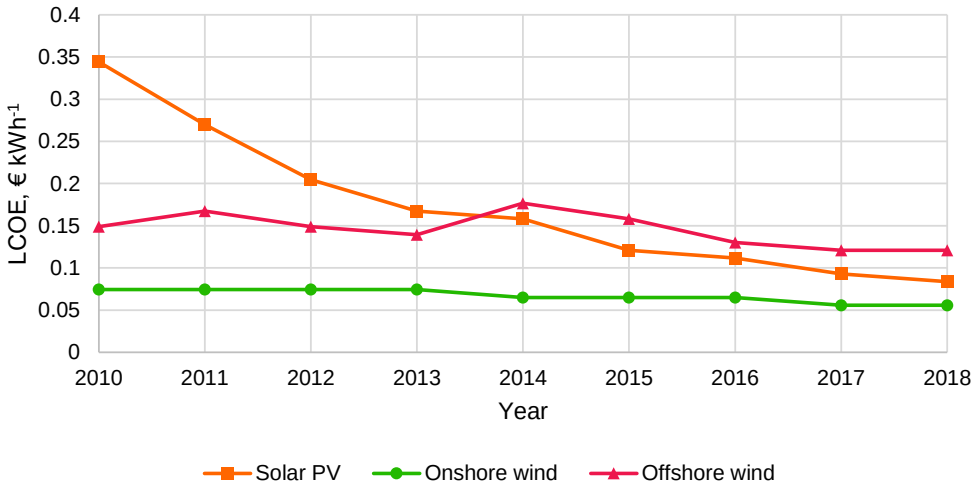

Figure 1.1 The levelized cost of electricity (LCOE) for completed renewable electricity projects from 2010 to 2018. Data from IRENA [6].

Furthermore, emissions from fossil-based power generation can be significantly reduced by the widespread implementation of carbon capture and storage (CCS) technologies [8]. CCS refers to a family of technologies aiming to capture CO_2 from emission sources, followed by pressurised long-term storage into geological features such as saline aquifers or depleted oil and gas fields [9, 10]. In this way, CCS can provide a bridging technology allowing the continuous use of fossil fuels while the share of renewables is continuously increased [11]. Regarding the relative magnitude of the key emission mitigation pathways, the International Energy Agency (IEA) has estimated that improved energy efficiency can provide 44%, renewables 36% and CCS 9% of the total cumulative CO_2 emission reduction until 2040 in a socially and environmentally sustainable transition scenario [2]. According to this estimate, the cumulative CO_2 emissions until 2040 would be reduced by 195 Gt compared to a more conservative scenario based on present energy policies.

In addition to limiting future emissions, NETs, which aim to directly remove CO_2 from the atmosphere, have been proposed as the second key element to help limit the magnitude of climatic change [12]. Numerous such technologies have been proposed, with examples including bioenergy with carbon capture and storage (BECCS), afforestation and reforestation and direct air carbon capture and storage (DACCS) [13]. Similar to CCS, BECCS and DACCS are based on the capture and storage of CO_2. However, their processes can be considered carbon negative because CO_2 is captured following the combustion of renewable biomass (BECCS) or directly from the atmosphere (DACCS), as opposed to fossil-based sources in conventional CO_2 capture and utilisation (CCU).

Although NETs have been assessed to offer carbon removal potential at the gigaton scale required, the technologies are still under development and a sufficiently quick large-scale deployment to limit temperature rise in the coming decades does not appear likely [14].

1.1 Carbon capture and utilization (CCU)

CCU is an evolution of CCS in that instead of disposal to long-term storage, the captured CO_2 is utilised directly or as a feedstock in chemical processes. The wider definition of CCU or CO_2 utilisation is considered to include all chemical and biological processes for the conversion or utilisation of CO_2, regardless of whether the CO_2 is originally captured from point emission sources or from the atmosphere [15]. However, this thesis places a more specific focus on the chemical conversion of CO_2 into fuels and chemical products. The capture and recycling of CO_2 originating from fossil point sources has been suggested as a bridging technology with the potential to mitigate current emissions and simultaneously introduce CO_2 as a carbon source into the energy and chemical value chains [16, 17].

The emission reduction potential of products synthesised from captured, fossil-based CO_2 is based on the substitution of fossil raw materials, provided that the emissions are compared over the entire product life cycle with indirect emissions included [18, 19]. The end-use and lifetime of the CO_2-based product is also to be considered because it dictates the timescale for which carbon is stored [15]. For instance, in the BECCS approach, atmospheric carbon is utilised by growing biomass, which is then combusted for its heating value. The released CO_2 is captured and permanently stored. This is an example of a ‘closed’ utilisation pathway, wherein CO_2 is not released at the end-of-life of the product.

In contrast, ‘cycled’ pathways constitute processes wherein the utilised CO_2 returns to the atmosphere after short time periods such as days or months [15]. The conversion of CO_2 into fuels or chemicals usually constitutes recycling processes where the net removal of CO_2 does not take place over the product cycle. The emission mitigation potential of these processes depends on decreasing the amount of CO_2 emitted in relation to an alternative fossil-based process [16]. This decrease can often be a result of replacing fossil carbon with recycled carbon as feedstock. When considering CCU processes as emission mitigation options, important factors include the potential scale of production, which is largely dictated by the market demand of the final product, and the timescale of CO_2 fixation in the product [20].

Ideally, in the long term, the capture of fossil-based CO_2 would be substituted by direct air capture (DAC) to recycle CO_2 within the atmosphere and eliminate further input of fossil carbon into the global carbon balance [21]. In the meantime, CCU based on point emission sources could be advanced to displace further use of fossil carbon sources and to provide economic incentives for carbon capture – that is, the production of valuable products instead of storage as a waste [22]. This could drive the further development of

capture and utilisation processes, which would be beneficial when carbon sources will no longer be fossil-based.

In terms of energetics, CO_2 conversion reactions can be divided into two categories [23]. In energetically favourable reactions, CO_2 is directly incorporated into the target molecule, yielding products that are lower in energy compared with CO_2. This category includes reactions of CO_2 with bases, amines, alkenes and other organic compounds. The most industrially relevant product obtained from these routes is urea (over 150 Mt produced per year [24]), which is afforded by the reaction of CO_2 with ammonia and is mainly used as fertilizer. Another emerging application of these reactions is synthesis of organic carbonates such as dimethyl carbonate (DMC), which are primarily used in the production of polycarbonate polymers. Although these types of reactions are energetically favourable, their potential application scales are expected to be limited to the megaton scale [24].

Owing to the thermodynamic stability of CO_2, reactions involving the reduction of carbon to lower oxidation states require sizable energy input [23]. The energy for these reactions can be supplied by heat, electrochemistry or radiation or using high-energy co-reactants such as hydrogen. Although electrochemical, photochemical and biological CO_2 reduction methods have been widely studied, they are still at early stages of research [16, 25] and are not considered further in this work. The use of hydrogen is convenient because hydrogen is readily produced by the electrolysis of water, which can be powered by renewable electricity sources. The integration of renewable electricity into the CO_2 conversion route is desirable because it provides the opportunity to store the electric energy in the form of chemical products.

A large number of heterogeneous and homogeneous catalytic systems have been developed for the efficient hydrogenation of CO_2 into products such as carbon monoxide (syngas), methane, methanol and hydrocarbons via the Fischer-Tropsch route [26, 27, 19, 28]. All these products are examples of potential synthetic fuels and energy vectors for the storage of renewable electricity and replacement of the current fossil-based fuels (Section 1.2). They could also provide carbon-containing platform chemicals as a substitute to fossil-based feedstock in chemical industries. Therefore, these catalytic routes could be implemented at a large scale with increasing availability of renewable electricity.

The annual CO_2 utilisation potential of CO_2-based fuels has been estimated at up to 4 Gt CO_2 in 2050 [15]. In another study, the CO_2 mitigation potential of CO_2-based chemicals (mainly methanol and derived compounds) is estimated at up to 3.5 Gt CO_2 by 2030, provided that a significant amount of renewable electricity is available [29]. The scale of these values is comparable to the expected contribution of major NETs such as BECCS, forestation and land management in the overall effort of reducing atmospheric CO_2 emissions [14].

1.2 CCU and chemical energy storage

As discussed, a major motivation for the development of CCU processes is the integration of CO_2 as a more sustainable carbon source into the present energy and chemical value chains based on fossil raw materials. To facilitate CO_2 utilisation at a large scale with potential for significant emission reductions, the production of synthetic fuels from CO_2 is appealing [16]. This approach provides the opportunity to integrate renewable electricity with the production of carbon-containing fuels and chemicals.

Owing to the variable and intermittent nature of renewable electricity sources such as wind or solar, an increase in the share of renewables in the overall electricity mix leads to increased flexibility demands on the overall energy system [30]. Options for the storage of electricity generated during peak production periods are required to ensure grid stability and to balance the supply and demand during periodic and hourly variations in renewable production rates [31].

Some of the potential energy storage technologies include batteries, pumped hydro, compressed air storage and flywheels [32, 33, 34]. Another option is chemical storage by utilising renewable electricity in the production of chemical fuels in which energy is stored in an energy-dense, storable and transportable form [35, 36]. This is achieved using electricity for the electrolysis of water, thus yielding hydrogen that can then be utilised in conversion processes to produce synthetic fuels. Performing electrolysis using the excess electricity available during production peaks could provide the economic case for such conversion processes [16].

Present industrial hydrogen production is almost entirely based on fossil raw materials [37]. The primary route is steam reforming of natural gas, yielding synthesis gas mainly hydrogen (H_2) and carbon monoxide (CO), from which hydrogen is then separated and purified. Water electrolysis, facilitating more sustainable hydrogen production compared to use of fossil feedstock by utilising renewable energy sources, is based on the utilisation of electric energy for the dissociation of water into hydrogen and oxygen [38]. Alkaline electrolysis constitutes the most established technology; proton exchange membrane (PEM) electrolysers are an emerging technology with particular advantages of flexible operation and rapid response under load variation [39], which is especially beneficial for energy storage applications. High-temperature solid oxide electrolysers (SOE) offer the potential for improved energy efficiency, but so far they are constrained by material limitations [38].

The use of hydrogen as a primary energy carrier is often suggested [40]. Hydrogen can provide an ideal clean fuel with no CO_2 or other harmful emissions resulting from its combustion. Direct and efficient conversion of hydrogen into electricity can also be achieved using hydrogen fuel cells [41]. However, owing to the difficulties involved in the storage and transportation of hydrogen [42, 43], the use of hydrogen for the production of more easily handled hydrocarbon or oxygenate fuels is attractive.

Energy density, both on volumetric and gravimetric basis, is an important criterion for the selection of chemical compounds for energy storage. High energy density is especially important in mobile applications such as transportation. Ideal chemical energy carriers should be simple to store, transport and handle. They should pose limited safety risks in terms of toxicity or flammability with limited environmental effects in case of accidental releases. In addition, the conversion efficiencies from electricity to end-use should be high to conserve the primary energy available from renewable sources. Versatility of the compound, with multiple potential uses in the energy, transportation and chemical sectors, is also beneficial.

Methane [44, 45], methanol [46, 47] and hydrocarbons generated by the Fischer-Tropsch route [48, 49] are potential energy storage compounds that are directly accessible via the hydrogenation of CO_2. Table 1.1 summarises the energy densities and estimated conversion efficiencies of these products in comparison with hydrogen and established fossil-based hydrocarbon fuels. Owing to their unique advantages and different potential end-uses, each of these compounds can be expected to be part of a future energy system with increasing reliance on synthetic fuels. However, in this Thesis, the main product of interest is methanol, the benefits of which include versatility and multiple end-uses, together with efficient synthesis and conversion routes (Section 1.3).

Table 1.1 The gravimetric and volumetric energy density and the conversion efficiency of CO_2 hydrogenation products and potential energy carrier compounds. Data for gasoline and diesel fuel is provided for comparison. Data from 1) Schüth [36], 2) Agarwal [50], 3) Thema et al. [44] and 4) Tremel et al. [51].

Product	**Gravimetric energy density, MJ/kg**	**Volumetric energy density, MJ/dm^3**	**Conversion efficiency, %**
Hydrogen	120[1)]	0.0107 (gas) 8.52 (liquid at -253 °C)[(1]	77%[(3] (from electricity)
Methane[1]	50[1)]	0.0357(gas) 21 (liquid at -162 °C) [(1]	83%[(4] (from hydrogen)
Synthetic hydrocarbons (Fischer-Tropsch)[1]	43[1)]	35[(1]	83%[(4] (from hydrogen)
Methanol[1]	20[1)]	16[(1]	89%[(4] (from hydrogen)
Gasoline[2]	43[2)]	32[2)]	-
Diesel[2]	42[2)]	36[2)]	-

1.3 Methanol – energy carrier and platform chemical

Methanol is both a potential fuel and an important platform chemical with an estimated annual demand (2016) of almost 100 Mt [52]. Major uses of methanol include further conversion into formaldehyde and acetic acid, conversion into alkenes by the methanol-to-olefins (MTO) process, fuel uses such as blending with gasoline and conversion into dimethyl ether (DME) or fuel additives such as methyl tert-butyl ether (MTBE). Methanol is also a commonly used solvent. Whereas the majority of methanol produced is used in chemical industries, methanol also possesses favourable characteristics as a fuel for internal combustion engines. These include high octane number [46], high efficiency and low emissions of nitrogen oxides, hydrocarbons and CO [53]. However, engine and fuel system modifications are required for the use of methanol in gasoline-powered engines. Methanol can be converted into electricity by combustion in gas turbines or potentially using direct methanol fuel cells [54].

The versatility of methanol and its multiple potential uses in both the chemical and energy sectors make this compound an interesting product for large-scale CO_2 utilisation [46, 47]. Liquid methanol is simple to store and handle compared with gaseous hydrogen or methane, which is favourable considering its use as an energy carrier compound for the storage of renewable electricity. In mobile applications, the need for higher energy density and the existing infrastructure make the use of synthetic hydrocarbons produced by Fischer-Tropsch route seem favourable compared with methanol. However, methanol itself can be effectively converted into similar hydrocarbon fuels via the methanol-to-gasoline (MTG) process described below. The use of methanol in static applications, such as power generation, seems feasible. In this application, methanol has the advantage of a highly selective and relatively energy effective synthesis process (Chapters 6–7).

Perhaps most interestingly, methanol has significant potential as a platform chemical and bridging compound for the large-scale introduction of renewable electricity and recycled CO_2 into the chemical sector [47, 29, 17]. Such a ‘power-to-methanol’ scheme is illustrated in Figure 1.2 (end of this section). Via further conversion into various important commodity chemicals, practically any chemical product currently produced from fossil raw materials is accessible through methanol [55]. Examples of products from the conversion of methanol include DME, gasoline-range hydrocarbons via the MTG process and alkenes via the MTO process. The versatility of methanol is highlighted in Table 1.2, which summarises the main fuel and chemical uses of hydrogen, methane, Fischer-Tropsch products and methanol.

Table 1.2 A summary of the main fuel and chemical uses of hydrogen and CO_2 hydrogenation products.

Compound	Fuel uses	Chemical uses
Hydrogen	Heat and power generation by combustion Conversion to electricity in fuel cells	Synthesis of ammonia and methanol Petroleum processing Fischer-Tropsch synthesis Steel production (reduction of iron ore)
Methane	Heat and power generation by combustion Electricity from solid oxide fuel cells (in development)	Production of synthesis gas Conversion into ethane, ethene and other chemical products (in development)
Fischer-Tropsch hydrocarbons	Powering internal combustion engines (gasoline and diesel)	Bulk and intermediate chemicals (alkenes, alcohols, aldehydes)
Methanol and derived products	Heat and power generation by combustion Blending with gasoline, conversion into gasoline via the MTG process Electricity from direct methanol fuel cells (in development) Production of fuel additives (e.g. MTBE) Dehydration to DME (diesel fuel substitute)	Synthesis of formaldehyde, acetic acid and other important chemicals Conversion into alkenes via the MTO process Common industrial solvent

DME, a gas at ambient conditions (boiling point: −24.8 °C), is a potential diesel fuel substitute possessing the advantages of clean combustion, high cetane number and high volatility that allow its low injection pressure in compression ignition engines [56]. DME can be stored as a liquid at pressures above 5 bar. The use of DME as a diesel fuel substitute in commercial road transportation has been demonstrated [57]. DME is produced by the dehydration of methanol on acidic catalysts. The reaction can also be integrated with methanol synthesis in a single reactor using a combination of methanol synthesis and dehydration catalysts [58].

The MTG process enables the conversion of methanol into gasoline fuel [59, 60]. In this process, methanol is converted on zeolite catalysts into a mixture containing saturated, unsaturated and aromatic hydrocarbons, mostly in the gasoline carbon-chain length range. The MTG process was commercially operated in New Zealand from 1986 until 1996, with natural gas as the raw material in the methanol synthesis stage [59]. More recently, commercial production has taken place in China using coal feedstock.

The MTO process is a variation of the MTG process, with the product selectivity adjusted towards the short-chain alkenes ethene and propene [61]. These products are important

feedstock chemicals in the polymer industry and are conventionally produced from oil-derived naphta in an energy-intensive cracking process. Because the reaction mechanism in the MTO process is similar to that in the MTG process, zeolite catalysts are also used in the MTO process [60]. In recent years, the MTO process has also been commercially operated at a significant scale in China [61].

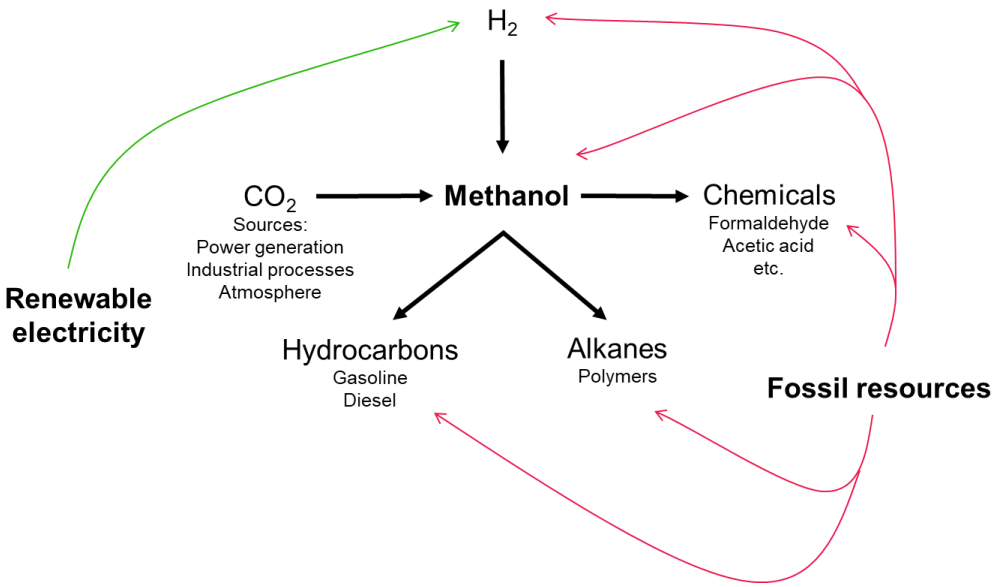

Figure 1.2 Power-to-methanol: the potential role of methanol as a platform chemical facilitating the integration of renewable electricity and captured CO_2 into the fuel and chemical value chains resulting in substitution of fossil resources.

1.4 Thesis goals

In this thesis, the CCU route of interest is the capture of CO_2 followed by hydrogenation to methanol using electrolytic hydrogen. In particular, alternative process options for the intensification of both CO_2 capture and methanol synthesis are investigated. These process options constitute alternatives to established methods of post-combustion CO_2 capture and CO_2 hydrogenation to methanol, ultimately aiming to improve the energy and cost efficiency of CO_2-based methanol synthesis as an option for large-scale CO_2 utilisation and chemical storage of renewable electricity.

Membrane contactors are an alternative to conventional gas–liquid contacting equipment in absorption-based CO_2 capture processes. Potential advantages of membrane contactors include high interfacial area per unit volume, flexible operation and modular structure facilitating simple scale-up. In this work, an experimental membrane-contactor–based CO_2 capture unit is developed, and the performance of the unit is characterised in terms of mass transfer and energy consumption. In this unit, a low-cost and readily scalable

polymeric membrane module is combined with an amino acid salt absorbent having improved compatibility with such membranes compared with conventional amine-based absorbents. In addition, vacuum is utilised for the regeneration of the absorption solution to reduce the regeneration temperature. The effects of key operating parameters are investigated. The established mass transfer models are applied to characterise the chemical absorption process taking place at the membrane contactor and to identify the controlling mass transfer resistance in this process.

Liquid-phase methanol synthesis using solid catalysts and co-catalytic alcoholic solvents facilitates the hydrogenation of CO_2 to methanol at reduced temperatures compared with conventional methanol synthesis processes. Lower temperatures are thermodynamically favourable for methanol synthesis, allowing improved methanol yield and selectivity. In addition, the liquid-phase methanol synthesis process could offer improved temperature control for the exothermic reaction system. In this work, the catalytic system for this process is experimentally investigated. Attempts are made to improve the productivity of methanol by means of rational combination of solid catalysts and solvent alcohol according to the established reaction mechanism. In addition, the continuous removal of by-product water during reaction using a molecular sieve adsorbent is investigated.

Following the experimental studies on low-temperature methanol synthesis, the feasibility of the liquid-phase methanol synthesis process is studied using techno-economic analysis. A functional flowsheet for the entire process is designed, and the process is modelled using process simulation software. Investment and operating costs of the process are estimated and compared with a more conventional gas-phase methanol synthesis process modelled and analysed using the same methodology. The use of different alcohols as solvent in the liquid-phase process is considered, and the resulting processes are compared in terms of mass and energy balances and process economics. Based on these analyses, opportunities and challenges concerning further the development of the liquid-phase process are identified.

1.5 Thesis outline

Chapter 1 introduces the thesis by first discussing the background, motivation and definition of CCU and the links between reduced CO_2 emissions, renewable energy sources and CCU processes. The role of methanol as a potential product for large-scale CO_2 utilisation is then explained. Section 1.4 establishes the subject and goals of the thesis and the research work involved. New findings and the contributions of this thesis in the scientific field are summarised in Section 1.6.

The structure of the thesis follows a progression from the subject of CO_2 capture to methanol synthesis and, specifically, CO_2 hydrogenation to methanol. Chapter 2 begins by introducing the established CO_2 capture processes, with a primary focus on processes based on chemical absorption. Chapter 3 introduces membrane contactors as an alternative contacting technology for CO_2 absorption processes and provides a literature review of membrane materials and absorbent solutions as well as the relevant mass

transfer theory and calculations. Key findings from this review are summarised in Section 3.4. Chapter 4 reviews alternative methods for the desorption of CO_2 from absorbent solutions.

Chapter 5 presents the research work involved with membrane-contactor–based CO_2 capture performed as part of this thesis and published in Publications I and II. The motivation and goals for this research are discussed in Section 5.1, and Section 5.2 describes the research methods used. The main results of this research are presented and discussed in Section 5.3. Section 5.4 provides a summary of key findings and discusses the outlook and needs for further research and development of the process and experimental unit.

Chapter 6 introduces methanol synthesis as the second subject of this thesis, beginning with conventional, fossil-based methanol synthesis. Section 6.1 reviews the structural and catalytic properties of the established copper/zinc oxide (Cu/ZnO) catalysts, and Section 6.2 discusses the reaction mechanism of methanol synthesis on such catalyst surfaces. Chapter 7 discusses CO_2 hydrogenation to methanol – that is, methanol synthesis from pure CO_2 and hydrogen instead of fossil-sourced synthesis gases. Section 7.1 reviews the developments in heterogeneous catalysts for CO_2-based methanol synthesis, and Section 7.2 reviews feasibility and techno-economic studies on the hydrogenation of CO_2 to methanol.

Chapter 8 discusses liquid-phase methanol synthesis processes. Of particular interest is the low-temperature methanol synthesis route utilising alcoholic solvents; studies relevant to this process are reviewed in Section 8.1. Cascade catalytic systems for liquid-phase methanol synthesis are reviewed in Section 8.2, whereas Section 8.3 discusses the use of amine-based solvents in liquid-phase methanol synthesis. Chapter 9 reviews the use of adsorbents and other means in the removal of water during methanol synthesis.

Chapter 10 presents the research work on low-temperature methanol synthesis conducted as part of this thesis and published in Publications III and IV. Section 10.1 begins by outlining the motivation and goals for this research. Section 10.2 explains the research methodology, and the results are presented and discussed in Section 10.3. Section 10.4 summarises the key findings of Publications III and IV and discusses the outlook for the low-temperature methanol synthesis process.

Chapter 11 concludes the work and recommends directions for future research, aiming to further develop the membrane-contactor–based CO_2 capture process and the low-temperature methanol synthesis route.

1.6 Contribution and new results

The following novel results were obtained in the research described in this thesis:

Membrane-contactor based CO_2 capture

The following results were published in Publications I and II and are discussed in Chapter 5.

i. A continuously operated CO_2 capture unit combining a polypropylene (PP) membrane module and an amino acid salt absorbent with vacuum solvent regeneration could be operated with good stability, and membrane wetting was not observed.

ii. Steady-state absorption rate was limited by the insufficient desorption of CO_2 from the absorbent solution. This limitation was analysed in detail in terms of the measured solvent CO_2 loadings and the mass transfer process taking place in the membrane contactor.

iii. Specific energy consumption for CO_2 capture was estimated based on direct experimental measurement. The limited desorption efficiency resulted in high energy consumption per unit of CO_2 captured.

iv. Both liquid-side and membrane resistance were found to significantly contribute to the overall mass transfer resistance in the membrane contactor. The gas-side resistance was comparably negligible.

v. Values of the enhancement factor for the chemical absorption of CO_2 into the amino acid salt solution were theoretically estimated, and the results corresponded well with the experimental findings.

Low-temperature methanol synthesis: experimental work

The following results were published in Publication III and are discussed in Chapter 10, Sections 10.3.1–10.3.4.

i. Water was effectively removed from the reaction solution during low-temperature methanol synthesis in alcoholic solvents using a molecular sieve adsorbent.

ii. Reduced concentrations of water with the use of the adsorbent resulted in significantly increased rates of methanol formation.

iii. The use of a copper chromite catalyst together with a Cu/ZnO-based methanol synthesis catalyst resulted in increased specific methanol productivity per total catalyst mass.

iv. By the characterisation of the Cu/ZnO catalyst prior and after methanol synthesis, the ongoing reduction of Cu and crystallisation of ZnO was observed during the reaction.

Low-temperature methanol synthesis: techno-economic analysis

The following results were published in Publication IV and are discussed in Chapter 10, Sections 10.3.5–10.3.8.

i. A complete flowsheet design for the liquid-phase, low-temperature methanol synthesis process was developed, and the process was modelled using process simulation software.

ii. The feasibility of the low-temperature methanol synthesis process was analysed using techno-economic analysis and compared with a more conventional gas-phase process.

iii. The presence of the alcoholic solvent in the low-temperature process was found to result in added complexity, increased energy consumption and higher methanol production cost compared with the gas-phase process.

iv. The comparison results of different alcohols as solvents showed that the use of less volatile alcohol resulted in more favourable mass and energy balances and reduced production cost.

2 Established CO_2 capture processes

This chapter provides an overview of established absorption-based CO_2 capture processes. Other types of capture processes are outside the scope of this work.

2.1 Sources of CO_2

CO_2 can be captured from point emission sources, such as industrial processes and flue gases from power generation, or alternatively directly from the atmosphere. Industrial processes associated with significant CO_2 emissions include the production of cement, iron and steel, pulp and paper, oil refineries, natural gas processing, ethylene, and ammonia synthesis [62]. The CO_2 content in the exhaust streams from these processes is relatively high. In addition, the CO_2-containing streams can be at elevated pressures which may simplify the separation of CO_2 and be beneficial concerning potential subsequent utilization processes. Table 2.1 summarizes the conditions of CO_2-containing exhaust streams from major stationary sources.

Table 2.1 Composition and conditions of CO_2-containing streams from power generation and industrial sources.

CO_2 source	**CO_2 concentration, mol-%**	**Main Impurities**	**Pressure, bar**	**Temperature, °C**
Coal power plant[1,2]	12–16	CO, NO_x, SO_x	1	50–75
Natural gas power plant[1]	7.5	CO, NO_x	1	50–75
Cement plant[1]	14–33	CO, NO_x, SO_x	1	
Steel plant[1,3]	15–20	CO	1	50–75
Hydrogen production[1]	70–90	CO	15–40	40–450
Refineries[3]	3–13			

References: [1] Ho et al. [63], [2] D'Alessandro et al. [64], [2] Wilcox [62].

In some of these processes, CO_2 is already separated as waste from the product streams utilising established CO_2 capture technologies. As a result, highly purified streams of CO_2 are already available for potential utilisation. A commercial example is the use of CO_2 from ammonia synthesis (originating from methane reforming) in the production of urea [20]. In cement and steel production, large amounts of CO_2 are produced as a side-product in carbon-intensive, difficult-to-replace processes and as part of flue gases associated with the combustion of fossil fuels for process heat. Although the resulting CO_2 concentrations are relatively high, the capture of CO_2 might be complicated owing to the associated impurities from combustion [63].

The largest share of total CO_2 emissions originates from the combustion of fossil fuels for heat and electricity generation in the energy sector [1]. Although partial decarbonisation via the increasing share of renewable electricity is expected in the coming decades [65], CO_2 capture is considered essential for the continued use of fossil during the low-cost transition to carbon-free energy sources [8]. As a result, the development of CO_2 capture technologies applicable for fossil-powered power plants is of major interest.

In the flue gases emitted from power plants, CO_2 concentration varies depending on the fuel used (Table 2.1). Combustion of coal leads to flue gases with high CO_2 concentration, whereas natural gas as a less carbon-intensive fuel yields flue gases with low CO_2 concentration. Major contaminants associated with combustion include nitrogen and sulphur oxides and CO. Heavy metals may also be present at low concentrations. These contaminants have to be considered in the selection and design of CO_2 capture processes. In addition, these components can cause problems in the utilisation of the captured CO_2, particularly the poisoning of catalysts used in CO_2 conversion processes [20].

The emission mitigation potential of CO_2 capture from point emission sources is generally limited to the reduction of the carbon intensity of the existing fossil-based processes by storage or long-term fixation of the emitted CO_2. In principle, CO_2 capture from the atmosphere (DAC) would constitute an ideal source of captured CO_2 [66]. DAC is independent of location and thus can capture emissions originating from mobile and distributed sources, where capture at the emission source is not practical [21]. Depending on the final use of the captured CO_2, DAC is a potential NET capable of reducing the amount of atmospheric CO_2 [67]. The captured CO_2 could also provide a completely fossil-free carbon source for the energy and chemical sectors [68]. The main challenge in DAC compared with capture from flue gas or industrial sources is the much lower CO_2 concentration in ambient air [21].

2.2 CO_2 capture by absorption

Various separation methods, including chemical or physical absorption into solvents, adsorption on solid materials and membrane separation, can be used for the separation of CO_2 from gas streams [69, 64, 70]. The suitability of each method primarily depends on the CO_2 concentration, the temperature and pressure of the gaseous stream, the fraction of CO_2 to be separated from the gas stream and the required purity of the CO_2 product. In general, a CO_2 removal fraction of 90% or higher is targeted in capture from stationary sources such as power plants [70]. To be utilised in chemical conversion processes, the final purity of CO_2 should usually be above 99% [63].

Of the various CO_2 capture processes, absorption-based processes are of interest in this thesis. Absorption processes are based on CO_2 removal from gaseous streams by contacting it with liquid solvents, resulting in the absorption of CO_2 from the gas into the liquid phase. By the nature of interaction between the solvent and CO_2, the absorbing liquids can be categorised as physical or chemical absorbents. Physical absorption utilises the solubility of CO_2 in the solvent at high partial pressures and low temperatures [71,

72]. The absorbed CO_2 can be removed by decreasing the pressure, and the weak interaction of CO_2 with the absorbent results in low energy consumption in the regeneration of the solvent.

Owing to the weak interaction between the absorbent and CO_2, the use of physical absorbents is limited to streams with high CO_2 concentration and high total pressure. In addition, the purity of the captured CO_2 can be low owing to the non-selective nature of the solvent. Physical solvents such as Selexol (DME of polyethylene glycol) and Rectisol (methanol chilled to −40 °C) have been widely used in the removal of acid gases (H_2S, CO_2) in natural gas and syngas processing. Such solvent systems are also feasible for pre-combustion or oxy-combustion capture from power plants but are not applicable to post-combustion capture.

Chemical absorbents are solvents that interact with CO_2 by chemical reaction, resulting in a reversible formation of reaction products that are soluble in the absorbent solution [69]. The stronger interaction between the absorbent and CO_2 compared with physical absorption results in a higher absorption capacity at lower CO_2 partial pressures, making the process feasible for streams at low CO_2 concentration and low pressure. As an acidic gas, CO_2 readily reacts with basic solvents. The industrial standard for the chemical absorption of CO_2 is the use of organic amines in aqueous solutions [71, 72]. The primary amine monoethanolamine (MEA) is a particularly common absorbent, but secondary amines such as diethanolamine (DEA) and tertiary amines such as methyldiethanolamine (MDEA) are also utilised. Amines are utilised as aqueous solutions, with 30 w-% MEA commonly considered the benchmark solution. An emerging solvent is the cyclic secondary amine piperazine (PZ) [73].

Regardless of the solvent used, the basic configuration of a CO_2 capture process based on chemical absorption is the same (Figure 2.1) [69, 70]. The CO_2-containing gas is counter-currently contacted with the solvent in an absorber column, where CO_2 is absorbed into the solution. The absorption temperature is typically between 40 and 60 °C. The CO_2-loaded (rich) solvent is then transferred to the solvent regeneration column, where CO_2 is desorbed from the solution at temperatures above 100 °C. The rich solvent leaving the absorber is heated by the heat transferred from the hot (lean) solvent exiting the desorption column, which is circulated to the absorption stage. Heat is also provided in the reboiler of the desorption column, where it is utilised to reverse the chemical absorption of CO_2. At the same time, water is evaporated, providing a flow of steam for stripping the released CO_2. The steam is condensed in an overhead condenser, providing a liquid reflux back to the column and yielding significantly pure CO_2 as a product.

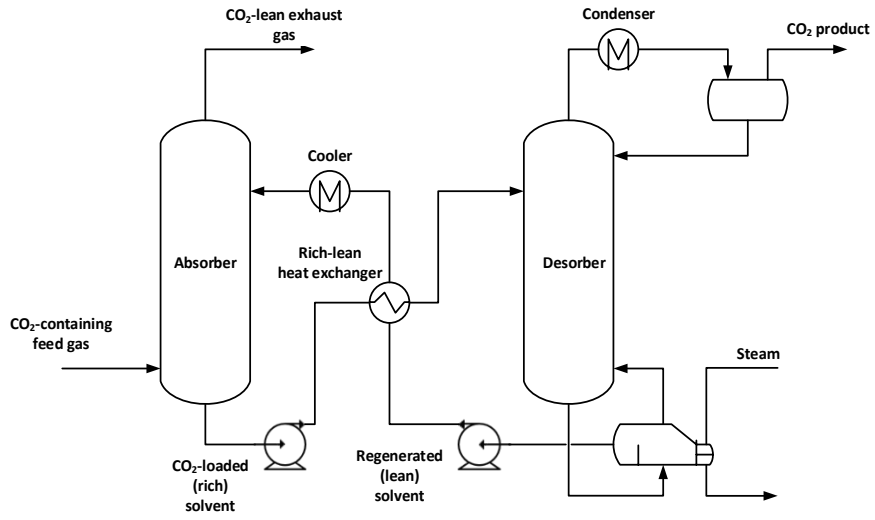

Figure 2.1. A simplified flowsheet of a CO_2 capture process based on chemical absorption.

The heat required in the reboiler constitutes the energy penalty for CO_2 capture. In post-combustion capture from power plants, heat is supplied by low-pressure steam removed from the power plant process, resulting in efficiency losses at the plant. Early post-combustion processes have been reported to require heat duties above 5.5 MJ per t CO_2 captured, whereas the more recently developed processes have achieved specific duties as low as 2.6 MJ per t CO_2 [9]. Together with the solvent selection, the energy consumption can be minimised by optimising the configuration of the absorption/desorption process [74, 75, 76]. Process intensification using alternative contactors in place of conventional absorption and stripping columns is also being pursued. Examples of this approach are the use of high-gravity equipment [77, 78] and membrane contactors (Chapter 3).

3 CO_2 absorption using membrane contactors

Membrane contactors are an alternative to conventional gas–liquid or liquid–liquid contacting equipment in mass transfer unit operations [79]. In conventional contactors such as packed or tray columns, the fluid phases are dispersed with the aim of maximising the interfacial area between the phases. Dispersion of the fluids may lead to operational difficulties including emulsion formation, foaming, unloading and flooding. In membrane contactors, the phases are not dispersed and are instead separated on the opposite sides of a microporous membrane. In this non-dispersive contact, mass transfer between the phases takes place at the phase interface located at the entrance of the membrane pores.

Unlike most membrane separation processes, the membranes used in gas–liquid or liquid–liquid contactors are not selective to the component to be separated or purified. Instead, the selectivity of the separation process is based on the selective absorption by the absorbing fluid. The role of the membrane is only to separate the bulk phases and to provide the interfacial area for mass transfer.

Compared with conventional equipment, membrane contactors offer a significantly large interfacial area per unit volume [80]. This results in reduced sizes of mass transfer equipment. Membrane contactors are commonly fabricated in the hollow fibre arrangement, in which the membrane fibres are usually packed in parallel bundles inside the module shell. One of the fluids, either gas or liquid, flows inside the fibres (lumen-side), and the other fluid flows outside the fibres (shell-side). The inner diameter of the membrane fibres is below 1.0 mm [81], and the modules often contain thousands of individual fibres, resulting in high total membrane surface area.

The mass transfer of the key component through the membrane is driven by the concentration gradient over the membrane and not by the pressure gradient as in membrane filtration processes. The interfacial area remains constant regardless of the operating conditions, allowing flexible operation with independent adjustment of the flow rates of the fluids. In addition, the orientation of the membrane module can be freely selected, and the modular design allows simple, linear scale-up by increasing the number of modules and total membrane surface area.

The main disadvantage of membrane contactors is the additional mass transfer resistance owing to the membrane. Mass transfer efficiency can also decrease owing to non-ideal flow such as by-passing, especially in large-scale modules. Membrane fouling may take place but is usually limited in effect compared with pressure-driven membrane separations [79]. In membrane gas–liquid contactors, membrane wetting – that is, the filling of the membrane pores by the liquid phase – is a more common difficulty compared to fouling and has a significant effect on the overall mass transfer performance. Membrane wetting needs to be avoided by careful design and operation of the membrane-contactor–based separation process, including the selection of a compatible membrane material and type of solvent used as the absorbing liquid, and careful control of the pressure difference over the membrane.

Large-scale CO_2 capture processes are largely based on post-combustion capture by chemical absorption with aqueous amines as the most common solvents [9]. Owing to the advantages of membrane contactors discussed above, the replacement of conventional absorbers in CO_2 capture processes with membrane contactors has attracted interest. The use of membrane contactors could intensify CO_2 capture by significantly reducing the equipment footprint and volume [82]. In terms of the volumetric mass transfer coefficient, intensification factors in the range of 2.5–5 in comparison to conventional equipment have been reported [83, 82]. In a membrane-contactor–based CO_2 absorption process, the CO_2-containing feed gas is separated from the absorbent liquid and CO_2 is transferred from the gas into the liquid phase through the membrane pores. As in conventional absorption processes, the selectivity of CO_2 absorption is provided by the chemical interaction between CO_2 and the solvent.

The performance of a membrane contactor for CO_2 separation is dependent on the proper selection of the membrane and the absorbent. As in conventional CO_2 capture processes, amine-based absorbents have been commonly considered for use in membrane contactors. However, alternative absorbents have been studied [84, 85]. In addition to the absorbent, the material and structure of the membrane have a significant influence on the contactor performance owing to their effects on the additional mass transfer resistance incurred by the membrane. The compatibility of the membrane and the absorbent is critical to avoid membrane wetting and to maintain stable and sufficient mass transfer performance over longer operating periods [86].

3.1 **Theory**

Mass transfer in membrane contactors is commonly described by the resistance-in-series model, in which the overall mass transfer resistance results from the sum contribution of the individual liquid-side, membrane and gas-side mass transfer resistances. This relatively simple approach is commonly utilised to analyse and predict the performance of membrane contactors with reasonable accuracy [87].

Empirical mass transfer correlations based on the membrane module configuration are often used in the estimation of the individual mass transfer coefficients on the liquid and gas side of the membrane. The increase in absorption rate owing to the chemical reaction between CO_2 and the absorbing liquid can be described by the enhancement factor, the value of which can be estimated using available equations.

Compared to the gas-side and liquid-side mass transfer coefficients, the accurate estimation of the membrane mass transfer coefficient is more difficult owing to the difficulty of estimating the precise structural properties of the membrane and the influence of membrane wetting. The incidence and effects of membrane wetting on the mass transfer performance have been experimentally and theoretically described, but the characterisation of partial wetting of the membrane pores under practical operating conditions is complicated.

3.1.1 Overall mass transfer coefficient

In a membrane contactor applied for CO_2 absorption, the overall mass transfer process includes the diffusion of CO_2 from bulk gas to the gas–membrane interface, diffusion through the membrane pores to the membrane–liquid interface and chemical and/or physical absorption into the liquid followed by diffusion to bulk liquid [85]. In non-wetted operation, with membrane pores filled with gas and liquid flowing inside the membrane fibres (lumen-side), the CO_2 flux N in the gas phase, membrane and liquid phase are given by the following:

$$N = k_{\mathrm{g}}\left(p_{\mathrm{g,b}} - p_{\mathrm{g,m}}\right) = k_{\mathrm{m}}\left(p_{\mathrm{g,m}} - p_{\mathrm{l,m}}\right) = k_{\mathrm{l}}\left(C_{\mathrm{l,m}} - C_{\mathrm{l,b}}\right) \tag{3.1}$$

where k_{g}, k_{m} and k_{l} are the gas, membrane and liquid individual mass transfer coefficients, respectively; p is the CO_2 partial pressure, and C is the CO_2 concentration in the liquid. The subscripts correspond to gas bulk (g,b), gas–membrane interface (g,m), liquid–membrane interface (l,m) and liquid bulk (l,b). The mass transfer process described by Equation 3.1 is illustrated in Figure 3.1.

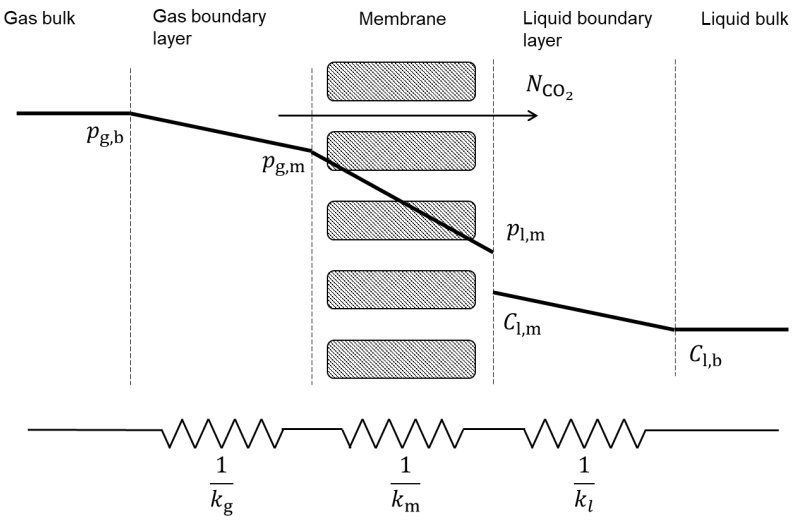

Figure 3.1 Schematic representation of mass transfer of CO_2 from gas to absorbing liquid through a non-wetted microporous membrane, and the involved mass transfer resistances

Assuming ideal gas, the CO_2 partial pressure in the gas phase in equilibrium with the CO_2 concentration dissolved in the liquid phase at the liquid–membrane interface is given by Henry's law:

$$p_{\mathrm{l,m}} = HC_{\mathrm{l,m}} \tag{3.2}$$

Where H is the Henry's law constant for CO_2 in the solvent used. The overall mass transfer coefficient can be described based on the gas phase (K_g) or the liquid phase (K_l):

$$N = K_g\left(p_{g,b} - p^*\right) = K_l\left(C^* - C_{l,b}\right) \tag{3.3}$$

Where $p^* = HC_{lb}$ and $p_{gb} = HC^*$. The gas-side overall mass transfer coefficient is usually used [88]. For convenient representation, the dimensionless gas-liquid partition coefficient m can be used instead of the Henry coefficient [89]:

$$m = \frac{C_l}{C_g^*} = RTH \tag{3.4}$$

where R is the ideal gas constant and T is the temperature. The gas-side overall mass transfer coefficient can be expressed using the resistance-in-series model by taking into account the individual mass transfer coefficients for the gas, liquid and membrane (Equation 3.5). This model is based on a number of assumptions: steady-state, equilibrium at the phase interface, uniform membrane-pore–size distribution and wall thickness, well-mixed bulk liquid and identical driving forces for physical and chemical absorption [84]. In addition, flat geometry is assumed, neglecting the curvature of the membrane fibre.

$$\frac{1}{K_g} = \frac{1}{k_g} + \frac{1}{k_m} + \frac{1}{Emk_l} \tag{3.5}$$

The effect of chemical absorption can be included in the expression for the overall mass transfer coefficient by introducing the enhancement factor E. In the absorption of CO_2 into basic solvents such as amines, mass transfer on the liquid side is enhanced by chemical reaction. Chemical absorption of CO_2 is based on the acid–base reaction between CO_2 and amine-based absorbents (Section 2.2), and the effect of this chemical interaction is the increased absorption rate compared with physical absorption based only on the physical solubility of CO_2 into the absorbing liquid. The enhancement factor is defined as the ratio of the absorption flux in the presence of reaction and the flux when only physical absorption takes place [84]:

$$E = \frac{N_{chem}}{N_{phy}} \tag{3.6}$$

The enhancement factor can be determined by the numerical solution of the differential mass balance equations over the membrane module [89] or using approximate solutions based on various mass transfer models [90]. The latter approach, described in Section 3.1.3, has been employed in this work. The gas-side overall mass transfer coefficient can be experimentally determined based on the gas-phase concentration change over the membrane module. For instance, the measured CO_2 flux through the membrane can be used:

$$K_{\mathrm{g}} = \frac{N}{\Delta C_{\mathrm{lm}}} = \frac{\dot{n}_{\mathrm{CO_2,in}} - \dot{n}_{\mathrm{CO_2,out}}}{A C_{\mathrm{lm}}} \tag{3.7}$$

where $\dot{n}_{\mathrm{CO_2,in}}$ and $\dot{n}_{\mathrm{CO_2,out}}$ are the molar flow rates of CO_2 in the inlet and outlet gas, respectively; A is the membrane surface area, and ΔC_{lm} is the logarithmic mean mass transfer driving force averaging the phase concentration in the membrane module:

$$\Delta C_{\mathrm{lm}} = \frac{\left(C_{\mathrm{g,in}} - C^{*}_{\mathrm{g,in}}\right) - \left(C_{\mathrm{g,out}} - C^{*}_{\mathrm{g,out}}\right)}{\ln\left[\left(C_{\mathrm{g,in}} - C^{*}_{\mathrm{g,in}}\right)\left(C_{\mathrm{g,out}} - C^{*}_{\mathrm{g,out}}\right)\right]} \tag{3.8}$$

where $C_{\mathrm{g,in}}$ and $C_{\mathrm{g,out}}$ are the measured CO_2 concentrations in the inlet and outlet gas, respectively, and $C^{*}_{\mathrm{g,in}}$ and $C^{*}_{\mathrm{g,out}}$ are the inlet and outlet gas-phase CO_2 concentrations in equilibrium with the corresponding liquid-phase concentrations, as determined using the Henry constant, partition coefficient or other equilibrium relations.

3.1.2 **Individual mass transfer coefficients**

The overall mass transfer coefficient in a gas–liquid membrane contactor includes the contributions of the gas, membrane and liquid mass transfer coefficients according to the resistance-in-series model (Equation 3.5). Although the overall mass transfer rate in the absorption process can be analysed using the overall mass transfer coefficient, a more detailed analysis can be performed by estimating the individual mass transfer coefficients. As a result, the controlling resistance limiting the overall mass transfer rate can be identified.

The gas- and liquid-side mass transfer coefficients are commonly estimated using empirical mass transfer correlations based on the membrane module configuration. In this work, the relevant module configuration constitutes the counter-current flow with liquid flowing inside the membrane fibres (lumen-side) and gas flowing outside the fibres (shell-side). This is a typical but not exclusive configuration for membrane contactors used for CO_2 absorption. Selected correlations developed in the literature for this configuration are utilised in the present work and described in this section.

Owing to the difficult estimation of the membrane mass transfer coefficient, this parameter is often fitted to the experimental data following the determination of the overall, gas and liquid mass transfer coefficients [87]. A theoretical value for the membrane mass transfer coefficient can be obtained based on the membrane pore properties, which are however difficult to accurately estimate. An experimental procedure known as the Wilson plot [79] method is also available for the estimation of the membrane mass transfer coefficient.

Gas-side mass transfer coefficient for shell-side flow

For shell-side flow of gas, the gas-side mass transfer coefficient is typically estimated by correlations of the following form [79]:

$$\mathrm{Sh} \propto \mathrm{Re}^{\gamma} \propto \mathrm{Sc}^{\zeta} f(\text{geometry}) \tag{3.9}$$

where Sh, Re and Sc are the Sherwood number, Reynolds number and Schmidt number, respectively; f describes a function of module geometry. The Sherwood number describes the ratio of the convective mass transfer rate and the diffusive mass transfer rate. For gas flowing on the shell side, the Sherwood number is given by the following [91]:

$$\mathrm{Sh} = \frac{k_{\mathrm{g}} d_{\mathrm{h}}}{D_{\mathrm{CO_2,g}}} \tag{3.10}$$

Where $D_{\mathrm{CO_2,g}}$ is the diffusivity of CO_2 in the feed gas, and d_{h} is the shell-side hydraulic diameter:

$$d_{\mathrm{h}} = \frac{{d_{\mathrm{c,i}}}^2 - n{d_{\mathrm{o}}}^2}{d_{\mathrm{c,i}} + n d_{\mathrm{o}}} \tag{3.11}$$

Here, $d_{\mathrm{c,i}}$ is the inner diameter of the membrane contactor (shell), d_{o} is the outer diameter of the membrane fiber and n is the number of fibers. The Reynolds number is obtained from the following:

$$\mathrm{Re} = \frac{4Q_{\mathrm{g}}}{n d_{\mathrm{o}} \nu_{\mathrm{g}}} \tag{3.12}$$

where Q_{g} is the feed gas volumetric flow rate and ν_{g} is the feed gas kinematic viscosity. The Schmidt number, describing the relative thickness of the hydrodynamic layer and the mass transfer boundary layer, is defined by the following:

$$\mathrm{Sc} = \frac{\nu_{\mathrm{g}}}{D_{\mathrm{CO_2,g}}} \tag{3.13}$$

Yang and Cussler [92] developed the following correlation for gas absorption and stripping processes based on parallel flow in randomly packed modules [91]:

$$\mathrm{Sh} = 1.25\left(\frac{Re\, d_{\mathrm{h}}}{l}\right)^{0.93} Sc^{0.33} \tag{3.14}$$

Where l is the membrane fibre length.

Liquid-side mass transfer coefficient for lumen-side flow

For laminar flow of liquid inside membrane fibres, correlations based on the Graetz number Gz have been developed for estimating the liquid-side mass transfer coefficient [93, 94, 95]. The Graetz number describes the development of the concentration profile in laminar flow inside a pipe. At low Graetz numbers (i.e. low residence time), the concentration of diffusing species is uniform in the radial direction, whereas at high Graetz numbers, a radial concentration gradient exists:

$$\mathrm{Gz} = \frac{v_\mathrm{l} {d_\mathrm{i}}^2}{D_{\mathrm{CO_2,l}} l} \tag{3.15}$$

where v_l is the liquid velocity inside the membrane fibre, d_i is the inner diameter of the fibre and $D_{\mathrm{CO_2,l}}$ is the diffusivity of CO_2 in the absorbent solution.

The Graetz-Lévéque solution, initially used to describe an analogic heat transfer situation, can be applied to estimate the liquid-side mass transfer coefficient for physical absorption [93]. Uniform, laminar flow of liquid inside membrane fibres and constant gas–liquid interface conditions are assumed. For developing flow with $\mathrm{Gz} > 20$, the following correlation can be used:

$$\mathrm{Sh} = 1.62\mathrm{Gz}^{1/3} \tag{3.16}$$

The Sherwood number for liquid flowing inside the fibres is described as follows.

$$\mathrm{Sh} = \frac{k_\mathrm{l} d_\mathrm{i}}{D_{\mathrm{CO_2,l}}} \tag{3.17}$$

For flow with a fully developed radial concentration profile, with $\mathrm{Gz} < 10$,

$$\mathrm{Sh} = 3.67 \tag{3.18}$$

A general solution applicable over the intermediate range of Graetz numbers was also developed as a geometric average of the above conditions:

$$\mathrm{Sh} = \sqrt[3]{3.67^3 + 1.62^3 \mathrm{Gz}} \tag{3.19}$$

The above correlations are applicable for the estimation of the liquid mass transfer coefficient in case of physical absorption with liquid flowing inside the membrane fibres, a module configuration of interest in the present work. In chemical absorption, the mass transfer on the liquid side of the membrane will be enhanced by the chemical reaction between CO_2 and the absorbent. The effect of the chemical reaction is included using the enhancement factor (Section 3.1.3). By utilising the enhancement factor, the liquid-side

correlations for physical absorption can also be used for cases involving chemical absorption [94].

Membrane mass transfer coefficient

In membrane contactors used for CO_2 absorption, CO_2 is transferred from the gas side through the membrane pores to the liquid side. Assuming only diffusive mass transfer through gas-filled pores with uniform pore structure and pore size distribution, Fick's law can be used to estimate the membrane mass transfer coefficient [84]:

$$k_{\mathrm{m}} = D_{\mathrm{CO_2,m}} \frac{\varepsilon}{\delta \tau} \tag{3.20}$$

where ε is the membrane porosity, $D_{\mathrm{CO_2,m}}$ is the effective diffusion coefficient of CO_2 in the membrane, δ is the membrane thickness and τ is the membrane tortuosity. In microporous membranes, porosity generally ranges from 0.2 to 0.9 and tortuosity from 2 to 3 [79]. The difficulty in the reliable estimation of these properties as well as the pore size distribution complicates the accurate estimation of the membrane mass transfer coefficient [87]. According to Equation 3.20, the use of thinner, more porous membranes leads to decreased mass transfer resistance when operating in gas-filled, non-wetted mode. The effective membrane diffusion coefficient is a combination of bulk and Knudsen diffusion coefficients, with the relative significance of both mechanisms dependent on the membrane pore size [84]:

$$\frac{1}{D_{\mathrm{CO_2,m}}} = \frac{1}{D_{\mathrm{CO_2,b}}} + \frac{1}{D_{\mathrm{CO_2,K}}} \tag{3.21}$$

where $D_{\mathrm{CO_2,b}}$ is the bulk diffusivity and $D_{\mathrm{CO_2,K}}$ is the Knudsen diffusivity for CO_2 in the membrane pores. For membrane pores with diameters below 1×10^{-7} m, Knudsen diffusion is the dominant mechanism, whereas bulk diffusion is dominant for pores with diameters above 1×10^{-5} m [84]. In the intermediate region, both mechanisms are significant. The bulk diffusion coefficient can be calculated based on the kinetic theory of gases. The Knudsen diffusion coefficient can be calculated from the following:

$$D_{\mathrm{CO_2,K}} = Z \sqrt{\frac{8RT}{\pi M_{\mathrm{CO_2}}}} \tag{3.22}$$

where $M_{\mathrm{CO_2}}$ is the molar mass of CO_2, and Z is a constant dependent on the membrane morphology and the interaction between the molecules and porous membrane structure. Based on the membrane morphology, Z can be estimated from the following:

$$Z = \frac{4\varepsilon d_{\mathrm{p}}}{3\delta} \tag{3.23}$$

where d_{p} is the membrane pore diameter. Experimental values of Z for single gas permeation through various commercial microporous membranes have also been reported [96].

The membrane mass transfer coefficient can be experimentally estimated by the Wilson plot method [79, 97]. In this method, the experimental overall mass transfer coefficient is calculated at different liquid velocities with the gas flow rate maintained constant. By feeding pure CO_2, the gas-side resistance can be considered negligible [98]. Alternatively, the gas-side resistance can be estimated using mass transfer correlations [99]. In either case, the membrane and gas-side resistances are assumed constant, making the overall mass transfer coefficient linearly proportional to the power of the liquid velocity: $\frac{1}{K_{\mathrm{g}}}$ is plotted against $v_l^{-\beta}$, where β is an empirical constant giving the best linear fit. The membrane resistance is then given by the intercept of this plot. Typically, the values of β are in the range of 0.3–0.9 [99]. The membrane mass transfer coefficient is typically in the range of 1.0×10^{-4}–1.0×10^{-3} m/s [99, 100, 101].

3.1.3 Enhancement factor for chemical absorption

The absorption of CO_2 into chemical absorbents such as amines is enhanced by the chemical reaction between CO_2 and the absorbing species at the gas–liquid interface. The reactions involved for aqueous amino acid salts are discussed in Section 3.3.2, respectively. During non-wetted operation of a membrane contactor, the gas–liquid interface is located at the entrance to the membrane pores on the liquid side of the membrane. Assuming that the gas–liquid contact time is sufficiently short to maintain a well-mixed, undisturbed bulk liquid outside the interface (towards the centre of the membrane fibre), the enhancement factor can be estimated based on the calculation of the Hatta number and the infinite enhancement factor using the properties of the bulk liquid [102, 94]. The Hatta number describes the ratio of reaction rate to the mass transfer flux at the gas–liquid interface:

$$\mathrm{Ha} = \frac{\sqrt{k_{\mathrm{y,z}} D_{\mathrm{CO_2,l}} C_{\mathrm{CO_2,l,b}}^{y-1} C_{\mathrm{a,b}}^{z}}}{k_{\mathrm{l}}} \tag{3.24}$$

where Ha is the Hatta number, $k_{y,\mathrm{z}}$ is the forward reaction rate constant for chemical absorption, y and z are the respective reaction orders in terms of CO_2 and the absorbent, $C_{\mathrm{CO_2,l,b}}$ is the CO_2 concentration in the bulk liquid and $C_{\mathrm{a,b}}$ is the concentration of the active absorbent component in the bulk liquid (at liquid inlet). The reaction rate constant and the reaction orders depend on the type of absorbent used. For primary amines or

amino acid salts with primary amine functionality, the reaction can be considered as first order with respect to both the CO_2 and absorbent, leading to the following equation [102]:

$$\mathrm{Ha} = \frac{\sqrt{k_1 D_{\mathrm{CO_2,l}} \mathrm{C_{a,b}}}}{k_l} \tag{3.25}$$

where k_1 is the forward reaction rate constant for a reaction between primary amine and CO_2. The infinite enhancement factor corresponds to the situation wherein the diffusion of the absorbent in the liquid phase limits the reaction rate [94, 103]:

$$E_\infty = \left(1 + \frac{C_{\mathrm{a,b}} D_{\mathrm{a}}}{\upsilon_{\mathrm{a}} m C_{\mathrm{CO_2,l,m}} D_{\mathrm{CO_2,l}}}\right)\left(\frac{D_{\mathrm{CO_2,l}}}{D_{\mathrm{a}}}\right)^q \tag{3.26}$$

Here, D_{a} is the diffusivity of the absorbent in solution, υ_{a} is the stoichiometric coefficient of the absorbent in the reaction with CO_2 (two in case of primary amines) and $C_{\mathrm{CO_2,lm}}$ is the CO_2 concentration at the liquid–membrane interface. The value of the exponent q varies depending on the mass transfer model used, ranging from $q = 0$ for the film model to $q = \frac{1}{2}$ for the penetration model [94].

The relative magnitudes of the Hatta number and infinite enhancement factor can be used to identify the reaction regime [103]. When $\frac{E_\infty}{\mathrm{Ha}} > 50$, the reactive absorption is controlled by the intrinsic reaction rate and is not limited by the depletion of reactants at the interface. In this case, the enhancement factor is equal to the Hatta number. When $\frac{E_\infty}{\mathrm{Ha}} < 0.02$, the reaction is limited by the diffusion of the absorbent, and the enhancement factor is equal to the infinite enhancement factor, $E = E_\infty$. In the intermediate regime, the absorption rate is partly controlled by the diffusion of the absorbent. In this case, the enhancement factor can be estimated using the following iterative solution [103].

$$E = \frac{\mathrm{Ha}\sqrt{(E_\infty - E)/(E_\infty - 1)}}{\tanh\left(\mathrm{Ha}(\sqrt{(E_\infty - E)/(E_\infty - 1)}\right)} \tag{3.27}$$

Other approximate solutions for estimating the enhancement factor in the intermediate regime have been developed depending on the type of reaction and the mass transfer model used [90]. For instance, the DeCoursey solution has been found to accurately predict the enhancement factor with the limitation that the residence time in the contactor is sufficiently short to avoid the depletion of the absorbent at the reactive interface (i.e. $Gz > 120\frac{D_{\mathrm{abs}}}{D_{\mathrm{CO_2,l}}}$) [94].

$$E = \frac{-(\mathrm{Ha})^2}{2(E_\infty - 1)} + \sqrt{\frac{(\mathrm{Ha})^4}{4(E_\infty - 1)^2} + \frac{E_\infty (\mathrm{Ha})^2}{(E_\infty - 1)} + 1} \tag{3.28}$$

3.1.4 **Membrane wetting**

To maintain efficient mass transfer in a membrane contactor, the membrane pores should remain filled with gas and not be wetted by the absorbent solution. Even partial wetting of the membrane pores leads to a significant increase in the membrane mass transfer resistance, resulting in decreased CO_2 fluxes [104]. The membrane mass transfer coefficients during non-wetted, partially wetted and completely wetted operation can be estimated using the wetting ratio – that is, the ratio of non-wetted pore length (or alternatively, pore volume) to the total pore length, which is equal to the membrane thickness:

$$\frac{1}{k_\mathrm{m}} = \frac{X}{k_\mathrm{m,w}} + \frac{1 - X}{k_\mathrm{m,nw}} \tag{3.29}$$

where X is the wetting ratio and $k_\mathrm{m,w}$ and $k_\mathrm{m,nw}$ are the membrane mass transfer coefficients of the wetted and non-wetted membranes, respectively. Partial membrane wetting has been successfully taken into account in the modelling of membrane contactors for CO_2 absorption [105, 106]. To prevent membrane wetting, the compatibility of the membrane and absorbent is critical. The wettability of a particular type of membrane in contact with an absorbent solution can be estimated from the breakthrough or liquid entry pressure [84, 85]. The breakthrough pressure corresponds to the minimum excess pressure required on the liquid side for liquid penetration into the membrane pores. This pressure can be calculated using the Laplace-Young equation:

$$\Delta \mathrm{p} = \frac{4\sigma_\mathrm{l} \cos\theta}{d_\mathrm{p,max}} \tag{3.30}$$

where σ_l is the surface tension of the absorbent solution, θ is the contact angle between the liquid and membrane and $d_\mathrm{p,max}$ is the maximum membrane pore diameter. The surface tension of water or aqueous solutions containing inorganic solutes is sufficiently high to generally prevent the wetting of commonly used hydrophobic membranes. However, the surface tension is significantly reduced even in the presence of low concentrations of organic components, such as amines.

Wetting can also be prevented by selecting the appropriate membrane material, as the contact angle of the aqueous solution to the membrane surface increases with increasing hydrophobicity of the membrane. Alternatively, the membrane pore size can be reduced. Denser (less porous) membranes can withstand higher differential pressures without

wetting, but the mass transfer resistance of the membranes is also increased. As a compromise, composite membranes comprising a thin dense layer deposited on a microporous support can be used. Surface modification of microporous membranes to increase their hydrophobicity can also be considered.

The breakthrough pressure can locally exceed owing to pressure fluctuations on the liquid or gas side of the membrane or to increasing pressure drop over the module length, resulting in partial membrane wetting [107]. Careful control of the pressure on both sides of the membrane is thus necessary to maintain stable and efficient operation. The type and size of membrane modules may be limited by the maximum allowable gas-side pressure drop. Furthermore, morphological changes on the membrane surface owing to chemical attack by the absorbent can cause wetting [108, 109].

3.2 **Membranes**

In membrane gas–liquid contactors, the membrane acts as a non-dispersive, non-selective barrier between the gas and liquid phases. Typically, hollow fibre membrane modules are used owing to their high surface area per unit volume. The properties of the membrane are critical to the overall performance of the contactor. For use in CO_2 absorption, the membrane is required to possess the following general properties [85]:

1. Thermal stability and resistance to degradation at elevated temperatures.
2. Chemical stability and compatibility with the absorbent.
3. High hydrophobicity to avoid wetting.
4. High porosity to minimise the mass transfer resistance.

3.2.1 **Hydrophobic microporous membranes**

Microporous hollow fibre membranes fabricated from hydrophobic polymers constitute the most common class of membranes used in gas–liquid contactors for CO_2 absorption. Polymers employed in hollow fibre membranes include polyethylene (PE), PP, polytetrafluoroethylene (PTFE), polyvinylidene fluoride (PVDF) and polyether ether ketone (PEEK). In gas–liquid contactors, microporous membranes are preferable to dense (non-porous) membranes owing to their lower membrane mass transfer resistance [110].

The absorption performance and wetting resistance of microporous membranes is determined by the membrane–absorbent compatibility and specific membrane properties, such as porosity and pore size [104, 111]. For instance, membranes fabricated from PE have been found to undergo degradation by amine absorbents [112, 113]. PP and PTFE membranes have been found to be stable and non-wetted when used with physical absorbents such as propylene carbonate, but the increased hydrophobicity and chemical stability of PTFE membranes is beneficial when using chemical absorbents [86]. The use of PP instead of PTFE membranes would be favourable owing their significantly lower cost and the availability of smaller diameter fibres allowing higher volumetric surface

area in the contactor [114]. However, in PP membranes, various morphological and chemical changes leading to membrane wetting have been observed following contact with amine solutions [104]. The chemical stability and wetting resistance of PTFE membranes is superior to that of PP membranes, especially over longer operating periods [88, 98, 114].

The robustness of PTFE membranes under practical operating conditions has also been demonstrated in pilot- and demonstration-scale processes. During the 1990s, a PTFE membrane contactor based process was developed for CO_2 capture from gas turbines on offshore oil and gas platforms [115]. In Japan, a pilot process has demonstrated the use of a PTFE membrane contactor with volumetric mass transfer coefficient five times that of a conventional absorption column and good stability during long-term operation [116]. On the contrary, pilot-scale studies in Australia have identified wetting of PTFE membranes caused by fluctuations in the pressure differential over the membrane, highlighting the need of careful control of operating conditions even with wetting-resistant membranes [107].

Asymmetric PEEK membranes with nanometre-scale surface pores and superhydrophobic surface treatment have been shown to offer stable CO_2 absorption performance with chemical (activated MDEA) and physical (activated potassium carbonate) absorbents [117, 118]. Based on pilot-scale studies utilising the PEEK membrane contactor, more than 20-fold intensification in terms of volumetric mass transfer coefficient compared with packed columns has been reported using the activated MDEA solvent. In addition, the performance was not affected by oxygen or nitrogen and sulphur oxides present in flue gas. A preliminary economic assessment suggested reduced costs for post-combustion capture compared with conventional amine processes.

3.2.2 **Composite membranes**

As with asymmetric membranes, the benefit of composite membranes in gas–liquid contactors is the improved wetting resistance and chemical and thermal stability provided by the dense outer layer. In composite membranes, the outer layer is composed of a material different from the porous membrane support. To avoid excessive mass transfer resistance, the outer layer should be as thin as possible and possess high CO_2 permeability [85].

Composite membranes for CO_2 absorption have been prepared by coating conventional microporous polymeric membranes with a dense outer layer. In particular, PP membranes coated with Teflon have shown similar absorption fluxes compared to uncoated PP membranes, with a much improved resistance to wetting [91, 114].

3.3 **Absorbents**

Both chemical and physical absorbents used in conventional CO_2 capture processes are in principle directly applicable in membrane gas–liquid contactors. Chemical absorbents

are generally favoured owing to their higher CO_2 absorption rate, capacity and selectivity at lower CO_2 partial pressures facilitated by the reactive interaction between CO_2 and the absorbent. The main performance criteria of chemical absorbents include the reaction rate and absorption capacity towards CO_2, the regeneration energy requirement and the thermal and chemical stability [71]. In membrane contactors, absorbent selection is further constrained by the compatibility of the absorbent with the membrane material. To maintain high and stable CO_2 absorption rate, the absorbent should not be able to wet and/or chemically degrade the membrane during long-term operation.

3.3.1 **Amines**

Amine-based absorbents, as the most common solvents in post-combustion CO_2 capture processes, are also often used in membrane contactors. Variations in the absorption fluxes of common amines using hollow fibre membrane contactors have been reported in the order of MEA > AMP > MDEA (PTFE membrane [119]), MEA > AMP > DEA (PVDF membrane [120]) and MEA > DEA > MDEA (PP membrane [121]). The relative absorption rates are largely determined by the reaction rate of the amines with CO_2. In the study by Wang et al. [121], the optimal concentrations for MEA and DEA solutions were identified at 30 and 20 w-%, respectively. At higher concentrations, the absorption rate was found to be limited by the increasing viscosity of the solutions and corresponding decrease in CO_2 diffusivity. Blended amines have also been considered for membrane contactors [121].

The use of amines such as MEA, DEA or AMP has been shown to lead to the wetting and/or degradation of low-cost microporous hydrophobic membranes fabricated from PP or PVDF [122, 108, 120, 109]. The hydrophobicity of PP membranes has been found to decrease in long-term contact with common amines, resulting in the diffusion of the absorbent into the membrane, membrane swelling and, finally, wetting [109]. As an example of the effect of wetting on membrane performance, the CO_2 flux through a PVDF membrane decreased by 26% (MEA), 39% (AMP) and 78% (DEA) over 12 days of operation [120]. To avoid membrane wetting, the use of more resistant membranes seems to be necessary with amine absorbents.

3.3.2 **Amino acid salts**

Aqueous amino acid salts have been proposed as alternative chemical CO_2 absorbents. The favourable characteristics of amino acid salt solutions include CO_2 absorption rates and capacities comparable to amines, low volatility and reported stability towards degradation [123]. Amino acid salts are particularly attractive for CO_2 capture using membrane contactors because unlike amines, they generally do not wet common hydrophobic membranes owing to the high surface tension of their aqueous solutions [102]. This could facilitate stable operation in the non-wetted mode using cost-effective microporous membranes such as those made from PP.

Amino acids contain both an amine and a carboxylic acid functional group, and their CO_2 absorption capability is based on the amine group, similarly to amine solvents [124]. Twenty standard amino acids are found in the proteins of living organisms. Except proline, all standard amino acids are primary amines, whereas except glycine, all standard amino acids are sterically hindered amines. In addition to the standard amino acids, several non-standard amino acids exist in nature.

In an aqueous solution, amino acids undergo an internal acid–base reaction between the amine and carboxylic acid functionalities. The proton transfer reaction yields a dipolar zwitterion form of the amino acid. The addition of an equimolar amount of strong base such as sodium or potassium hydroxide fully converts the zwitterion into the amine form that is active for CO_2 absorption. For visualisation, Figure 3.2 presents the chemical structures of glycine, sarcosine and L-alanine in the amine form.

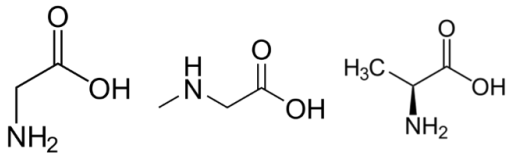

Figure 3.2 Chemical structure of the amino acids glycine, sarcosine, and L-alanine in the amine form active for CO_2 absorption.

Various amino acid salts have been considered for CO_2 absorption. Examples include the potassium salts of glycine [125, 123, 126], taurine [125, 126], sarcosine [127, 128, 126], proline [127, 129] and alanine [129, 130]. As is the case with conventional amine absorbents, the performance of different amino acid salt solutions is primarily differentiated by their CO_2 absorption rates and capacities at different temperatures and by the regeneration energy [124, 126]. Water solubility and viscosity should also be considered, and high surface tension is favourable when considering their use in membrane contactors. In contrast to amines, the surface tension of amino acid salt solutions is generally higher than that of water and increases with increasing amino acid salt concentration [102]. This directly results in higher breakthrough pressures and decreased membrane wetting tendency for amino acid salt solutions.

Neutralised amino acid salts exist in the amine form and are weakly basic. CO_2 absorption is considered to take place by the zwitterion mechanism, represented by the equations below for the case of potassium glycinate. Dissolved CO_2 and the amino acid salt form a zwitterion intermediate (Equation 3.31), which is then deprotonated by a base present in the solution (Equation 3.32) to form carbamate [123]. CO_2 may also react with the hydroxide ions present in the solution, forming bicarbonate (Equation 3.33).

$$H_2NCH_2COOK^+ + CO_2 \rightleftharpoons {}^-OOC^+H_2NCH_2COO^-K^+ \tag{3.31}$$

$$^{-}OOC^{+}H_2NCH_2COO^{-}K^{+} + B_i \rightarrow {}^{-}OOCHNCH_2COO^{-}K^{+} + B_iH^{+} \quad (3.32)$$

$$CO_2 + OH^{-} \rightarrow HCO_3^{-} \quad (3.33)$$

B_i refers to H_2O, OH^- or the amino acid salt, all capable of deprotonating the zwitterion. The ratio of carbamate and bicarbonate formed varies with the type of amino acid salt, reaction conditions and CO_2 loading of the solution [124, 131]. Owing to the weak basicity of many amino acid salts, the formation of bicarbonate can often be considered negligible at lower amino acid salt concentrations [102].

The kinetics of CO_2 absorption into potassium salts of glycine and taurine have been characterised by Kumar et al. [125]. Assuming the zwitterion reaction mechanism described above, the overall forward rate for the chemical absorption of CO_2 is given by the following:

$$r_{CO_2} = \frac{k_1 C_{CO_2} C_A}{1 + \frac{k_{-1}}{\sum_1^j k_{b,j} C_{b,j}}} \quad (3.34)$$

where C_A is the amino acid salt concentration, and the second-order kinetic constants k_1 and k_{-1} refer to the forward and reverse reactions described by Equation 3.31. $\sum_1^j k_{b,j} C_{b,j}$ refers to the contribution of all present bases in the removal of protons (Equation 3.32); $k_{OH^-} C_{OH^-}$ represents hydroxide ions, $k_{H_2O} C_{H_2O}$ represents water and $k_A C_A$ represents the amino acid salt. The kinetic equation can be simplified in selected cases. First, if $\frac{k_{-1}}{\sum_1^j k_{b,j} C_{b,j}} \ll 1$, which corresponds to fast deprotonation compared with the reverse reaction of the zwitterion formation (Equation 3.31), the kinetics can be described by the following.

$$r_{CO_2} = k_1 C_{CO_2} C_A \quad (3.35)$$

In an opposite case, where $\frac{k_{-1}}{\sum_1^j k_{b,j} C_{b,j}} \gg 1$ and the reverse reaction rate is significant,

$$R_{CO_2} = k_1 C_{CO_2} C_A \left(\frac{\sum_1^j k_{b,j} C_{b,j}}{k_{-1}} \right) \quad (3.36)$$

For potassium taurate, the reaction order in terms of the amino acid salt concentration was found to range from approximately one at the amino acid salt concentration of 1 M to 1.5 at the concentration of 4 M [125]. This indicates that the deprotonation step is not

significantly faster than the zwitterion formation step. In addition, the contribution of water to deprotonation was found to be significant. Both of these observations differ from the kinetic behaviour of aqueous amine solutions. The kinetic constants found at 295 K for potassium taurate and glycinate are presented in Table 3.1. Similar kinetic data for the potassium and lithium salts of proline and sarcosine were reported by van Holst et al. [127].

Table 3.1 Values of kinetic constants related to the zwitterion reaction mechanism for the aqueous amino acid salts potassium taurate and potassium glycinate at 295 K [125].

Amino acid salt	k_1	k_A	k_{H_2O}
Potassium taurate	12.60	$1.30 \cdot 10^{-4}$	$3.39 \cdot 10^{-6}$
Potassium glycinate	49.68	$6.04 \cdot 10^{-5}$	$2.69 \cdot 10^{-6}$

Although the absorption capacities and rates of amino acid salt solutions have been found to be comparable to those of amines [126], absorption energy must also be considered to facilitate an energy-effective CO_2 capture process. For instance, the energy requirement using potassium glycinate in a pilot-scale post-combustion process (5.5 GJ/t CO_2) was found to be higher than that using MEA (3.68 GJ/t CO_2) [132]. In addition, operational difficulties including significant solvent degradation were reported in the same study, highlighting the major challenges in the direct replacement of amines in conventional capture processes.

The energy requirement of potassium sarcosine was also found to be higher than that of MEA in another pilot plant report [128]. On the contrary, the potassium salt of L-alanine was identified as a potentially energy-saving absorbent based on its relatively low heat of absorption [129], suggesting that the energy intensity could be reduced by proper selection of the amino acid. To improve the solvent properties, the promotion of amino acid salt solutions by amines such as piperazine has also been suggested [130].

The precipitation of reaction products at high CO_2 loading may take place in concentrated amino acid salt solutions [133, 124]. This may lead to operational issues or limitations in conventional post-combustion capture processes [132]. However, precipitation can also be utilised to maximise the CO_2 absorption capacity and reduce energy consumption. This was demonstrated in a novel capture process based on the precipitation of the zwitterion product of CO_2 absorption and increased equilibrium CO_2 loading in the solution [134, 135]. Utilising 4-M potassium taurate as the absorbent, the regeneration energy for this process (2.4 GJ/t CO_2) was reported to be 35% lower than that for a MEA absorption process.

Although amino acid salts may not offer clear and significant advantages over amines in a conventional CO_2 capture process, the decreased tendency of membrane wetting is a

major motivation for considering their use in membrane-contactor–based capture processes.

Feron and Jansen [136] reported pilot plant studies of CO_2 absorption utilising a proprietary amino acid salt–based absorbent solution and a patented, transversal flow PP hollow fibre contactor. The mass transfer performance of the unit was found to be competitive with membrane contactors using MEA as the absorbent. The overall mass transfer coefficient was reported at 1.6×10^{-3} m/s. The mass transfer resistance was dominated by the liquid-side resistance. The cyclic loading – that is, the difference in the CO_2 loading of the lean and rich solvent – was limited to 0.11 mol CO_2 per mol of active component. The corresponding equilibrium value based on CO_2 solubility at the absorption and desorption temperatures was 0.45 mol/mol. In the absorption temperature range of 25–40 °C, the CO_2 flux increased with increasing temperature owing to increased rates of reaction and diffusion.

In contrast, Yan et al. [137] reported a decreasing CO_2 absorption flux with increasing temperature (30–50 °C) using potassium glycinate as the absorbent in a PP membrane contactor. Compared with MDEA and MEA, the absorption rate with potassium glycinate was found to be higher. A slight increase in the CO_2 flux was found with increasing absorbent concentration (0.5–3.0 M). A stable flux over 40 h of operations was reported, indicating good resistance to membrane wetting. With a PP contactor, Lu et al. [138] found that the overall mass transfer coefficient increased by 30% using potassium glycinate (0.75 M) promoted with PZ (0.25 M) compared with pure 1-M potassium glycinate. A novel approach based on the promotion of potassium glycinate by the addition of phosphate or borate salts was also reported [139].

3.3.3 **Physical absorbents**

Studies on the use of physical CO_2 absorbents in membrane contactors are limited. The low surface tension of physical solvents, resulting in poor compatibility with microporous membranes, is considered a major limitation [140]. Dindore et al. [86] studied the wetting characteristics of various combinations of membranes and physical solvents and found that low-cost microporous membranes such as PP or PVDF are not compatible with the majority of physical solvents applicable in CO_2 absorption. However, propylene carbonate was identified as a potential solvent to be used with PP membranes. The absorption of CO_2 at pressures up to 20 bar with this membrane–absorbent combination has been demonstrated, but potential membrane wetting was still observed during longer operating periods [141].

3.4 **Summary**

The advantages of membrane contactors over conventional gas–liquid contacting equipment in CO_2 absorption processes include higher interfacial area per unit volume, physical separation of the gas and liquid phases and simple modular scale-up. The

additional mass transfer resistance of the membrane can be offset by the significant increase in interfacial area, resulting in increased volumetric mass transfer coefficients compared with conventional equipment. Moreover, owing to the separation of the gas and liquid phases, hydrodynamic issues such as foaming and flooding can be avoided, and the gas and liquid flow rates can be independently adjusted. The modularity of membrane contactors allows simple scale-up by increasing the number of modules and the membrane surface area.

Membrane modules in the hollow fibre configuration are often employed as gas–liquid contactors owing to the high interfacial area provided by bundles of thin fibres in a shell. The absorbent liquid may flow on the lumen or shell side of the contactor with the selection based on the type of membrane and the hydrodynamic conditions. Microporous membranes are most commonly used, with the non-selective membrane acting as a non-dispersive barrier between the two phases. Selectivity for the absorption of CO_2 from the gas phase into the liquid is depends on the selection of the absorbent liquid. In general, absorbents used in conventional CO_2 capture processes are also applied in membrane contactors. Although both physical and chemical CO_2 absorbents can be used, chemical absorbents are favoured owing to their higher absorption rates and capacities, especially at lower CO_2 partial pressures.

According to the resistance-in-series model, the overall mass transfer in a membrane contactor includes the gas-side, membrane and liquid-side resistances. For reference, Table 3.2 presents a comparison of the overall mass transfer coefficients measured for various membrane and absorbent combinations. For efficient mass transfer, operation in the non-wetted mode, with the membrane pores occupied by the gas and not the liquid, is critical. To maintain non-wetted operation, hydrophobic membranes are employed with aqueous absorbent solutions. However, the membrane wetting tendency of aqueous solutions containing organic components such as amines increases with increasing organic concentration. Careful selection of the membrane–absorbent combination is thus necessary to avoid membrane wetting and to maintain stable and high CO_2 fluxes.

Table 3.2 Values of gas-side overall mass transfer coefficient for CO_2 absorption measured for various membrane and absorbent combinations.

Ref.	Membrane	Absorbent	Overall mass transfer coefficient, m s^{-1}
[119]	PTFE	AMP	2.5×10^{-5}
[136]	PP (transversal flow module)	Proprietary amino acid salt-based	1.6×10^{-3}
[100]	PTFE, PVDF	MEA	9.0×10^{-4} (PVDF) 4.0×10^{-4} (PTFE)
[86]	PTFE, PP	Propylene carbonate	2.0×10^{-5} (PP) 1.5×10^{-5} (PTFE)
[142]	PP	MDEA, MDEA+PZ	3.0×10^{-5} (MDEA) 6.0×10^{-5} (MDEA+PZ)
[99]	PP, PTFE, PVDF	MEA	2.8×10^{-4} (PTFE) 4.3×10^{-4} (PP) 1.4×10^{-4} (PVDF)
[138]	PP	PG, PG+PZ	$1.7 \cdot 10^{-4}$ (PG) $2.3 \cdot 10^{-4}$ (PG+PZ)
[101]	PVDF, PP	PZ, MDEA, AMP	4.4×10^{-5} (PVDF, MDEA) 1.7×10^{-4} (PVDF, AMP) 3.3×10^{-4} (PP, AMP) 7.7×10^{-5} (PP, MDEA)
[114]	PP, PTFE, PP with dense layer	MEA	3.3×10^{-4} (PP) 3.3×10^{-4} (PTFE) 2.8×10^{-4} (PP-PMP) 2.9×10^{-4} (PP-Teflon)
[121]	PP	MEA, DEA, MDEA, MEA+MDEA	5.7×10^{-4} (MEA) 2.5×10^{-4} (DEA) 0.5×10^{-4} (MDEA) 6.8×10^{-4} (MEA+MDEA)
[91]	PP, PP with dense layer	MEA	5.5×10^{-6} (PP) 1.0×10^{-3} (PP, PTMSP) 1.1×10^{-3} (PP, PIM-1) 6.0×10^{-4} (PP, Teflon)

Membranes fabricated from low-cost hydrophobic polymers such as PP and PVDF have been found to be prone to degradation and wetting in long-term contact with amine-based absorption solutions. PTFE membranes offer improved stability but at significantly higher cost. Asymmetric and dense-layer composite membranes have been suggested as alternatives to porous membranes. The thin, dense outer layer on these membranes offers

improved wetting resistance; however, it results in increased membrane mass transfer resistance. Instead of using novel membrane materials, wetting can be minimised by the selection of absorbents with higher surface tension. Instead of organic amines, alternative chemical absorbents such as aqueous amino acid salts have been found to be effective when used in membrane contactors.

4 Alternative methods for CO_2 desorption

A continuous CO_2 capture process comprises the absorption stage and the solvent regeneration stage, wherein the CO_2 is desorbed from the absorbent and released from the solution. The regeneration step is based on the reversal of the reactions taking place during CO_2 absorption. This is conventionally facilitated by increasing the solution temperature. The efficiency of the desorption stage is critical to the economics of CO_2 capture, as solvent regeneration constitutes the majority of the energy input to the capture process.

The use of membrane contactors in place of conventional contacting equipment in CO_2 capture processes has mostly been focused on the absorption stage. The desorption stage could also be intensified using membrane contactors. Similarly to the absorption stage, the principal benefits of membrane contactors in the desorption stage would be the increased volumetric mass transfer rate (owing to increased surface area per unit volume) and the physical separation of the gas and liquid phases by the membrane, which allows flexible operation [143]. A challenge in membrane-contactor–based desorption is the membrane stability at elevated temperatures, which can be low especially when using common microporous polymeric materials. As a result, alternatives including inorganic membranes and dense layer composite membranes have received research interest for CO_2 desorption and stripping (Section 4.1).

Furthermore, the use of vacuum has been suggested to facilitate effective solvent regeneration at reduced temperatures (Section 4.2). The potential benefits of reduced regeneration temperature include energy savings, the possibility to use low-grade heat sources and decreased rate of solvent degradation. On the other hand, these benefits need to be balanced with the increased electric energy required for compression of the CO_2 product. Vacuum desorption at reduced temperatures combined with the use of membrane contactors for CO_2 stripping also appears promising because the demand for membrane stability at high temperatures is reduced.

4.1 Membrane contactors for stripping

In a conventional CO_2 desorption column, the CO_2 released from the solution is transported from the liquid to the gas phase and then stripped by the steam evaporated from the aqueous solution. In a membrane contactor, the CO_2 released from the solution on the liquid side of the membrane is transported through the membrane to the gas side. A flow of stripping or sweeping gas is often maintained on the gas side to transport the gaseous CO_2 away from the contactor and to maintain the mass transfer driving force. The desorption process is controlled by mass transfer (and not by the reaction rate), and the liquid-side mass transfer resistance usually dominates, contributing up to 90% of the total resistance [143, 144]. Desorption at elevated temperatures is necessary both for driving the absorption reactions towards free CO_2 and for accelerating the CO_2 desorption

flux. Accordingly, the stripping flux has been shown to increase with increasing temperature [144, 145, 146].

Owing to the elevated temperatures required, avoiding membrane degradation and wetting and maintaining stable performance are primary concerns in the selection of the membrane material. Even PTFE membranes, which are generally stable under absorption conditions, have been shown to be prone to wetting at higher temperatures [144]. Wetting of a PTFE membrane by propylene carbonate under desorption conditions has also been reported [147]. Correspondingly, lower-cost polymeric membranes with a lower wetting resistance than PTFE do not appear feasible for CO_2 desorption [148]. On the other hand, coating of microporous membranes with dense layers fabricated from various glassy polymers or Teflon appears promising [149, 146].

4.2 Vacuum desorption

The primary goal of utilising vacuum in CO_2 desorption from loaded absorbent solutions is the reduction of desorption temperature. The potential benefits of performing solvent regeneration at reduced temperatures include the reduction in specific energy consumption, the possibility to use low-grade heat sources instead of steam and the improvement in solvent stability owing to slower degradation [150]. If combined with the use of membrane contactors, the reduced temperature could also improve the stability of the membrane. The promoting effect of vacuum for CO_2 desorption is attributable to the reduction in CO_2 partial pressure and the resulting increase in the mass transfer driving force [151]. To save energy, the amount of water evaporating from the absorbent solution could be reduced under vacuum, leading to the reduction in the latent heat consumed [152]. In addition, the sensible heat required for heating the solution is reduced.

Conventionally, solvent regeneration is performed at the boiling temperature of the loaded solution, with the evaporated water sweeping the released CO_2 away from the gas–liquid interface and maintaining a low CO_2 partial pressure. Correspondingly, the effectiveness of vacuum desorption is increased when the pressure is reduced to the level corresponding to the water vapour pressure at the operation temperature. Using potassium and sodium carbonate solutions, Nii et al. [152] found a continuously increasing CO_2 desorption rate with decreasing pressure, with a sharp increase at pressures below the water vapour pressure. However, the amount of water evaporated also sharply increased at the low pressures, resulting in a significantly higher water evaporation rate compared with the CO_2 desorption rate. To maximise the ratio of CO_2 released to water evaporated, simultaneously maximising the energy efficiency, maintaining the vacuum at the water vapour pressure was suggested.

The use of hollow fibre membranes for vacuum desorption has also been pursued.. Fang et al. [150] performed CO_2 stripping from MEA under vacuum using a PP hollow fibre membrane contactor. With the loaded solution flowing inside the fibres, steam was used as a sweeping gas on the shell side. The CO_2 desorption rate increased with decreasing pressure (10–35 kPa) and increasing temperature (40–70 °C). The steam sweep was found

to increase the desorption rate owing to reduced CO_2 partial pressure on the gas side. Wang et al. [153] estimated the energy consumption during vacuum regeneration using PP or PVDF membrane contactors. A minimum energy consumption of 0.78 MJ/kg CO_2 was found at a desorption temperature of 70 °C and pressure of 20 kPa. This was estimated to be 28% lower than the thermal energy requirement of thermal regeneration without vacuum.

5 Membrane-contactor based CO_2 capture unit (Publications I–II)

The subject of Publications I and II is CO_2 capture by absorption in a membrane-contactor–based continuous system. Publication I discusses the design aspects and operational findings related to an experimental CO_2 capture unit. Factors limiting the CO_2 capture performance of the unit are identified and discussed. Experimental results in terms of the overall mass transfer and specific energy consumption are reported and compared with literature data. Publication II is a direct continuation of Publication I, providing a more detailed analysis of the mass transfer performance of the membrane-contactor–based CO_2 capture unit.

5.1 Background and motivation

CO_2 capture technologies facilitating the storage and/or utilisation of CO_2 captured from emission sources are considered an important component in the overall effort to reduce atmospheric CO_2 emissions (Chapter 1). Established technologies for the capture of CO_2 from point emission sources such as fossil-fired power plants are largely based on chemical absorption processes using aqueous amine solutions (Chapter 2). Although such processes are technically feasible, their large-scale implementation is hindered by the high costs involved. This fuels the development of alternative capture processes and technologies.

Membrane contactors are an alternative to absorption (and desorption) columns used in conventional CO_2 capture processes (Chapters 3–4). The CO_2 capture unit discussed in Publications I and II integrates a membrane contactor into a continuous absorption/desorption process. Aqueous amino acid salt solutions (Section 3.3.2) are used as solvent to facilitate the use of cost-effective and commercially available polymeric hollow fibre membrane modules as the absorber. Such modules are known to suffer from wetting and stability issues when used with amine-based absorption solutions (Section 3.1.4).

The integration of the absorption and desorption stages yields a complete and practical capture process and allows the characterisation of the separate process stages in a combined system. Publication I investigates this integration and identifies the factors limiting the performance of the entire unit. In the continuous unit, CO_2 is released from the solution by means of increased temperatures and the use of vacuum. The implementation of vacuum solvent regeneration (Section 4.2) is motivated by the possibility to reduce the temperature required for effective CO_2 desorption. This could reduce the amount of heat energy consumed in the process, which constitutes a major fraction of the operating costs in conventional CO_2 capture processes. To complete the analysis, electric energy consumed in the process is also measured.

Building on the findings presented in Publication I, Publication II aims to provide a more detailed mass transfer analysis of the CO_2 capture unit. The main focus of this analysis is on the membrane contactor as a well-defined and functional operational unit. The mass transfer performance of the contactor is assessed by varying the main operating parameters such as flow rates and temperatures. Using calculational methods established in the relevant literature, the individual mass transfer resistances and enhancement factor for chemical absorption are evaluated to identify the limiting resistance. The effect of desorption conditions is also investigated. However, this is done by studying the resulting effects on absorption at the membrane contactor rather than by a detailed analysis of the mass transfer processes involved in desorption.

5.2 Methodology

A detailed description of the experimental unit and procedure is given in Publication I. A flowsheet of the unit is presented in Figure 5.1. The continuously operated CO_2 capture unit comprises a membrane module as the absorber and a glass vessel as a desorption vessel/stripper. The glass vessel also acts as a buffer tank for the absorbent solution. The Liqui-Cel 2.5 × 8 Extra-Flow membrane contactor, containing PP hollow fibres, was supplied by 3M. The membrane surface area of the module is 1.4 m^2. The module is configured in counter-current flow with the absorbent liquid flowing upwards inside the membrane fibres (lumen side) and gas flowing outside the fibres (shell side).

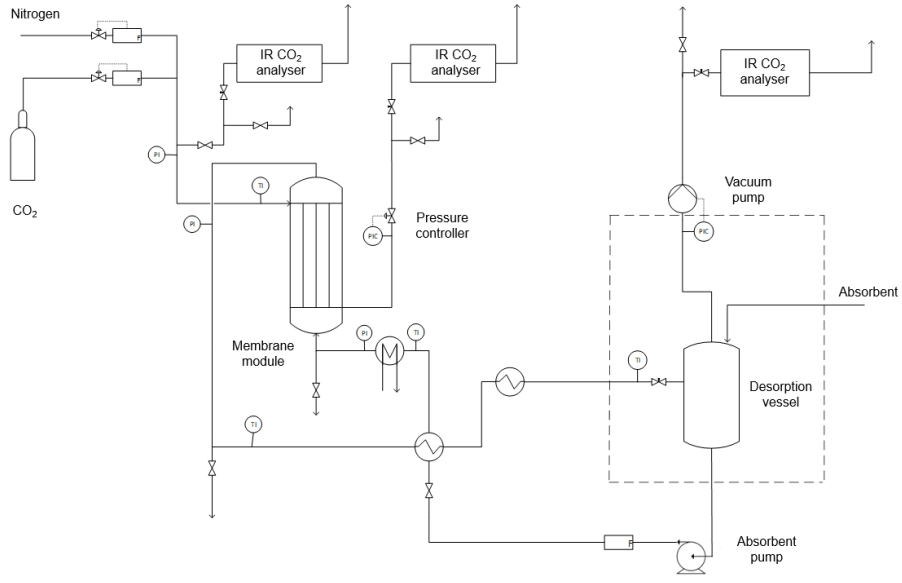

Figure 5.1 Flowsheet of the experimental CO_2 capture unit.

Inlet gas entering the contactor comprises mixtures of CO_2 and nitrogen at a CO_2 concentration of 10 vol-%, unless otherwise stated. The gas flows are controlled by mass

flow controllers (calibrated under NTP conditions), and the concentration in the mixed gas is verified using an infrared (IR) analyser. The gas pressure is controlled using a back-pressure controller located at the gas outlet from the contactor. The gas-side pressure is automatically controlled at 0.1 bar below the liquid-side pressure to avoid bubbling of gas through the membrane and liquid penetration in the membrane pores. The CO_2 concentration in the outlet gas is also measured by an IR analyser.

The absorbent solution is circulated through the system by a magnetic drive gear pump, and the liquid flow rate is measured using a flow meter (calibrated using water, NTP) located directly after the pump. The CO_2-lean absorbent at the regeneration temperature (60–80 °C) is cooled in a heat exchanger in which heat is transferred to the cold absorbent exiting the membrane module. The solution is further cooled to the absorption temperature (10–30 °C) in another heat exchanger using cooling water. The cooling water temperature is controlled by a circulating cooler. After flowing through the membrane module, the CO_2-rich absorbent is first heated in the heat exchanger and then heated to the regeneration temperature in a hot water heater.

The gas outlet from the desorption vessel is connected to a vacuum pump via an automatic vacuum control unit. The CO_2 concentration in the outlet gas from the vacuum pump is measured by an IR CO_2-analyser. The analyser also measures oxygen concentration in the outlet gas. Process control and data acquisition are performed in LabVIEW software; the details of this system are also provided in Publication I.

In all publications, potassium glycinate absorbent solutions were prepared by the neutralisation of glycine (>99%) using an equimolar amount of potassium hydroxide (>85w-%) in purified water. Potassium glycinate concentrations were verified by potentiometric titration using 1-M hydrochloric acid. All concentrations were within 1% of the nominal concentration. Nitrogen (>99.5%) and CO_2 (>99.99%) supplied from gas cylinders were mixed in the feed gas for CO_2 capture experiments.

Unless stated otherwise, all data were collected under steady-state conditions, indicated by stable operating conditions and a stable CO_2 concentration in the membrane outlet gas. Steady-state data were collected during a period of approximately 1 min using the LabVIEW environment. Results were then calculated as mean values during the sampling period. Repeatability of results was checked by a series of repeat experiments performed both without vacuum and with vacuum at 600 mbar, both at a desorption temperature of 80 °C.

In Publication I, the standard deviations observed in these experiments were multiplied by a factor of 1.96 to estimate the 95% confidence interval, which was then assumed to hold for experiments under all operating conditions. The confidence intervals are represented as error bars in the relevant figures. In Publication II, repeatability was estimated by determining the standard error of the mean (instead of standard deviation) from the same repeat experiments. The standard error of the mean was then multiplied by a factor of 1.96 to evaluate the 95% confidence interval.

Liquid samples were also collected under steady-state conditions to measure the CO_2 loading of the absorbent (mol CO_2 absorbed per mol of potassium glycinate). One rich solvent sample (collected after the membrane module) and one lean solvent sample (collected before the membrane module) were collected. Each sample was analysed three times by titration using 1 M hydrochloric acid and the volumetric measurement of the CO_2 gas released. A maximum relative standard deviation of 3.0% for the triplicate measurements was accepted.

For Publication II, a stability test with six days of operation was performed with the system continuously running during daytime and shut off during night. The same batch of absorbent was used throughout the test. Instead of nitrogen, CO_2 was mixed with air in the feed gas to investigate any effects from oxygen.

5.2.1 Calculations

The CO_2 capture efficiency – that is, the fraction of CO_2 absorbed from the feed gas – was calculated using the following expression:

$$\eta_{\text{abs}} = \frac{\dot{n}_{\text{CO}_2,\text{in}} - \dot{n}_{\text{CO}_2,\text{out}}}{\dot{n}_{\text{CO}_2,\text{in}}} \cdot 100\% \tag{5.1}$$

where η is the capture (absorption) efficiency, and $\dot{n}_{\text{CO}_2,\text{in}}$ and $\dot{n}_{\text{CO}_2,\text{out}}$ are the molar flow rates of CO_2 in the inlet and outlet gas, respectively. The flow rates were determined from the mass balance over the membrane module, assuming that nitrogen was not transferred through the membrane. According to Equation 3.7, the molar flux of CO_2 through the membrane and absorbed in the liquid was calculated using the following:

$$N = \frac{\dot{n}_{\text{CO}_2,\text{in}} - \dot{n}_{\text{CO}_2,\text{out}}}{A} = \frac{(C_{\text{CO}_2,\text{in}} - C_{\text{CO}_2,\text{out}})Q_{\text{n}}}{A} \tag{5.2}$$

where $C_{\text{CO}_2,\text{in}}$ and $C_{\text{CO}_2,\text{out}}$ are the molar CO_2 concentrations in the inlet and outlet gas, respectively, and Q_{n} is the inert gas volumetric flow rate. Equation 5.2 is also an approximation that assumes that inert components are not transferred over the membrane. An exact solution of the CO_2 flux over the membrane would require that the mass transfer of all components is taken into account in the mass balance over the membrane module. The overall mass transfer coefficient was then calculated using Equation 3.7, with the logarithmic mean mass transfer driving force calculated using Equation 3.8.

The liquid concentrations at the contactor inlet and outlet were calculated from the lean and rich solvent loadings, respectively. Solubility data of CO_2 in 1-M potassium glycinate from Portugal et al. [131] were used to determine the gas-phase concentrations in equilibrium with the corresponding liquid concentrations. The gas-phase concentration was plotted against the liquid-phase concentration in the CO_2 partial pressure range relevant to the present experiments (100–1000 kPa), and an exponential curve was fitted to the data. As a result, the following correlation was found:

$$C^*_{\mathrm{CO_2,g}} = 1.4 \cdot 10^{-4} e^{0.014 C_{\mathrm{CO_2,l}}} \tag{5.3}$$

where $C_{\mathrm{CO_2,l}}$ is the liquid-phase CO_2 concentration, and $C^*_{\mathrm{CO_2,g}}$ the corresponding gas-phase equilibrium concentration.

The heat duty required for heating the absorbent from the absorption temperature to the desorption temperature was estimated from the following:

$$P_t = \rho Q_\mathrm{l} c_\mathrm{p} \Delta T \tag{5.4}$$

where P_t is the thermal duty, Q_l is the liquid volumetric flow rate, ΔT is the temperature difference between the desorption temperature and the temperature of the pre-heated absorbent leaving the plate heat exchanger, ρ is the solution density approximated by the density of water (1000 kg/m^3) and c_p is the absorbent heat capacity approximated by the heat capacity of pure water (4186 J/kg K).

The specific heat consumption per mol of CO_2 captured was calculated as follows.

$$e_t = \frac{P_t}{NA} \tag{5.5}$$

The specific electricity consumption was similarly calculated:

$$e_e = \frac{P_e}{NA} \tag{5.6}$$

where P_e is the total measured electrical power of the absorbent pump and the vacuum pump. The desorption efficiency was calculated from the following:

$$\eta_\mathrm{des} = \frac{\alpha_\mathrm{rich} - \alpha_\mathrm{lean}}{\alpha_\mathrm{rich}} \cdot 100\% \tag{5.7}$$

where η_des is the desorption efficiency, and α_rich and α_lean are the CO_2 loadings of the rich absorbent leaving the membrane contactor and the lean absorbent entering the membrane contactor, respectively.

The individual mass transfer coefficients were calculated for a series of experiments where the liquid flow rate was varied. Experimental correlations presented in the literature were used to estimate the liquid and gas mass transfer coefficients. These correlations and other equations involved are discussed in Section 3.1. The liquid and gas mass transfer coefficients were estimated using Equation 3.19 and Equation 3.14, respectively. The parameters used in the calculation of the individual mass transfer coefficients are summarized in Publication IV, Table 2.

The membrane mass transfer coefficient was estimated based on the resistance-in-series model (Equation 3.5). First, the gas and liquid mass transfer coefficients were estimated

using correlations, and the enhancement factor using the method described below. The membrane mass transfer coefficient was then calculated using the experimentally calculated values of the overall mass transfer coefficient. A constant value of the membrane mass transfer coefficient was assumed, with the average value over the liquid flow rate data points taken as the estimate. For comparison, a theoretical value of the membrane mass transfer coefficient was calculated using Equation 3.20.

The procedure for calculating the enhancement factor is described in Section 3.1.3. The Hatta number was calculated using Equation 3.25. The infinite enhancement factor was then calculated with Equation 3.26. The DeCoursey solution (Equation 3.28) was then used to estimate the value of the enhancement factor under the experimental conditions.

5.3 Results and discussion

This section presents and discusses the results obtained using the membrane-contactor–based CO_2 capture unit and published in Publications I and II. The following subsections are organised according to the type of experiments performed and findings obtained in the two publications. Sections 5.3.1–5.3.4 correspond to the results presented in Publication I, and Sections 5.3.5–5.3.9 to the results presented in Publication II. Section 5.4 summarises these findings and provides an outlook for the further development of the membrane contactor-based CO_2 capture process.

5.3.1 Start-up and operational findings

The CO_2 capture unit could be continuously operated with good stability, providing consistent and reliable data for steady-state measurements. Automatic gas-side pressure control could maintain an appropriate trans-membrane pressure under all operating conditions. During limited time of operation, any indication of membrane wetting (i.e. decline in performance) was not observed, suggesting good compatibility of the amino acid salt solutions with the PP membrane.

Publication I, Figure 3 presents an example of the evolution of the CO_2 concentration at the membrane outlet and the CO_2 capture efficiency during start-up of the unit using fresh batches of absorbent solution – in this case, 3 M potassium glycinate. For comparison, profiles obtained with atmospheric desorption and desorption under 800-mbar vacuum are presented, with otherwise identical conditions. As observed in the figure, during the first hour of operation, nearly 100% of the CO_2 entering the contactor is absorbed into the unloaded solution. Because the CO_2 absorbed in the solution is not completely desorbed at the desorption stage, the CO_2 loading of the solution continuously increases. This build-up of CO_2 then decreases the absorption flux, resulting in decreasing capture efficiency. Steady-state operation is reached when the absorption flux is equal to the flux of CO_2 released from the solution at the desorption stage.

During vacuum desorption at 800 mbar, the steady-state CO_2 capture efficiency is higher than that in non-vacuum operation. With the aid of vacuum, CO_2 is more effectively

desorbed, which allows a corresponding increase in the steady-state absorption flux. At the same time, the steady-state condition is reached slightly faster (after about 5 h) than in the non-vacuum case. This is attributable to the faster build-up of CO_2 in the solution owing to an increased CO_2 flux enabled by the more efficient desorption. However, even under vacuum conditions, the steady-state CO_2 flux is limited by the desorption rate, and the capture efficiency only remains at approximately 16% under these conditions. The desorption performance and its effect on the steady-state absorption flux is discussed further in Section 5.3.5.

5.3.2 Overall mass transfer coefficient

Figure 5.2 presents the overall mass transfer coefficients calculated at different desorption pressures at 80 °C. The driving force for the physical mass transfer is included in the calculation of the overall mass transfer coefficient via the logarithmic mean concentration (Equation 3.8). Thus, the variation in the mass transfer coefficient is probably linked to the variation in the rate of chemical absorption. Higher lean loading under less favourable desorption conditions (higher vacuum pressure) seems to lead to a lower reaction rate, as discussed in more detail in Section 5.3.6. The lean CO_2 loading varies from 0.48 mol/mol at 800 mbar to 0.42 mol/mol at 500 mbar in the present experiments.

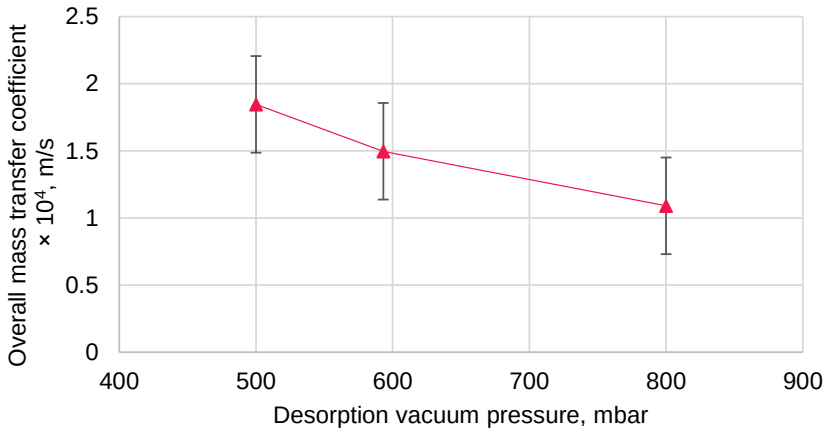

Figure 5.2 Effect of desorption pressure on the overall mass transfer coefficient during vacuum desorption at 80 °C. Absorbent flow rate: 1.0 l/min (NTP, 1 M potassium glycinate), feed gas flow rate: 5.0 l/min (NTP, 10% CO_2 in nitrogen), absorption temperature: 20 °C. Line added for visual guidance.

The highest value for the overall mass transfer coefficient is 1.9×10^{-4} m/s, at the desorption temperature of 80 °C and pressure of 500 mbar. Table 5.1 compares this value to literature values obtained using PP hollow fibre modules and various absorbent solutions. The value calculated here is well within the range of values found in the literature, as reviewed in Table 5.1. This can be considered a validation of the experimental and calculational procedure employed to determine the overall mass transfer

coefficient; moreover, it suggests a reasonably good (absorption) mass transfer performance of the experimental unit.

Table 5.1 Comparison of experimental overall mass transfer coefficients in CO_2 absorption using polypropylene membrane contactors and various absorbents.

Reference	Absorbent	Liquid velocity, m s^{-1}	Overall mass transfer coefficient, m s^{-1}
This work	Potassium glycinate (PG)	0.04	1.9×10^{-4} (lean loading 0.42)
Feron and Jansen, 2002 [136]	CORAL (Proprietary amino acid salt based)	N/A	1.6×10^{-3}
Mavroudi et al., 2003 [154]	DEA	0.16	3.5×10^{-4}
Dindore et al., 2004 [86]	Propylene carbonate	0.38	2.0×10^{-5}
Kosaraju et al., 2005 [155]	Polyamidoamine dendrimer	0.062	2.15×10^{-5}
Lu et al., 2005 [142]	MDEA MDEA+PZ	3.9	3.0×10^{-5} (MDEA) 0.8×10^{-5} (MDEA, lean loading 0.3) 6.0×10^{-5} (MDEA+PZ)
Franco et al., 2008 [99]	MEA	0.014	4.3×10^{-4} (lean loading 0.27-0.30)
Lu et al., 2009 [138]	PG PG+PZ	3.0	1.7×10^{-4} (PG) 2.3×10^{-4} (PG+PZ)
Lin et al., 2009 [101]	MDEA, AMP	N/A	3.3×10^{-4} (AMP) 7.7×10^{-5} (MDEA)
Chabanon et al., 2011 [114]	MEA	N/A	3.3×10^{-4} 1.6×10^{-4} (after 1200 h)
Wang et al., 2013 [121]	MEA+MDEA (various amines and blends)	0.09	6.2×10^{-4}
Scholes et al., 2015 **[91]**	MEA	N/A	5.5×10^{-6} (35 °C) 8.0×10^{-6} (65 °C) (wetted membrane)

The reference most relevant to the present study is that of Lu et al. [138], who also employed a potassium glycinate solution and found an almost identical value of the overall mass transfer coefficient (1.7×10^{-4} m/s). This result was obtained using a fresh, unloaded absorbent solution as opposed to the relatively highly loaded solution in the present study. The effect of the lean loading has been studied by Lu et al. [142] using MDEA solutions. They found a rather significant decrease in the overall mass transfer coefficient when the loading increased from 0 to 0.3 mol/mol. The effect of loading with various amino acid salt solutions was investigated in a screening study by He et al. [126], who noted a significant decrease in the absorption rate beginning from about 0.2 mol/mol, regardless of the type of amino acid salt used. These findings highlight the importance of effective desorption for maintaining high steady-state absorption fluxes.

5.3.3 Purity of CO_2 product

Measurement of CO_2 concentration in the outlet gas from the desorption stage allows the assessment of the purity of the CO_2 product from the capture unit. In addition, this provides insights into the selectivity of CO_2 absorption over that of nitrogen. Usually, absorption of nitrogen is considered negligible owing to the high CO_2 selectivity of chemically absorbing solutions. The CO_2 concentration of the product following vacuum desorption at 60–80 °C and 500–800 mbar is presented in Figure 5.3. The CO_2 concentration in the experiments ranges from 84 to 95 vol-%, with no trend observed in terms of the desorption temperature or pressure. Comparative data from literature is not readily available, as the CO_2 concentration following desorption is usually not reported. Considering a practical CO_2 capture process, the purity requirement of CO_2 produced depends on the intended use of CO_2. For chemical conversion, the purity should generally be above 99% [63].

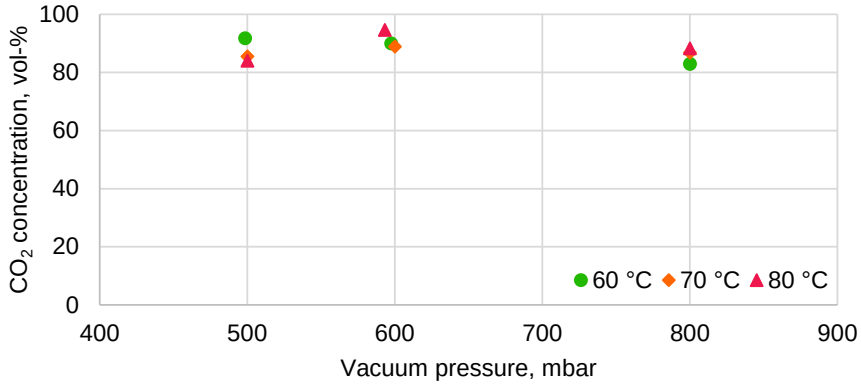

Figure 5.3 Effect of vacuum pressure and desorption temperature on the CO_2 concentration of the outlet gas leaving desorption. Absorbent flow rate: 1.0 l/min (NTP, 1 M potassium glycinate), feed gas flow rate: 5.0 l/min (NTP, 10% CO_2 in nitrogen), absorption temperature: 20 °C.

Assuming that the rest of the outlet gas consists of only nitrogen, the implied CO_2/nitrogen selectivity would range from 5 to 20. However, oxygen concentrations of up to 3 vol-% were also measured in these experiments. This suggests air remaining in the system or minor leaks in the vacuum system. Owing to the inaccuracies involved, the measured CO_2 concentrations should only be considered as rough estimates, probably corresponding to the lower limit of the actual concentration range. However, it appears that the absorption of nitrogen may not be negligible under the present conditions. This might be explained by the high CO_2 loading in the lean solution, limiting the CO_2 absorption rate, and by the more efficient desorption of physically absorbed nitrogen compared with chemisorbed CO_2.

5.3.4 Specific energy consumption

Energy consumption by the capture unit was estimated by calculating the sensible heat required for heating the absorbent to the desorption temperature and measuring the electricity consumed by the absorbent and vacuum pumps. The specific heat requirement and electricity consumption per mole of CO_2 captured at the desorption temperature of 80 °C and pressures of 500–800 mbar are presented in Figure 5.4. The electricity consumption is significant compared with the heat requirement. The specific heat requirement is higher at lower desorption temperatures. Although the heat required for solvent heating is reduced, this decrease is offset by significantly decreased CO_2 desorption rates. Reducing the desorption pressure also results in lower specific heat consumption owing to increased desorption rate.

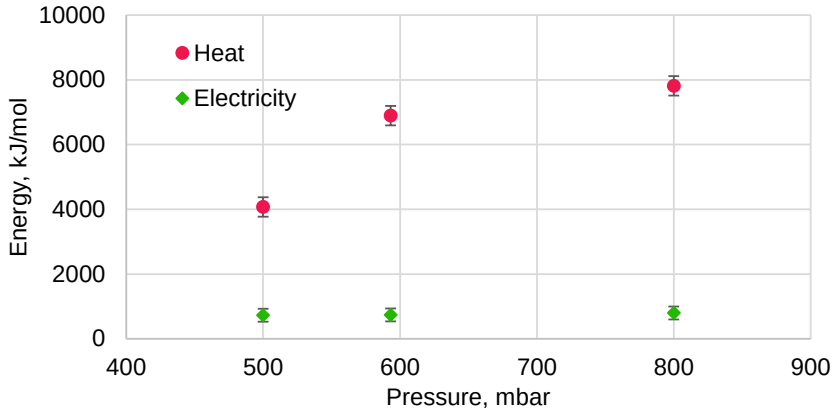

Figure 5.4 Specific heat and electricity consumption per mole of CO_2 captured during desorption at 80 °C and 500–800 mbar vacuum. Absorbent flow rate: 1.0 l/min (NTP, 1 M potassium glycinate), feed gas flow rate: 5.0 l/min (NTP, 10% CO_2 in nitrogen), absorption temperature: 20 °C.

The specific energy values are compared to a limited number of literature references in Publication I. In brief, the magnitude of the results can be significantly different depending on the type of experiments performed and the method used for estimating the energy consumption. In the present study, the aim is to directly estimate the energy based on measurements obtained from the unit, with the idea that the results can be directly extrapolated to larger capacity capture units.

This approach differs from a commonly used theoretical approach of estimating the energy consumption in post-combustion capture processes – for example, based on the concept of equivalent work, which takes into account the lost electricity generation capacity owing to steam extraction to the reboiler [156]. This approach has also been used in the context of membrane stripping of CO_2 under vacuum [153]. The approach used in the present study may lead to the overestimation of the heat energy owing to the inefficiencies related to the experimental setup (insulation and heat integration). On the

contrary, the present approach ignores the contribution of absorption heat (approximately 69 kJ/mol for potassium glycinate [9]), water evaporation and CO_2 compression in the overall energy balance.

Regardless of the methodological limitations, the lowest estimated heat requirement (80 °C, 500 mbar) is very high, corresponding to over 100 MJ/t of CO_2 captured. This is close to two orders of magnitude higher than the figures for industrial amine-based capture processes [9]. The main explanation for the high energy consumption is the insufficient CO_2 desorption performance of the current setup. Some improvements could be expected by optimising the operating conditions (absorbent concentration, temperature, pressure and liquid flow rate), but more significant results would probably require equipment modifications to the unit at the desorption stage. Potential developments are summarised in Section 5.4.

For a comparative analysis, the energy requirement in terms of the equivalent work is estimated with a procedure adapted from Wang et al. [153]. The equivalent work is applicable for the case of post-combustion capture from power generation and is estimated using the following equation [156]:

$$w = \frac{P_{\mathrm{t}} \dfrac{(T_{\mathrm{des}} + T_{\mathrm{app}}) - T_{\mathrm{cond}}}{(T_{\mathrm{des}} + T_{\mathrm{app}})} + P_{\mathrm{vp}} + P_{\mathrm{comp}}}{\dot{n}_{\mathrm{CO_2}} M_{\mathrm{CO_2}}} \tag{5.8}$$

where $\dot{n}_{\mathrm{CO_2}}$ is the molar flow rate of the CO_2 product, which is equal to the absorption rate at the membrane contactor during steady-state operation. A temperature difference of 10 K, assumed as the temperature approach in the rich/lean heat exchanger [153], is used to estimate the sensible heat required for heating the solvent to the desorption temperature (Equation 5.4). The first term in Equation 5.8 estimates the lost electricity generation following extraction of steam from the power plant [156]. The condensing temperature of the steam is assumed to be 10 K above the desorption temperature, constituting a temperature approach T_{app} of 10 K in the reboiler. T_{cond} represents the condensing temperature in the steam turbine, assumed as 313 K.

The electric power required by the vacuum pump and the CO_2 compressor (assuming single-stage compression to 2 bar [153]) is estimated using the following equation [157].

$$P = \frac{\dot{n}_{\mathrm{CO_2}} \mathrm{R} \mathrm{T} \kappa}{(1-\kappa)\eta} \left[\left(\frac{p_{\mathrm{in}}}{p_{\mathrm{out}}} \right)^{\frac{(\kappa-1)}{\kappa}} - 1 \right] \tag{5.9}$$

T is the gas temperature after water condensation (assumed as 293.15 K), κ is the heat capacity ratio of CO_2, p_{in} and p_{out} are the inlet and outlet pressures, respectively, of the vacuum pump and compressor and η is the efficiency, assumed as 75% for both the vacuum pump and compressor.

The results of this analysis are presented in Figure 5.5. The lowest equivalent work, found at 70 °C and 400 mbar, is 6.0 MJ/t CO_2, which is 94% lower than the estimated energy requirement based on experimental measurements (Figure 5.4). For reference, a comparable benchmark value for absorption-based CO_2 capture is 2.6 MJ/t CO_2 [9]. A significant part of the reduction is explained by the reduced amount of sensible heat owing to the assumed temperature difference of only 10 °C; the temperature differences measured at the experimental unit are up to 35 °C at the desorption temperature of 80 °C. Regardless, the equivalent work is dominated by the sensible heat, as the heat requirement is almost 700 W, compared with only approximately 1 W for work required by the vacuum pump and compressor. The latter can be explained by the small flow rate of the CO_2 product.

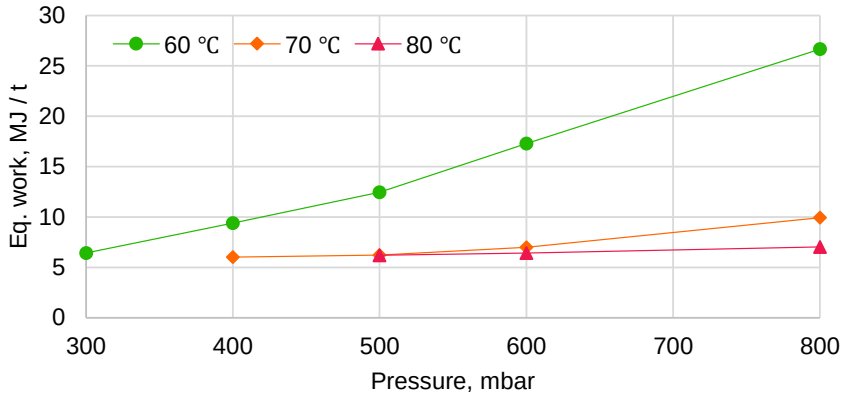

Figure 5.5 Equivalent work for CO_2 capture at desorption temperatures of 60–80 °C and pressures of 300–800 mbar.

Note that this calculation only provides a simplified estimate for the energy requirement, allowing a rough comparison to established CO_2 capture processes. Based on the present experiments and assumptions involved in Equation 5.8, the equivalent work seems to converge to a minimum value of approximately 6 MJ/t CO_2. However, according to the discussion in Section 5.3.6, the desorption performance would be expected to improve with further decrease in the vacuum pressure owing to increasing evaporation of water and therefore increasing CO_2 flux. As a result, the equivalent work would also be expected to decrease, and for these reasons, the extrapolation of Figure 5.5 to lower pressures should not be performed.

5.3.5 Varied operating parameters (non-vacuum desorption)

In Publication II, the mass transfer performance, measured by the capture efficiency and the overall mass transfer coefficient, was investigated during both non-vacuum and vacuum desorption. During vacuum desorption, desorption efficiency was also assessed, with a particular focus on the effects of the CO_2 loading of the absorbent on the steady-state absorption performance. The individual mass transfer coefficients and the

enhancement factor were estimated at different absorbent flow rates. Moreover, a stability test investigating the system stability during six days of operation was performed.

The effect of the absorbent flow rate during non-vacuum desorption at 80 °C is presented in Figure 5.6. A linear increase in both the capture efficiency and overall mass transfer coefficient are observed with increasing flow rate. A similar trend has been previously observed with potassium glycinate absorbent [137, 138], and the values of the overall mass transfer coefficient are similar to those previously reported for a similar system by Lu et al. [138]. The increase in the mass transfer coefficient can be explained by the decreasing thickness of the liquid boundary layer, resulting in decreased liquid-side mass transfer resistance [84]. As a result, the CO_2 flux increases, resulting in higher capture efficiency.

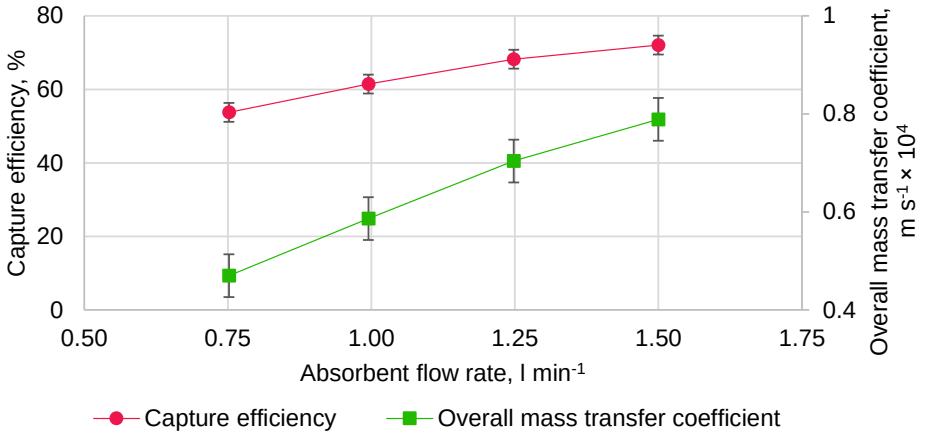

Figure 5.6 Effect of absorbent flow rate on the CO_2 capture efficiency and overall mass transfer coefficient during non-vacuum desorption. Absorbent: 1 M potassium glycinate, feed gas flow rate: 5.0 l/min (NTP, 10% CO_2 in nitrogen), absorption temperature: 20 °C, desorption temperature 80 °C. Lines added for visual guidance.

These results can also be used to provide insights on the chemically absorbing system under the present conditions, according to the discussion by Kumar et al. [102, 125]. At conditions characterised by low liquid flow rates and/or high CO_2 loading of the solution, free amino acid salt is depleted at the liquid interface, and the absorption rate is controlled by the diffusion of the reacting species to the interface. Under such conditions, which are also observed in the present experiments, the overall absorption rate (and the overall mass transfer coefficient) increases with increasing liquid flow rate. Here, the lean CO_2 loading varies from 0.49 at the flow rate of 0.75 l/min to 0.51 at 1.5 l/min, suggesting that some degree of amino acid salt depletion could be expected.

At a higher flow rate and/or lower CO_2 loadings, excess amino acid salt is present at the interface, and the absorption rate is controlled by the rate of chemical absorption [102, 125], as described by Equation 3.34 for the second-order reaction between amino acid

salts and CO_2. In this regime, the CO_2 flux and overall mass transfer coefficient are no longer significantly increased with increasing liquid flow rate.

Figure 5.7 presents the effect of the absorption temperature during non-vacuum desorption at 80 °C. A decrease in both the overall mass transfer coefficient and capture efficiency is found with increasing temperature. This result contradicts the usual findings with amine absorbents [119], and an opposing trend showing an increase in the mass transfer coefficient has also been observed with potassium glycinate [138]. On the contrary, Yan et al. found decreasing absorption rate with increasing temperature using potassium glycinate [137]. In general, the absorption rate is expected to increase with increasing temperature because the rates of diffusion and chemical reaction both increase.

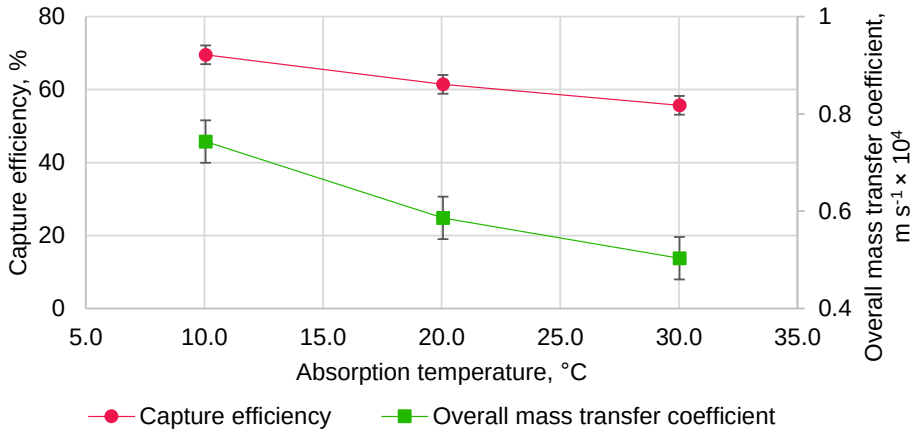

Figure 5.7 Effect of absorption temperature on the CO_2 capture efficiency and overall mass transfer coefficient during non-vacuum desorption. Absorbent flow rate: 1.0 l/min (NTP, 1 M potassium glycinate), feed gas flow rate: 5.0 l/min (NTP, 10% CO_2 in nitrogen), desorption temperature 80 °C. Lines added for visual guidance..

The present result can likely be explained by the equilibrium effects of the high solvent CO_2 loading under the experimental conditions. At absorption temperatures of 10–30 °C, the lean loading varies from 0.50 to 0.52, with no trend observed with respect to the temperature. As the temperature increases, the equilibrium loading corresponding to the CO_2 partial pressure in the membrane module decreases. As a result, the mass transfer driving force is decreased, which offsets the favourable effects of higher temperature and results in a lower absorption rate and mass transfer coefficient.

Figure 5.8 presents the effect of the feed gas CO_2 concentration on the capture efficiency and overall mass transfer coefficient. The corresponding CO_2 fluxes (not shown) increase with increasing CO_2 concentration owing to the increasing mass transfer driving force (partial pressure). However, the capture efficiency decreases because the increased absorption rate does not offset the higher amount of CO_2 present in the feed gas; thus, a

higher fraction of CO_2 entering the membrane module passes through the module unabsorbed.

The overall mass transfer coefficient also decreases with increasing CO_2 concentration. This decline can be explained by the changes in the rate of chemical absorption. Because the CO_2 loading in these experiments is high (approximately 0.50), the concentration of free amino acid salt at the reactive interface is limited, which reduces the overall absorption rate. Because increased CO_2 partial pressure also results in an increased reaction rate (Equation 3.34), it is reasonable that the depletion of amino acid salt concentration at the membrane interface is more significant at higher CO_2 concentrations. This then results in the decrease of the overall mass transfer coefficient owing to the decrease in the enhancement factor (Equation 3.5).

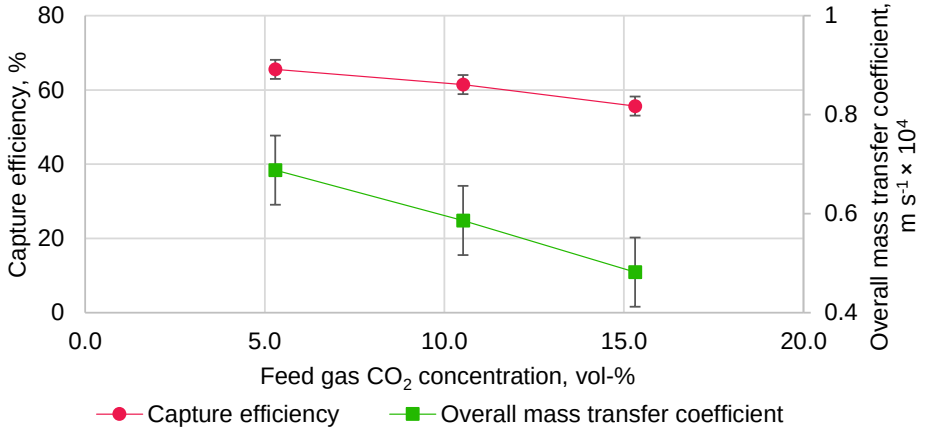

Figure 5.8 Effect of feed gas CO_2 concentration (balance nitrogen) on the CO_2 capture efficiency and overall mass transfer coefficient during non-vacuum desorption. Absorbent flow rate: 1.0 l/min (NTP, 1 M potassium glycinate), feed gas flow rate: 5.0 l/min (NTP), absorption temperature: 20 °C, desorption temperature: 80 °C. Lines added for visual guidance.

The effect of desorption temperature during non-vacuum desorption is presented in Figure 5.9. With the temperature increased from 60 to 80 °C, a drastic effect is found both in terms of the capture efficiency, increasing from only 10% to over 60%, and the overall mass transfer coefficient, showing a six-fold increase. Compared with the other investigated parameters (Figures Figure 5.6–Figure 5.8), desorption temperature clearly has the most significant effect on the resulting absorption performance. This points to desorption performance as the main limiting factor on the steady-state absorption rate.

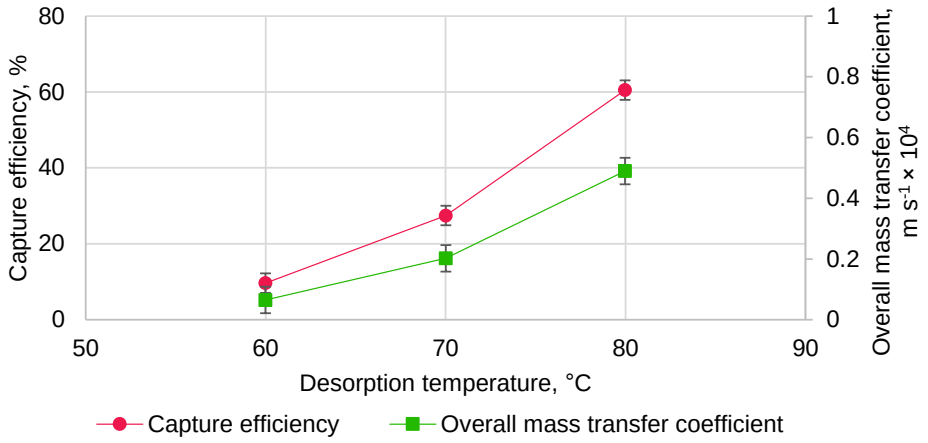

Figure 5.9 Effect of desorption temperature on CO_2 capture efficiency and overall mass transfer coefficient during non-vacuum desorption. Absorbent flow rate: 1.0 l/min (NTP, 1 M potassium glycinate), feed gas flow rate: 5.0 l/min (NTP, 10% CO_2 in nitrogen), absorption temperature: 20 °C. Lines added for visual guidance.

Temperature has a vital effect on CO_2 desorption because the equilibrium solubility (loading) of CO_2 decreases with increasing temperature [123]. The solubility is essentially dictated by the chemical equilibrium of the reactions involved in the chemical absorption, described by Equations 3.31–3.33 for amino acid salt absorbents. In addition to the equilibrium effect, beneficial kinetic factors are involved with increasing desorption temperature. The reverse reactions leading to CO_2 desorption are accelerated, and the mass transfer rate of released CO_2 from the solution to the gas phase is higher owing to increased CO_2 diffusivity and lower solution viscosity.

In particular, the high lean CO_2 loading, ranging from 0.55 mol/mol at 60 °C to 0.50 mol/mol at 80 °C, seems to be the limiting factor for the steady-state absorption rate. The CO_2 absorption rate of amino acid salt solutions has been shown to be strongly dependent on CO_2 loading [126]. This is also observed in the present investigation by measurement of the absorption rate during accumulation of CO_2 into a fresh absorbent solution (Publication II, Figure 8). The effect of CO_2 loading on the absorption rate can be explained by both physical and chemical effects: higher loading results in decreased driving force for physical mass transfer, and the rate of chemical absorption decreases owing to the low availability of free amino acid salt for reaction.

5.3.6 Vacuum desorption: effects of temperature and pressure

Desorption under vacuum provides a means to improve the driving force for desorption without increasing the temperature. By utilising vacuum, the CO_2 partial pressure in the gas phase can be reduced, leading to decreased equilibrium solubility in the liquid. Operating at a lower desorption temperature would be preferable because the heat

consumption could be minimised and low-grade heat sources could be utilised to provide heat for solvent regeneration. In addition, solvent losses via evaporation and degradation could be minimised.

To this end, the effects of temperature and pressure during vacuum desorption are further investigated. Figure 5.10 presents the CO_2 capture efficiency and the overall mass transfer coefficient at the membrane contactor with the desorption temperature varied at 60–80 °C and vacuum pressure at 300–800 mbar. The low limit of the vacuum pressure at each temperature is determined by the corresponding water vapour pressure. Clearly, the capture efficiency and overall mass transfer coefficient are both improved with increasing desorption temperature and decreasing pressure, with the effect of temperature more pronounced.

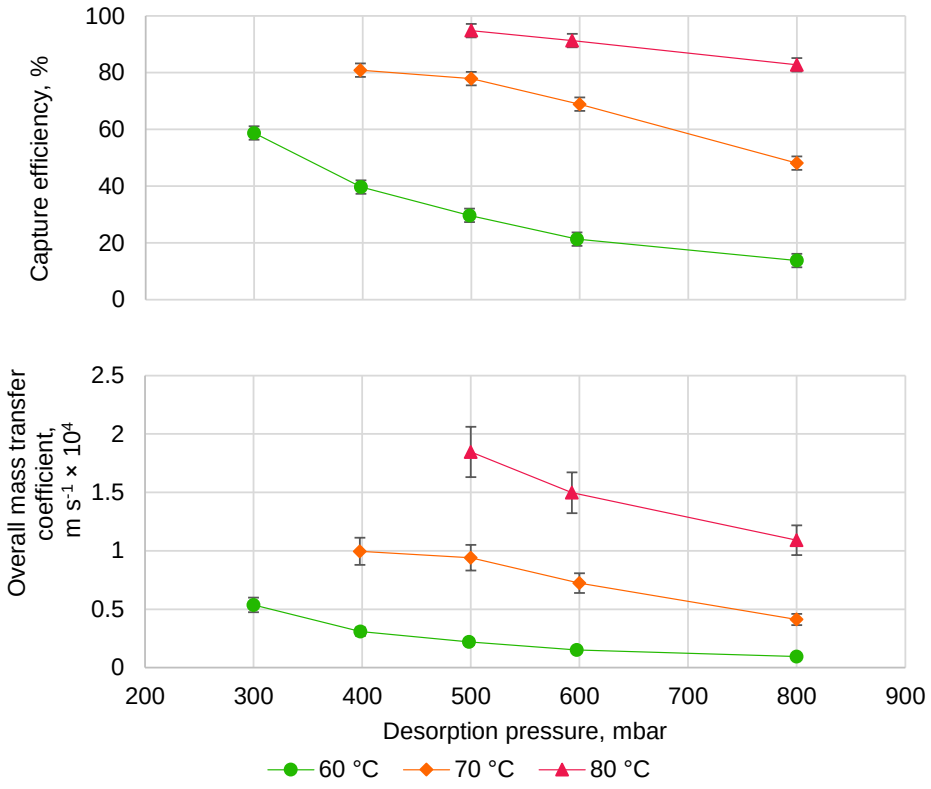

Figure 5.10 Effect of desorption temperature and pressure on CO_2 capture efficiency and (absorption) overall mass transfer coefficient during vacuum desorption. Absorbent flow rate: 1.0 l/min (NTP, 1 M potassium glycinate), feed gas flow rate: 5.0 l/min (NTP, 10% CO_2 in nitrogen), absorption temperature: 20 °C. Lines added for visual guidance.

The improved steady-state absorption at more favourable desorption conditions is explained by the lean absorbent loading, presented in Figure 5.11. The lower lean loading results in a higher absorption rate in the membrane contactor owing to increased rate of chemical reaction with increased availability of free amino acid salt in the bulk solution and at the reactive interface. However, even at 80 °C and 500 mbar, the desorption efficiency remains low, at 5.5% ± 1.42%. As a result, the cyclic capacity (the difference between rich and lean solvent loadings) is only 0.02 ± 0.006 mol, compared with above 0.2 mol in benchmark amine absorption processes [82]. Thus, the steady-state CO_2 capture rate remains strongly limited by ineffective desorption.

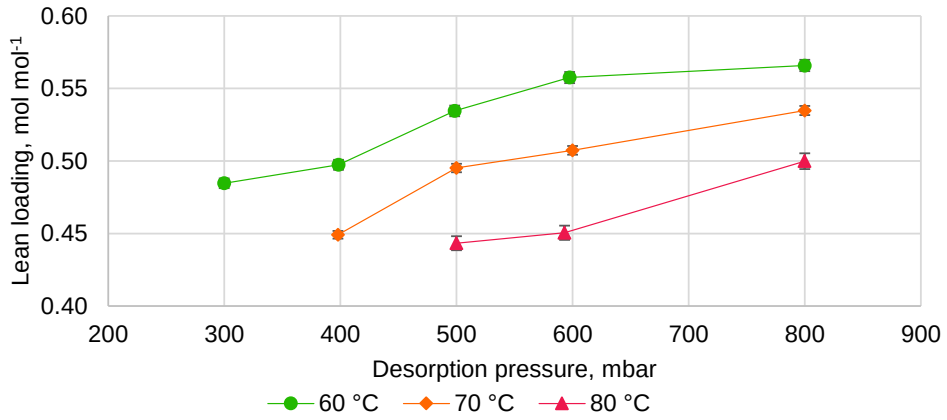

Figure 5.11 Effect of desorption temperature and pressure on CO_2 loading of the lean absorbent solution. Absorbent flow rate: 1.0 l/min (NTP, 1 M potassium glycinate), feed gas flow rate: 5.0 l/min (NTP, 10% CO_2 in nitrogen), absorption temperature: 20 °C. Error bars represent the standard deviation from three repeated titrimetric analyses of a single liquid sample. Lines added for visual guidance.

The CO_2 equilibrium under the desorption conditions is analysed for a deeper understanding of the limited performance of the desorption stage. Figure 5.12 presents the rich CO_2 loading and the estimated CO_2 partial pressure in the desorption vessel at desorption temperature of 80 °C and pressures of 500–800 mbar. The data are compared with corresponding equilibrium data from Portugal et al. [131], available at the temperature of 78 °C. The partial pressure is evaluated assuming 100% CO_2 concentration in the gas space of the vessel, with the corresponding water vapour pressure subtracted from the total pressure. This is an approximation that does not take into account the actual molar flows of water vapour and CO_2 taking place in the vessel. According to Figure 5.3, and similar data collected under the present experiments, the actual CO_2 concentration would be slightly lower, at 85%–95%.

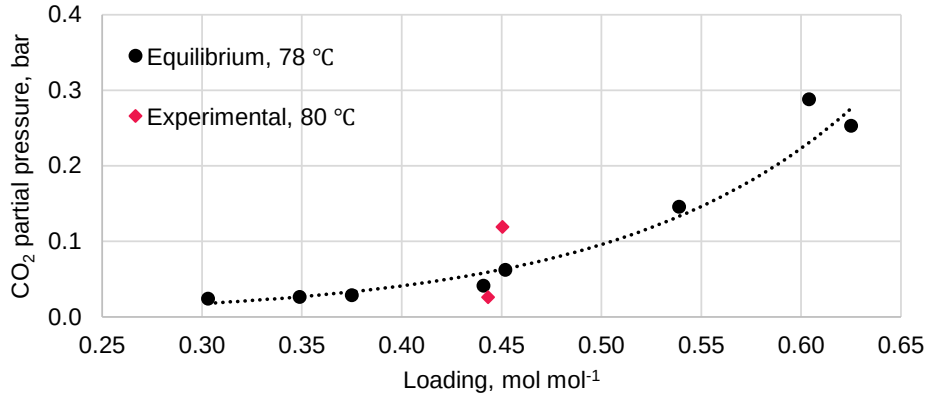

Figure 5.12 The rich CO_2 loading and estimated CO_2 partial pressure in the vacuum desorption experiments at 80 °C and 500–600 mbar, compared with the equilibrium data from Portugal et al. at 78 °C [131].

Considering the uncertainties involved, the estimated CO_2 partial pressure in the experiments at 500 and 600 mbar seems to approach the corresponding equilibrium partial pressure. This suggests that the desorption performance is limited by the equilibrium and not by the mass transfer rate. To overcome the equilibrium limitation, operating at boiling water conditions seems to be necessary to provide a flux of sweeping steam for the dilution of CO_2 and lowering the partial pressure. Nii et al. [152] previously found that vacuum desorption is strongly enhanced at pressures below the water vapour pressure. Operation at the boiling point is found to be energetically optimal, as further lowering the pressure results in excessive steam generation and consequent increase in the latent heat consumption.

At 80 °C, the water vapour pressure is approximately 470 mbar. Operating at this pressure would likely improve the performance of the present unit. To allow stable and continuous operation under boiling conditions, the unit should be equipped with a reflux condenser and preferably also a reboiler to maintain the temperature and provide a constant flux of steam throughout the bulk liquid. At the same time, heat should be provided to overcome the absorption heat of CO_2 in the solution, facilitating the continuous release of free CO_2 and subsequent mass transfer to the gas phase. With such modifications, the desorption stage would more closely replicate a conventional desorption column. Addition of packing material to the vessel could further improve the mass transfer performance in this configuration.

An alternative approach for improving the desorption performance is the use of alternative contactors. The use of membrane contactors for CO_2 desorption and stripping has been demonstrated (Section 4.1) and seems to constitute an effective method, provided that adequately stable membrane materials are used at the elevated temperatures. In addition, the membrane must resist wetting at high differential pressures over the membrane if low vacuum pressures are used to aid desorption. The use of composite

membranes appears to be particularly promising considering these requirements [146, 158]. A further emerging approach is the use of high-gravity equipment such as rotating packed beds [77].

5.3.7 Vacuum desorption: effects of liquid flow rate

Figure 5.13 presents the variations in the CO_2 flux and overall mass transfer coefficient at the membrane contactor, with desorption performed at 80 °C and 600 mbar. The measured CO_2 fluxes are in the order of 50% lower than the values from Yan et al. [137]. In that study, however, the feed CO_2 concentration was higher (14%) and unloaded potassium glycinate was used. Because the CO_2 flux does not significantly increase with increasing liquid flow rate, the absorption rate seems to be primarily controlled by reaction kinetics and not by the diffusion of reactants. This situation is different from similar experiments under non-vacuum desorption (Figure 5.6) that suggest absorption limited by diffusion. Improved desorption enabled by vacuum and the resulting decrease in the lean CO_2 loading seems to lead to a shift in the absorption regime.

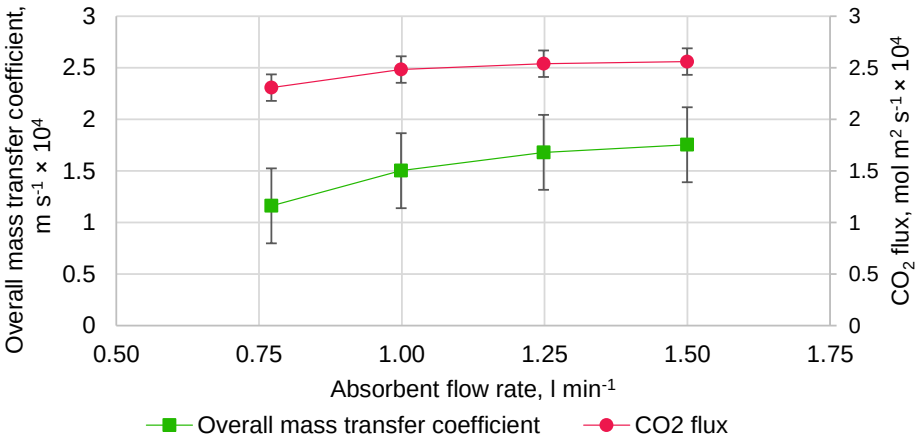

Figure 5.13 Effect of liquid flow rate on CO_2 flux and (absorption) overall mass transfer coefficient. Absorbent: 1M potassium glycinate, feed gas flow rate: 5.0 l/min (NTP, 10% CO_2 in nitrogen), absorption temperature: 20 °C, desorption temperature: 80 °C, desorption pressure: 600 mbar. Lines added for visual guidance.

Figure 5.14 presents the rich and lean CO_2 loading measured at different liquid flow rates during desorption at 80 °C and 600 mbar. The lean loading clearly decreases with increasing flow rate. However, as seen in Figure 5.13, the decrease in loading does not result in a significant increase in the CO_2 flux. This also suggests that absorption is controlled by intrinsic reaction kinetics under the present conditions, as the increased availability of free amino acid salt does not result in an increased absorption rate. Because the absorption rate remains constant, the amount of CO_2 absorbed into the solution

decreases with increasing flow rate, as the residence time decreases. The amount of CO_2 absorbed (or the cyclic capacity) decreases from 0.024 to 0.013 mol when the flow rate is increased from 0.70 to 1.5 l/min. Based on these findings, it appears that the absorbent is more effectively utilised at the lower range of the flow rates studied. Higher flow rates would only result in unnecessary increases in operating costs from circulation and heating of the solvent.

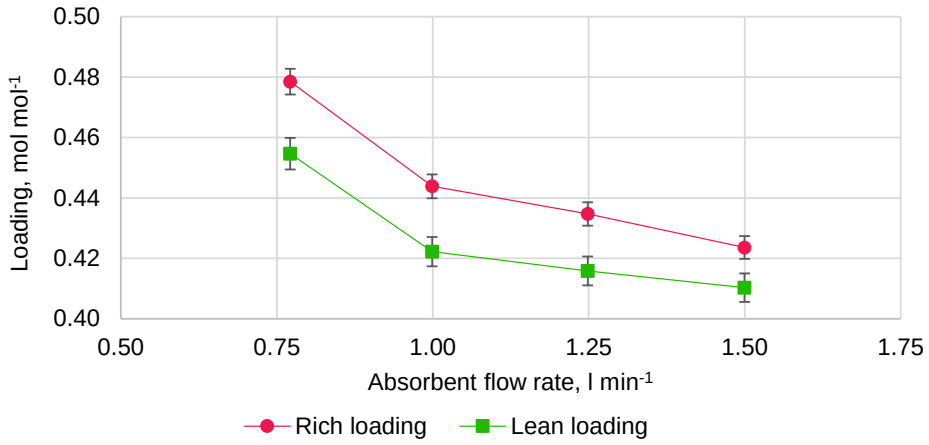

Figure 5.14 Variation in CO_2 loading of the rich and lean absorbent with absorbent flow rate varied. Absorbent: 1 M potassium glycinate, feed gas flow rate: 5.0 l/min (NTP, 10% CO_2 in nitrogen), absorption temperature: 20 °C, desorption temperature: 80 °C, desorption pressure: 600 mbar. Lines added for visual guidance.

The values of the overall mass transfer coefficient presented in Figure 5.13 are consistent in magnitude to those presented by Lu et al. [138] for potassium glycinate in a PP membrane contactor. Compared with the CO_2 flux, a more significant increase is observed in the mass transfer coefficient with increasing flow rate. This increase is likely explained by the change in the logarithmic mean driving force (Equation 3.8) with decreasing solvent CO_2 loading. Because absorption seems to be limited by the chemical reaction rate, the flux does not increase despite the increasing driving force for physical mass transfer. This results in a decrease in the overall mass transfer coefficient, according to Equation 3.5.

5.3.8 Individual mass transfer coefficients and resistances

The values of the individual mass transfer coefficients and enhancement factor are estimated at the same data points described in Figures Figure 5.13 and Figure 5.14. The results of this analysis are presented in Table 5.2. The liquid velocities correspond to volumetric flow rates of 0.75–1.5 l/min. The liquid mass transfer coefficient, calculated using Equation 3.19, increases with increasing liquid velocity, but the increase is not significant. At liquid velocities of 0.043–0.064 m/s, the enhancement factor also remains

constant. These findings appear to be consistent with the results in Figure 5.13, where the changes in CO_2 flux and overall mass transfer coefficient are not significant in this velocity (flow rate) range. The lower enhancement factor at 0.033 m/s (0.75 l/min) is explained by the higher lean loading (Figure 5.14). The lower enhancement factor, suggesting a lower rate of chemical absorption, is also reflected in the decreased CO_2 flux and overall mass transfer coefficient at the lowest flow rate (Figure 5.13).

Table 5.2 Variation in the values of the Reynolds number, enhancement factor, and individual mass transfer coefficients with liquid velocity. Absorbent 1 M potassium glycinate, feed gas flow rate 5.0 l min^{-1} (NTP, 10% CO_2 in nitrogen), absorption temperature 20 °C, desorption temperature 80 °C and pressure 600 mbar.

Liquid velocity, m s^{-1}	**Re, -**	**E, -**	**$k_L \times 10^5$, m s^{-1}**	**$K_g \times 10^3$, m s^{-1}**	**$k_m \times 10^4$, m s^{-1} (calculated from experiments)**	**$k_m \times 10^2$, m s^{-1} (theoretical)**
0.033	6.1	12.9	2.78	1.14	2.92 ± 0.40	1.55
0.043	7.9	24.9	2.87			
0.054	9.9	22.3	2.98			
0.064	11.9	26.2	3.07			

The calculated membrane mass transfer coefficient, assumed constant at all flow rates, is comparable in magnitude to the values reported for PP modules and amine absorbents [100, 99, 101]. A more detailed comparison is presented in Publication II. However, the calculated value is very low compared with the theoretical value of the membrane mass transfer coefficient, based on Equation 3.20. The theoretical value assumes completely non-wetted operation, and the significant deviation might reflect partial wetting of the membrane during the present conditions.

More likely, the large difference reflects the uncertainties involved in both methods of estimating the membrane mass transfer coefficient. In the mass transfer analysis performed here, the membrane mass transfer coefficient is a lumped parameter compensating the uncertainties involved in the rest of the analysis [87]. A particularly likely source of uncertainty is the estimation of the enhancement factor under the high CO_2-loading conditions in the present experiments, as the methodology used here has been previously utilized to assess chemical absorption at lower CO_2-loading conditions [94]. On the contrary, the theoretical value is highly sensitive to the parameter values (e.g. porosity and tortuosity) used in the calculation. Accurate estimation of these parameters is known to be difficult and prone to significant errors [82].

Calculation of the individual mass transfer coefficients also allows the calculation of the corresponding mass transfer resistances, according to Equation 3.5. Table 5.3 presents the mass transfer resistances at different liquid velocities and the contribution of the individual resistances to the total mass transfer resistance. At the lowest liquid velocity

(0.033 m/s), the liquid-side resistance is slightly higher than the membrane resistance, whereas at higher velocities, the membrane resistance contributes the major fraction of the overall resistance. These findings correlate with the corresponding values of the enhancement factor Table 5.2 as an increase in the enhancement factor results in decreased liquid-side resistance at the higher liquid velocities. The contributions of the individual resistances are comparable to those reported by Franco et al. [99] for a PP module and MEA absorbent, at 11% (gas), 61% (membrane) and 28% (liquid).

Table 5.3 Calculated mass transfer resistances and contributions to the overall mass transfer resistance at different liquid velocities. Absorbent 1 M potassium glycinate, feed gas flow rate 5.0 l min^{-1} (NTP, 10% CO_2 in nitrogen), absorption temperature 20 °C, desorption temperature 80 °C and pressure 600 mbar.

Liquid velocity, m s^{-1}	**Gas-side resistance, s m^{-1}**	**Membrane resistance, s m^{-1}**	**Liquid-side resistance, s m^{-1}**
0.033	880 (11%)	3422 (42%)	3839 (47%)
0.043	880 (14%)	3422 (55%)	1919 (31%)
0.054	880 (14%)	3422 (54%)	2062 (32%)
0.064	880 (15%)	3422 (57%)	1702 (28%)

5.3.9 Stability during long-term operation

The CO_2 concentration at the membrane outlet during the stability test run for a total of 33 h is presented in Publication IV, Figure 12. The desorption temperature was 70 °C and pressure was 500 mbar during this test. The CO_2 concentration remains stable during the test period, suggesting stable performance of the membrane contactor and the rest of the unit. Importantly, any decline in the membrane performance suggesting potential wetting is not observed. Thus, the compatibility of the membrane and absorbent solution seems to be sufficient in longer-term contact. During this test, CO_2 (product) concentration after desorption varied between 84.4 and 89.4 vol-%, whereas the concentration of oxygen was between 6.1 and 8.5 vol-%. This implies that the co-absorption of oxygen takes place, and the apparent CO_2/oxygen selectivity is in the range of 10.5–14.4. Under the present conditions, absorption of oxygen is not negligible.

5.4 Summary and outlook

Publications I and II provide a relatively comprehensive assessment of a membrane-contactor–based CO_2 absorption process. In terms of the mass transfer performance of the membrane contactor, the experimental unit performed well, showing CO_2 fluxes and

overall mass transfer coefficients comparable to the data presented in literature for similar processes. The highest value of the overall mass transfer coefficient was 1.8×10^{-4} m/s. In addition, the performance of the unit remained stable during long operating periods, suggesting no wetting issues and good compatibility of the amino acid salt absorbent with the PP membrane module. Analyses of the individual mass transfer resistances showed that the contributions of liquid-side (28%–47%) and membrane (42%–57%) resistances were significant and that the gas-side resistance was small in comparison.

The steady-state absorption rate of the present unit is limited by insufficient desorption of CO_2 from the loaded absorbent solution. Desorption was performed at temperatures of up to 80 °C and under vacuum at pressures as low as 300 mbar. Higher temperature and lower pressure favoured the release of CO_2, with the effect of temperature being more pronounced. However, even under optimal conditions (80 °C, 500 mbar), only 5.5% of CO_2 absorbed in the solution was desorbed. As a result, the CO_2 loading of the lean solution remained high, which in turn limited the absorption rate at the membrane contactor owing to the reduced rate of chemical absorption. Publication II discusses in detail the effects of lean loading on the absorption rate under varied operating conditions, providing valuable data for further development of the unit.

Ineffective desorption also resulted in high specific energy requirement per mole of CO_2 captured: over 100 MJ/t of CO_2 captured. However, note that this figure is subject to the uncertainties involved with the estimation method and was attained under non-optimised conditions in terms of liquid flow rate and absorbent concentration. Increasing the absorbent concentration to more industrially relevant concentrations (up to 6 M for potassium glycinate [9]) would improve the energetic performance because the CO_2 capacity of the solution would be maximised and the heat and electric energy involved with the circulation and heating of the solvent would remain constant. The performance could also be improved using other amino acid salt solutions. For instance, previous research has identified potassium salts of sarcosine [126], lysine [124] and alanine [130] as promising examples.

Liquid flow rate is an important optimising parameter affecting both the absorption and desorption stages of the process. Optimum selection of the flow rate requires the identification of the prevailing absorption regime in the membrane contactor. The absorption regime shifts from diffusion-controlled at low flow rates (and/or high lean CO_2 loading) to reaction-kinetics–controlled at high flow rates (low lean CO_2 loading). In the former regime, the absorption rate increases with increasing flow rate as the liquid-side mass transfer resistance is minimised. However, in the latter regime, further increase in the flow rate does not significantly improve the absorption rate and would only constitute a waste of energy. Optimal operating conditions would be found at the intersection of these two absorption regimes.

The observed limitations in the desorption performance seem to be more a result of the specific design of the present experimental unit than an inherent flaw in the process

concept. Two alternative approaches for improving the performance by equipment modifications can be identified.

First, desorption could be performed under conditions resembling those of conventional solvent regeneration columns. Thus, desorption would be performed under boiling water conditions to provide a flux of steam to minimise CO_2 partial pressure above the gas–liquid interface. To maximise the effectiveness, the temperature would be maximised depending on the intended heat source; vacuum pressure would then be set to a value equal to the corresponding water vapour pressure. Water would be separated from the CO_2 product by condensation and refluxed to the desorption vessel. A reboiler would be installed to maintain the temperature of the liquid at the boiling point and to provide heat for the continuous desorption of CO_2. Packing could be installed to maximise the gas–liquid interfacial area in this type of setup. An interesting approach would be the use of ultrasound to intensify mass transfer in the desorption vessel [159].

Second, the use of alternative contacting equipment at the solvent regeneration stage could be investigated. The use of membrane contactors for CO_2 stripping would provide the same advantages as those found at absorption: compact equipment with high specific interfacial area, flexible operation and modularity allowing simple scale-up. A requirement would be the use of membrane materials with sufficient stability and wetting resistance at elevated temperatures. The use of vacuum would help by reducing the temperature required for effective desorption. Beyond membrane contactors, the use of high-gravity contactors such as rotating packed beds could provide an interesting intensification option for both the absorption and desorption stages [77].

6 Conventional methanol synthesis

Methanol is an important fuel and industrial compound and has potential as a chemical energy carrier for the storage of renewable electricity. Current industrial synthesis of methanol is based on the catalytic conversion of synthesis gas generated from fossil sources. However, methanol can also be produced by the direct hydrogenation of CO_2. The conversion of CO_2, captured from point emission sources or even directly from the atmosphere, could provide a sustainable route for methanol synthesis.

Methanol synthesis is commonly performed by the conversion of syngas containing CO, CO_2 and hydrogen on Cu/ZnO catalysts at temperatures of 200–300 °C and pressures of 50–100 bar [53]. These types of low-temperature methanol synthesis processes were developed in the 1960s, replacing previous processes performed at 320–450 °C and 250–350 bar using ZnO/Cr_2O_3 catalysts. This transition was enabled by improved feedstock purification that allowed the use of the highly sulphur- and chlorine-sensitive Cu-based catalysts [160].

Syngas is generated by the reforming of fossil feedstocks, most often natural gas. The syngas composition varies depending on the type of feedstock. Syngas produced from methane is rich in hydrogen, whereas that produced from higher hydrocarbons and coal is hydrogen deficient. The syngas composition can be described by the stoichiometric number S (Equation 6.1), with values below 2.0 representing hydrogen deficiency and values above 2.0 representing excess hydrogen in relation to the stoichiometric composition [53]. Ideally, the stoichiometric number is slightly above 2.0 to maximise methanol selectivity while avoiding unnecessary hydrogen accumulation.

$$S = \frac{C_{\mathrm{H_2}} - C_{\mathrm{CO_2}}}{C_{\mathrm{CO}} + C_{\mathrm{CO_2}}} \tag{6.1}$$

The stoichiometric number can be adjusted by the addition of CO_2 to hydrogen-rich syngas or using the water–gas shift (WGS) reaction (Equation 6.4) to convert CO into hydrogen in hydrogen-deficient syngas. The presence of CO_2 in the syngas has been found to be essential for high methanol productivity and catalyst stability, and the syngas typically contains 2%–8% CO_2 [161]. However, experimental studies have found that maximum methanol productivity is achieved in the range of 1%–4% CO_2 of total carbon in the feed [162, 163, 164].

The methanol synthesis process can be described by three equilibrium reactions.

$$\mathrm{CO_2 + 3\ H_2 \rightleftharpoons CH_3OH + H_2O} \quad \Delta H = -49.8\ \mathrm{kJ/mol} \tag{6.2}$$

$$\mathrm{CO + 2\ H_2 \rightleftharpoons CH_3OH} \quad \Delta H = -91.0\ \mathrm{kJ/mol} \tag{6.3}$$

$$\mathrm{CO + H_2O \rightleftharpoons CO_2 + H_2} \quad \Delta H = -41.2\ \mathrm{kJ/mol} \tag{6.4}$$

The exothermic reactions in Equation (6.2) and Equation (6.3) represent the hydrogenation of CO_2 and CO to methanol, respectively. Equation (6.4) describes the WGS reaction, which is also activated by Cu-based methanol synthesis catalysts [161]. Depending on the gas composition, this reaction can proceed in the reverse direction (reverse water-gas shift, RWGS). Because both methanol synthesis reactions are exothermic and result in a reduction of molar volume, methanol synthesis is favoured at low temperatures and high pressures. However, higher temperatures lead to increased reaction rate, and the operating temperatures represent a compromise between the kinetics and thermodynamic equilibrium. The upper limit for the reaction temperature is set by catalyst stability, as temperatures above 300 °C lead to significant deactivation of the catalyst owing to sintering of the active Cu particles [165].

Methanol selectivity on Cu/ZnO catalysts typically exceeds 99%, with the main by-products being higher alcohols, DME and hydrocarbons [53]. Methanol selectivity has been shown to be even higher from feed gas containing only CO_2 and H_2, compared with mixed syngas feeds containing CO [166]. The equilibrium yield of methanol depends on the feed gas composition, with higher ratios of CO to CO_2 leading to higher equilibrium conversions [167]. For illustration, Figure 6.1 presents the effect of temperature on the total carbon conversion for stoichiometric CO/H_2 and CO_2/H_2 mixtures at total pressures of 40 and 100 bar. The equilibrium compositions are calculated using the predictive Soave-Redlich-Kwong (SRK) equation of state, which combines the SRK equation of state with the group-contribution–based UNIFAC activity coefficient model [168]. As a result, systems containing polar and supercritical components can be predicted with improved accuracy.

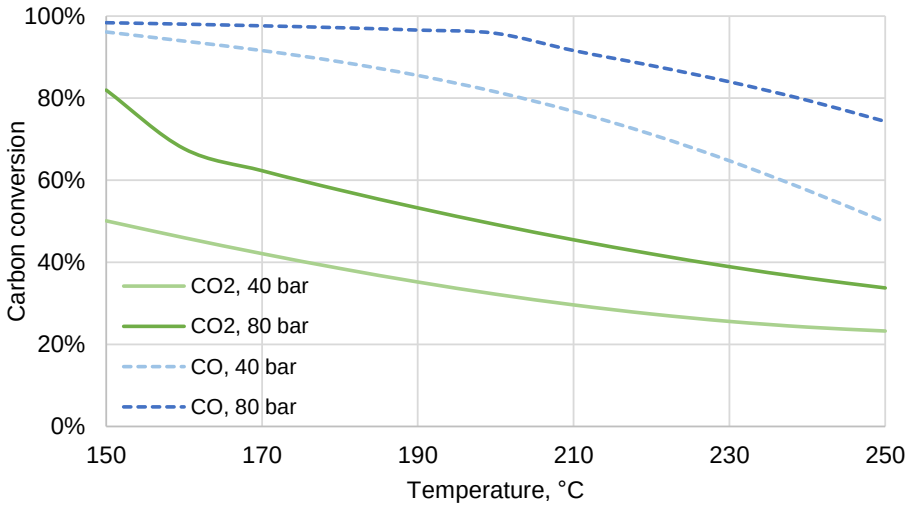

Figure 6.1 The equilibrium carbon conversion from stoichiometric CO_2:H_2 (1:3) and CO:H_2 (1:2) mixtures at total pressures of 40 and 80 bar and at temperatures of 150–250 °C. Equilibrium compositions are calculated with the predictive Soave-Redlich-Kwong equation of state.

The basic configuration of the methanol synthesis section is illustrated in Figure 6.2. Owing to the thermodynamic equilibrium, carbon conversion can only reach 50%–80% in a single pass through the reactor. Conversion levels may be further limited to avoid excessive reaction temperatures [169]. After the separation of methanol and water formed in the reaction by condensation, the unreacted gases are recycled and mixed with fresh syngas in the reactor feed. The ratio of the recycled to fresh gas depends on the technology applied, typically being in the range of 7–9 [170]. A fraction of the recycled gas is purged to limit the accumulation of inert components and to adjust the stoichiometric number of the mixed gas [53]. The crude methanol separated from the unreacted gases contains water and a small amount of other by-products [53]. Separation and purification of methanol is then performed in a sequence of distillation columns.

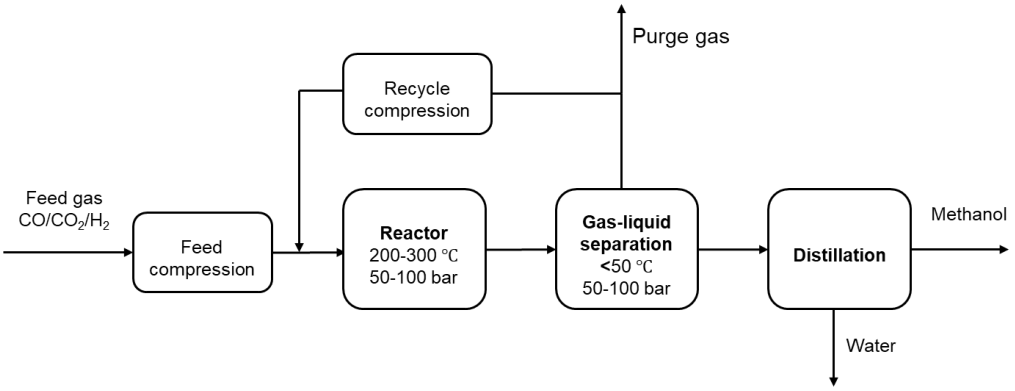

Figure 6.2 Simplified block diagram of a conventional methanol synthesis process excluding syngas generation.

Temperature control is a key factor in reactor design. The heat generated by the exothermic reactions has to be effectively removed both to increase the methanol yield and to protect the catalyst. The reactors generally comprise a heat-exchanger–type structure with the catalyst installed either in the tubes or on the shell side. The reactor systems can be based on adiabatic or quasi-isothermal reactors [53]. Adiabatic reactor systems may include quench reactors or multiple adiabatic reactors in series [171, 170].

6.1 Cu/ZnO catalysts

Industrial methanol synthesis catalysts are commonly based on the $Cu/ZnO/Al_2O_3$ composition, containing 50%–75% Cu, 10%–30% Zn and 5%–20% Al on a molar basis [53]. In recent years, interfaces of Cu and ZnO have been identified as the active surfaces on the catalyst [172], whereas Al_2O_3 seems to act as a structural and electronic promoter improving both the Cu dispersion and the intrinsic catalytic activity [173]. The catalysts are commonly prepared by co-precipitation from solutions of the corresponding metal salts using basic precipitants. The catalysts are activated by reduction, typically under diluted hydrogen at 150–250 °C. The activation results in the reduction of copper oxide into metallic Cu particles, which are surrounded by the ZnO/Al_2O_3 matrix [174]. The size of the spherical Cu particles in the activated catalyst is in the range of 5–15 nm.

Promotion of Cu-based catalysts by ZnO is well-known and has been explained by various structural, electronic and morphological effects. As a structural promoter, ZnO acts as a physical spacer between the Cu particles, increasing their dispersion and stability under reaction conditions [175]. The morphology of Cu particles has been found to dynamically change depending on the redox potential of the gas phase [176, 177, 178]. Changes in the interfacial energy between Cu and ZnO result in changes in Cu surface area and migration of Zn onto Cu particles [179]. These types of structural changes have been correlated with increasing methanol synthesis activity of the catalyst [180]. ZnO has also been found to increase the reducibility of Cu compared with other support materials,

and this difference has been correlated with increased catalytic activity [181]. These findings support the conclusion that ZnO affects the intrinsic activity of Cu/ZnO catalysts and does not only act as a stabiliser of Cu particles.

A more detailed description of the active sites might be provided by the presence of imperfections and faults in the catalyst microstructure. The presence of microstructural strain in the Cu and ZnO phases has been correlated with increasing methanol synthesis activity [182]. Such defects have been suggested to form during the preparation of the catalyst [183], and they have been observed to remain stable under methanol synthesis conditions [184]. Combined experimental and modelling studies have shown that defects in Cu nanoparticles result in step surfaces, which constitute the active sites for methanol synthesis [172]. Even higher activity has been modelled on Cu step sites on which Cu was partially substituted by Zn in a partially oxidised form. The partially oxidized ZnO species have been suggested to act as adsorption sites for the intermediate species of methanol synthesis that are bound to the surface through oxygen atoms.

In further studies, insights into the role of ZnO have been provided based on the different behaviours of Cu/ZnO and Cu/MgO catalysts when the feed gas composition was changed from CO/H_2 to mixed $CO/CO_2/H_2$ and to CO_2/H_2 [185]. Whereas Cu/ZnO was found active for CO_2 hydrogenation, Cu/MgO was active for CO hydrogenation. The activity of Cu/ZnO increased with increasing fraction of CO_2 in the feed, whereas the activity of Cu/MgO deteriorated following the addition of CO_2. The Cu/ZnO interfaces were thus identified as the active site for CO_2 hydrogenation, whereas Cu particles on the inert MgO support were identified as active sites for CO hydrogenation.

6.2 Reaction mechanism and kinetic models

Studies on the reaction mechanism are closely linked to the development of increasingly detailed kinetic reaction models aiming to model methanol synthesis under varied reaction conditions and reactor configurations. In addition to simplified empirical models, microkinetic models [186] attempting to deduce the elementary reaction steps and describe the surface chemistry of the relevant reactants, intermediates and products have been developed for this purpose.

Methanol synthesis on Cu-based catalysts has usually been suggested to proceed through a formate (HCOO) intermediate. Evidence for this reaction pathway is provided by the observation of formate as the most abundant species on the catalyst surface under methanol synthesis conditions [187, 188]. Often but not always, further hydrogenation of the formate intermediate is considered the rate-limiting step in methanol synthesis [189, 190]. The formate route has been considered in a number of kinetic models describing the elementary steps and overall kinetics in methanol synthesis [191, 192, 193, 194, 195]. An often-cited example of these types of models is described below. Some models also consider dynamic changes in the catalyst under reaction conditions [196]. Note that principally simpler, power-law type kinetic models have also been used to accurately describe methanol synthesis on Cu/ZnO-based catalysts [197, 198].

The model by Vanden Bussche and Froment [194] considers Cu as the active catalytic component and CO_2 as the main carbon source in methanol synthesis. The elementary steps of this model are presented in Table 6.1. The WGS is also included in this model. A reaction mechanism with formate as key intermediate is suggested for methanol synthesis. H_2 and CO_2 dissociatively adsorb on the Cu surface. CO_2 also adsorbs via oxidation by adsorbed oxygen, forming adsorbed carbonate. Carbonate is quickly hydrogenated into bicarbonate (HCO_3) species and successively into formate, formaldehyde, methoxy and methanol. Hydrogenation of formate is considered the rate-determining step.

Table 6.1 Proposed elementary steps for methanol synthesis and the reverse water-gas shift reaction on Cu/ZnO catalysts, based on the kinetic model from Vanden Bussche & Froment [194]. The rate-determining steps are bolded. * Represents adsorption site on the catalyst

	Methanol synthesis		**(Reverse) water-gas shift**
1	$H_2(g) + 2^* \rightleftharpoons 2\ H^*$	1	$H_2(g) + 2^* \rightleftharpoons 2\ H^*$
2	$CO_2(g) + O^* + * \rightleftharpoons CO_3^{**}$	**2**	$\mathbf{CO_2(g) + * \rightleftharpoons O^* + CO(g)}$
3	$CO_3^{**} + H^* \rightleftharpoons HCO_3^{**} + *$	3	$O^* + H^* \rightleftharpoons OH^* + *$
4	$HCO_3^{**} + * \rightleftharpoons HCOO^{**} + O^*$	4	$OH^* + H^* \rightleftharpoons H_2O^* + *$
5	$\mathbf{HCOO^{**} + H^* \rightleftharpoons H_2CO^* + O^* + *}$	5	$H_2O^* \rightleftharpoons H_2O(g) + *$
6	$H_2CO^* + H^* \rightleftharpoons H_3CO^* + *$	6	
7	$H_3CO^* + H^* \rightleftharpoons CH_3OH(g) + 2^*$	7	

Langmuir-Hinshelwood–type kinetic equations describing the rates of methanol synthesis and RWGS were derived by assuming pseudo-steady-state concentration of surface intermediates [194]. The concentrations of adsorbed bicarbonate, formaldehyde, methoxy, methanol and hydroxyl species were not considered, as they have been shown to be negligible under the reaction conditions. The following kinetic equations, giving the rates of methanol synthesis and RWGS (unit mol/kg_{cat} s), were derived.

$$r_{\mathrm{MeOH}} = \frac{k'_{5a}K'_2K_3K_4K_{\mathrm{H_2}}p_{\mathrm{CO_2}}p_{\mathrm{H_2}}\left(1-\left(\frac{1}{K^*}\right)\left(\frac{p_{\mathrm{H_2O}}p_{\mathrm{CH_3OH}}}{p_{\mathrm{H_2}}^3 p_{\mathrm{CO_2}}}\right)\right)}{\left(1+\left(\frac{K_{\mathrm{H_2O}}}{K_8K_9K_{\mathrm{H_2}}}\right)\left(\frac{p_{\mathrm{H_2O}}}{p_{\mathrm{H_2}}}\right)+\sqrt{K_{\mathrm{H_2}}p_{\mathrm{H_2}}}+K_{\mathrm{H_2O}}p_{\mathrm{H_2O}}\right)^3} \qquad (6.5)$$

$$r_{\mathrm{RWGS}} = \frac{k_1' p_{\mathrm{CO_2}} \left(1 - K_3^* \left(\frac{p_{\mathrm{H_2O}} p_{\mathrm{CO}}}{p_{\mathrm{CO_2}} p_{\mathrm{H_2}}}\right)\right)}{\left(1 + \left(\frac{K_{\mathrm{H_2O}}}{K_8 K_9 K_{\mathrm{H_2}}}\right)\left(\frac{p_{\mathrm{H_2O}}}{p_{\mathrm{H_2}}}\right) + \sqrt{K_{\mathrm{H_2}} p_{\mathrm{H_2}}} + K_{\mathrm{H_2O}} p_{\mathrm{H_2O}}\right)} \tag{6.6}$$

The values of the kinetic and equilibrium model parameters are given in the reference [194]. Model parameters were fitted to experimental data obtained on an industrial Cu/ZnO catalyst under industrial reaction conditions, with pressure ranging from 15 to 51 bar, temperature from 180 to 280 °C and the CO:CO_2 ratio from 0 to 4.1. The influence of temperature, pressure and feed gas composition was accurately predicted when extrapolated outside the original experimental conditions.

More recently, Grabow and Mavrikakis [199] developed a detailed microkinetic model for methanol synthesis and WGS. Cu was considered as the active site, and the effects of ZnO were not included in the model. However, the authors concluded that the Cu surfaces may not provide an accurate representation of the active sites. Instead, partially oxidised step or defect sites are suggested as the active sites, similarly to other recent studies (Section 6.1). A notable result was that both CO_2 and CO hydrogenation significantly contribute to methanol formation, with 1/3 of methanol formed via CO hydrogenation under typical industrial reaction conditions. WGS was found to have a favourable effect on CO_2 hydrogenation, limiting the inhibiting effect of water (Chapter 7) by removal of water-derived hydroxyl from the catalyst surface.

7 CO_2 hydrogenation to methanol

Conventional methanol synthesis processes are thermodynamically limited to low per-pass conversion, as operation at unfavourably high temperatures is required to achieve sufficient reaction rates. The thermodynamic equilibrium is even more unfavourable for pure CO_2 hydrogenation – that is, when mixtures of CO_2 and H_2 are converted instead of mixed syngas containing CO. However, the presence of CO_2 in the feed has been found necessary in conventional methanol synthesis. Under typical reaction conditions, CO_2 hydrogenation to methanol is significantly faster than CO hydrogenation [200, 164]. Indeed, methanol synthesis on Cu/ZnO has been shown to primarily occur via CO_2 hydrogenation, even at very low CO_2 concentrations in the feed [201].

In terms of process technology and design, methanol synthesis from CO_2 does not significantly differ from conventional methanol synthesis processes [166, 171, 202]. However, alternative process and reactor options have been pursued to overcome the thermodynamic limitations of CO_2 hydrogenation. By significantly increasing the reaction pressure (i.e. over 400 bar), nearly 100% per-pass CO_2 conversion can be achieved with a significantly high methanol selectivity and very high reaction rate [203, 204]. Condensation of the reaction products can also be utilised to achieve higher conversions [167]. This approach has been experimentally demonstrated both by increasing the pressure [205] and by developing novel reactors with internal cooling [206, 207].

Water produced as a by-product of CO_2 hydrogenation is known to inhibit methanol synthesis on Cu/ZnO catalysts [208, 200, 163]. The suggested mechanism of inhibition is the blocking of catalytic sites by absorbed oxygen or hydroxyl species [164]. At low CO_2 concentrations, the WGS reaction removes these water-derived species from the catalyst surface, simultaneously creating more CO_2 to be converted into methanol. The forward WGS reaction is thus favourable for methanol synthesis. However, the reaction reverses at higher CO_2 concentrations, consuming CO_2 and hydrogen to form CO and water, which results in decreased methanol selectivity and hindered reaction rates owing the effects of water on the catalyst.

The technical feasibility of CO_2 conversion to methanol has been demonstrated in several pilot- or demonstration-scale operations. Utilising a conventional methanol synthesis catalyst and technology, a pilot plant developed by Lurgi demonstrated good productivity combined with promising catalyst stability [166, 202]. The process utilised a commercial $Cu/ZnO/Al_2O_3$ catalyst and a two-stage reactor design with an adiabatic reactor followed by an isothermal water-cooled reactor. At 80 bar and 240–280 °C, per-pass CO_2 conversions of 35%–45% with methanol selectivity above 99.9% over the reactor loop (63.5% including water) were reported. Another pilot plant developed by Mitsui Chemicals with a capacity of 100 t of methanol per year began operation in 2009 [209, 202]. The process utilised a Cu/ZnO-based multicomponent catalyst developed at RITE in Japan [210, 211].

The CAMERE process developed in South Korea is based on a separate RWGS reactor and methanol synthesis reactor [202, 212]. In the RWGS step, part of the CO_2 is converted to CO and H_2O and the resulting gas mixture is fed to the methanol synthesis reactor following removal of water. This configuration reportedly results in twice the yield of methanol compared with direct CO_2 hydrogenation. The concept was demonstrated by a pilot plant producing 100 kg of methanol per day.

So far, the only commercial plant converting CO_2 to methanol is operated by Carbon Recycling International in Iceland [213, 47]. The plant became operational in 2011 with an initial capacity of 10 t of methanol per day. The process is based on the availability of CO_2 from a geothermal power station and the production of hydrogen by electrolysis using cheap geothermally produced electricity. The methanol product is used as fuel by blending with gasoline.

7.1 Catalyst developments in CO_2 hydrogenation

The fundamental role of a catalyst in improving the rate of a chemical reaction is to lower the activation energy for the target reaction by providing a low-energy reaction pathway that is not accessible for the uncatalysed reaction [214]. Moreover, the selectivity for the intended product is improved as the activation energy is lowered compared with that of potential side-reactions. Although conventional Cu/ZnO-based catalysts are effective for CO_2 conversion to methanol, modifications and alternative catalysts compositions have been developed to improve the activity, selectivity and stability under CO_2/H_2 feed conditions [171, 47, 27, 215].

Developments in heterogeneous catalysts for CO_2 hydrogenation to methanol range from the modification of the Cu/ZnO structure with additional promoting or stabilising components to the development of catalysts based on entirely different active components. With Cu/ZnO-based catalysts, the goal of further catalyst development might involve the further reduction of the activation energies of rate-determining elementary steps along the established reaction pathways (Section 6.2) by the addition of promoting materials. Another aim might involve the stabilisation of the active surface features under CO_2 hydrogenation conditions characterised by high concentrations of water. Catalysts based on components other than Cu and ZnO in turn aim to provide alternative reaction routes on novel reactive surfaces that might be intrinsically more stable and selective for methanol under CO_2 hydrogenation conditions. Table 7.1 presents a comparison of a number of catalysts with particularly promising performance in CO_2 hydrogenation to methanol.

Table 7.1 Performance of selected catalysts in CO_2 hydrogenation to methanol.

Catalyst	**Temperature °C**	**Pressure bar**	**CO_2 Conversion %**	**Methanol selectivity %**	**Methanol productivity[1] g/kg$_{cat}$ h**	**Ref.**
$Cu/ZnO/Al_2O_3$	230	30	3.1	-	1200	[216]
$Cu/ZnO/ZrO_2$	240	50	9.7	62	1200	[217]
$Cu/ZnO/ZrO_2/Ga_2O_3$	250	70	22	72	704	[218]
$Cu/ZnO/Al_2O_3$/Y	250	50	26.9	47.1	520	[219]
$Cu/ZnO/Al_2O_3$	250	50	19.7	39.7	340	[219]
Pd/Ga/CNT[2]	250	50	16.5	52.5	512	[220]
$NiGa/SiO_2$	200	1	10.1	42.9	90	[221]
ZnO/ZrO_2	300	20	3.4	86	248	[222]
In_2O_3/ZrO_2	300	50	-	100	300	[223]
Pd/In_2O_3	300	50	20	70	890	[224]
Pd/In_2O_3	280	50	9.2	78	960	[225]

1) g of methanol formed per kg of catalyst per hour 2) carbon nanotubes

Principally, a good catalyst should possess high methanol selectivity as well as high activity. Here, activity is measured by methanol productivity (also referred to as space-time yield or mass-time yield). However, direct comparison of the catalytic activity of different catalysts is complicated by the differences in reaction conditions such as temperature, pressure and space velocity. Differences in methanol selectivity and productivity can also be caused when the experiments are conducted at different CO_2 conversion levels. At low conversion levels – that is, under differential conditions [226] – the intrinsic reaction rate on the catalyst can be measured without interference from equilibrium limitations or the influence of reaction products, arguably providing a best estimate for the intrinsic activity of the catalyst in the target reaction. However, in this case, the activity should not be directly extrapolated to industrial, high-conversion-level conditions.

$Cu/ZnO/Al_2O_3$ remains the benchmark catalyst for methanol synthesis. The performance of this catalyst system has been maximised by careful optimisation of the catalyst composition and preparation procedure based on decades of research and industrial experience [174, 216]. At methanol productivity values above 1000 g/kg h, the CO_2

hydrogenation rates on high-activity $Cu/ZnO/Al_2O_3$ catalysts are comparable to those of industrial methanol synthesis from mixed syngas [202].

Despite the high performance of the established catalyst composition, multicomponent catalysts based on further promotion of the Cu/ZnO structure by the addition of various promoting materials show promising results, especially in terms of potentially improved stability in the presence of water. For example, the performance of multicomponent catalysts with added zirconia (ZrO_2) and gallia was demonstrated in bench-scale methanol synthesis from CO_2 [210, 211], and a similar catalyst was utilised in the two-stage CAMERE process based on RWGS followed by conversion to methanol [212].

ZrO_2 has been found to be a particularly effective component for Cu-based methanol synthesis catalysts [227]. Instead of purely structural promotion, the addition of ZrO_2 might affect the reaction mechanism in methanol synthesis [228]. An added advantage is the hydrophobicity of ZrO_2, making $Cu/ZnO/ZrO_2$-based catalysts more tolerant to water compared with Cu/ZnO [229, 230]. As another development, increasing the fraction of Zn in industrial-like $Cu/ZnO/Al_2O_3$ catalysts was found to inhibit the RWGS reaction and the methanol synthesis rate was increased, resulting in improved methanol selectivity [231]. Further promotion of this catalyst by gold resulted in a significantly higher activity than a commercial methanol synthesis catalyst.

Catalysts based on active components other than Cu (or copper oxide interfaces) are interesting, particularly owing to the possibility of achieving significantly higher methanol selectivity compared with Cu/ZnO-based catalysts. The key to improved selectivity appears to be the suppression of RWGS, which is always present on Cu-based catalysts. Catalysts based on palladium (Pd) [232] and Pd-containing bimetallic phases [220], Ni–Ga alloys [221], ZnO supported on ZrO_2 [222] and indium oxide [223, 225] have been demonstrated as industrially relevant supported catalyst compositions showing high activity and selectivity in CO_2 hydrogenation to methanol.

7.2 Feasibility and techno-economic analyses

This section provides a review of the techno-economic studies on CO_2 hydrogenation to methanol. Interest in methanol synthesis from CO_2 arises from the recycling of captured CO_2 into a useful fuel and chemical product and the storage of renewable electricity in a storable, transportable and versatile liquid energy carrier. These goals can be achieved by utilising hydrogen, generated by the electrolysis of water using renewable electricity, in the CO_2-based methanol synthesis process. This process scheme is often referred to as power-to-liquid or power-to-methanol in the relevant literature.

The principle aim of techno-economic studies is to assess the present or future feasibility of the process under investigation. In a power-to-methanol process, feasibility is commonly measured by economic metrics and by the overall energy efficiency of the cycle beginning from renewable electricity and ending in the final methanol product. Efficiency is commonly measured as the ratio of the chemical energy (lower heating

value) of the methanol product to the heat and electrical energy consumed in the process. Environmental impacts, primarily direct and indirect CO_2 emissions and the amount of CO_2 utilised in the process, are also considered in some studies.

The assessment generally begins with the review and selection of process and technology options, setting of the boundary conditions, such as the source and composition of feed streams, and the process capacity. Often, comparative scenarios based on alternative processes or feeds are generated. The mass and energy balances are then determined via flowsheet simulation, other mathematical models, assumptions and/or literature data. Finally, the process economics are investigated by estimating the capital and operating costs and revenues over the lifetime of the project.

Multiple techno-economic studies on the power-to-methanol process have been published. Although the studies are focused on the same general process, significant differences in the scale, focus and methods of analysis can be found. Many of the studies pay close attention to the design and modelling of the methanol synthesis process, whereas others are primarily focused on the electrolysis technology. Some studies consider the grid-scale implications of large-scale CO_2-based methanol production as part of a renewable-based energy system. Accordingly, the detail and rigor of the modelling and discussion of the various components of the overall process are varied. Table 7.2 summarises the key findings from the reviewed studies.

Table 7.2 Summary of techno-economic and feasibility studies on CO_2 hydrogenation to methanol.

Ref.	CO_2 source	Hydrogen source	Key results
Ibrahim, et al., 2008 [32]	Coal-fired power plant	Alkaline electrolysis (atmospheric or pressurized at 30 bar)	Overall conversion efficiency 51–58% (58–68% if waste heat from power plant available) Positive NPV at methanol price of 114 €/t with oxygen sales and pressurized electrolyser
Hadjipaschalis, et al., 2009 [33]	Natural gas-fired power plant, oxyfuel combustion	Alkaline electrolysis, 617 MW	Energy conversion efficiency of methanol synthesis 46% Methanol production cost 479 €/t or 495 €/t depending on the cost of natural gas
Van-Dal & Bouallou, 2013 [233]	Coal-fired power plant	Pressurized (30 bar) electrolysis, 645 MW	Power plant efficiency decreased by 3% with heat integration of methanol synthesis and CO_2 capture CO_2 abatement 1.2 t CO_2 per t methanol produced if synthesis powered by fossil and electrolysis by renewable electricity

Table 7.2 (cont.)

Anicic, et al., 2014 [234]	Flue gas	Electrolysis (260/309 MW)	Annual profit 15 M€ and 12 M€ for direct and two-step methanol synthesis, respectively
Tremel, et al., 2015 [51]	Supplied by tanks	Supplied at 20 bar from PEM electrolysis	Methanol is the most feasible product, with a production cost of 980€/t (alternatives: Fischer-Tropsch, DME, SNG, ammonia)
Pérez-Fortes, et al., 2016 [235]	Coal-fired power plant	Supplied by pipeline	Large-scale CO_2-based methanol synthesis not financially feasible under present conditions Capital costs 451 €/t MeOH/a, variable costs 641 €/t MeOH, fixed costs 25 €/t MeOH Cost of hydrogen is the most important factor in sensitivity analysis
Atsonios, et al., 2016 [236]	Coal-fired power plant	Pressurized (30 bar) alkaline electrolysis	Methanol production costs 850–900 €/t Methanol production using cheap electricity from a thermal power plant at high operating hours is most competitive route Maximization of plant operating hours is vital
Kourkoumpas, et al., 2016 [237]	Lignite power plant	Alkaline electrolysis, 120 MW	MeOH production cost 421 €/t for power plant owner, 580 €/t for private owner (higher cost of electricity, lower electrolyser operating hours) Methanol production cost 342 €/t
Rivera-Tinoco, et al., 2016 [238]	Not specified	PEM or SOEC electrolysis, total plant capacity 24.2 MW	Methanol production costs 890 €/t with PEM and 5460 €/t with SOE Capital costs dominate with SOE especially due to low lifetime and need of replacements Operating costs (electricity) dominate with PEM
Bellotti, et al., 2017 [239]	Coal-fired power plant	PEM electrolysis (30 bar), capacity 5, 13 or 63 MW	PEM electrolysis accounts for over 75% of total capital costs Selling of oxygen is critical for economic feasibility Economies of scale are significant

Table 7.2 (cont.)

Varone & Ferrari, 2015 [240]	Oxy-fuel power plant	SOEC electrolysis (50 MW)	The production cost is dependent on the amount of surplus renewable electricity available in 2050 Methanol production cost 81 or 88 €/MWh (559 or 520 €/t)

Figure 7.1 summarises the methanol production costs versus methanol production capacity found in the reviewed studies. Figure 7.2 presents the production costs versus electrolyser capacity and identifies the type of electrolyser considered. For studies with comparative scenarios, the methanol production cost found in the optimal scenario is presented. For reference, the current European market price for methanol is below 300 € [241]. As such, CO_2-based methanol production does not presently appear competitive with fossil-based methanol production.

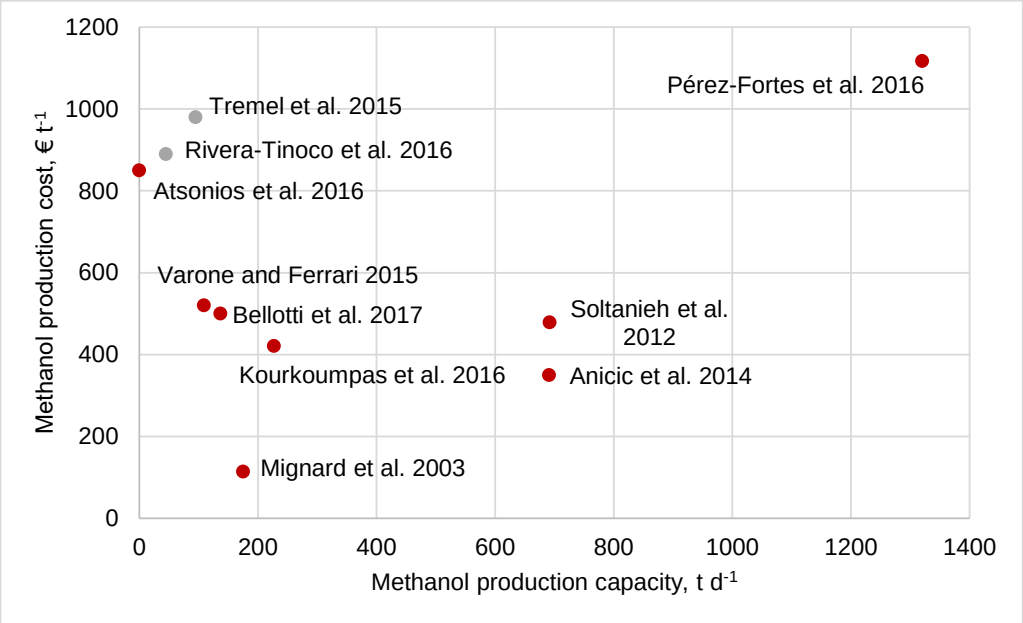

Figure 7.1 Methanol production capacity and cost in the reviewed studies. Colour coding represents the CO_2 source. Red: captured from flue gas, grey: not specified. Non-specified capacities are represented as 0 t/d.

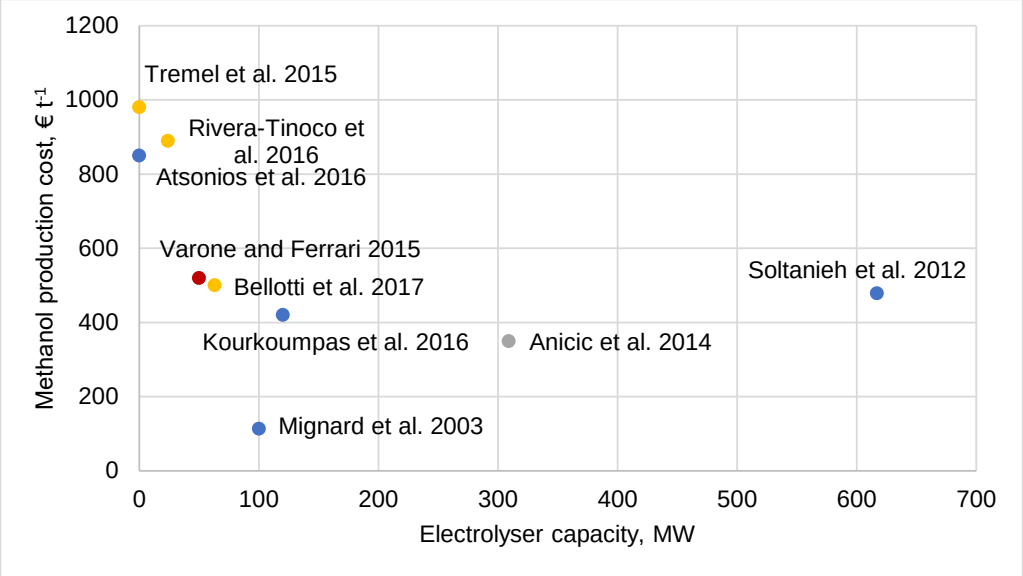

Figure 7.2 Electrolyser capacity and methanol production cost in the reviewed studies. Colour coding represents the type of electrolyser. Blue: alkaline, yellow: PEM, red: SOE, grey: not specified. Non-specified capacities are represented as 0 MW.

The methanol production cost is expected to decrease at increasing plant capacities owing to economies of scale in both electrolysis and methanol synthesis. The outline of such a trend can be observed, if not very clearly, in Figure 7.1 and Figure 7.2. Bellotti et al. [239] directly compared different plant capacities and found that the overall production cost decreases with increasing capacity. Relatively large capacity plants have been considered by Anicic et al. [234], Soltanieh et al. [242] and Pérez-Fortes et al. [235]. Anicic et al. [234] found a low methanol production cost of 350 €/t, showing potential present-day competitiveness with fossil-based methanol production. However, the capital and operating costs were not estimated very rigorously compared with Pérez-Fortes et al. [235], who reported significantly higher production costs of above 1000 €/t. In general, the methods and detail of cost estimation significantly vary in the reviewed studies, making direct comparison of the costs difficult.

Soltanieh et al. [242] considered an integrated process based on the combination of power generation by oxy-fuel combustion and methanol synthesis using electrolytic hydrogen. This type of integration is interesting owing to the elimination of CO_2 emissions and production of methanol at a relatively competitive cost. In general, the integration of fossil power generation and methanol synthesis might provide an effective near-to-medium-term solution for the reduction of CO_2 emissions, simultaneously allowing stable power plant operation via the conversion of excess electricity into methanol. In addition, Van-Dal and Bouallou [233] showed that heat integration between CO_2 capture and methanol synthesis can lead to significantly low efficiency losses incurred to power generation from post-combustion capture.

Owing to the significant power consumption of the electrolysis unit, the cost of electricity has a major effect on the economics of a power-to-methanol process. In fact, electricity generally constitutes the main operating cost in the overall process. In addition to the electricity cost, the availability of electricity is critical. Stable input of electricity allows continuous operation at high load factors, which simplifies operation and improves the economics. The total production costs have been shown to be highly sensitive to the operating time and capacity factor [240, 236]. Intermittent operation also creates difficulties in methanol synthesis, especially in reactor operation. Part-load operation requires the careful optimisation of the reactor configuration to maintain adequate temperature control [243]. If intermittent renewable electricity is used for electrolysis, buffering storage of hydrogen may be necessary to allow sufficiently stable operation of the synthesis unit.

In the electrolysis unit, the performance in intermittent and part-load operation can be improved by employing PEM electrolysers instead of alkaline electrolysers. However, as a more mature technology, hydrogen production cost is at present significantly lower with alkaline electrolysers than with PEM electrolysers. Processes based on alkaline electrolysis are at present more competitive than those utilising PEM electrolysers (Figure 7.2). For SOE electrolysers, the costs are currently significantly higher compared to PEM and alkaline electrolysers [238]. However, with future development of SOE technology, the higher inherent energy efficiency of high-temperature electrolysis may lead to superior results [240]. Overall, decreasing electrolyser capital costs are necessary because they contribute to a large fraction of the overall capital expenditure in power-to-methanol processes.

Power plant flue gases are most often considered the source of CO_2. Usually, post-combustion capture by amine (MEA) absorption is assumed. In many studies, the source of CO_2 and technology of capture are not considered in much detail, and post-combustion amine capture can be considered as a ‘default’ choice utilising established technology. This might be justifiable owing to the relatively low impact of CO_2 capture on the total capital and operating costs compared with electrolysis. Potential benefits of oxy-fuel combustion, especially its integration possibilities with CO_2 capture, electrolysis and methanol synthesis, have been demonstrated [242].

The faith of the oxygen by-product from water electrolysis has a clear impact on the overall economics. Especially if pressurised electrolysers are used, the oxygen compression and storage costs are relatively insignificant and venting the potentially valuable by-product is wasteful. The feasibility of selling the oxygen would probably be highly dependent on the plant location and the presence of potential customers in the vicinity.

8 Liquid-phase methanol synthesis

Methanol synthesis in the presence of liquid solvents is an alternative approach to the catalytic gas-phase processes discussed in the previous sections. Both heterogeneous (solid) and homogeneous (liquid) catalysts have been considered in these types of processes. Some processes even use a combination of both types of catalysts, either combined in a single reaction step or in a cascade system with separated reaction steps performed using different catalysts. The carbon source for these liquid processes also differs: some processes can only convert CO_2-free syngas, whereas others are applicable for the direct hydrogenation of CO_2 to methanol, which is the reaction route of interest in the present work.

The primary focus of this work is heterogeneous catalysts and the corresponding three-phase processes where solids, liquids and gases/vapours are all present. The solvents used in liquid-phase methanol synthesis can be inert or have a co-catalytic effect. The potential benefits of liquid-phase methanol synthesis include the more favourable thermodynamics and increased per-pass conversion compared to conventional methanol synthesis, which can be achieved by operation at lower temperatures and condensation or by solvation of liquid reaction products. In CO_2 hydrogenation, the methanol selectivity can be improved because CO formation via RWGS is reduced at lower temperatures. In addition, improved temperature control of the exothermic reaction can be provided by the large heat capacity of the liquid solvent.

Early developments in the field of liquid-phase methanol synthesis were based on a cyclic process with carbonylation of methanol to methyl formate, followed by the hydrogenation of methyl formate to methanol [244].

$$CH_3OH + CO \rightarrow HCOOCH_3 \tag{8.1}$$

$$HCOOCH_3 + 2\,H_2 \rightarrow 2\,CH_3OH \tag{8.2}$$

This process is catalysed by alkali alkoxides, such as potassium or sodium methoxide, in combination with heterogeneous copper chromite [245, 246, 247] or Ni-based catalysts [248, 249, 250]. Inert solvents such as xylene are used. The alkali alkoxide catalyses the carbonylation reaction, whereas the metal catalysts are active for formate hydrogenation. With these catalytic systems, methanol has been synthesised at temperatures as low as 100 °C and pressures of 30–65 bar [251]. However, the basic catalysts are not compatible with CO_2 or water, the presence of which even at trace amounts leads to rapid catalyst deactivation [250]. Thus, only purified CO_2-free syngas can be used in these processes.

The same issue occurs in the liquid-phase methanol synthesis method developed at Brookhaven National Laboratory, which is similarly based on the CO conversion by basic catalysts [252]. The catalytic system comprises nickel acetate, tert-amyl alcohol and sodium hydride, allowing methanol synthesis at good yields in the temperature range of

80–120 °C and at a pressure of 20 bar. Here, the liquid-phase comprises the alcohol and an additional solvent such as tetrahydrofuran.

The LPMEOH™ liquid-phase methanol synthesis process was developed by the Air Products and Eastman companies in co-operation with the US Department of Energy [253, 254, 255]. The aim was to develop a process capable of utilising the syngas generated by coal gasification, allowing the integration of methanol synthesis into a coal gasification power plant. The developed process is based on a slurry bubble column reactor containing conventional methanol synthesis catalyst in a powder form suspended in inert mineral oil. The oil acts a heat transfer medium, transferring the reaction heat to an internal heat exchanger. The process allows the conversion of syngas feeds with varied compositions, including any content of CO or CO_2.

A demonstration plant with a design capacity of 235 t of methanol per day began operation in 1997 and was run for 69 months. The production rate exceeded the design capacity, and the overall process runtime was as high as 97.5% of the planned runtime. Overall, the project was reported successful and the integration of methanol synthesis to IGCC power generation was considered promising. The main challenges were considered the cost of syngas generated by coal gasification, the required gas purification for the protection of the catalyst and the scale-up of the slurry bubble column reactor.

8.1 Alcohol-promoted methanol synthesis

A liquid-phase methanol synthesis process based on the combination of conventional methanol synthesis catalysts and a liquid alcohol solvent was first proposed by Fan et al. [256]. In this process, the alcoholic solvent acts as a co-catalytic solvent. The alcohol promotes methanol synthesis by facilitating an altered reaction route that allows operation at low temperatures compared with conventional methanol synthesis. The reduced temperature allows higher per-pass conversion owing to the more favourable thermodynamic equilibrium. In particular, the reaction proceeds through the formate ester of the corresponding alcoholic solvent, with various alcohols used as the promoter. Importantly, the process does not employ basic catalysts sensitive to deactivation by CO_2. This allows the conversion of CO_2-containing syngas and even pure CO_2.

Alcohol-promoted methanol synthesis from CO_2 and H_2 was first studied by comparing a commercial Cu/ZnO catalyst, a copper chromite catalyst and a Pd-promoted (5% Pd) copper chromite catalyst, with ethanol as the solvent [256]. At 200 °C and 30 bar, the commercial catalyst showed the highest activity, with CO_2 conversion of 7.5% and methanol selectivity of 73.3% after 2 h of reaction. The copper chromite catalyst also showed reasonable activity with CO_2 conversion of 5.2% and methanol selectivity of 59.6%. The main by-product was CO formed via RWGS. The addition of Pd was not found to be beneficial. Ethyl formate, the expected intermediate product, was also found among the reaction products in each of the experiments.

The effect of reaction temperature and time was also studied [256]. At 117–157 °C, ethyl formate was the main product, whereas at 157–197 °C, a decrease in ethyl formate was accompanied by increasing methanol formation. With the reaction time increasing from 2 to 20 h, a decrease in the concentration of ethyl formate was accompanied by methanol accumulation in the products. These results pointed to ethyl formate being the intermediate in methanol formation. Supporting evidence was provided by a blank experiment with no ethanol added, which resulted in very slow methanol formation. Furthermore, methanol was formed at a significantly increased rate when ethyl formate was added to the reaction mixture. As a result, the following reaction steps were proposed, with ethyl formate hydrogenation as the rate-determining step:

1. Hydrogenation of carbon dioxide into formic acid

$$CO_2 + H_2 \rightleftharpoons HCOOH \tag{8.3}$$

2. Reaction of formic acid with ethanol, forming ethyl formate

$$HCOOH + C_2H_5OH \rightleftharpoons HCOOC_2H_5 + H_2O \tag{8.4}$$

3. Hydrogenation of ethyl formate, forming methanol and ethanol

$$HCOOC_2H_5 + 2\,H_2 \rightleftharpoons CH_3OH + C_2H_5OH \tag{8.5}$$

Tsubaki et al. [257] reported the conversion of CO_2-containing syngas (5% CO_2) on Cu/ZnO in ethanol solvent. In the absence of ethanol, methanol synthesis did not occur below 210 °C, whereas the formation of both methanol and ethyl formate was observed at 150 °C following the addition of ethanol. A more detailed reaction route for the alcohol-promoted methanol synthesis was presented.

$$CO + H_2O \rightleftharpoons CO_2 + H_2 \tag{8.6}$$

$$CO_2 + \frac{1}{2}H_2 + Cu \rightleftharpoons HCOOCu \tag{8.7}$$

$$HCOOCu + ROH \rightleftharpoons HCOOR + CuOH \tag{8.8}$$

$$HCOOR + 2\,H_2 \rightleftharpoons ROH + CH_3OH \tag{8.9}$$

$$CuOH + \frac{1}{2}H_2 \rightleftharpoons H_2O + Cu \tag{8.10}$$

Net reaction:

$$CO_2 + 2\,H_2 \rightleftharpoons CH_3OH \tag{8.11}$$

Cu represents catalytic sites on the Cu catalyst and ROH is the alcoholic solvent. The formation of the formate ester and the subsequent hydrogenation to methanol were thus proposed to be initiated by the hydrogenation of CO_2 (and not CO), a view which is generally accepted for the conventional gas-phase reaction. CO, when present, is first converted to CO_2 via the WGS reaction. Instead of further hydrogenation of the formate intermediate species (Table 6.1), formate readily reacts with the alcohol to form the ester. The elimination of the slow formate hydrogenation step, which requires higher temperatures in the conventional gas-phase reaction, then explains the promoting effect of the alcohol.

Tsubaki et al. [257] also tested the reaction with a Cu/Al_2O_3 catalyst, yielding only ethyl formate but no methanol as product. Addition of Cu/ZnO with Cu/Al_2O_3 resulted in methanol formation. Based on these findings, it was proposed that Cu/Al_2O_3 (i.e. Cu) is active in the formation of the formate ester intermediate, whereas Cu/ZnO catalyses the hydrogenation of the ester into methanol. Zeng et al. [258] tested the effect of the $CO:CO_2$ ratio in the feed gas and found that the reaction rate increased with increasing CO_2 content. Highest rate was found with pure CO_2 and H_2.

The reaction mechanism was further studied by means of in situ infrared spectroscopy [259]. With ethanol as the solvent, formate adsorption species were identified on the Cu/ZnO surface. Formate was found to react with gas-phase ethanol to form ethyl formate. In a subsequent study, this step has been identified to take place via a Rideal type mechanism – that is, by direct reaction between absorbed formate and gas-phase ethanol [260]. Ethyl formate was then readily hydrogenated by hydrogen absorbed on the catalyst surface [259]. Both the formation and hydrogenation of ethyl formate occurred at temperatures below those required in conventional methanol synthesis. An identical mechanism was identified with 2-propanol as the alcohol [261]. In a kinetic study, both the reaction of alcohol with formate and the hydrogenation of the resulting ester were found to be faster with 2-propanol than with ethanol, pointing to the superiority of 2-propanol to ethanol as a catalytic solvent [262].

Based on the above findings, the alcohol used does not seem to fundamentally alter the low-temperature reaction route. However, different alcohols have been shown to possess varying effectiveness in promoting methanol synthesis. Tsubaki et al. found linear alcohols more effective than the branched counterparts, with n-butanol showing the best results [257]. Zeng et al. [258] reported that the yield of both methanol and the corresponding ester decreased with the increasing carbon number of primary alcohols from ethanol to 1-hexanol. For alcohols with the same carbon number but different structure, secondary alcohols were found to have higher activity. The highest promoting effect was found with 2-propanol. Low activity was found for alcohols with bulky molecular structures. Iso-butanol, tert-butyl alcohol and cyclopentanol showed low activity, whereas ethylene glycol and benzyl alcohol showed no activity at all.

The structural differences of alcohols with the same carbon number were proposed to affect the reaction rate via both spatial and electronic effects [258]. The electron density

of the oxygen atom is higher on the bulkier and more branched alcohols, leading to increasing rate of nucleophilic attack on the formate intermediate. However, the same nucleophilic reaction is simultaneously hindered by the spatial obstacle caused by the bulkier molecular structure. It was postulated that from four different butyl alcohols tested, 2-butanol shows the optimal balance between these two factors, leading to the highest activity.

Continuous alcohol-promoted methanol synthesis has been demonstrated using a semi-batch autoclave reactor with CO_2 containing (5%) syngas, Cu/ZnO catalyst and 2-butanol solvent [263]. For synthesis, 3g catalyst and 20-ml alcohol were used. Reaction occurred at 170 °C and 50 bar with continuous feed of reactant gas and removal of product gases. In steady state, the total carbon conversion was 47%, with methanol selectivity of 98.9% (excluding CO). However, the activity of the catalyst in terms of methanol productivity was not reported and direct comparison to gas-phase CO_2 hydrogenation (Section 7.1) by this metric cannot be performed.

The catalysts used in the alcohol-promoted methanol synthesis process are similar to the conventional Cu/ZnO catalysts used in gas-phase methanol synthesis. The various alternative catalysts developed for CO_2 hydrogenation to methanol may be effective for performing the reaction via the low-temperature route. The variety of catalysts tested for this reaction is so far limited, but some optimisation of Cu/ZnO catalysts has been reported. An equimolar ratio of Cu and Zn in the catalyst was found to result in the highest activity in low-temperature methanol synthesis [263, 264]. Catalytic activity was also found to be almost proportional to the metallic Cu surface area, but the activity of Cu/ZnO interfaces was considered important for the reaction [264]. The utilisation of alternative catalyst preparation methods [265, 266, 267, 268] has also been pursued, but these studies use mixed syngas and do no report performance in terms of methanol productivity.

Improvements in catalysts are needed because the rate of the alcohol-promoted reaction on Cu/ZnO catalysts seems to be low compared with gas-phase methanol synthesis. Methanol productivity is not directly reported in most of the studies, but Yang et al. [264] reported a rate of 6.1 g of methanol per kg of catalyst per hour from syngas containing both CO and CO_2. The methanol synthesis rate is expected to be of the same magnitude in other studies with similar catalysts and solvents. This would be two orders of magnitude below the values reported for gas-phase CO_2 hydrogenation to methanol (Table 7.1).

As another development, alkali metal salts have been added to the Cu–alcohol catalytic system. Potassium salts have been used in combination with Cu-based catalysts in ethanol solvent, with the alkali formate catalysing the formation of ethyl formate and the Cu catalysts catalysing further hydrogenation of the formate [269, 270]. Addition of the alkali was found to significantly increase the methanol synthesis rate. The process has been further developed by the impregnation of Cu-based catalysts with basic components [271, 272]. However, the use of basic catalysts makes the system intolerant of CO_2-containing feed gas, and the process is thus only applicable for CO hydrogenation.

8.2 Cascade catalytic systems

In cascade catalytic systems for CO_2 hydrogenation to methanol, the overall methanol synthesis reaction is divided into separate steps that are performed using different catalysts. Huff and Sanford [273] demonstrated the concept by homogeneous CO_2 hydrogenation to methanol via the following steps:

1. Hydrogenation of CO_2 into formic acid
2. Esterification of formic acid to form a formate ester
3. Hydrogenation of the ester to form methanol

This reaction route is principally similar to the alcohol-promoted route discussed above. In the absence of the solid catalyst, the key intermediate is formic acid instead of formate absorbed on the catalyst surface. The reaction sequence was performed in a single vessel using multiple catalysts and using a strategy of separating thermodynamically unfavourable and unstable intermediates to improve the overall reaction. Using a combination of homogeneous ruthenium complex catalysts in liquid solvents at low temperature (135 °C), the initial feasibility of this type of process was established. However, the cascade system suffered some incompatibility both among the catalysts and between CO_2 and the catalysts, and further optimisation of the catalyst system was found necessary [273].

Successively, a cascade catalytic system using heterogeneous catalysts was reported by Chen et al. [274]. A major advantage of using heterogeneous catalysts is the easier separation of the catalyst from the product mixture. Catalysts based on Cu and molybdenum carbide were investigated, and the combination of copper chromite and Cu/Mo_2C was found to be the most effective. 1,4-dioxane was used as inert solvent, with its high hydrogen solubility identified as a favourable property. The addition of ethanol improved the rate of reaction, leading to the reaction proceeding through the formate intermediate instead of formic acid in the absence of alcohol.

In the cascade system, copper chromite was identified to be effective for the formation of ethyl formate, whereas Cu/Mo_2C was active in the further conversion of the formate into methanol [274]. This reaction route is the same as the alcohol-promoted methanol synthesis route. As such, this approach can be considered a development of the same concept utilising a more advanced system of heterogeneous catalysts. The turnover frequency was found to be in a similar range to that of the homogeneous system reported by Huff and Sanford [273], and the methanol productivity was measured at 10.2 g/kg h at 135 °C, 10 bar CO_2 and 30 bar H_2. Good stability of the catalysts was observed during 72 h of reaction.

8.3 Amine-based systems

Low-temperature methanol synthesis has been demonstrated with amines as co-catalysts. Because amine solution are commonly used as absorbents in CO_2 capture processes, this approach provides an interesting opportunity to integrate CO_2 capture and further hydrogenation of the captured CO_2 [275, 276]. Direct hydrogenation of absorbed CO_2 to methanol could eliminate the energy-intensive desorption stage from CO_2 capture. This has been demonstrated using not only homogeneous catalysts [277, 275] but also heterogeneous catalysts, which are of main interest in the present work.

The use of amines has been demonstrated in combination with an alcoholic component, with methanol synthesis proceeding through the formate ester route [278]. Amines have also been shown to allow lower reaction temperatures without the presence of alcohol via novel reaction routes [279, 280]. Methanol productivity values of up to 133.5 g/kg h have been reported at 170 °C [279]. Performing methanol synthesis in amine-based solvents is a particularly promising approach owing to the possibility to directly integrate CO_2 hydrogenation with a preceding CO_2 capture process. Because amine solvents are commonly used in CO_2 capture processes based on chemical absorption, the conversion of the absorbed CO_2 directly from the absorption solution could eliminate the need for the high-energy regeneration of the solvent. This could lead to significantly reduced costs in the overall capture and utilisation process.

9 Water removal during methanol synthesis

Owing to the harmful effects of water in methanol synthesis, especially when converting CO-free syngas, continuous removal of water produced in the reaction would be interesting. Such an approach could improve the per-pass conversion and methanol yield, as removal of water by-product drives the CO_2 hydrogenation reaction (Equation 6.2) towards the product side.. In addition, the reaction rate could be improved by limiting the inhibiting effect of water, and catalyst stability improved.

Water removal during methanol synthesis has been pursued by the use of membrane reactors. A lithium-exchanged Nafion dense polymeric membrane was utilised to remove both water and methanol from reacting gases via the selective permeability of the vapour reaction products [281]. Using a commercial methanol synthesis catalyst at 200 °C and low pressure (4.3 bar), the methanol yield from CO_2 and H_2 was increased at low space velocities in a membrane tube reactor.

A zeolite membrane reactor was suggested for the selective permeation of water and methanol [282]. At 20 bar and temperature range of 206–263 °C, both CO_2 conversion and methanol selectivity improved in the membrane reactor compared with a conventional tubular reactor. The improvement was most significant when operating below the critical temperature of methanol (238 °C), as the permeability of methanol was reduced at higher temperatures.

As an alternative to the use of membrane reactors, water can be removed by adsorption using molecular sieve adsorbents. These types of absorbents can selectively absorb water from solutions based on molecular size exclusion and are commonly used in processes such as ethanol dehydration in biofuel production [283]. The use of molecular sieve absorbents in a sorption-enhanced methanol synthesis process is a novel application that has been discussed in a number modelling studies, but experimental reports seem to be scarce.

A non-steady state model showed that both methanol and DME yields can be improved by the absorption of water during DME synthesis [284]. The use of a 4-Å zeolite molecular sieve was considered for methanol synthesis from syngas [285]. A steady-state model was prepared for a novel reactor, where the absorbent flows with the reacting gases inside reactor tubes filled with commercial methanol synthesis catalyst. The model suggested a decrease in the water concentration over the length of reactor and a corresponding increase in the rate of methanol synthesis when the absorbent was introduced. It also suggested an increase in the CO concentration because RWGS was driven further when water was removed.

A sorption-enhanced CO_2 hydrogenation to methanol process utilising a 4-Å molecular sieve was compared with a similar process without water adsorption by means of flowsheet simulation [286]. Equilibrium-based reactor modelling, neglecting the kinetics of reaction and absorption, suggested that the complete removal of water from the

reacting mixture resulted in 100% CO_2 conversion. Methanol selectivity progressively decreased with increasing temperature, as the selectivity to CO via RWGS was increased. At 230 °C and 50 bar, the per-pass methanol yield could be improved from 19% to 58% with the addition of absorbent. Consequently, the recycle ratio in the reactor loop could be reduced from 3.1 to 0.5.

10 Low-temperature CO_2 hydrogenation to methanol (Publications III-IV)

The subject of Publication III is low-temperature, liquid-phase CO_2 hydrogenation to methanol utilising heterogeneous Cu-containing catalysts and co-catalytic alcoholic solvents. The work presents experiments conducted for evaluating and improving the performance of the catalytic system. Cascade catalysis and water adsorption during the reaction are investigated as novel approaches to this process. In Publication IV, a techno-economic analysis is conducted to assess the feasibility of a power-to-methanol process based on the alcohol-promoted CO_2 hydrogenation reaction in comparison to a more conventional gas-phase CO_2 hydrogenation process.

10.1 Background and motivation

CO_2 can be effectively converted into methanol utilising similar catalysts and processes to those used in industrial, fossil-based methanol synthesis (Chapters 6–7). However, the conversion of CO_2/H_2 mixtures instead of CO-containing syngas results in less favourable thermodynamics and lower equilibrium conversion in a single reactor pass. In a practical process, this conversion results in an increased recycle ratio because larger amounts of unreacted gases need to be recycled. Correspondingly, the capital and operating costs are increased owing to the recompression and transport of large gas volumes in the reactor loop. Another difficulty in the conversion of CO-free syngas is the increased formation of water both as a by-product of CO_2 hydrogenation to methanol and via RWGS. The higher concentration of water is suggested to result in reduced reaction rate owing to the kinetic inhibition caused by the adsorption of oxygen or hydroxyl species on the catalyst surface [163, 164].

To increase the equilibrium conversion, the operating conditions in methanol synthesis should be changed to increased pressures and/or reduced temperatures. By operating at sufficiently high pressures, nearly full conversion of reactant gases can be achieved without changes in the reaction temperature. However, operating at very high pressures can also lead to increased costs related to compression and pressure rating of all process equipment. The lower limit for reaction temperature in a conventional methanol synthesis process is in turn dictated by the activity of established catalysts. The reaction is kinetically hindered at lower temperatures because the formate reaction route from CO_2 to methanol cannot proceed when the activation energy barrier of the key reaction steps is not overcome.

The alcohol-promoted methanol synthesis process (Section 8.1) provides an opportunity to reduce the operating temperature via alteration of the reaction route. In the presence of alcoholic solvents, formate absorbed on Cu-based catalysts is readily converted into formate ester of the corresponding alcohol. This reaction step bypasses the slow (high-energy) step of conventional methanol synthesis and facilitates CO_2 hydrogenation to methanol at reduced temperatures. Moreover, methanol selectivity is increased because

the conversion of CO_2 into CO via RWGS, and the resulting formation of additional water, is limited at reduced temperatures by the reaction equilibrium [167]. Finally, an added benefit of the liquid-phase system is the increased temperature control of the exothermic reaction system facilitated by the transfer of heat from the catalyst into the heat-absorbing solvent.

Previously published literature (Section 8.1) has demonstrated the basic feasibility of the alcohol-promoted catalytic system. Both mixed ($CO/CO_2/H_2$) syngas and CO_2/H_2 have been converted to methanol using Cu/ZnO and other Cu-based catalysts at reduced temperatures compared with the gas-phase reaction. Comparisons of different alcohols have shown differences in their performance as co-catalytic solvents. Continuous synthesis at high carbon conversion has also been demonstrated with high methanol selectivity. However, the catalytic activity in terms of methanol productivity (mass-time yield) is usually not reported. Based on the limited available data, the activity is very low compared with gas-phase CO_2 hydrogenation using Cu/ZnO or alternative heterogeneous catalysts.

The reaction route proceeding through formate ester intermediates has also been utilised in cascade catalytic systems using homogeneous or heterogeneous catalysts (Section 8.2). In such systems, combinations of different catalysts are used to catalyse the separate reaction steps, with the aim of improving the rate and selectivity of the overall reaction from CO_2 to methanol. Chen et al. [274] tested different Cu-based catalysts in the presence of an inert solvent and added ethanol. A combination of copper chromite and Cu/Mo_2C was identified to be the most effective for methanol synthesis. Copper chromite was identified to be particularly effective for the formation of ethyl formate, whereas Cu/Mo_2C was active in the further conversion of the formate into methanol. The resulting methanol productivity was of similar magnitude to that in previous reports on the alcohol-promoted reaction but at a reduced temperature (135 °C) and relatively low pressure (10 bar CO_2, 30 bar H_2).

10.1.1 Publication III: developing the catalytic system

Publication III pursues a similar cascade catalytic system utilising a combination of Cu/ZnO and copper chromite catalysts in 2-butanol solvent. Both catalysts are commonly used in industrial processes and are readily available at low cost. Compared with the previous report on a similar catalytic system by Chen et al., we pursue higher methanol productivity by performing the reaction at a higher temperature (180 °C), which is still well below temperatures of conventional methanol synthesis. We also investigate whether optimisation in terms of methanol productivity can be achieved by varying the relative amount of each catalyst present in the system. This approach is believed to be effective because the limiting reaction step in the overall reaction could be accelerated by increasing the amount of catalyst that is more active for that particular step.

Another point of interest in Publication III is the amount and effects of water present in the system. Water concentrations have not been reported in previous publications on

similar reaction systems. This is apparently explained by analytical methods: water is not detected by the flame ionisation detectors (FID) commonly used in the gas chromatographic analysis of reaction products in methanol synthesis. Using a thermal conductivity detector (TCD), we can measure the concentration of water in the reaction solution. Methanol and major by-products can also be quantified, albeit at reduced sensitivity compared with FID.

Publication III further pursues the in-situ removal of water from the reaction solution by utilising zeolite molecular sieve absorbents (Chapter 9). There are two points of interest. (1) As the addition of the absorbent allows the concentration of water to be reduced under otherwise identical reaction conditions, the effect of water on the alcohol-promoted methanol synthesis reaction can be evaluated. (2) At the same time, the technical feasibility of sorption enhancement in this reaction can be evaluated on a basic level.

10.1.2 **Publication IV: techno-economic analysis**

None of the reviewed published work on alcohol-promoted or similar liquid-phase methanol synthesis processes has considered process design beyond the combinations of catalysts and solvents facilitating methanol formation at temperatures below those employed in gas-phase methanol synthesis (Section 8.1). Without consideration of the reactor and overall process design, the actual benefits of the reduced temperature in a practical process have not been clarified. Moreover, the complications caused by the addition of the solvent or the influence of different solvents on the overall process have not been discussed.

The aim of Publication IV is to assess the technical and economic feasibility of a methanol synthesis process based on the conversion of captured CO_2 using the liquid-phase, low-temperature reaction route. The first step in this assessment is the design of a complete methanol synthesis process including the reactor loop and product separation. Based on the resulting mass and energy balances and a subsequent economic analysis, the feasibility of this novel process is compared with that of a more conventional CO_2-based methanol synthesis process. As reviewed in Section 7.2, the economic feasibility of methanol synthesis based on gas-phase CO_2 hydrogenation has been assessed in several previous studies. By utilising similar methodology to these previous reports, Publication IV provides a comparative assessment of the gas-phase and liquid-phase CO_2 hydrogenation processes.

10.2 **Methodology**

10.2.1 **Catalytic experiments**

Figure 10.1 presents a flowsheet of the experimental apparatus. A detailed description of the experimental equipment and procedure is given in Publication III. Reaction experiments were performed in an autoclave reactor (volume: 450 ml). Reaction

temperature and mixing speed were controlled using an attached control unit. The mixing speed was set at 600 rpm in all experiments. Liquid samples from the reaction mixture were collected using a water-cooled sample collection vessel, in which any vapours present in the sample were condensed prior to sample collection. Experiments were performed in semi-batch mode with a constant pressure maintained by continuous feed of gas. The total reaction time was 6 h, and liquid samples were collected every 2 h.

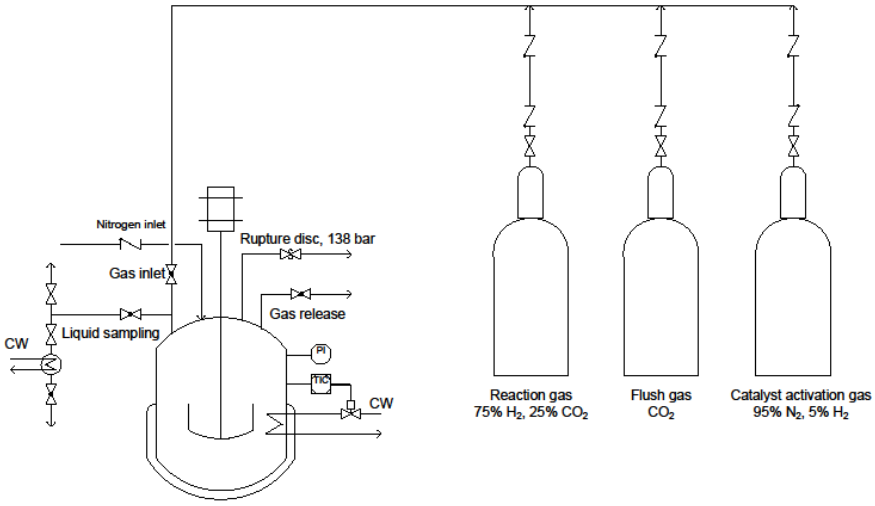

Figure 10.1 Experimental setup used in the reaction experiments.

Analysis grade 1-butanol and 2-butanol were used as solvents. A commercial Cu/ZnO-based methanol synthesis catalyst was used. The catalyst was ground and sieved to 150–500 µm for each experiment. Powdered copper chromite was used in the dual catalyst experiments. A 3-Å molecular sieve was used in the adsorption experiments. The absorbent was ground and sieved to 150–500 µm prior to use and was activated by heating to 250 °C under air. A mixed gas containing 75 mol-% hydrogen and 25 mol-% CO_2 was used as the reaction feed gas, and a mixed gas containing 5 mol-% hydrogen in nitrogen was used for catalyst reduction.

Liquid samples were analysed by gas chromatography using a TCD. Analysis uncertainty was estimated by repeated measurements and by estimating the uncertainty related to the preparation and analysis of the calibration standards. The total uncertainty is expressed as the relative standard deviation for each product compound, presented as error bars in

the relevant figures. The uncertainty related to the experimental procedure was estimated as relatively insignificant compared with the analytical error.

To observe any structural changes in the catalyst during reaction, a batch of Cu/ZnO catalyst was characterised prior to reaction in the unreduced form and following the reaction in 1-butanol at 180 °C. A separate batch of ground catalyst was characterised following reduction. Characterisation was performed by powder X-ray diffraction (XRD) and scanning electron microscopy-energy dispersive X-ray spectroscopy (SEM-EDS).

10.2.2 **Process modelling**

Steady-state flowsheet models of alternative CO_2 hydrogenation to methanol processes were created using Aspen Plus V9. The processes include a gas-phase process and a liquid-phase process utilising four alternative alcoholic solvents: 2-butanol, 1-butanol, 1-pentanol and 1-hexanol. Other than the solvent, the design of these liquid-phase processes is identical. In addition, an alternative liquid-phase process configuration utilising 1-pentanol solvent and improved solvent recovery by decantation was modelled.

All methanol synthesis processes are based on the utilisation of capture CO_2 and hydrogen-generated renewable electricity-powered water electrolysis. Electrolysis is assumed to be powered by 30 MW of wind electricity, with the scale of electricity generation set according to data on recent and upcoming wind energy installations in Finland [287]. Alkaline pressurised (30 bar) electrolysis with a system efficiency of 30% is assumed for hydrogen generation. The capacity of the methanol synthesis unit is based on the amount of hydrogen available from the electrolysis unit. The process scale and boundaries are illustrated in Figure 10.2. The design and costing of the CO_2 capture and water electrolysis units are outside the scope of the analysis.

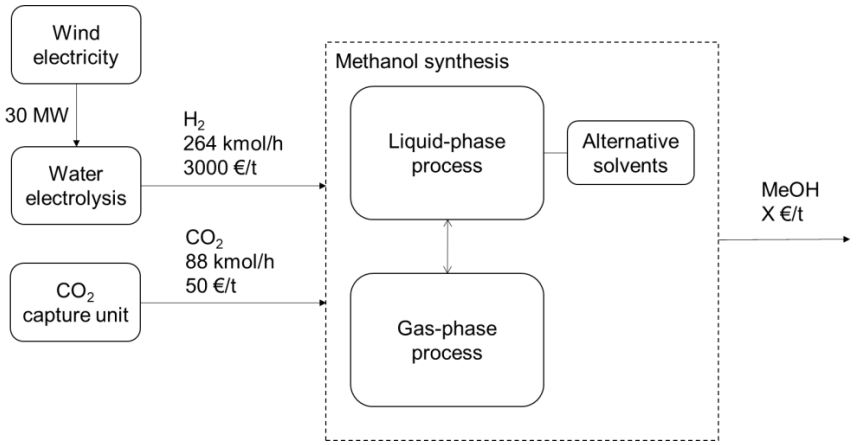

Figure 10.2 Scope and boundaries of the techno-economic analysis of CO_2 hydrogenation to methanol. The design capacity is based on renewable electricity input of 30 MW.

Details on the modelling of the alternative processes in Aspen Plus, including the flowsheets and process descriptions of the modelled processes, are presented in Publication IV. Two separate property methods were used in all process models. High-pressure (>10 bar) process sections were modelled using the Redlich-Kwong-Soave equation of state with modified Huron-Vidal mixing rules (RKSMHV2). The low-pressure sections were modelled using the NRTL-RK property method, which uses the activity-coefficient–based non-random two-liquid model for the liquid phase and the Redlich-Kwong equation of state for the gas phase. The selection of the methods was based on the guidelines provided by Aspen Plus and on previous modelling studies on similar processes (Section 7.2).

The process design and modelling methods (including the selection and specification of the unit operation blocks) were kept similar between the gas-phase and liquid-phase processes to maintain comparability of the results. The basic configuration (Figure 6.2) of each process consists of the feed gas compression, the reactor section and the separation section involving the separation and recycle of unreacted gases followed by the separation and purification of the methanol product. Compared with the gas-phase process, a key additional feature of the liquid-phase processes is the separation of the solvent alcohol within the separation section and recycle of the solvent to the reactor. Owing to this feature, the liquid-phase processes require two distillation columns, compared with a single column in the gas-phase process.

In the gas-phase process, the reactor was modelled by an adiabatic plug flow model (RPLUG), with the reaction kinetics of methanol synthesis and WGS modelled by the Vanden Bussche and Froment model [194] (Equations 6.5–6.6) utilising readjusted parameters from Mignard and Pritchard . The Langmuir-Hinshelwood–type kinetic model [243]was implemented in Aspen Plus following the methodology from Van-Dal and Bouallou [233]. The reactor inlet pressure was set at 50 bar, and the inlet temperature was 215 °C based on the heat integration in the process model. The reactor was sized to approach equilibrium of both methanol synthesis and WGS according to the kinetic model.

A less rigorous, equilibrium-based modelling approach was selected for the liquid-phase processes. Because a detailed kinetic model for the alcohol-promoted reaction is not available, CO_2 hydrogenation to methanol and the RWGS were modelled as equilibrium reactions. Full approach to equilibrium was assumed for the reactions, and the chemical and phase equilibrium were calculated using the continuous stirred tank (RCSTR) model block. The reactor was set to isothermally operate at 180 °C and 50 bar in each of the liquid-phase processes. A reactor configuration consisting of separate inlets for the feed gas and circulated solvent and separate outlets for gas/vapour phase and liquid phase was adopted. A rough sizing for the reactor was performed based on the amount of methanol formed and the catalyst-mass-specific methanol formation rate observed in the gas-phase reactor. This procedure is explained in detail in the Supplementary material to Publication IV.

10.2.3 Economic and environmental analysis

Capital costs were estimated by the factorial method described by Towler and Sinnott [288]. Installed equipment costs were obtained from the cost functions integrated into the Aspen Plus software. Appropriate material (stainless steel) and location (Western Europe) factors were then applied to obtain the inside battery limits (ISBL) cost of the process. Overall capital costs including off-site (OSBL), engineering and contingency costs were then estimated using typical factors for a process with low complexity and relatively limited off-site demands [288]. These factors, providing an order of magnitude estimate for the overall costs, are summarised in Table 10.1. In the economic analyses of the process, the capital costs were annualised based on an assumed plant lifetime of 20 years and an interest rate of 5%.

Table 10.1 Method and factors used in the estimation of process capital costs.

Item	Basis
ISBL capital cost	Installed equipment cost from Aspen Plus Exchange rate 0.8085 €/USD Material factor 1.3 (304 stainless steel) Location factor 1.043 (Western Europe)
OSBL capital cost	25% of ISBL
Engineering cost	20% of ISBL and OSBL
Contingency	30% of ISBL and OSBL

Fixed operating costs primarily including labour, overhead and maintenance costs were estimated using a factorial method from Towler and Sinnott [289]. The factors and assumptions used are detailed in Publication IV.

The costs of hydrogen and feedstock CO_2, constituting the major variable costs, were assumed based on literature references. Based on Levene et al. [290], the cost of hydrogen generated by wind electricity–powered water electrolysis was assumed at 3000 €/t. The cost of captured CO_2, comprising the capital and operating costs of an amine-based post-combustion capture unit, was estimated at 50 €/t based on a report from the IEA [291]. CO_2 transportation costs and the specific source of CO_2 to the capture unit were not considered.

Use of grid electricity to power the methanol synthesis processes was assumed for maintaining constant operation. A market cost of 60 €/MWh was assumed for grid electricity [292]. Cost of medium-pressure steam was estimated at 35 €/t based on fuel (natural gas) cost and a factorial correction taking into account non-fuel costs. Identical cost was assumed for low-pressure steam. The costs of cooling water, wastewater and

catalyst were set according to literature references. The cost of the alcoholic solvents was assumed at 500 €/t, regardless of the type of alcohol used.

Revenues were estimated using an assumed methanol price of 400 €/t based on available market data for recent years. Sales of oxygen produced as a by-product in water electrolysis were considered at a price of 70 €/t based on literature data. Based on the revenues and production costs, an economic analysis was performed to determine the net present value (NPV) of each alternative process. A plant lifetime of 20 years and a discount rate of 8% were assumed for this analysis.

A simple environmental analysis comprising the CO_2 balance, electricity consumption and water balance was performed. The CO_2 balance considers the feedstock CO_2, CO_2 removed within process outlet streams and indirect emissions from steam generation. Cooling water input and wastewater output and composition were considered in the water balance.

10.3 Results and discussion

The results published in Publication III are discussed in sub-sections 10.3.1–10.3.4, and results published in Publication IV are discussed in sub-sections 10.3.5–10.3.8.

10.3.1 Preliminary findings

Dehydrogenation of the alcoholic solvents was observed as a key side reaction. This reaction yields hydrogen and the aldehyde or ketone corresponding to the alcohol used. Alcohol dehydrogenation is known to be catalysed by copper [293] and has also been previously reported in connection with alcohol-promoted methanol synthesis [264]. In the present experiments, 1-butanol was dehydrogenated into butanal, whereas 2-butanol was dehydrogenated into 2-butanone. A typical concentration profile of reaction products in 1-butanol is presented in Figure 10.3. Similar profiles were found in all experiments, regardless of the conditions and alcohol used as solvent.

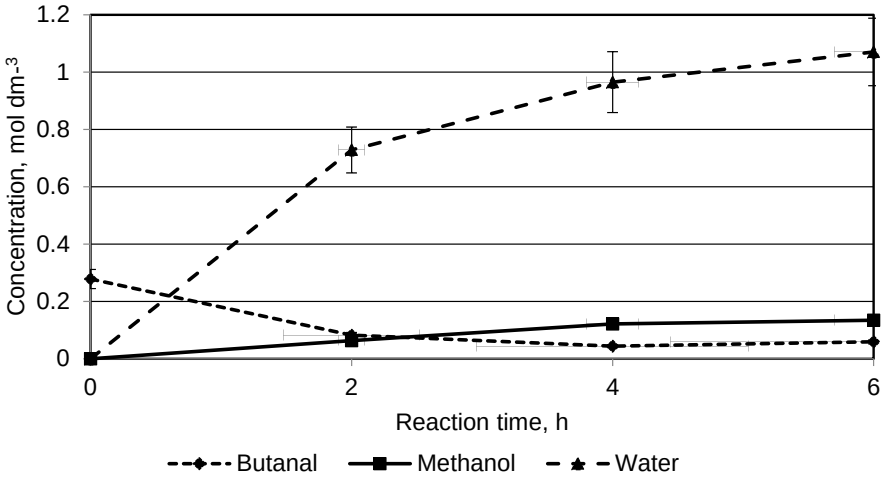

Figure 10.3 A typical concentration profile of reaction products in 1-butanol. 20 g of Cu/ZnO catalyst in 200 ml of alcohol, temperature: 180 ºC, feed gas CO_2:H_2 = 1:3, total pressure: 60 bar.

The reaction time depicted in Figure 10.3 begins from the pressurisation of the reactor with the reacting gas, following the heating of the reactor under a low-pressure nitrogen atmosphere. Correspondingly, the concentration of the dehydrogenation products (in this case, butanal) reaches the maximum during heating of the reactor. The peak concentration of the dehydrogenation products varies depending on the temperature and the alcohol but always remains below 10 w-% of the total solution. The concentration begins to decrease during reaction time. Because alcohol dehydrogenation is a reversible, equilibrium-limited reaction [294], it appears that the reaction is reversed under the reaction gas atmosphere with high hydrogen partial pressure. As the concentration seems to stabilise during the final hours of reaction, the concentration of butanal seems to reach a level corresponding to the equilibrium composition for this reaction.

Owing to the reversibility of these reactions and the rather low apparent equilibrium concentration of the dehydrogenation products, this side reaction is not considered particularly harmful for the overall process. Assuming that a large excess of the solvent alcohol would be used in a practical process, the dehydrogenation of a small fraction of the solvent does not appear problematic. Potential problems might be encountered in the separation and purification of reaction products owing to the presence of an additional component at a small but non-negligible concentration.

According to Figure 10.3, the concentration of methanol continuously increases during reaction time, but the rate of increase seems to decrease after 4 h of reaction. A similar pattern was generally observed in the experiments. The continuous increase suggests that methanol formation is not limited by the equilibrium of the CO_2 hydrogenation to methanol reaction (Equation 6.2). Instead, kinetic inhibition of the reaction rate is

suspected to be caused by the by-product water. The concentration of water also increases during the reaction time because water is formed both as the by-product of methanol synthesis and in RWGS (reverse reaction of Equation 6.4); moreover, the amount of water formed is significantly higher than that of methanol. Similar relative concentrations were found in all experiments.

If water is only formed as the by-product of methanol synthesis, the molar amounts of methanol and water formed should be equal. Thus, the much higher concentrations of water compared to methanol suggest that a significant majority of the water is formed in the RWGS reaction. This also implies that RWGS is the main reaction under the present conditions, and the selectivity of CO is much higher than that of methanol. If water is only formed as the by-product of methanol synthesis, the molar amounts of methanol and water formed should be equal. Under the present conditions, further conversion of CO directly into methanol is not expected to take place. The alcohol-promoted reaction has been identified to proceed via CO_2, with CO only reacting via conversion into CO_2 by WGS [257, 259]. In addition, mechanistic studies have identified that CO hydrogenation to methanol is blocked by the formate coverage of Cu/ZnO catalysts under methanol synthesis conditions [185].

In the experiments depicted in Figure 10.3, the molar ratio of water to methanol is approximately 10:1, which implies that methanol selectivity from the raw materials is apparently only 10%. However, final methanol selectivity in theoretically calculated chemical equilibrium at 180 °C and 60 bar approaches 100% (with a corresponding CO_2 conversion of approximately 50%) [167]. Thus, it seems that the RWGS reaction proceeds faster than methanol formation and the system remains far from equilibrium after 6 h of reaction time.

Formate esters, which are the intermediate products of alcohol-promoted methanol synthesis, were not detected in any of the experiments. It appears that the esters are rapidly further hydrogenated into methanol and their concentrations remain below the detection limit of the analysis method. However, because the intermediates were not detected, confirming that the methanol synthesis proceeded through the suggested reaction route was not possible. The promoting effect of alcohols is supported by a blank experiment in hexane at 180 °C, which yielded no methanol.

The next point of investigation is the effects of reaction temperature and pressure on the methanol productivity. Here, note that in the presence of a volatile alcoholic solvent, a significant fraction of the total pressure in the reactor is the vapour pressure of the solvent. As a result, the combined partial pressure of the reacting gases CO_2 and H_2 is not equal to the total pressure in the reactor, as would be the case in a gas/vapour-phase reaction without solvent. This factor is illustrated in Figure 10.4, which shows the variation in methanol productivity in 1-butanol with the temperature varied from 180 to 220 °C.

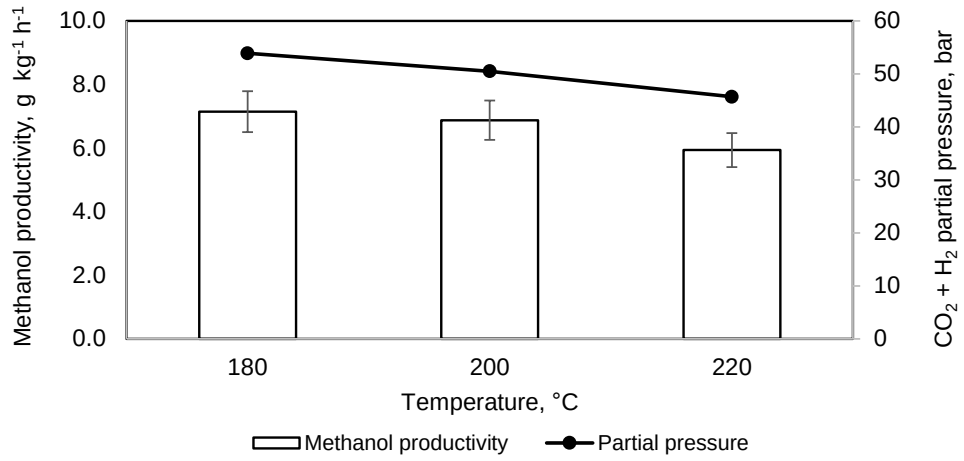

Figure 10.4 Effect of reaction temperature on methanol productivity with 20 g of Cu/ZnO catalyst in 200 ml of 1-butanol. Reaction time: 6 h, feed gas CO_2:H_2 = 1:3, total pressure: 60 bar.

Figure 10.4 also presents the calculated CO_2 + H_2 partial pressure at the reaction temperatures. This partial pressure was calculated by subtracting the vapour pressure of 1-butanol from the total reactor pressure. Note that the partial pressure of the reacting gases is significantly reduced with increasing reactor temperature. This reduction in partial pressure is suggested to be the cause of the observed decrease in methanol productivity (i.e. reaction rate) with increasing temperature.

Under otherwise identical conditions, the reaction rate would usually be expected to show an increase with increasing temperature. It appears that operating this liquid-phase reaction at lower temperatures might be beneficial owing to not only the more favourable equilibrium but also the higher reactant pressure resulting in a faster reaction rate. In practical terms, operation at higher temperature would still entail compression of the reactant gases to the total reactor pressure, but a fraction of the total pressure would be wasted by the vapour pressure of the solvent.

This was further investigated by adjusting the total reaction pressure to maintain constant CO_2 + H_2 partial pressure at different reaction temperatures. Figure 10.5a shows the results for the reaction performed in 2-butanol at temperatures of 160–200 °C. A significant increase in productivity is found with increasing temperature under the otherwise identical conditions. Figure 10.5b shows the effect of varying the gas partial pressure while maintaining a constant reaction temperature. A significant increase in the productivity is found with increasing pressure.

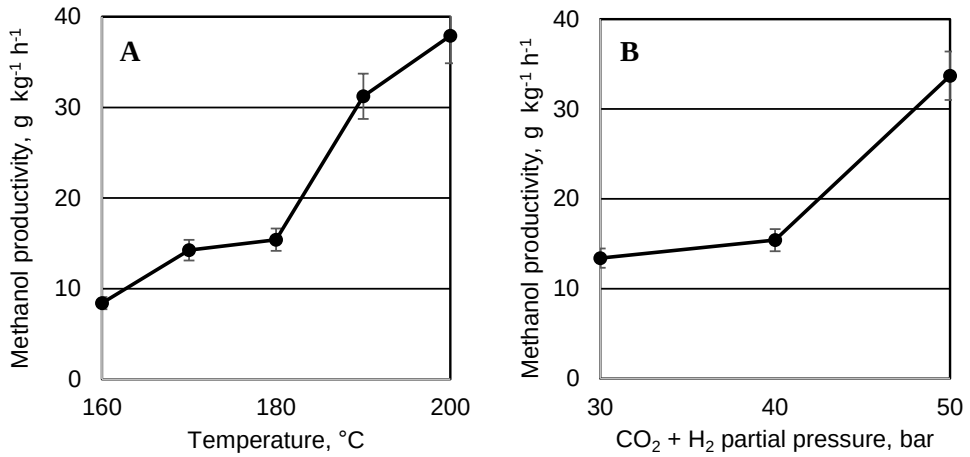

Figure 10.5 Variation of methanol productivity with a) temperature at constant $CO_2 + H_2$ partial pressure (40 bar) and b) $CO_2 + H_2$ partial pressure at constant temperature (180 °C). 10 g of Cu/ZnO catalyst in 200 ml of 2-butanol. Feed gas: CO_2:H_2 = 1:3. Reaction time: 6 h.

10.3.2 **Water removal by adsorption**

Next, the removal of water from the reaction mixture using a molecular sieve adsorbent was investigated. First, the limiting effect of water on the alcohol-promoted methanol synthesis process was confirmed by an experiment where 1.4 mol/dm^3 of water was added to 2-butanol prior to reaction at 180 °C and 60 bar. This amount of water is slightly above the highest concentrations of water found in other experiments (Figure 10.3 provides an example). The methanol productivity was approximately 74% lower than a comparable base experiment with no water added. The water-added experiment showed a relatively stable concentration of water close to the initial concentration. Apparently, the initial water concentration is close to the equilibrium water concentration under the reaction conditions.

The effect of adding the absorbent on water concentration and methanol productivity was then studied by varying the relative amount of catalyst and absorbent while maintaining a constant mass (50 g) of solids in the reactor. The results are shown in Figure 10.6. The results from a base experiment with 20 g of catalyst and no adsorbent and a preliminary test with 20 g of catalysts and 20 g of unground (pelletised) adsorbent are included.

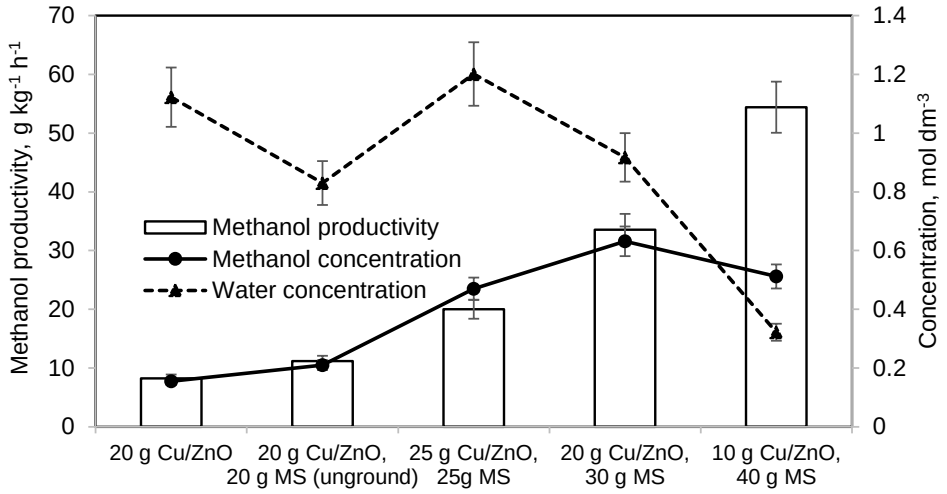

Figure 10.6 Effect of catalyst and adsorbent (MS, molecular sieve) mass on the concentration of methanol and water and the methanol productivity in 2-butanol. Temperature: 180 °C, feed gas CO_2:H_2 = 1:3, total pressure: 60 bar, reaction time: 6 h.

Note that adding the adsorbent in the unground state results in a noticeable but limited impact on the methanol productivity. The water concentration decreases, showing that adsorption takes place but does not result in a significant increase in the methanol production rate. A more significant improvement is found with the use of ground (150–300 µm) absorbent, which implies that the adsorption of water is significantly limited by diffusion when using unground adsorbent. Compared with the base case with 20 g of catalyst, the addition of 30 g of adsorbent results in increased methanol productivity by over 300%.

Moreover, the water concentration is not significantly decreased when the amount of adsorbent is 30 g or less. The data presented is collected following the full reaction time of 6 h. It appears that the water concentration is suppressed during the earlier stages of the reactor, allowing methanol synthesis to proceed faster while the water formed as by-product is effectively adsorbed. Towards the end of the reaction time, water still builds up to concentration levels of the same magnitude as those found without the adsorbent.

This pattern is illustrated by the methanol and water concentration profiles collected during the reaction. Figure 10.7 shows this data from the experiment with 20 g of catalyst and 30 g of molecular sieve. Similar results were found in other experiments with the added adsorbent. Increase in the water concentration during the experiment might imply gradual saturation of the water-adsorbing capacity of the adsorbent. As a result, the formation of methanol would likely be slower if the reaction were to be continued after 6 h.

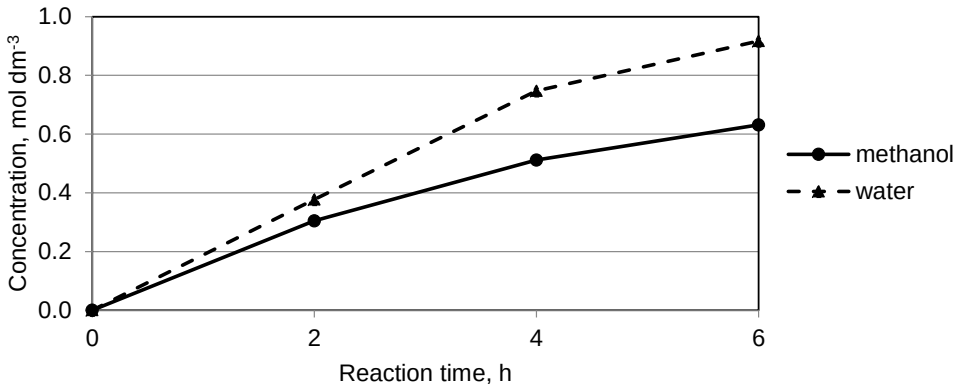

Figure 10.7 Methanol and water concentration during reaction with 20 g of catalyst and 20 g of adsorbent in 2-butanol. Temperature: 180 °C, feed gas CO_2:H_2 = 1:3, total pressure: 60 bar.

The situation is different when the relative amount of adsorbent to catalyst is further increased. Data from the experiment with 40 g of adsorbent and 10 g of catalyst shows a significant decrease in the water concentration after the reaction time and a significant increase in the methanol productivity (Figure 10.6). The increased amount of adsorbent can more effectively limit the build-up of water during the reaction time. In fact, the concentration of water remains below that of methanol throughout the experiment (Figure 10.8).

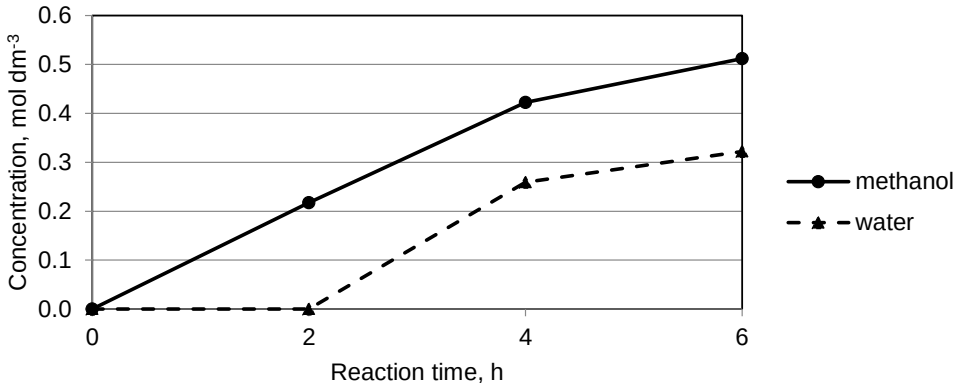

Figure 10.8 Methanol and water concentration during reaction with 10 g of catalyst and 40 g of adsorbent in 2-butanol. Temperature: 180 °C, feed gas CO_2:H_2 = 1:3, total pressure: 60 bar.

As a result of the suppressed water concentration, methanol synthesis proceeds more efficiently, leading to higher specific productivity per catalyst mass. The amount of catalyst is more efficiently utilised. However, owing to the reduced catalyst mass compared with the other experiments, the final methanol concentration remains below that found with 20 g of adsorbent and 20 g of catalyst. This situation would likely be reversed if the reaction time were extended, as methanol formation at increased rate would continue after 6 h of reaction owing to the limited water concentration until the adsorbent begins to be saturated.

Two key findings arise from the above results. First, a clear inverse relationship is observed between methanol productivity and water concentration. Limiting the amount of water present clearly increases the specific rate of methanol synthesis. This correlates with previous results presented for gas-phase methanol synthesis, especially for CO_2 hydrogenation. However, such findings have apparently not been reported for low-temperature methanol synthesis in solvent-based systems. The values of methanol productivity measured with any combination of (ground) adsorbent and catalyst are significantly high compared with previously published values for comparable reaction systems.

Second, the water concentration can be controlled by adding solid absorbents with a capability to selectivity adsorb water from the reaction solution. The adsorbent used here, a zeolite molecular sieve with pore size of 3 Å, appears to be a promising candidate. The adsorbent can effectively limit the water concentration and the co-adsorption of methanol does not seem to take place, implying good selectivity.

Note that the present results are obtained during a limited reaction time and low CO_2 conversion conditions. Even then, progressive saturation of the adsorbent appears to take place when the adsorbent is added at a mass similar to that of the catalyst. The amount of water formed when approaching equilibrium in methanol synthesis would be higher compared to the present conditions. Based on these preliminary findings, the mass of the adsorbent in relation to the catalyst should be high under practical operating conditions. With regard to the reaction conditions, further lowering of the reaction temperature would likely be favourable for sorption-enhanced methanol synthesis, as the water-adsorbing capacity of the adsorbent is increased at a lower temperature. In either case, adjusting the relative amounts of adsorbent and catalyst would pose an important optimisation problem.

Furthermore, this study does not consider the regeneration of the absorbent. Regeneration would entail adsorbent treatment under elevated temperature and/or moisture-free gas atmospheres. Developing a practical process for sorption-enhanced, liquid-phase methanol synthesis would be an interesting design challenge, including non-steady state adsorption and regeneration cycles combined with solids handling involving both the adsorbent and catalyst.

10.3.3 **Dual catalysts**

A combination of copper chromite (CuCr) and Cu/ZnO catalysts was used to investigate the dual, or cascade, catalysis concept in alcohol-promoted CO_2 hydrogenation to methanol. A series of experiments was performed in 2-butanol solvent at 180 °C and 60 bar of total pressure, which corresponds to a $CO_2 + H_2$ partial pressure of 50.1 bar. The ratio of the two catalysts was varied with 20 g of Cu/ZnO combined with 10 g of CuCr, and vice versa. The results were then compared with those of a base experiment with 20 g of Cu/ZnO and no CuCr under otherwise identical conditions. The results are shown in Figure 10.9.

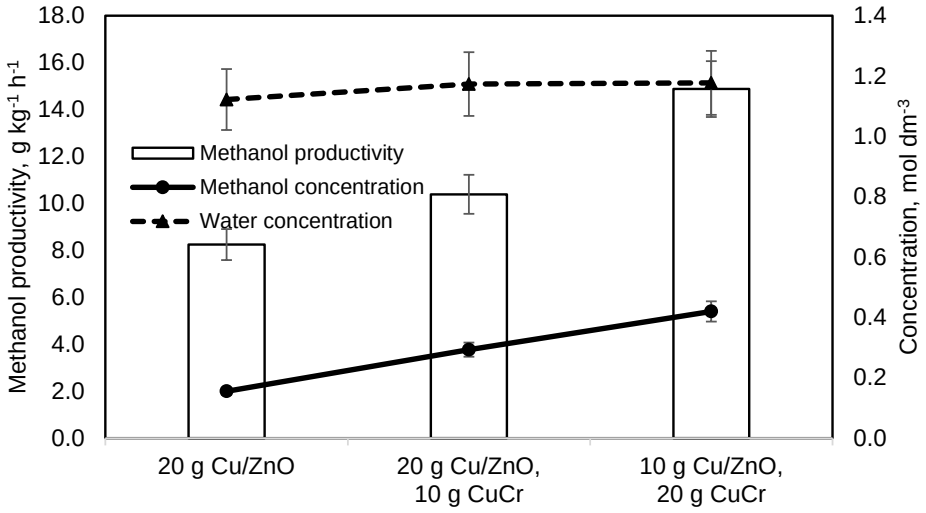

Figure 10.9 The effect of varied mass of Cu/ZnO and CuCr catalysts on the methanol and water concentration and the methanol productivity in 2-butanol. Reaction time: 6 h. Temperature: 180 °C, feed gas CO_2:H_2 = 1:3, total pressure: 60 bar.

An increase in both methanol concentration and catalyst-mass-specific methanol productivity is found by the addition of the copper chromite catalyst. Thus, methanol formation is clearly promoted by the use of the combined catalysts. Two alternative explanations (at least) could be provided for this promoting effect. The targeted synergistic effect – that is, the high activity of the two catalysts in two separate reaction steps – might be taking place, leading to an optimised performance in the overall reaction of methanol synthesis. Support for this explanation can be provided by separate experiments using only copper chromite and experiments with prior addition of the suspected formate ester intermediates. However, such experiments were not performed in the present study.

Alternatively, the copper chromite catalyst might itself be more active than the Cu/ZnO catalyst in the overall reaction. The latter could also be supported or ruled out by a

separate experiment using only copper chromite. Such experiments have been reported in the literature and do not support this explanation. Both Chen et al. [274] and Fan et al. [295] reported a higher activity of Cu/ZnO than that of copper chromite in CO_2 hydrogenation to methanol in the presence of alcohol. Chen et al. [274] clearly demonstrated the different activity of these two catalysts in the two reaction steps. Based on these findings, it is strongly suspected that this type of synergistic effect is also witnessed in our experiments.

The water concentration is unchanged between the experiments using different catalyst masses (Figure 10.9). Both the catalysts seem to be active for CO formation via RWGS [295, 274], and the identical water concentrations may suggest that RWGS proceeds similarly during each of the present experiments. The final water concentration is similar to those found in other experiments discussed above (e.g. Figure 10.3). It thus appears that this concentration of water corresponds to the equilibrium of RWGS under the reaction conditions.

As the rate of methanol synthesis increases when the two catalysts are combined, the apparent selectivity of methanol over CO (estimated by the ratio of methanol to water) is increased. This conclusion assumes that CO is not directly converted into methanol under the present conditions [257, 185]. However, as discussed above (Section 10.3.1), this only represents the selectivity after limited CO_2 conversion observed during 6 h of reaction, and the selectivity under equilibrium-limited conditions would be significantly in favour of methanol, regardless of the relative rates of RWGS and methanol synthesis on the two catalysts.

The above findings show that the rate of methanol synthesis via CO_2 hydrogenation in alcoholic solvents can be improved using two different catalysts in combination. The combination of Cu/ZnO and copper chromite presents a potentially effective catalyst combination. The exact nature of the observed promoting effect is not confirmed by the present experiments, but literature data suggest a synergistic effect based on the distinct activity of the two catalysts in separate steps of the overall reaction. It is found that the methanol productivity is also affected by the relative amount of the two catalysts, suggesting an optimisation issue in a practical process.

The values of methanol productivity found using the combined catalysts are high compared with the previous results in the literature but not as high as those observed with the use of water-selective adsorbent (Figure 10.6). However, compared with that approach, the combination of separate catalysts containing similar active components and presenting similar mechanical form and properties does not appear as challenging to apply in a practical methanol synthesis process.

10.3.4 **Catalyst characterization**

Structural features of the Cu/ZnO catalysts were investigated before and after reaction in 1-butanol at 180 °C by means of XRD and SEM-EDS. The X-ray diffractograms of the

catalyst as supplied in the calcined form, reduced form and following the methanol synthesis reaction are presented in Figure 10.10. The same batch of catalyst was analysed in the calcined form and reduced form, whereas the reduced catalyst was separately prepared and analysed.

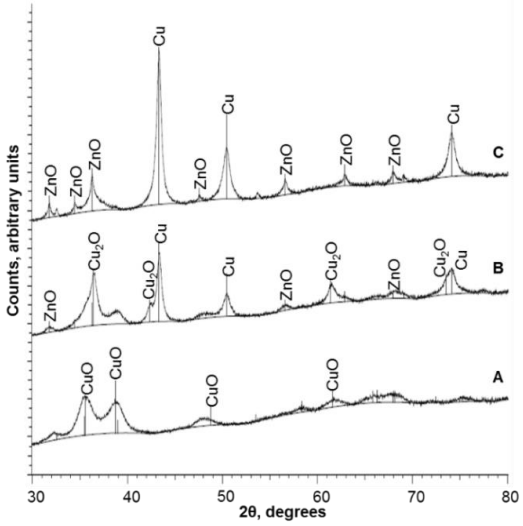

Figure 10.10 X-ray diffractograms of the Cu/ZnO catalyst in the calcined form (A), reduced form (B) and following methanol synthesis (C). Reaction in 1-butanol, temperature: 180 °C, feed gas CO_2:H_2 = 1:3, total pressure: 60 bar. Reaction time: 6 h.

The calcined catalyst is largely amorphous, showing a minor pattern corresponding to copper(II)oxide (CuO), whereas the reduced catalyst presents a pattern consistent with crystalline copper(I)oxide (Cu_2O) and metallic Cu. Weak features of crystalline ZnO are also identifiable in the reduced catalyst. These patterns are typical for unreduced and reduced Cu/ZnO catalysts [184, 296].

The reduction of Cu has been shown to proceed stepwise from CuO via Cu_2O to Cu metal [297]. The significant presence of Cu_2O in the reduced catalyst (Figure 10.10) suggests incomplete reduction of the catalyst in the present study. This might be explained by the insufficient reduction time or temperature or the otherwise non-optimal reduction conditions (i.e. gas–solid contact and gas flow). Alternatively, the catalyst may have been partly re-oxidised during transfer from the reactor into the XRD equipment.

Following methanol synthesis, the catalyst only shows XRD patterns consistent with metallic Cu and ZnO. It appears that the ongoing reduction of the catalyst has taken place under the reaction conditions, and the catalyst seems to be maintained in an active state after the reaction time. This finding is also consistent with previous studies identifying structural changes in the catalysts under reaction conditions [180].

The more clearly defined peaks corresponding to ZnO in the used catalyst compared with the reduced catalyst may also indicate crystallisation of ZnO during the reaction. Previously, the crystallisation of ZnO has been found to lead to the loss of reactive Cu/ZnO interfaces on the catalyst surface, resulting in the initial deactivation of the catalyst [298]. This phenomenon is supported by the SEM-EDS elemental maps of Cu and Zn in the calcined and used catalyst, presented in Figure 10.11. A relatively homogeneous distribution of both Cu and Zn is found in the unused catalyst, whereas the used catalyst presents some degree of segregation of Cu and Zn. Particularly, distinct areas with high Zn content can be identified in the used catalyst.

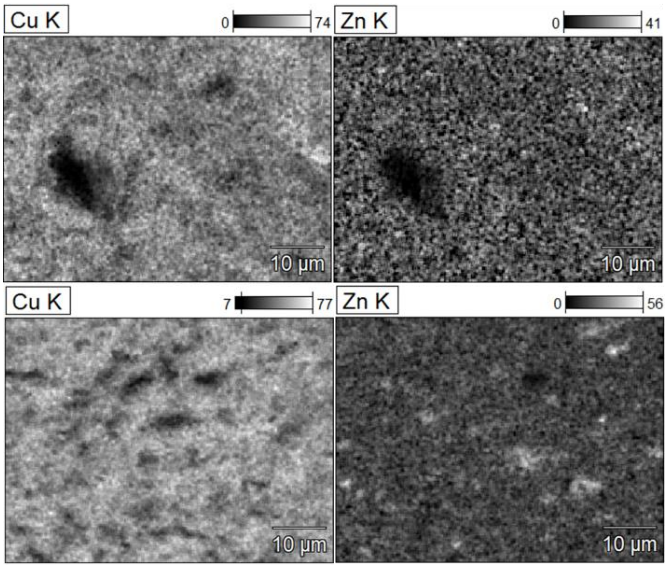

Figure 10.11 SEM-EDS elemental maps of Cu and Zn in the calcined Cu/ZnO catalyst (upper part) and the catalyst following methanol synthesis (lower part). Reaction in 1-butanol, temperature: 180 °C, feed gas CO_2:H_2 = 1:3, total pressure: 60 bar. Reaction time: 6 h. Composition scales in weight percent.

SEM images of the used catalyst, presented in Figure 10.12, provide further insights. Micrometre-scale crystals, identified as ZnO by a concurrent EDS analysis (not shown), can be identified. Such features were not observed in the calcined catalyst, suggesting that the agglomeration and crystallisation of ZnO has taken place during the reaction. This could act as a potential deactivation mechanism for the catalyst; however, this can only be proven by long-term catalyst stability tests combined with correlation of the methanol synthesis activity with the observed degree of ZnO crystallisation during reaction.

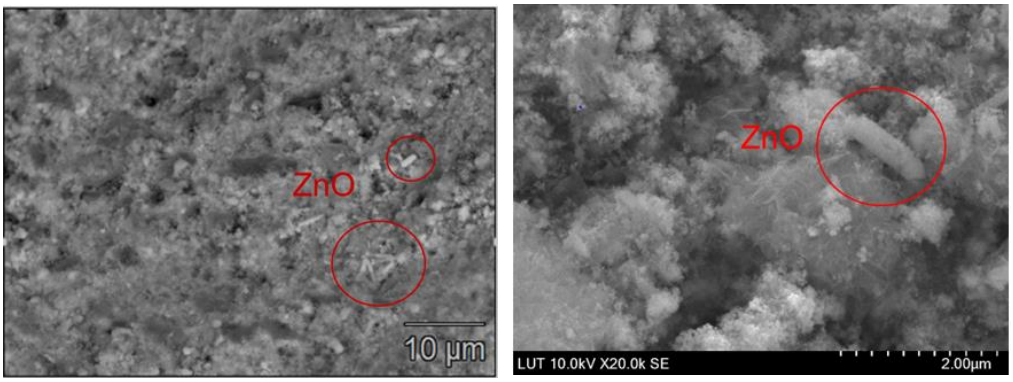

Figure 10.12 SEM micrographs of the Cu/ZnO catalyst following methanol synthesis in 1-butanol. Temperature: 180 °C, feed gas CO_2:H_2 = 1:3, total pressure: 60 bar. Reaction time: 6 h. ZnO crystals are highlighted.

The stability of Cu/ZnO catalysts during the alcohol-promoted methanol synthesis reaction has been previously studied by Reubroycharoen et al. [263], who reported stable performance during 40 h of continuous reaction at 170 °C, and by Jeong et al. [299], who found no decline in activity during 60 h of reaction at 150 °C. The latter study also presented XRD profiles of the catalyst prior and after reaction. In contrast to the present study, no changes in the crystalline structure were found. The different results could be explained by different feed gas composition, as the referenced studies used CO-rich syngas instead of CO_2 and H_2 used here. Because methanol synthesis from CO_2 and H_2 results in increased water concentration, it is suggested that the observed changes in the catalyst structure might be caused or accelerated by the significant amount of water present. However, confirmation of this effect would require further studies correlating the water concentration with the observed changes in the catalyst structure.

10.3.5 Mass and energy balances

Table 10.2 compares the mass balances of the assessed processes. In the table, methanol yield is calculated as the ratio of the mass flow of methanol product to the theoretical mass flow at 100% yield based on the stoichiometric feed of CO_2 and hydrogen. The methanol yield is reduced by losses of methanol, CO_2 and hydrogen within waste streams removed from the process. These streams consist of a purge from the unreacted gas recycle stream (1% in the gas-phase process and 0.5% in the liquid-phase processes), wastewater removed by distillation and gases removed from flash separation stages. In addition, an additional purge (0.5%) is removed from the solvent recycle in the liquid-phase processes.

Table 10.2 Comparison of mass balances of the alternative methanol synthesis processes.

Flow, kg/h	Gas-phase	2-butanol	1-butanol	1-pentanol	1-hexanol	1-pentanol + decant
Hydrogen in	533	533	533	533	533	533
CO_2 in	3882	3882	3882	3882	3882	3882
Methanol out	2272	2452	2560	2588	2540	2586
Methanol losses	52	161	57	65	102	63
CO_2 losses	560	289	231	236	251	242
Hydrogen losses	89	40	32	32	35	33
CO_2 conversion per pass	21%	86%	88%	87%	86%	86%
Methanol yield	81%	87%	92%	92%	90%	92%
Solvent loss, kg/h	-	3526	1727	1026	609	190
Solvent loss	-	13%	7%	4%	2%	1%

The methanol yield in the liquid-phase processes is higher than that in the gas-phase processes. This difference is largely explained by a higher conversion in the reactor in the liquid-phase processes, resulting in a decreased amount of recycled and purged gases. The per-pass CO_2 conversion in the liquid-phase processes is above 85%, whereas that in the gas-phase process is approximately 21%. The conversion in the liquid-phase processes is well above that of the single-phase equilibrium conversion under the reaction conditions [167]. Thus, the conversion seems to be increased by the effect of the phase distribution of the reactants and products in the reactor. The solubility of water and methanol in the solvent might further drive the conversion of the gas-phase reactants, which presents a potential advantage for a well-designed liquid-phase reactor. However, experimental confirmation of this effect would be in order owing to the uncertainties involved with the prediction of the phase equilibrium under high-pressure conditions.

A major difficulty in the liquid-phase processes is caused by the separation of the alcoholic solvent from the liquid reaction products. All the alcohols form azeotropic mixtures with water, and the complete separation of these components is thus not possible via conventional distillation. Thus, significant amount of solvent is lost as part of the wastewater stream removed after distillation. In Table 10.2, the fractional solvent loss represents the ratio of the solvent mass flow removed from the process to the solvent mass flow entering the reactor. The fraction of solvent lost varies depending on the molar composition of the alcohol–water azeotrope. Alcohols with higher carbon numbers form azeotropes with lower alcohol content, resulting in smaller solvent loss. A more detailed discussion of the azeotropes is presented in Publication IV.

The 1-pentanol + decant process utilised decantation to separate two separate liquid phases to improve solvent recovery compared with the base 1-pentanol process. This

scheme is explained in detail in Publication IV. The limited solubility of higher alcohols in water allows the separation of water- and alcohol-rich phases from the azeotropic mixture. As a result, the solvent recovery is much improved, and most of the solvent losses remaining in the 1-pentanol + decant process are from the solvent recycle purge and not from the wastewater stream.

Compared with the gas-phase process, the presence of the solvent in large quantities in the liquid-phase processes leads to a significant increase in the amount of energy required for distillation. This is shown in the process energy balances summarised in Table 10.3 in terms of the thermal and electric duties and specific energy consumption per ton of methanol product. In the gas-phase process, all process heating is covered by heat integration utilising the reaction heat. In contrast, all liquid-phase processes require external heating by means of steam. Use of alcohols with higher carbon number and higher boiling point decreases the heat requirement owing to their easier separation from methanol and water. A particularly high energy need is found with 2-butanol with a boiling point of 99 °C.

Table 10.3 Thermal and electric duties and specific energy consumption in the alternative CO_2 hydrogenation to methanol processes.

Duty, kW	**Gas-phase**	**2-butanol**	**1-butanol**	**1-pentanol**	**1-hexanol**	**1-pentanol + decant**
Hot utility	0	11379	8250	4580	5026	4617
Cold utility	2969	14519	11509	7847	8340	7904
Heat integrated	5245	4307	3725	4077	4586	4137
Electricity	502	559	546	556	573	558
Energy, GJ/t MeOH						
Thermal	0.0	0.0	16.7	11.6	6.4	7.1
Electricity	1.0	0.8	0.8	0.8	0.8	0.8

The higher per-pass conversion in the liquid-phase processes reduces the amount of recycled gases, thus decreasing the electric power required by the recycle compressor. However, this reduction is offset by the addition of the solvent recycle pump. As a result, the electricity consumption is higher in the liquid-phase processes than in the gas-phase process. The electricity consumption reported in Table 10.3 does not include the electricity used in water electrolysis, which is included in the cost of hydrogen.

10.3.6 Environmental analysis

The CO_2 and water balances of the alternative processes are summarized in Table 10.4. The CO_2 balance of all processes is negative, meaning that the amount of CO_2 consumed in methanol synthesis is higher than the amount released from the process and indirectly

emitted from steam generation. Because the gas-phase process does not require steam, the highest net CO_2 input is found for this process.

Table 10.4 CO_2 and water balances of the alternative CO_2 hydrogenation to methanol processes.

	Gas-phase	**2-butanol**	**1-butanol**	**1-pentanol**	**1-hexanol**	**1-pentanol + decant**
CO_2 balance, kg/h						
Inlet streams	3882	3882	3882	3882	3882	3882
Outlet streams	560	289	231	236	251	242
Steam generation using natural gas	0	3150	2331	1295	1648	1306
Balance	-3322	-443	-1321	-2351	-1983	-2334
Water balance						
Cooling water consumption, t/h	361	402	490	557	626	552
Wastewater generation, kg/h	1374	4924	3098	2382	1963	1534
Alcohol in wastewater, w-%*	0.3%	68%	52%	37%	23%	3%

* Methanol in the gas-phase process, solvent in the liquid-phase processes

The environmental impact of cooling water consumption is not considered particularly significant, assuming that water is readily available and the used water (25 °C) can be released without treatment. The solvent/water waste streams constitute mixtures of water and the solvent alcohol removed from the process. Ideally, nearly pure water would be removed, requiring minimal waste treatment. However, owing to the alcohol–water azeotropes, large amounts of alcohols are necessarily contained in these streams.

The amount of alcohol varies depending on the azeotropic composition, with the alcohol content decreasing with higher carbon number of the alcohol. The amount of liquid waste released also correspondingly decreases. This, together with the corresponding CO_2 balances, suggests that the use of alcohols with higher carbon number would be environmentally favourable in this type of process. The 1-pentanol + decant process shows a significant reduction in the amount of alcohol released compared with the base 1-pentanol process. The use of decantation or other, more complex separation methods to

overcome the azeotropes seems to be necessary to avoid excessive release of alcohol waste.

The methanol synthesis processes are assumed to use grid electricity, and the environmental impact would depend on the sources of electricity supporting the grid at a particular time and location. The annual electricity consumption in the processes (Table 10.3) ranges from 4.0 to 4.6 GWh. Assuming a grid carbon intensity of 170 g CO_2/kWh (representative of the Finnish grid in 2018), the corresponding indirect CO_2 emissions would range from 85 to 97 kg/h. These emissions would be insignificant compared with the process CO_2 balances presented in Table 10.4.

10.3.7 **Economic analysis**

The overall methanol production cost comprises the variable and fixed operating costs and the annualised capital investment. Figure 10.13 compares the production cost of the alternative processes. A detailed overview of the capital and operating costs is given in the Supplementary material to Publication IV. The lowest production cost is found with the gas-phase process (1008 €/t). The 1-pentanol + decant process with improved solvent recovery shows a production cost almost as low (1068 €/t) as the gas-phase process. The cost of the other liquid-phase processes is inflated by the excessive loss of solvent, even when a relatively low cost of solvent (500 €/t) is assumed for all alcohols. The effective solvent recovery is thus necessary both from the environmental (Section 10.3.6) and economic viewpoints. The highest production cost is found with 2-butanol (1973 €/t) owing to the highest solvent loss and most energy-intensive separation. The production cost is decreased using the higher-boiling 1-pentanol or 1-hexanol.

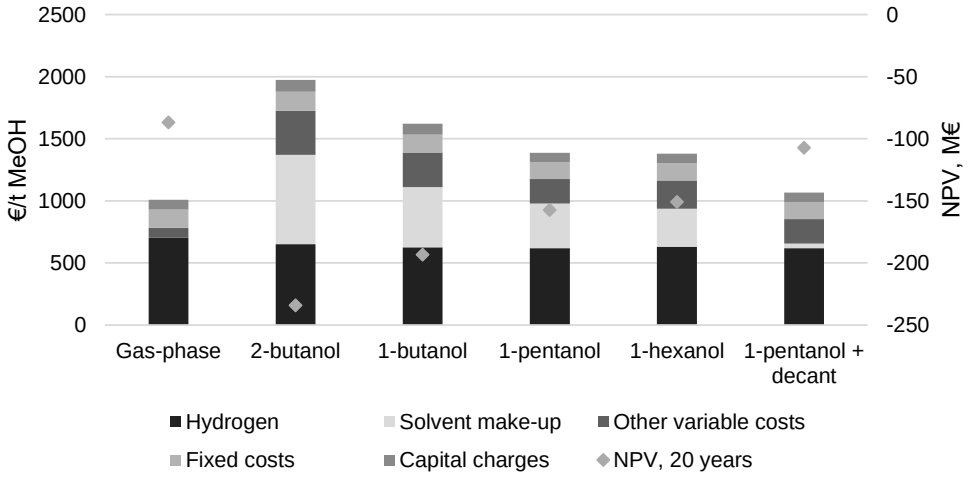

Figure 10.13 Methanol production cost and net present value (NPV) of the alternative CO_2 hydrogenation processes.

Figure 10.13 shows the calculated NPV for each process option over the assumed plant lifetime of 20 years. The NPV for each process is negative, and no process appears economically feasible under the present conditions and assumptions. In accordance with the corresponding production costs, the highest NPV is found with the gas-phase process (−86.7 M€) and lowest with the 2-butanol process (−234.2 M€). The NPV of the most feasible liquid-phase process (1-pentanol + decant) is 24% lower than that of the gas-phase process.

According to Figure 10.13, the capital costs (represented as the annual capital charges) are insignificant compared with the operating costs. The contribution of different types of equipment to the capital costs is detailed in Publication IV. In summary, compressors constitute the largest fraction of installed equipment costs.

Fixed operating costs are also relatively small compared with the variable operating costs. In all processes, the cost of hydrogen constitutes the main variable cost, whereas the cost of CO_2 is comparatively insignificant. Figure 10.14 breaks down the variable costs in the gas-phase process, the base 1-pentanol process and the 1-pentanol + decant process with improved solvent recovery. In these respective processes, the cost of hydrogen constitutes 70%, 45% and 58% of the total methanol production cost. In the base 1-pentanol process, cost of solvent make-up is large, but this cost is effectively minimised in the 1-pentanol + decant process, where the solvent is more effectively recovered. Steam costs are also significant in the liquid-phase processes owing to the requirement of external heating for distillation.

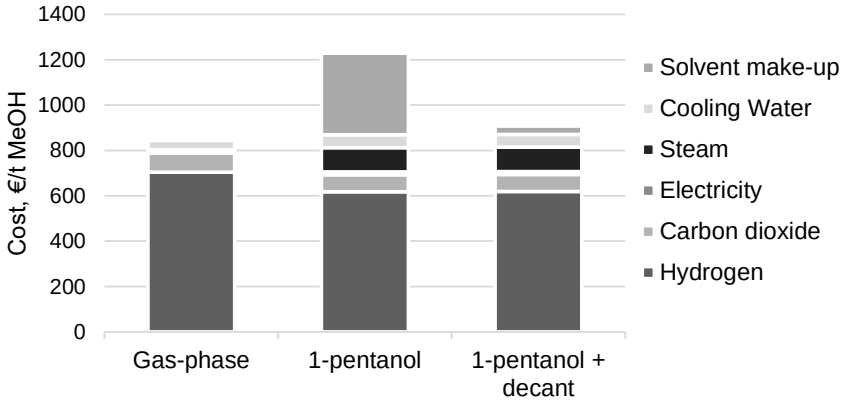

Figure 10.14 Distribution of the variable production costs in three CO_2 hydrogenation to methanol processes: the gas-phase process, the liquid-phase process with 1-pentanol solvent, and the liquid-phase process with 1-pentanol solvent and solvent recovery by decantation.

10.3.8 **Sensitivity analysis**

The effect of selected key variables on the economic feasibility of the alternative methanol synthesis processes was assessed by sensitivity analysis. Sensitivity analysis was performed in terms of the overall production cost, and the NPV was not considered. The cost of hydrogen, a major fraction of the overall cost, was included in the analysis, and the impact of the CO_2 cost was assessed. In addition, the variables considered included the price for by-product oxygen and the total capital investment. The gas-phase process and 1-pentanol + decant process were selected for the sensitivity analysis, the latter presenting the most feasible liquid-phase process. Solvent cost was considered as an additional variable for the 1-pentanol + decant process. The results of the analysis are shown in Figure 10.15 for the gas-phase process and in Figure 10.16 for the 1-pentanol + decant process.

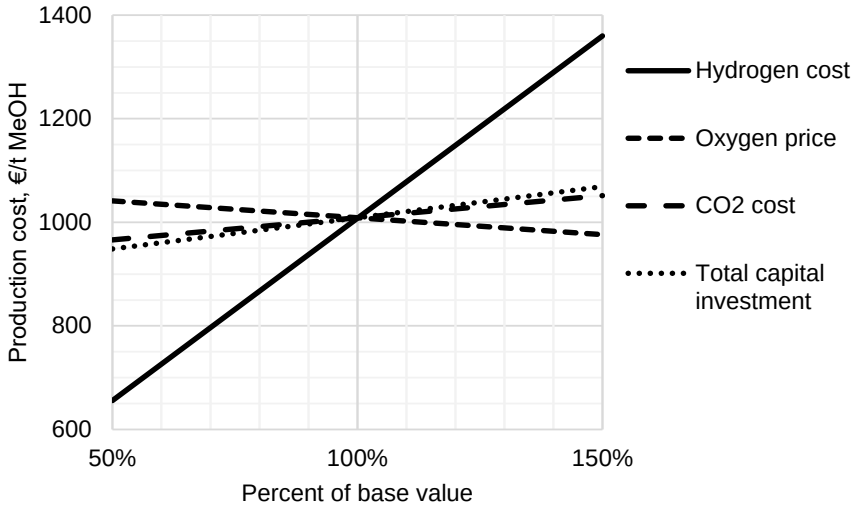

Figure 10.15 Sensitivity of methanol production cost to variation in selected parameters in the gas-phase methanol synthesis process. Base values: hydrogen cost, 3000 €/t; oxygen price, 70 €/t; CO_2 cost, 50 €/t; total capital investment 18.0 M€.

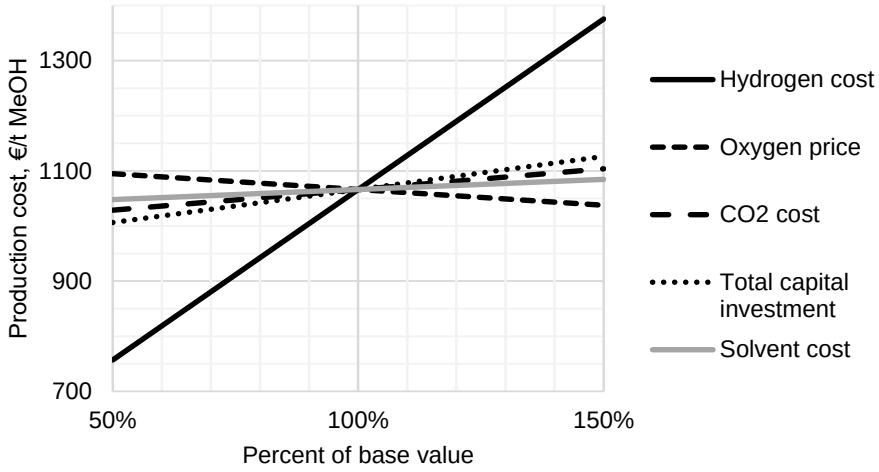

Figure 10.16 Sensitivity of methanol production cost to variation in selected parameters in the liquid-phase methanol synthesis process with 1-pentanol solvent and improved solvent recovery. Base values: hydrogen cost, 3000 €/t; oxygen price, 70 €/t; CO_2 cost, 50 €/t; total capital investment, 19.8 M€; solvent cost, 500 €/t.

Hydrogen cost clearly has the most significant impact on the overall production cost in both processes. Future decreases in the renewable hydrogen cost are expected with the development of electrolyser technology and decreasing renewable electricity costs.

Significant reduction (i.e. more than 50%) in hydrogen cost would be required to make the processes competitive at present methanol prices. For instance, the required hydrogen cost to reach a methanol production cost of 400 €/t with the gas-phase process would be 400 €/t. With the 1-pentanol + decant process, this threshold is not reached even at zero hydrogen cost owing to the higher non-hydrogen costs of the process.

The impact of oxygen cost is found to be more significant than that of CO_2 cost. Sales of oxygen at a reasonably high price would be an important contributor to the overall economics of a renewable energy-based methanol synthesis process. As is the case with renewable hydrogen, the cost of captured CO_2 would also be expected to decrease with the development in capture technology. However, this development seems relatively insignificant to the process economic compared with the developments in hydrogen generation.

An additional sensitivity analysis was performed in terms of the reactor per-pass conversion in the 1-pentanol + decant process. This analysis was performed by developing a new process model with the conversion for CO_2 hydrogenation to methanol limited to 75%. The results are shown in Table 10.5.

Table 10.5 The effect of the reactor per-pass conversion on the mass balance and methanol production cost of the liquid-phase methanol synthesis process with 1-pentanol solvent and improved solvent recovery.

CO_2 conversion per pass	**86%**	**75%**
Methanol yield	92%	84%
Solvent loss, kg/h	190	349
Solvent loss	0.7%	0.6%
Production cost, €/t MeOH	1068	1178

With decreased conversion, a larger amount of unreacted gases are recycled and purged from the process, which results in decreased methanol yield. As the total gas flow (fresh + recycled gas) entering the reactor is increased, the amount of circulated solvent also has to be increased to maintain the volumetric ratio of liquid to gas in the reactor. As a result, the amount of solvent purged from the liquid recycle is increased, and the production cost is increased owing to the increased cost of solvent make-up. In addition, the capital and operating costs involved with solvent circulation are increased. It is evident that the feasibility of the liquid-phase process is dependent on maximising the per-pass conversion.

10.4 Summary and outlook

The main advantage of the liquid-phase methanol synthesis process using alcoholic solvents is the reduced reaction temperature that allows higher conversion in a single reactor pass. According to the process modelling performed in this study, the conversion

can even be increased beyond the single-phase equilibrium owing to the favourable distribution of reactants and products in the gas/vapour and liquid phases. However, experimental verification of this effect would be in order owing to the uncertainties involved with the prediction of phase equilibrium under high-pressure conditions.

In the present study, the liquid-phase processes were modelled based on equilibrium reaction models; this is in contrast to the more rigorous kinetics-based modelling of the gas-phase process. In practice, the reaction rate at reduced temperature in the liquid-phase processes should be of similar magnitude to the reaction rate in the gas-phase process to avoid excessive amounts of catalyst and reactor size. As discussed in the literature review (Section 8.1), catalyst systems with high activity have not been reported for the alcohol-promoted reaction.

Improvement in methanol productivity was pursued by means of a cascade catalytic system combining a Cu/ZnO catalyst and a copper chromite catalyst and by water removal using a molecular sieve adsorbent. Both of these approaches led to improved methanol productivity, with the use of water-selective adsorbent showing more significant impact. The combination of 10 g of catalyst with 40 g of absorbent resulted in methanol productivity of over 50 g/kg h^{-1}, which is higher than the value previously reported for the alcohol-promoted reaction route but still significantly below the values reported for gas-phase CO_2 hydrogenation to methanol (Table 7.1). A clear inverse relationship between methanol productivity and water concentration was observed, highlighting the inhibiting effect of water on methanol synthesis. The present investigation was conducted at low conversion levels and did not consider the regeneration of the absorbent. Operation at industrially relevant, high-conversion conditions would entail challenges in terms of the absorption capacity of the absorbent; moreover, a practical reactor and process design must incorporate the cyclical adsorption/desorption process.

The practical benefit of higher per-pass conversion is the reduction in the amount of gases recycled in the reactor loop. Assuming that a constant fraction of the recycled gases is purged, this leads to an increased overall methanol yield through the process as a smaller amount of gases are purged. In addition, the capital and operating costs related to the gas recycle and compression are reduced. However, in the present study, the economic benefit involved is found insignificant because these costs form a minor fraction of the overall production cost.

To achieve significant benefits in process simplicity and economics, full single-pass conversion by means of decreasing the temperature, increasing the pressure and/or utilising phase separation effects and condensation of reaction products should be aimed for. Based on a thermodynamic analysis reported by Stangeland et al. [167], full conversion could be achieved at temperatures as low as 150 °C at 50 bar in a multi-phase system involving product condensation. To facilitate a feasible liquid-phase process, a key research area would be the development of catalyst/solvent systems capable of sufficiently high reaction rates at reduced temperatures. Besides activity, issues such as catalyst and solvent stability and side reactions should be considered.

The downside of introducing the co-catalytic solvents is the added complexity of the overall process. Compared with the relatively simple tubular reactors used in conventional methanol synthesis, reactor design is complicated for three-phase systems utilising volatile alcoholic solvents. Downstream from the reactor, the liquid reaction products are contained in a mixture with the solvent, presenting increased demands on product separation and purification. The capital and energy intensity of the separation stage is therefore increased compared with conventional processes, as found in the results of the present study. Further complication is caused by the formation of azeotropic mixtures between alcohols and water. Because these mixtures cannot be separated by simple distillation, a feasible process should employ alternative means of separation to allow effective recovery of the solvent alcohol.

The energy and cost effectiveness can be improved using higher-boiling alcohols. Ideally, even solvents with higher boiling points, such as long-chain or complex alcohols, might be used to allow the selective evaporation of methanol and water from the reactor. However, research (Section 8.1) has shown that the catalytic activity in low-temperature methanol synthesis is maximised using short-chain alcohols such as butanol and that use of alcohols with significantly higher boiling points does not appear feasible.

Based on the present analysis, the liquid-phase processes in their current design do not appear competitive with the more conventional gas-phase process. The higher production cost for the liquid-phase processes is explained by the more complex and energy-intensive separation stage. The present study suggested a preliminary design for a liquid-phase methanol synthesis process that could likely be improved and optimised to reduce the production cost. The production cost for the gas-phase process (1080 €/t) is consistent with that obtained in previous studies (Section 7.2) and suggests that power-to-methanol processes are not presently competitive with fossil-based methanol processes. The largest cost component in both the gas-phase and liquid-phase processes is the cost of renewable hydrogen. Development of electrolysis technology with improved efficiency and lower capital costs together with the reduction in the cost of renewable electricity are necessary to improve the economic performance of power-to-methanol processes.

11 Conclusion and suggestions for future work

In this work, intensified approaches to CO_2 capture and methanol synthesis were investigated in the context of CO_2 utilisation and energy storage. These approaches included absorption-based CO_2 capture using membrane contactors as alternative gas-liquid contacting equipment and low-temperature CO_2 hydrogenation to methanol using a combination of solid catalysts and co-catalytic alcoholic solvents.

In the experimental CO_2 capture unit, the steady-state absorption rate was limited by insufficient desorption of CO_2 from the loaded absorbent solution, which then limited the rate of chemical absorption in the membrane contactor. The observed limitation in the desorption performance of the CO_2 capture unit seems to result from the design of the present experimental unit and not from an inherent flaw in the process concept (Section 5.4). Because the membrane contactor used at the absorption stage functioned well, further development of the unit should prioritise the desorption stage. Improvement of the desorption performance by equipment modification could be pursued by two alternative approaches:

i. Desorption could be performed under conditions resembling those of conventional solvent regeneration columns. Operation under boiling water conditions, providing a steam flux to reduce the CO_2 partial pressure, would be facilitated by installing a reflux condenser and, preferably, a heating element as a reboiler. Desorption temperature would be maximised depending on the intended heat source (i.e. steam and heat pumps), and the vacuum pressure would be set to a value equal to the corresponding water vapour pressure. Installation of packing and flow distributors (e.g. nozzles) into the desorption vessel could improve the mass transfer performance.

ii. The use of a membrane contactor for stripping could provide the same advantages as those found at the absorption stage (e.g. compactness and modularity). The use of membrane materials with sufficient stability and wetting resistance at the desorption temperature would be critical. Vacuum could be used to reduce the desorption temperature and improve the driving force by creating a pressure gradient over the membrane. The driving force could be further improved by introducing a steam sweep on the gas side of the membrane. This would also help to maintain the desorption temperature inside the membrane module.

iii. Other alternative contactors could be used for desorption. An example would be high-gravity equipment such as rotating packed beds. The use of such

equipment at the absorption stage could also be investigated. Another option is the use of ultrasound to intensify mass transfer inside the desorption vessel.

Besides modification of the equipment, the performance of the capture unit could be improved by optimising the operating conditions:

i. The use of amino acid salt based absorbent solutions appears favourable owing to their good compatibility with low-cost polymeric membranes, such as the PP module used here. However, the use of different amino acid salts and even blends of different amino acid salts should be investigated to maximise the steady-state performance. Key parameters in the selection of absorbents should be the absorption and desorption rates at different temperatures and CO_2 loadings and the CO_2 absorption capacity. Solvent stability and degradation should also be investigated using appropriate analytical methods.

ii. The amino acid salt concentration of the solution should be increased to improve the absorption rate and capacity (i.e. moles of CO_2 per kg of solvent). Energy efficiency would be improved as the working capacity of the solvent would increase while the heat and electric energy involved in the circulation and heating of the solvent would remain constant. The upper limit for the concentration would be set by the water solubility of the selected amino acid salts and the formation of precipitates following absorption of CO_2. Increases in solution viscosity and the resulting effects on mass transfer should also be considered.

After reaching satisfactory performance in terms of mass transfer rate and specific energy, further research should aim for practical applications:

i. Comprehensive modelling of the capture unit should be performed to predict the performance under different operating conditions and to facilitate scale-up and techno-economic analyses. Modelling approaches would vary depending on the final configuration of the unit. Membrane contactors could facilitate relatively simple modelling of the mass transfer processes in absorption and desorption owing to the well-defined gas–liquid interface. Effective modelling approaches are available in the literature [87]. Scale-up would also be simplified by the modular nature of membrane contactors.

ii. For optimal performance, the unit should be finally configured for a specific application. Preferably, the benefits of using a membrane-contactor–based CO_2 capture process should be relevant for the intended application. For

instance, the compact nature of the contactors could be favourable in applications where equipment footprint should be limited (e.g. oil platforms or marine transportation). Configuration of the unit should consider issues such as heat integration, provision of heat, packaging and modularisation.

In the low-temperature methanol synthesis process, methanol productivity was increased both by using dual heterogeneous catalysts and by using a molecular sieve adsorbent to remove water from the reaction mixture (Section 10.4). Based on the present findings, the process presents two major challenges for further development. First, to avoid excessive reactor sizes, the catalytic activity should be improved to facilitate methanol production rates comparable to those obtained in gas-phase CO_2 hydrogenation to methanol while maintaining thermodynamically favourable, reduced temperatures. Second, the selection of the solvent as well as the reactor and overall process design should facilitate simple separation of the solvent from the reaction products to improve the energy and cost effectiveness of the process.

Following approaches could be pursued:

Heterogeneous catalysts with high activity should be selected and developed. Catalysts showing high activity in gas-phase CO_2 hydrogenation (Table 7.1) could be used as a starting point. The fundamental role of a catalyst in improving the rate of a chemical reaction is to lower the activation energy for the target reaction by providing a low-energy reaction pathway that is not accessible for the uncatalysed reaction [214]. Moreover, the selectivity for the intended product is improved as the activation energy is lowered compared with that of potential side-reactions. Although conventional Cu/ZnO-based catalysts are effective for CO_2 conversion to methanol, modifications and alternative catalysts compositions have been developed to improve the activity, selectivity and stability under CO_2/H_2 feed conditions [171, 47, 27, 215].

Developments in heterogeneous catalysts for CO2 hydrogenation to methanol range from the modification of the Cu/ZnO structure with additional promoting or stabilising components to the development of catalysts based on entirely different active components. With Cu/ZnO-based catalysts, the goal of further catalyst development might involve the further reduction of the activation energies of rate-determining elementary steps along the established reaction pathways (Section 6.2) by the addition of promoting materials. Another aim might involve the stabilisation of the active surface features under CO_2 hydrogenation conditions characterised by high concentrations of water. Catalysts based on components other than Cu and ZnO in turn aim to provide alternative reaction routes on novel reactive surfaces that might be intrinsically more stable and selective for methanol under CO_2 hydrogenation conditions. Table 7.1 presents a comparison of a number of catalysts with particularly promising performance in CO_2 hydrogenation to methanol.

i. Fundamental work on catalyst development should consider a more detailed characterisation of the reaction mechanism in the low-temperature process.

This information could be utilised in the identification and development of active catalytic surfaces with high activity. Such investigations have been performed on the gas-phase reaction route using various spectroscopic and computational methods (Sections 6.1–6.2). The identification of particularly active components would be followed by the development of practical supported catalysts. This work includes studying the involved solid-state chemistry and experimentation with catalyst preparation methods.

ii. Reaction temperature and pressure should preferably be selected to allow (near) complete CO_2 conversion at close to 100% selectivity to methanol at the chemical equilibrium. The latter would require the suppression of RWGS by operating at a sufficiently low temperature or using catalysts that do not catalyse this reaction. Under these conditions, recycle of unreacted gases could potentially be eliminated. In this way, the benefits of the alternative reaction route could be fully realised, and the competitiveness of the process compared with the gas-phase process could be improved.

iii. The use of adsorbents or other methods for the removal of water from the reactor should be considered. The present work shows that water can be effectively removed using a molecular sieve adsorbent; as a result, the methanol synthesis rate is increased. In addition to the kinetic benefit, the removal of water would be beneficial for the reaction equilibrium and even product separation. The adsorbent-based process should be developed to function at practical reaction conditions, with regeneration of the absorbent also considered in the reactor and process design.

iv. Alcoholic solvents with both high co-catalytic activity and physical properties facilitating simple separation should be selected. Based on present knowledge, this selection presents a difficult optimisation problem. Linear alcohols with shorter carbon chains have been shown to possess higher activity in the methanol synthesis reaction (Section 8.1); however, according to the process modelling performed in the present work, the use of longer chain alcohols with higher boiling points would be favourable for separation. A further complication is the formation of alcohol–water azeotropes.

v. Use of alternative separation sequences involving unit operations such as reactive distillation, integrating the separation of reaction products from the solvent in the reactor, or extractive distillation to break the alcohol-water azeotropes.

vi. The use of other solvents with co-catalytic function should be considered. Although alcoholic solvents facilitate the reaction route discussed, other combinations of catalysts and solvents might be used to enable similar low-temperature reaction routes. In recent reports, amine-based solutions, both in the presence of alcohols and by themselves, have been shown to facilitate liquid-phase methanol synthesis at low temperatures (Section 8.3). The use of amines appears promising owing to the possibility of direct integration of the CO_2 conversion process with a preceding capture process. Elimination of energy-intensive solvent regeneration in absorption-based capture processes could be a major break-through for CCU.

vii. Design and modelling of reactors and the overall process should be performed to realise the above suggestions into a functional and effective methanol synthesis process. Creative reactor designs and separation sequences, together with efficient heat integration both within the process and potentially with connected facilities (e.g. electrolysis and CO_2 capture), should be investigated. Successive economic and environmental analyses should be performed to assess the feasibility of the resulting processes.

References

[1] IPCC, “Climate Change 2014: Synthesis Report. Contribution of Working Groups I, II and III to the Fifth Assessment Report of the Intergovernmental Panel on Climate Change [Core Writing Team, R.K. Pachauri and L.A. Meyer (eds.)],” IPCC, Geneva, Switzerland, 2014.

[2] IEA, “World Energy Outlook 2017,” IEA, Paris, France, 2017.

[3] C. Le Quéré, R. M. Andrew, P. S. S. Friedlingstein, J. Hauck, J. Pongratz, P. A. Pickers, J. I. Korsbakken, G. Peters, J. G. Canadell and A. Arneth, “Global Carbon Budget 2018,” *Earth Syst. Sci. Data,* vol. 10, p. 2141–2194, 2018.

[4] T. F. Stocker, D. Qin, G.-K. Plattner, M. M. B. Tignor, S. K. Allen, J. Boschung, A. X. Y. Nauels, V. Bex and P. M. Midgley, “Climate Change 2013: The Physical Science Basis,” Intergovernmental Panel on Climate Change, 2013.

[5] IPCC, “Climate Change 2014: Mitigation of Climate Change. Contribution of Working Group III to the Fifth Assessment Report of the Intergovernmental Panel on Climate Change [Edenhofer, O. et al. (eds.)],” Cambridge University Press, Cambridge, United Kingdom, 2014.

[6] IRENA, “Renewable Power Generation Costs in 2018,” International Renewable Energy Agency, Abu Dhabi, 2019.

[7] D. F. J. Bogdanov, K. Sadovskaia, A. Aghahosseini, M. Child, A. Gulagi, A. S. Oyewo, L. Barbosa and C. Breyer, “Radical transformation pathway towards sustainable electricity via evolutionary steps,” *Nat. Commun.,* vol. 10, 2019.

[8] IEA, “CO_2 Capture and Storage: A Key Carbon Abatement Option,” OECD Publishing, Paris, France, 2008.

[9] M. E. Boot-Handford, J. C. Abanades, E. J. Anthony, M. J. Blunt, S. Brandani, N. Mac Dowell, J. R. . Fernández, M.-C. Ferrari, R. Gross, J. P. Hallett, R. S. Haszeldine, P. Heptonstall, A. Lyngfelt, Z. Makuch, E. Mangano and R. T. J. Porter, “Carbon capture and storage update,” *Energy Environ. Sci.,* vol. 7, pp. 130-189, 2014.

[10] M. A. C. S. Bui, A. Bardow, E. J. Anthony and A. Boston, “Carbon capture and storage (CCS): the way forward,” *Energy Environ. Sci.,* vol. 11, pp. 1062-1176, 2018.

[11] C. F. Heuberger, I. Staffell, N. Shah and N. Mac Dowell, "Quantifying the value of CCS for the future electricity system," *Energy Environ. Sci.*, vol. 9, pp. 2497-2510, 2016.

[12] R. S. Haszeldine, S. Flude, G. Johnson and V. Scott, "Negative emissions technologies and carbon capture and storage to achieve the Paris Agreement commitments," *Phil. Trans. R. Soc. A,* vol. 376, p. 20160447, 2018.

[13] C. J. Minx, "Negative emissions—Part 1: Research landscape and synthesis," *Environ. Res. Lett.*, vol. 13, p. 063001, 2018.

[14] S. Fuss, "Negative emissions—Part 2: Costs, potentials and side," *Environ. Res. Lett.*, vol. 13, p. 063002, 2018.

[15] C. Hepburn, E. Adlen, J. Beddington, E. A. Carter, S. Fuss, N. Mac Dowell, J. C. Minx, P. Smith and C. K. Williams, "The technological and economic prospects for CO_2 utilization and removal," *Nature,* vol. 575, pp. 87-97, 2019.

[16] M. Aresta, A. Dibenedetto and A. Angelini, "Catalysis for the Valorization of Exhaust Carbon: from CO_2 to Chemicals, Materials, and Fuels. Technological Use of CO_2," *Chem. Rev.*, vol. 114, p. 1709−1742, 2014.

[17] C. Ampelli, S. Perathoner and G. Centi, "CO_2 utilization: an enabling element to move to a resource and energy-efficient chemical and fuel production," *Phil. Trans. R. Soc. A,* vol. 373, p. 20140177, 2015.

[18] N. von der Assen, *From life-cycle assessment towards life-cycle design of carbon dioxide capture and utilization (Ph.D. Thesis),* Lehrstuhl für Technische Thermodynamik und Institut für Thermodynamik, RWTH Aachen, 2016.

[19] J. Artz, T. E. Müller and K. Thenert, "Sustainable Conversion of Carbon Dioxide: An Integrated Review of Catalysis and Life Cycle Assessment," *Chem. Rev.,* vol. 118, pp. 434-504, 2018.

[20] M. Peters, "Chemical Technologies for Exploiting and Recycling Carbon Dioxide into the Value Chain," *ChemSusChem,* vol. 4, p. 1216 – 1240, 2011.

[21] A. Goeppert, M. Czaun, G. K. Surya Prakash and G. A. Olah, "Air as the renewable carbon source of the future: an overview of CO_2 capture from the atmosphere," *Energy Environ. Sci.*, vol. 5, pp. 7833-7853, 2012.

[22] E. A. Quadrelli, G. Centi, J.-L. Duplan and S. Perathoner, "Carbon Dioxide Recycling: Emerging Large-Scale Technologies with Industrial Potential," *ChemSusChem,* vol. 4, p. 1194 – 1215, 2011.

[23] M. Aresta and A. Dibenedetto, "Utilisation of CO_2 as a chemical feedstock: opportunities and challenges," *Dalton Trans.,* p. 2975–2992, 2007.

[24] M. Aresta, A. Dibenedetto and A. Angelini, "The changing paradigm in CO_2 utilization," *J.* CO_2 *Util.,* Vols. 3-4, pp. 65-73, 2013.

[25] E. V. Kondratenko, G. Mul, J. Baltrusaitis, G. O. Larrazábal and J. Pérez-Ramírez, "Status and perspectives of CO_2 conversion into fuels and chemicals by catalytic, photocatalytic and electrocatalytic processes," *Energy Environ. Sci.,* vol. 6, p. 3112–3135, 2013.

[26] W. Wang, S. Wang, X. Ma and J. Gong, "Recent advances in catalytic hydrogenation of carbon dioxide," *Chem. Soc. Rev.,* vol. 40, p. 3703–3727, 2011.

[27] M. D. Porosoff, B. Yan and J. G. Chen, "Catalytic reduction of CO_2 by H_2 for synthesis of CO, methanol and hydrocarbons: challenges and opportunities," *Energy Environ. Sci.,* vol. 9, pp. 62-72, 2016.

[28] J. Klankermayer, S. Wesselbaum, K. Beydoun and W. Leitner, "Selective Catalytic Synthesis Using the Combination of Carbon Dioxide and Hydrogen: Catalytic Chess at the Interface of Energy and Chemistry," *Angew. Chem. Int. Ed.,* vol. 55, p. 7296 – 7343, 2016.

[29] A. Kätelhön, R. Meys, S. Deutz, S. Suh and A. Bardow, "Climate change mitigation potential of carbon capture and utilization in the chemical industry," *Proc. Natl. Acad. Sci. U. S. A.,* vol. 116, p. 11187–11194, 2019.

[30] H. Kondziella and T. Bruckner, "Flexibility requirements o frenewable energy based electricity systems – a review of research results and methodologies," *Renewable Sustainable Energy Rev.,* vol. 53, pp. 10-22, 2016.

[31] International Electrotechnical Commission, "Electrical Energy Storage," IEC, Geneva, Switzerland, 2011.

[32] H. Ibrahim, A. Ilinca and J. Perron, "Energy storage systems—Characteristics and comparisons," *Renewable and Sustainable Energy Reviews,* vol. 12, pp. 1221-1250, 2008.

[33] I. Hadjipaschalis, A. Poullikkas and V. Efthimiou, “Overview of current and future energy storage technologies for electric power applications,” *Renewable and Sustainable Energy Reviews,* vol. 13, pp. 1513-1522, 2009.

[34] F. Schüth, “Energy Storage Strategies,” in *Chemical Energy Storage*, Berlin, Germany, Walter de Gruyter GmbH, 2013, pp. 35-48.

[35] C. Graves, S. D. Ebbesen, M. Mogensen and K. S. Lackner, “Sustainable hydrocarbon fuels by recycling CO_2 and H_2O with renewable or nuclear energy,” *Renewable Sustainable Energy Rev.,* vol. 15, pp. 1-23, 2011.

[36] F. Schüth, “Chemical Compounds for Energy Storage,” *Chem. Ing. Tech.,* vol. 83, no. 11, pp. 1984-1993, 2011.

[37] P. Häussinger, R. Lohmüller and A. Watson, “Hydrogen, 2. Production,” in *Ullmann's Encyclopedia of Industrial Chemistry*, Weinheim, Wiley-VCH, 2012, pp. 249-307.

[38] A. Ursua, “Hydrogen Production From Water Electrolysis: Current Status and Future Trends,” *Proc. IEEE,* vol. 100, no. 2, 2012.

[39] M. Carmo, D. Fritz, J. Mergel and D. Stolten, “A comprehensive review on PEM water electrolysis,” *Int. J. Hydrogen Energy,* vol. 38, pp. 4901-4934, 2013.

[40] National Research Council, The Hydrogen Economy - Opportunities, Costs, Barriers, and R&D Needs, Washington, D.C.: The National Academies Press, 2004.

[41] J. H. Scott, “The Development of Fuel Cell Technology for Electric Power Generation: From NASA’s Manned Space Program to the "Hydrogen Economy"," *Proc. IEEE,* vol. 94, pp. 1815-1825, 2006.

[42] U. Eberle, M. Felderhoff and F. Schüth, “Chemical and Physical Solutions for Hydrogen Storage,” *Angew. Chem. Int. Ed.,* vol. 48, p. 6608 – 6630, 2009.

[43] P. Häussinger, R. Lohmüller and A. Watson, “Hydrogen, 5. Handling,” in *Ullmann's Encyclopedia of Industrial Chemistry*, Weinheim, Wiley-VCH, 2012, pp. 341-352.

[44] M. Thema, F. Bauer and M. Sterner, "Power-to-Gas: Electrolysis and methanation status review," *Renewable Sustainable Energy Rev.,* vol. 112, pp. 775-787, 2019.

[45] S. Rönsch, J. Schneider, S. Matthischke, M. Schlüter, M. Götz, J. Lefebvre, P. Prabhakaran and S. Bajohr, "Review on methanation – From fundamentals to current projects," *Fuel,* vol. 166, pp. 276-296, 2016.

[46] G. Olah, A. Goeppert and G. Prakash, Beyond Oil and Gas: The Methanol Economy, 2nd ed., Weinheim: Wiley-VCH, 2009.

[47] A. Goeppert, M. Czaun, J.-P. Jones, G. K. Surya Prakash and G. A. Olah, "Recycling of carbon dioxide to methanol and derived products – closing the loop," *Chem. Soc. Rev.,* vol. 43, pp. 7995-8048, 2014.

[48] M. E. Dry, "Practical and theoretical aspects of the catalytic Fischer-Tropsch process," *Appl. Catal., A,* vol. 138, pp. 319-344, 1996.

[49] R. W. Dorner, D. R. Hardy, F. W. Williams and H. D. Willauer, "Heterogeneous catalytic CO_2 conversion to value-added hydrocarbons," *Energy Environ. Sci.,* vol. 3, pp. 884-890, 2010.

[50] A. K. Agarwal, "Biofuels (alcohols and biodiesel) applications as fuels for internal combustion engines," *Prog. Energy Combust. Sci.,* vol. 33, pp. 233-271, 2007.

[51] A. Tremel, P. Wasserscheid, M. Baldauf and T. Hammer, "Techno-economic analysis for the synthesis of liquid and gaseous fuels based on hydrogen production via electrolysis," *Int. J. Hydrogen Energy,* vol. 40, pp. 11457-11464, 2015.

[52] IHS, "Global Methanol Market Review," IHS, 2012.

[53] J. Ott, V. Gronemann, F. Pontzen, E. Fiedler, G. Grossmann, Kersebohm, B. D., G. Weiss and C. Witte, "Methanol," in *Ullmann's Encyclopedia of Industrial Chemistry,* Weinheim, Wiley-VCH Verlag GmbH & Co. KGaA, 2012.

[54] M. Hogarth and G. Hards, "Direct Methanol Fuel Cells," *Platinum Met. Rev.,* vol. 40, no. 4, pp. 150-159, 1996.

[55] M. Bertau, H. J. Wernicke and F. Schmidt, "Methanol Utilisation Technologies," in *Methanol: The Basic Chemical and Energy Feedstock of the Future*, Berlin Heidelberg, Springer-Verlag, 2014, pp. 327-601.

[56] C. Arcoumanis, C. Bae, R. Crookes and E. Kinoshita, "The potential of di-methyl ether (DME) as an alternative fuel for compression-ignition engines: A review," *Fuel,* no. 87, pp. 1014-1030, 2008.

[57] Volvo, "Volvo Bio-DME: Unique field test in commercial operations, 2010-2012," 2012. [Online]. Available: http://www.volvotrucks.com/SiteCollectionDocuments/VTC/Corporate/News%20and%20Media/publications/Volvo%20BioDME.pdf. [Accessed 8 March 2016].

[58] G. Centi and S. Perathoner, "Opportunities and prospects in the chemical recycling of carbon dioxide to fuels," *Catal. Today,* vol. 148, pp. 191-205, 2009.

[59] L. Reichelt and F. Schmidt, "Methanol-to-Gasoline Process," in *Methanol: The Basic Chemical and Energy Feedstock of the Future*, M. Bertau, H. Offermanns, L. Plass, F. Schmidt and H. Wernicke, Eds., Springer-Verlag Berlin Heidelberg, 2014, pp. 440-453.

[60] M. Stöcker, "Methanol-to-hydrocarbons: catalytic materials and their behavior," *Microporous Mesoporous Mater.*, vol. 29, pp. 3-48, 1999.

[61] F. Schmidt and C. Pätzold, "Methanol-to-Olefins Processes," in *Methanol: The Basic Chemical and Energy Feedstock of the Future*, M. Bertau, H. Offermann, L. Plass, F. Schmidt and H. Wernicke, Eds., Springer-Verlag Berlin Heidelberg, 2014, pp. 454-472.

[62] J. Wilcox, "Introduction to Carbon Capture," in *Carbon Capture*, New York, Springer Science+Business Media, LLC, 2012, pp. 1-34.

[63] H.-J. Ho, A. Iizuka and E. Shibata, "Carbon Capture and Utilization Technology without Carbon Dioxide Purification and Pressurization: A Review on Its Necessity and Available Technologies," *Ind. Eng. Chem. Res.*, vol. 58, pp. 8941-8954, 2019.

[64] D. M. D'Alessandro, B. Smit and J. Long, "Carbon Dioxide Capture: Prospects for New Materials," *Angew. Chem. Int. Ed.,* vol. 49, pp. 6058-6082, 2010.

[65] O. Edenhofer, " Renewable energy sources and climate change mitigation: Special report of the intergovernmental panel on climate change," Intergovernmental Panel on Climate Change, 2012.

[66] D. W. Keith, M. Ha-Duong and J. K. Stolaroff, "Climate Strategy with CO_2 Capture from the Air," *Clim. Change*, vol. 74, pp. 17-45, 2006.

[67] K. S. Lackner, "The urgency of the development of CO_2 capture from ambient air," *PNAS*, vol. 109, p. 13156–13162, 2012.

[68] G. Olah, G. Surya Prakash and A. Goeppert, "Anthropogenic Chemical Carbon Cycle for a Sustainable Future," *J. Am. Chem. Soc.*, vol. 133, pp. 12881-12898, 2011.

[69] N. MacDowell, N. Florin, A. Buchard, J. Hallett, A. Galindo, G. Jackson, C. S. Adjiman, C. K. Williams, N. Shah and P. Fennell, "An overview of CO_2 capture technologies," *Energy Environ. Sci*, vol. 3, pp. 1645-1669, 2010.

[70] P. Markewitz, W. Kuckshinrichs, W. Leitner, J. Linssen, P. Zapp, R. Bongartz, A. Schreiber and T. E. Müller, "Worldwide innovations in the development of carbon capture technologies and the utilization of CO_2," *Energy Environ. Sci.*, vol. 5, pp. 7281-7305, 2012.

[71] K. A. Mumford, Y. Wu, K. H. Smith and G. W. Stevens, "Review of solvent based carbon-dioxide capture technologies," *Front. Chem. Sci. Eng.*, vol. 9, pp. 125-141, 2015.

[72] W. Boll, "Gas Production, 3. Gas Treating," in *Ullmann's Encyclopedia of Industrial Chemistry*, Weinheim, Wiley-VCH Verlag GmbH & Co. KGaA, 2012, pp. 483-539.

[73] G. Rochelle, E. Chen, S. Freeman, D. Van Wagener, Q. Xu and A. Voice, "Aqueous piperazine as the new standard for CO_2 capture technology," *Chem. Eng. J.*, vol. 171, p. 725– 733, 2011.

[74] B. Dutcher, M. Fan and A. Russell, "Amine-Based CO_2 Capture Technology Development from the Beginning of 2013 - A Review," *ACS Appl. Mater. Interfaces*, vol. 7, p. 2137−2148, 2015.

[75] H. Ahn, M. Luberti, Z. Liu and S. Brandani, "Process configuration studies of the amine capture process for coal-fired power plants," *Int. J. Greenhouse Gas Control*, vol. 16, p. 29–40, 2013.

[76] Y.-J. Lin, E. Chen and G. T. Rochelle, "Pilot plant test of the advanced flash stripper for CO_2 capture," *Faraday Discuss.,* vol. 192, p. 37–58, 2016.

[77] M. Wang, A. S. Joel, C. Ramshaw, D. Eimer and N. M. Musa, "Process intensification for post-combustion CO_2 capture with chemical absorption: A critical review," *Appl. Energy*, vol. 158, p. 275–291, 2015.

[78] B. Zhao, W. Tao, M. Zhong, Y. Su and G. Cui, "Process, performance and modeling of CO_2 capture by chemical absorption using high gravity: A review," *Renewable Sustainable Energy Rev.,* vol. 65, p. 44–56, 2016.

[79] A. Gabelman and S.-T. Hwang, "Hollow fiber membrane contactors," *J. Membr. Sci.,* vol. 159, no. 1-2, pp. 61-106, 1999.

[80] E. Cussler, "Hollow fiber contactors," in *Membrane Processes in Separation and Purification*, Netherlands, Kluwer Academic Publishers, 1994, pp. 375-394.

[81] M. Mulder, Basic Principles of Membrane Technology, 2nd ed., Kluwer Academic Publishers, 2003.

[82] E. Favre and H. F. Svendsen, "Membrane contactors for intensified post-combustion carbon dioxide capture by gas–liquid absorption processes," *J. Membr. Sci.,* Vols. 407-408, pp. 1-7, 2012.

[83] D. deMontigny, P. Tontiwachwuthikul and A. Chakma, "Comparing the Absorption Performance of Packed Columns and Membrane Contactors," *Ind. Eng. Chem. Res.,* vol. 44, pp. 5726-5732, 2005.

[84] J.-L. Li and B.-H. Chen, "Review of CO_2 absorption using chemical solvents in hollow fiber membrane contactors," *Sep. Purif. Technol.,* vol. 41, pp. 109-122, 2005.

[85] S. Zhao, P. H. M. Feron, L. Deng, E. Favre, E. Chabanon, S. Yan, J. Hou, V. Chen and H. Qi, "Status and progress of membrane contactors in post-combustion carbon capture: A state-of-the-art review of new developments," *J. Membr. Sci.,* vol. 511, pp. 180-206, 2016.

[86] V. Y. Dindore, D. W. F. Brilman, F. H. Geuzebroek and G. F. Versteeg, "Membrane–solvent selection for CO_2 removal using membrane gas–liquid contactors," *Sep. Purif. Technol.,* vol. 40, pp. 133-145, 2004.

[87] E. Chabanon, D. Roizard and E. Favre, “Modeling strategies of membrane contactors for post-combustion carbon capture: A critical comparative study,” *Chem. Eng. Sci.,* vol. 87, p. 393–407, 2013.

[88] D. deMontigny, P. Tontiwachwuthikul and A. Chakma, “Using polypropylene and polytetrafluoroethylene membranes in a membrane contactor for CO_2 absorption,” *J. Membr. Sci.,* vol. 277, pp. 99-107, 2006.

[89] H. Kreulen, C. A. Smolders, G. F. Versteeg and W. P. M. van Swaaij, “Microporous hollow fibre membrane modules as gas-liquid contactors. Part 2. Mass transfer with chemical reaction,” *J. Membr. Sci.,* vol. 78, pp. 217-238, 1993.

[90] W. P. M. van Swaaij and G. F. Versteeg, “Mass Transfer Accompanied With Complex Reversible Chemical Reactions In Gas-Liquid Systems: An Overview,” *Chem. Eng. Sci.,* vol. 47, pp. 3181-3195, 1992.

[91] C. A. Scholes, S. E. Kentish, G. W. Stevens and D. deMontigny, “Comparison of thin film composite and microporous membrane contactors for CO_2 absorption into monoethanolamine,” *Int. J. Greenhouse Gas Control,* vol. 42, pp. 66-74, 2015.

[92] M.-C. Yang and E. L. Cussler, “Designing hollow-fiber contactors,” *AIChE J.,* vol. 32, pp. 1910-1915, 1986.

[93] H. Kreulen, C. A. Smolders, G. F. Versteeg and W. P. M. van Swaaij, “Microporous hollow fibre membrane modules as gas-liquid contactors. Part 1. Physical mass transfer processes - A specific application: Mass transfer in highly viscous liquids,” *J. Membr. Sci.,* vol. 78, pp. 197-216, 1993.

[94] P. S. Kumar, J. A. Hogendoorn, P. H. M. Feron and G. F. Versteeg, “Approximate solution to predict the enhancement factor for the reactive absorption of a gas in a liquid flowing through a microporous membrane hollow fiber,” *J. Membr. Sci,* vol. 213, pp. 231-245, 2003.

[95] V. Y. Dindore, D. W. F. Brilman and G. F. Versteeg, “Hollow fiber membrane contactor as a gas–liquid model contactor,” *Chem. Eng. Sci.,* vol. 60, pp. 467-479, 2005.

[96] C. M. Guijt, I. Rácz, T. Reith and A. B. de Haan, “Determination of membrane properties for use in the modelling of a membrane distillation module,” *Desalination,* vol. 132, pp. 255-261, 2000.

[97] S. Atchariyawut, C. Feng, R. Wang, R. Jiraratananon and D. T. Liang, "Effect of membrane structure on mass-transfer in the membrane gas–liquid contacting process using microporous PVDF hollow fibers," *J. Membr. Sci.,* vol. 285, p. 272–281, 2006.

[98] S. Khaisri, D. deMontigny, P. Tontiwachwuthikul and R. Jiraratananon, "Comparing membrane resistance and absorption performance of three different membranes in a gas absorption membrane contactor," *Sep. Purif. Technol.,* vol. 65, p. 290–297, 2009.

[99] J. Franco, D. deMontigny, S. Kentish and J. S. G. Perera, "A Study of the Mass Transfer of CO_2 through Different Membrane Materials in the Membrane Gas Absorption Process," *Sep. Sci. Technol.,* vol. 43, p. 225–244, 2008.

[100] S.-H. Yeon, B. Sea, Y.-I. Park and K.-H. Lee, "Determination of Mass Transfer Rates in PVDF and PTFE Hollow Fiber Membranes for CO_2 Absorption," *Sep. Sci. Technol.,* vol. 38, pp. 271-293, 2003.

[101] S.-H. Lin, C.-F. Hsieh, M.-H. Li and K.-L. Tung, "Determination of mass transfer resistance during absorption of carbon dioxide by mixed absorbents in PVDF and PP membrane contactor," *Desalination,* vol. 249, pp. 647-653, 2009.

[102] P. S. Kumar, J. A. Hogendoorn, P. H. M. Feron and G. F. Versteeg, "New absorption liquids for the removal of CO_2 from dilute gas streams using membrane contactors," *Chem. Eng. Sci.,* vol. 57, pp. 1639-1651, 2002.

[103] S. Rode, P. T. Nguyen, D. Roizard, R. Bounaceur, C. Castel and E. Favre, "Evaluating the intensification potential of membrane contactors for gas absorption in a chemical solvent: A generic one-dimensional methodology and its application to CO_2 absorption in monoethanolamine," *J. Membr. Sci.,* vol. 389, pp. 1-16, 2012.

[104] S. Mosadegh-Sedghi, D. Rodrigue, J. Brisson and M. Iliuta, "Wetting phenomenon in membrane contactors – Causes and prevention," *J. Membr. Sci.,* vol. 452, pp. 332-353, 2014.

[105] J.-G. Lu, Y.-F. Zheng and M.-D. Cheng, "Wetting mechanism in mass transfer process of hydrophobic membrane gas absorption," *J. Membr. Sci.,* vol. 308, p. 180–190, 2008.

[106] S. Khaisri, D. deMontigny, P. Tontiwachwuthikul and R. Jiraratananon, "A mathematical model for gas absorption membrane contactors that studies the

effect of partially wetted membranes," *J. Membr. Sci.,* vol. 347, p. 228–239, 2010.

[107] C. A. Scholes, A. Qader, G. W. Stevens and S. E. Kentish, "Membrane Gas-Solvent Contactor Pilot Plant Trials of CO_2 Absorption from Flue Gas," *Sep. Sci. Technol.,* vol. 49, pp. 2449-2458, 2014.

[108] R. Wang, H. Y. Zhang, P. H. M. Feron and D. T. Liang, "Influence of membrane wetting on CO_2 capture in microporous hollow fiber membrane contactors," *Sep. Purif. Technol.,* vol. 46, pp. 33-40, 2005.

[109] Y. Lv, X. Yu, S.-T. Tu, J. Yan and E. Dahlquist, "Wetting of polypropylene hollow fiber membrane contactors," *J. Membr. Sci.,* vol. 362, pp. 444-452, 2010.

[110] H. Al-Saffar, B. Ozturk and R. Hughes, "A comparison of porous and non-porous gas-liquid membrane contactors for gas separation," *Chem. Eng. Res. Des.,* vol. 75, no. 7, pp. 685-692, 1997.

[111] S.-C. Chen, S.-H. Lin, R.-D. Chien and P.-S. Hsu, "Effects of shape, porosity, and operating parameters on carbon dioxide recovery in polytetrafluoroethylene membranes," *J. Hazard. Mater.,* vol. 179, pp. 692-700, 2010.

[112] S. M. Sedghi, J. Brisson, D. Rodrigue and M. Iliuta, "Chemical alteration of LDPE hollow fibers exposed to monoethanolamine solutions used as absorbent for CO_2 capture process," *Sep. Purif. Technol.,* vol. 80, pp. 338-344, 2011.

[113] S. Mosadegh-Sedghi, J. Brisson, D. Rodrigue and M. Iliuta, "Morphological, chemical and thermal stability of microporous LDPE hollow fiber membranes in contact with single and mixed amine based CO_2 absorbents," *Sep. Purif. Technol.,* vol. 96, pp. 117-123, 2012.

[114] E. Chabanon, D. Roizard and E. Favre, "Membrane Contactors for Postcombustion Carbon Dioxide Capture: A Comparative Study of Wetting Resistance on Long Time Scales," *Ind. Eng. Chem. Res.,* vol. 50, p. 8237–8244, 2011.

[115] O. Falk-Pedersen, Y. Bjerve, G. Glittum and S. Rønning, "Separation of carbon dioxide from offshore gas turbine exhaust," *Energy Convers. Manag.,* vol. 69, p. 393–396, 1995.

[116] N. Nishikawa, M. Ishibashi, H. Ohta, N. Akutsu, H. Matsumoto, T. Kamata and H. Kitamura, "CO_2 removal by hollow-fiber gas–liquid contactor," *Energy Convers. Manag.*, vol. 36, pp. 415-418, 1995.

[117] S. Li, D. J. Rocha, S. J. Zhou, H. S. Meyer, B. Bikson and Y. Ding, "Post-combustion CO_2 capture using super-hydrophobic, polyether ether ketone, hollow fiber membrane contactors," *J. Membr. Sci.,* vol. 430, pp. 79-86, 2013.

[118] S. Li, J. Zhou, T. Pyrzynski, A. Makkuni and H. Meyer, "Hybrid Membrane/Absorption Process for Post-combustion CO_2 Capture. Final Scientific/Technical Report," Gas Technology Institute, 2014.

[119] Y.-S. Kim and S.-M. Yang, "Absorption of carbon dioxide through hollow fiber membranes using various aqueous absorbents," *Sep. Purif. Technol.,* vol. 21, pp. 101-109, 2000.

[120] W. Rongwong, R. Jiraratananon and S. Atchariyawut, "Experimental study on membrane wetting in gas–liquid membrane contacting process for CO_2 absorption by single and mixed absorbents," *Sep. Purif. Technol.,* vol. 69, pp. 118-125, 2009.

[121] Z. Wang, M. Fang, S. Yan, H. Yu, C.-C. Wei and Z. Luo, "Optimization of Blended Amines for CO_2 Absorption in a Hollow-Fiber Membrane Contactor," *Ind. Eng. Chem. Res.,* vol. 52, p. 12170−12182, 2013.

[122] R. Wang, D. F. Li, C. Zhou, M. Liu and D. T. Liang, "Impact of DEA solutions with and without CO_2 loading on porous polypropylene membranes intended for use as contactors," *J. Membr. Sci.,* vol. 229, pp. 147-157, 2004.

[123] A. F. Portugal, P. W. J. Derks, G. F. Versteeg, F. D. Magalhães and A. Mendes, "Characterization of potassium glycinate for carbon dioxide absorption purposes," *Chem. Eng. Sci.,* vol. 62, pp. 6534-6547, 2007.

[124] B. M. Lerche, E. H. Stenby and K. Thomsen, CO_2 Capture from Flue gas using Amino acid salt solutions., Kgs. Lyngby: Technical University of Denmark (DTU), 2012.

[125] P. S. Kumar, J. A. Hogendoorn and G. F. Versteeg, "Kinetics of the reaction of CO_2 with aqueous potassium salt of taurine and glycine," *AIChE J.,* vol. 49, pp. 203-213, 2003.

[126] F. He, T. Wang, M. Fang, Z. Wang, H. Yu and Q. Ma, "Screening Test of Amino Acid Salts for CO_2 Absorption at Flue Gas Temperature in a Membrane Contactor," *Energy Fuels,* vol. 31, p. 770−777, 2017.

[127] J. van Holst, G. F. Versteeg, D. W. F. Brilman and J. A. Hogendoorn, "Kinetic study of CO_2 with various amino acid salts in aqueous solution," *Chem. Eng. Sci.,* vol. 64, pp. 59-68, 2009.

[128] H. Knuutila, U. E. Aronu, H. M. Kvamsdal and A. Chikukwa, "Post combustion CO_2 capture with an amino acid salt," *Energy Procedia,* vol. 5, p. 1550–1557, 2011.

[129] J. Lim, D. H. Kim, Y. Yoon, S. K. Jeong, K. T. Park and S. C. Nam, "Absorption of CO_2 into Aqueous Potassium Salt Solutions of L-Alanine and L-Proline," *Energy Fuels,* vol. 26, p. 3910−3918, 2012.

[130] H.-J. Song, S. Park, H. Kim, A. Gaur, J.-W. Park and S.-J. Lee, "Carbon dioxide absorption characteristics of aqueous amino acid salt solutions," *Int. J. Greenhouse Gas Control,* vol. 11, pp. 64-72, 2012.

[131] A. F. Portugal, J. M. Souda, F. D. Magalhães and A. Mendes, "Solubility of carbon dioxide in aqueous solutions of amino acid salts," *Chem. Eng. Sci.,* vol. 64, pp. 1993-2002, 2009.

[132] M. Rabensteiner, G. Kinger, M. Koller and C. Hochenauer, "PCC pilot plant studies with aqueous potassium glycinate," *Int. J. Greenhouse Gas Control,* vol. 42, pp. 562-570, 2015.

[133] P. S. Kumar, J. A. Hogendoorn, P. H. M. Feron and G. F. Versteeg, "Equilibrium Solubility of CO_2 in Aqueous Potassium Taurate Solutions: Part 1. Crystallization in Carbon Dioxide Loaded Aqueous Salt Solutions of Amino Acids," *Ind. Eng. Chem. Res.,* vol. 42, pp. 2832-2840, 2003.

[134] E. Sanchez Fernandez and E. Goetheer, "DECAB: process development of a phase change absorption process," *Energy Procedia,* vol. 4, pp. 868-875, 2011.

[135] E. Sanchez Fernandez, K. Heffernan, L. van der Ham, M. Linders, E. Eggink, F. Schrama, D. Brilman and E. V. T. Goetheer, "Conceptual Design of a Novel CO_2 Capture Process Based on Precipitating Amino Acid Solvents," *Ind. Eng. Chem. Res.,* vol. 52, no. 34, p. 12223–12235, 2013.

[136] P. H. M. Feron and A. E. Jansen, "CO_2 separation with polyolefin membrane contactors and dedicated absorption liquids: performances and prospects," *Sep. Purif. Technol.,* vol. 27, p. 231–242, 2002.

[137] S. Yan, M.-X. Fang, W.-F. Zhang, S.-Y. Wang, Z.-K. Xu, Z.-Y. Luo and K.-F. Cen, "Experimental study on the separation of CO_2 from flue gas using hollow fiber membrane contactors without wetting," *Fuel Process. Technol.,* vol. 88, pp. 501-511, 2007.

[138] J.-G. Lu, Y.-F. Zheng and M.-D. Cheng, "Membrane contactor for CO_2 absorption applying amino-acid salt solutions," *Desalination,* vol. 249, pp. 498-502, 2009.

[139] J.-G. Lu, H. Zhang, Y. Ji, F. Fan and C. Liu, "Amino Acid-Salt-Based Complex Absorbents for CO_2 Capture in a Membrane Contactor," *Energy Fuels,* vol. 24, p. 4617–4626, 2010.

[140] E. Chabanon, B. Belaissaoui and E. Favre, "Gas–liquid separation processes based on physical solvents: opportunities for membranes," *J. Membr. Sci.,* vol. 459, pp. 52-61, 2014.

[141] V. Y. Dindore, D. W. F. Brilman, P. H. M. Feron and G. F. Versteeg, "CO_2 absorption at elevated pressures using a hollow fiber membrane contactor," *J. Membr. Sci.,* vol. 235, pp. 99-109, 2004.

[142] J. Lu, L. Wang, X. Sun, J. Li and X. Liu, "Absorption of CO_2 into Aqueous Solutions of Methyldiethanolamine and Activated Methyldiethanolamine from a Gas Mixture in a Hollow Fiber Contactor," *Ind. Eng. Chem. Res.,* vol. 44, pp. 9230-9238, 2005.

[143] S. Koonaphapdeelert, Z. Wu and K. Li, "Carbon dioxide stripping in ceramic hollow fibre membrane contactors," *Chem. Eng. Sci.,* vol. 64, pp. 1-8, 2009.

[144] S. Khaisri, D. deMontigny, P. Tontiwachwuthikul and R. Jiraratananon, "CO_2 stripping from monoethanolamine using a membrane contactor," *J. Membr. Sci.,* vol. 376, pp. 110-118, 2011.

[145] A. Mansourizadeh and A. F. Ismail, "CO_2 stripping from water through porous PVDF hollow fiber membrane contactor," *Desalination,* vol. 273, pp. 386-390, 2011.

[146] C. A. Scholes, S. E. Kentish, G. W. Stevens, J. Jin and D. deMontigny, "Thin-film composite membrane contactors for desorption of CO_2 from

Monoethanolamine at elevated temperatures," *Sep. Purif. Technol.,* vol. 156, pp. 841-847, 2015.

[147] M. Simioni, S. E. Kentish and G. W. Stevens, "Membrane stripping: Desorption of carbon dioxide from alkali solvents," *J. Membr. Sci.,* vol. 378, pp. 18-27, 2011.

[148] R. Naim, A. Ismail and A. Mansourizadeh, "Effect of non-solvent additives on the structure and performance of PVDF hollow fiber membrane contactor for CO_2 stripping," *J. Membr. Sci.,* vol. 423–424, pp. 503-513, 2012.

[149] A. Trusov, S. Legkov, L. van den Broeke, E. K. V. Goetheer and A. Volkov, "Gas/liquid membrane contactors based on disubstituted polyacetylene for CO_2 absorption liquid regeneration at high pressure and temperature," *J. Membr. Sci.,* vol. 383, pp. 241-249, 2011.

[150] M. Fang, S. Yan, Z. Luo, M. Ni and K. Cen, "CO_2 chemical absorption by using membrane vacuum regeneration technology," *Energy Procedia,* vol. 1, pp. 815-822, 2009.

[151] S. Yan, M. Fang, Z. Luo and K. Cen, "Regeneration of CO_2 from CO_2-rich alkanolamines solution by using reduced thickness and vacuum technology: Regeneration feasibility and characteristic of thin-layer solvent," *Chem. Eng. Process.: Process Intensification,* vol. 48, pp. 515-523, 2009.

[152] S. Nii, Y. Iwata, K. Takahashi and H. Takeuchi, "Regeneration of CO_2-loaded carbonate solution by reducing pressure," *J. Chem. Eng. Jpn.,* vol. 28, pp. 148-153, 1995.

[153] Z. Wang, M. Fang, Q. Ma, Z. Zhao, T. Wang and Z. Luo, "Membrane stripping technology for CO_2 desorption from CO_2-rich absorbents with low energy consumption," *Energy Procedia,* vol. 63, pp. 765-772, 2014.

[154] M. Mavroudi, S. P. Kaldis and G. P. Sakellaropoulos, "Reduction of CO_2 emissions by a membrane contacting process," *Fuel,* vol. 82, pp. 2153-2159, 2003.

[155] P. Kosaraju, A. S. Kovvali, A. Korikov and K. K. Sirkar, "Hollow Fiber Membrane Contactor Based CO_2 Absorption-Stripping Using Novel Solvents and Membranes," *Ind. Eng. Chem. Res.,* vol. 44, pp. 1250-1258, 2005.

[156] B. A. Oyenekan and G. T. Rochelle, "Energy Performance of Stripper Configurations for CO_2 Capture by Aqueous Amines," *Ind. Eng. Chem. Res.,* vol. 45, pp. 2457-2464, 2006.

[157] N. Matsumiya, M. Teramoto, S. Kitada and H. Matsuyama, "Evaluation of energy consumption for separation of CO_2 in flue gas by hollow fiber facilitated transport membrane module with permeation of amine solution," *Sep. Purif. Technol.,* vol. 46, p. 26–32, 2005.

[158] G. A. Dibrov, V. V. Volkov, V. P. Vasilevsky, A. A. B. S. D. Shutova, V. S. Khotimsky, A. van de Runstraat, E. L. V. Goetheer and A. V. Volkov, "Robust high-permeance PTMSP composite membranes for CO_2 membrane gas desorption at elevated temperatures and pressures," *J. Membr. Sci.,* vol. 470, p. 439–450, 2014.

[159] J. Ying, D. A. Eimer, F. Brakstad and H. A. Haugen, "Ultrasound intensified CO_2 desorption from pressurized loaded monoethanolamine solutions. I. parameters investigation and modelling," *Energy,* vol. 163, pp. 168-179, 2018.

[160] M. Muhler and S. Kaluza, "Syngas to Methanol and Ethanol," in *Fuel Production with Heterogeneous Catalysis,* J. Sá, Ed., Boca Raton, CRC Press, 2014, pp. 169-192.

[161] S. Lee, "Methanol Synthesis from Syngas," in *Handbook of Alternative Fuel Technologies*, S. Lee, J. G. Speight and S. K. Loyalka, Eds., Boca Raton, CRC Press, 2007, pp. 297-321.

[162] K. Klier, V. Chatikavanij, R. G. Herman and G. W. Simmons, "Catalytic synthesis of methanol from COH_2: IV. The effects of carbon dioxide," *J. Catal.,* vol. 74, pp. 343-360, 1982.

[163] M. Sahibzada, I. S. Metcalfe and D. Chadwick, "Methanol Synthesis from $CO/CO_2/H_2$ over Cu/ZnO/Al2O3 at Differential and Finite Conversions," *J. Catal.,* vol. 174, pp. 111-118, 1998.

[164] O. Martin and J. Pérez-Ramírez, "New and revisited insights into the promotion of methanol synthesis catalysts by CO_2," *Catal. Sci. Technol.,* vol. 3, pp. 3343-3352, 2013.

[165] J. A. Moulijn, M. Makkee and A. van Diepen, "Methanol," in *Chemical Process Technology,* J. A. Moulijn, M. Makkee and A. van Diepen, Eds., Chichester, John Wiley & Sons, 2001, pp. 180-193.

[166] F. Pontzen, W. Liebner, V. Gronemann, M. Rothaemel and B. Ahlers, "CO_2-based methanol and DME – Efficient technologies for industrial scale production," *Catal. Today,* vol. 171, pp. 242-250, 2011.

[167] K. Stangeland, H. Li and Z. Yu, "Thermodynamic Analysis of Chemical and Phase Equilibria in CO_2 Hydrogenation to Methanol, Dimethyl Ether, and Higher Alcohols," *Ind. Eng. Chem. Res.,* vol. 57, p. 4081−4094, 2018.

[168] S. Horstmann, K. Fischer and J. Gmehling, "Application of PSRK for Process Design," *Chem. Eng. Comm.,* vol. 192, p. 336–350, 2005.

[169] X. Liu, G. Q. Lu, Z. Yan and J. Beltramini, "Recent Advances in Catalysts for Methanol Synthesis via Hydrogenation of CO and CO_2," *Ind. Eng. Chem. Res.,* vol. 42, pp. 6518-6530, 2003.

[170] H.-J. Wernicke, "Methanol Generation," in *Methanol: The Basic Chemical and Energy Feedstock of the Future*, M. Bertau, H. Offermanns, L. Plass, F. Schmidt and H. Wernicke, Eds., Berlin , Springer-Verlag , 2014, pp. 51-301.

[171] F. Arena, G. Mezzatesta, L. Spadaro and G. Trunfio, "Latest Advances in the Catalytic Hydrogenation of Carbon Dioxide to Methanol/Dimethylether," in *Transformation and Utilization of Carbon Dioxide*, B. M. Banage and M. Arai, Eds., Berlin, Springer-Verlag, 2014, pp. 103-130.

[172] M. Behrens, F. Studt, I. Kasatkin, S. Kühl, M. Hävecker, F. Abild-Petersen, S. Zander, F. Girgsdies, P. Kurr, B.-L. Kniep, M. Tovar, R. W. Fischer, J. K. Norskov and R. Schlögl, "The Active Site of Methanol Synthesis over Cu/ZnO/Al2O3 Industrial Catalysts," *Science,* vol. 336, pp. 893-897, 2012.

[173] M. Behrens, S. Zander, P. Kurr, N. Jacobsen, J. Senker, G. Koch, T. Ressler, R. W. Fischer and R. Schlögl, "Performance Improvement of Nanocatalysts by Promoter-Induced Defects in the Support Material: Methanol Synthesis over Cu/ZnO:Al," *J. Am. Chem. Soc.,* vol. 135, p. 6061−6068, 2013.

[174] M. Behrens and R. Schlögl, "How to Prepare a Good Cu/ZnO Catalyst or the Role of Solid State Chemistry for the Synthesis of Nanostructured Catalysts," *Z. Anorg. Allg. Chem.,* vol. 639, pp. 1683-2695, 2013.

[175] M. S. Spencer, "The role of zinc oxide in Cu/ZnO catalysts for methanol synthesis and the water–gas shift reaction," *Top. Catal.,* vol. 8, pp. 259-266, 1999.

[176] R. d'Alnoncourt, X. Xia, J. Strunk, E. Löffler, O. Hinrichsen and M. Muhler, "The influence of strongly reducing conditions on strong metal–support interactions in Cu/ZnO catalysts used for methanol synthesis," *Phys. Chem. Chem. Phys.,* vol. 8, pp. 1525-1538, 2006.

[177] C. Holse, C. Elkjær, A. Nierhoff, S. J, I. Chorkendorff, S. Helveg and J. Nielsen, "Dynamic Behavior of CuZn Nanoparticles under Oxidizing and Reducing Conditions," *J. Phys. Chem. C,* vol. 119, pp. 2804-2812, 2015.

[178] K. F. Kalz, R. Kraehnert, M. Dvoyashkin, R. Dittmeyer, R. Gläser, U. Krewer, K. Reuter and J.-D. Grunwaldt, "Future Challenges in Heterogeneous Catalysis: Understanding Catalysts under Dynamic Reaction Conditions," *ChemCatChem,* vol. 9, pp. 17-29, 2017.

[179] B. S. Clausen, J. Schiotz, L. Gråbaek, C. V. Ovesen, K. W. Jacobsen, J. K. Norskov and H. Topsoe, "Wetting/ non-wetting phenomena during catalysis: Evidence from in situ on-line EXAFS studies of Cu-based catalysts," *Top. Catal.,* vol. 1, pp. 367-376, 1994.

[180] J. D. Grunwaldt, A. M. Molenbroek, N.-Y. Topsoe, H. Topsoe and B. S. Clausen, "In Situ Investigations of Structural Changes in Cu/ZnO Catalysts," *J. Catal.,* vol. 194, pp. 452-460, 2000.

[181] N.-Y. Topsøe and H. Topsøe, "FTIR studies of dynamic surface structural changes in Cu-based methanol synthesis catalysts," *J. Mol. Catal. A: Chem.,* vol. 141, pp. 95-105, 1999.

[182] M. M. Günter, T. Ressler, B. Bems, C. Büscher, T. Genger, O. Hinrichsen, M. Muhler and R. Schlögl, "Implication of the microstructure of binary Cu/ZnO catalysts for their catalytic activity in methanol synthesis," *Catal. Lett.,* vol. 71, pp. 37-44, 2001.

[183] I. Kasatkin, P. Kurr, B. Kniep, A. Trunschke and R. Schlögl, "Role of Lattice Strain and Defects in Copper Particles on the Activity of Cu/ZnO/Al2O3 Catalysts for Methanol Synthesis," *Angew. Chem.,* vol. 119, pp. 7465-7468, 2007.

[184] T. Kandemir, F. Girgsdies, T. C. Hansen, K. Liss, I. Kasatkin, E. L. Kunkes, G. Wowsnick, N. Jacobsen, R. Schlögl and M. Behrens, "In Situ Study of Catalytic Processes: Neutron Diffraction of a Methanol Synthesis Catalyst at Industrially Relevant Pressure," *Angew. Chem. Int. Ed.,* vol. 52, pp. 5166-5170, 2013.

[185] F. Studt, M. Behrens, E. L. Kunkes, T. Nygil, S. Zander, A. Tarasov, J. Schumann, E. Frei, J. B. Varley, F. Abild-Petersen, J. K. Norskov and R. Sclögl, "The Mechanism of CO and CO_2 Hydrogenation to Methanol over Cu-Based Catalysts," *ChemCatChem,* vol. 7, pp. 1105-1111, 2015.

[186] Stoltze, "Microkinetic simulation of catalytic reactions," *Prog. Surf. Sci.,* vol. 65, pp. 65-150, 2000.

[187] I. Chorkendorff, P. A. Taylor and P. B. Rasmussen, "Synthesis and hydrogenation of formate on Cu(100) at high pressures," *J. Vac. Sci. Technol., A,* vol. 10, pp. 2277-2281, 1992.

[188] G. J. Millar, C. H. Rochester and K. C. Waugh, "An in situ high pressure FT-IR study of CO_2/H_2 interactions with model ZnO/SiO2, Cu/SiO2 and Cu/ZnO/SiO2 methanol synthesis catalysts," *Catal. Lett.,* vol. 14, pp. 289-295, 1992.

[189] M. Bowker, R. Hadden, H. Houghton, J. Hyland and K. Waugh, "The mechanism of methanol synthesis on copper/zinc oxide/alumina catalysts," *J. Catal.,* vol. 109, pp. 263-273, 1988.

[190] K. Waugh, "Methanol Synthesis," *Catal. Lett.,* vol. 142, pp. 1153-1166, 2012.

[191] G. H. Graaf, E. J. Stamhuis and A. A. C. M. Beenackers, "Kinetics of low-pressure methanol synthesis," *Chem. Eng. Sci.,* vol. 43, pp. 3185-3195, 1988.

[192] P. B. Rasmussen, P. M. Holmblad, T. Askgaard, C. V. Ovesen, P. Stoltze, J. K. Norskov and I. Chorkendorff, "Methanol synthesis on Cu(100) from a binary gas mixture of CO_2 and H_2," *Catal. Lett.,* vol. 26, pp. 373-381, 1994.

[193] T. Askgaard, J. Norskov, C. Ovesen and P. Stoltze, "A Kinetic Model of Methanol Synthesis," *J. Catal.* , vol. 156, pp. 229-242, 1995.

[194] K. M. Vanden Bussche and G. F. Froment, "A Steady-State Kinetic Model for Methanol Synthesis and the Water Gas Shift Reaction on a Commercial Cu/ZnO/Al2O3 Catalyst," *J. Catal.,* vol. 161, pp. 1-10, 1996.

[195] N. Park, M.-J. Park, Y.-J. Lee, K.-S. Ha and K.-W. Jun, "Kinetic modeling of methanol synthesis over commercial catalysts based on three-site adsorption," *Fuel Process. Technol.,* vol. 125, p. 139–147, 2014.

[196] C. Ovesen, B. Clausen, J. Schiotz, P. Stoltze, H. Topsoe and J. Norskov, "Kinetic Implications of Dynamical Changes in Catalyst Morphology during

Methanol Synthesis over Cu/ZnO Catalysts," *J. Catal.,* vol. 168, pp. 133-142, 1997.

[197] M. Peter, M. B. Fichtl, H. K. S. Ruland, M. Muhler and O. Hinrichsen, "Detailed kinetic modeling of methanol synthesis over a ternary copper catalyst," *Chem. Eng. J.,* vol. 203, p. 480–491, 2012.

[198] K. Kobl, S. Thomas, Y. Zimmermann, K. Parkhomenko and A.-C. Roger, "Power-law kinetics of methanol synthesis from carbon dioxide and hydrogen on copper–zinc oxide catalysts with alumina or zirconia supports," *Catal. Today,* vol. 270, p. 31–42, 2016.

[199] L. C. Grabow and M. Mavrikakis, "Mechanism of Methanol Synthesis on Cu through CO_2 and CO Hydrogenation," *ACS Catal.,* vol. 1, pp. 365-384, 2011.

[200] J. S. Lee, K. H. Lee, S. Y. Lee and Y. G. Kim, "A Comparative Study of Methanol Synthesis from CO_2/H_2 and CO/H_2 over a Cu/ZnO/Al2O3 Catalyst," *J. Catal.,* vol. 144, pp. 414-424, 1993.

[201] G. C. Chinchen, P. J. Denny, D. G. Parker, M. S. Spencer and D. A. Whan, "Mechanism of methanol synthesis from $CO_2/CO/H_2$ mixtures over copper/zinc oxide/alumina catalysts: use of 14C-labelled reactants," *Appl. Catal.,* vol. 30, pp. 333-338, 1987.

[202] T. Lorenz, M. Bertau, F. Schmidt and L. Plass, "Methanol Production from CO_2," in *Methanol: The Basic Chemical and Energy Feedstock of the Future,* M. Bertau, H. Offermanns, L. Plass, F. Schmidt and H. Wernicke, Eds., Springer-Verlag Berlin Heidelberg, 2014, pp. 266-276.

[203] A. Bansode and A. Urakawa, "Towards full one-pass conversion of carbon dioxide to methanol and methanol-derived products," *J. Catal.,* vol. 309, pp. 66-70, 2014.

[204] R. Gaikwad, A. Bansode and A. Urakawa, "High-pressure advantages in stoichiometric hydrogenation of carbon dioxide to methanol," *J. Catal.,* vol. 343, pp. 127-132, 2016.

[205] J. G. van Bennekom, R. H. Venderbosch, J. G. M. Winkelman, E. Wilbers, D. Assink, K. P. J. Lemmens and H. J. Heeres, "Methanol synthesis beyond chemical equilibrium," *Chem. Eng. Sci.,* vol. 87, p. 204–208, 2013.

[206] M. J. Bos and D. W. F. Brilman, "A novel condensation reactor for efficient CO_2 to methanol conversion for storage of renewable electric energy," *Chem. Eng. J.*, vol. 278, p. 527–532, 2015.

[207] W. Wu, K. Xie, D. Sun, X. Li and F. Fang, "CuO/ZnO/Al2O3 Catalyst Prepared by Mechanical-Force-Driven Solid-State Ion Exchange and Its Excellent Catalytic Activity under Internal Cooling Condition," *Ind. Eng. Chem. Res.*, vol. 56, pp. 8216-8223, 2017.

[208] M. Saito, T. Fujitani, M. Takeuchi and T. Watanabe, "Development of copper/zinc oxide-based multicomponent catalysts for methanol synthesis from carbon dioxide and hydrogen," *Appl. Catal., A,* vol. 138, pp. 311-318, 1996.

[209] J. Tremblay, "CO_2 As Feedstock," *Chem. Eng. News,* vol. 86, no. 35, p. 13, 2008.

[210] M. Saito, M. Takeuchi, T. Fujitani, J. Toyir, S. Luo, J. Wu, H. Mabuse, F. Ushikoshi, K. Mori and T. Watanabe, "Advances in joint research between NIRE and RITE for developing a novel technology for methanol synthesis from CO," *Appl. Organometal. Chem.* , vol. 14, pp. 763-772, 2000.

[211] J. Toyir, R. Miloua, N. E. Elkadri, M. Nawdali, H. Toufik, F. Miloua and M. Saito, "Sustainable process for the production of methanol from CO_2 and H_2 using Cu/ZnO-based multicomponent catalyst," *Phys. Procedia,* vol. 2, pp. 1075-1079, 2009.

[212] O. Joo, K. Jung, I. Moon, A. Y. Rozovskii, G. I. Lin, S. : Han and S. Uhm, "Carbon Dioxide Hydrogenation To Form Methanol via a Reverse-Water-Gas-Shift Reaction (the CAMERE Process)," *Ind. Eng. Chem. Res.,* vol. 38, pp. 1808-1812, 1999.

[213] Chemicals-technology.com, "George Olah CO_2 to Renewable Methanol Plant, Reykjanes, Iceland," 2016. [Online]. Available: http://www.chemicals-technology.com/projects/george-olah-renewable-methanol-plant-iceland/. [Accessed 24 March 2020].

[214] S. Arndt and R. Schomäcker, "Chemical Kinetics: A Practical Guide," in *Chemical Energy Storage*, Berlin, Walter de Gruyter GmbH, 2013, pp. 249-276.

[215] J. Zhong, X. W. Z. Yang, B. Liang, Y. Huang and T. Zhang, "State of the art and perspectives in heterogeneous catalysis of CO_2 hydrogenation to methanol," *Chem. Soc. Rev.,* vol. 49, pp. 1385-1413, 2020.

[216] J. Schumann, T. Lunkenbein, A. Tarasov, N. Thomas, R. Schlögl and M. Behrens, "Synthesis and Characterisation of a Highly Active Cu/ZnO:Al Catalyst," *ChemCatChem,* vol. 6, pp. 2889-2897, 2014.

[217] F. Arena, G. Mezzatesta, F. Zafarana, G. Trunfio, F. Frusteri and L. Spadaro, "Effects of oxide carriers on surface functionality and process performance of the Cu–ZnO system in the synthesis of methanol via CO_2 hydrogenation," *J. Catal.,* vol. 300, pp. 141-151, 2013.

[218] R. Ladera, F. Pérez-Alonso, J. González-Carballo, M. Ojeda, S. Rojas and J. Fierro, "Catalytic valorization of CO_2 via methanol synthesis with Ga-promoted Cu–ZnO–ZrO2 catalysts," *Appl. Catal., B,* Vols. 142-143, pp. 241-248, 2013.

[219] Z. Gao and C. T. Au, "CO_2 Hydrogenation to Methanol on a YBa2Cu3O7 Catalyst," *J. Catal.,* vol. 189, pp. 1-15, 2000.

[220] Kong, H. Li, G. Lin and H. Zhang, "Pd-Decorated CNT-Promoted Pd-Ga2O3 Catalyst for Hydrogenation of CO_2 to Methanol," *Catal. Lett.,* vol. 141, pp. 886-694, 2011.

[221] Studt, I. Sharafutdinov, F. Abild-Pedersen, C. F. Elkjaer, J. S. Hummelshoj, S. Dahl, I. Chorkendorff and J. K. Norskov, "Discovery of a Ni-Ga catalyst for carbon dioxide reduction to methanol," *Nat. Chem.,* vol. 6, pp. 320-324, 2014.

[222] L. G. Wang, Z. Li, C. Tang, Z. Feng, H. An, H. Liu, T. Liu and C. Li, "A highly selective and stable ZnO-ZrO2 solid solution catalyst for CO_2 hydrogenation to methanol," *Sci. Adv.,* vol. 3, p. e1701290, 2017.

[223] Martin, A. J. Martín, C. Mondelli, S. Mitchell, T. F. Segawa, R. Hauert, C. Drouilly, D. Curulla-Ferré and Pérez-Ramírez, "Indium Oxide as a Superior Catalyst for Methanol Synthesis by CO_2 Hydrogenation," *Angew. Chem. Int. Ed.,* vol. 55, p. 6261 –6265, 2016.

[224] Rui, Z. Wang, K. Sun, J. Ye, Q. Ge and C. Liu, "CO_2 hydrogenation to methanol over Pd/In2O3: effects of Pd and oxygen vacancy," *Appl. Catal., B,* vol. 218, pp. 488-497, 2017.

[225] S. Frei, C. Mondelli, R. García-Muelas, K. S. Kley, B. Puértolas, N. López, O. V. Safonova, J. A. Stewart, D. C. Ferré and J. Pérez-Ramírez, "Atomic-scale engineering of indium oxide promotion by palladium for methanol production via CO_2 hydrogenation," *Nat. Commun.,* vol. 10, pp. 1-11, 2019.

[226] A. Vannice, Kinetics of Catalytic Reactions, New York: Springer Science+Business Media, 2005.

[227] Raudaskoski, E. Turpeinen, R. Lenkkeri, E. Pongrácz and R. Keiski, "Catalytic activation of CO_2: Use of secondary CO_2 for the production of synthesis gas and for methanol synthesis over copper-based zirconia-containing catalysts," *Catal. Today,* vol. 144, pp. 318-323, 2009.

[228] F. Arena, G. Italiano, K. Barbera, S. Bordiga, G. Bonura, L. Spadaro and F. Frusteri, "Solid-state interactions, adsorption sites and functionality of Cu-ZnO/ZrO2 catalysts in the CO_2 hydrogenation to CH3OH," *Appl. Catal., A,* vol. 350, pp. 16-23, 2008.

[229] F. Arena, K. Barbera, G. Italiano, G. Bonura, L. Spadaro and F. Frusteri, "Synthesis, characterization and activity pattern of Cu–ZnO/ZrO2 catalysts in the hydrogenation of carbon dioxide to methanol," *J. Catal.,* vol. 249, pp. 185-194, 2007.

[230] C. Li, X. Yuan and K. Fujimoto, "Development of highly stable catalyst for methanol synthesis from carbon dioxide," *Appl. Catal., A,* vol. 469, pp. 306-311, 2014.

[231] O. Martin, C. Mondelli, D. Curulla-Ferré, C. Drouilly, R. Hauert and J. Pérez-Ramírez, "Zinc-Rich Copper Catalysts Promoted by Gold for Methanol Synthesis," *ACS Catal.,* vol. 5, pp. 5607-5616, 2015.

[232] Y. Song, X. Liu, L. Xiao, W. Wu, J. Zhang and X. Song, "Pd-Promoter/MCM-41: A Highly Effective Bifunctional Catalyst for Conversion of Carbon Dioxide," *Catal. Lett.,* vol. 145, pp. 1272-1280, 2015.

[233] È. Van-Dal and C. Bouallou, "Design and simulation of a methanol production plant from CO_2 hydrogenation," *J. Cleaner Prod.,* vol. 57, pp. 38-45, 2013.

[234] B. Anicic, P. Trop and D. Goricanec, "Comparison between two methods of methanol production from carbon dioxide," *Energy,* vol. 77, pp. 279-289, 2014.

[235] M. Pérez-Fortes, J. C. Schöneberger, A. Boulamanti and E. Tzimas, "Methanol synthesis using captured CO_2 as raw material: Techno-economic and environmental assessment," *Appl. Energy,* vol. 161, pp. 718-732, 2016.

[236] K. Atsonios, K. D. Panopoulos and E. Kakaras, "Investigation of technical and economic aspects for methanol production through CO_2 hydrogenation," *Int. J. Hydrogen Energy,* vol. 41, pp. 2202-2214, 2016.

[237] D. S. Kourkoumpas, E. Papadimou, K. Atsonios, S. Karellas, P. Grammelis and E. Kakaras, "Implementation of the Power to Methanol concept by using CO_2 from lignite power plants: Techno-economic investigation," *Int. J. Hydrogen Energy,* vol. 41, pp. 16674-16687, 2016.

[238] R. Rivera-Tinoco, M. Farran, C. Bouallou, F. Auprêrte, S. Valentin, P. Millet and J. R. Ngameni, "Investigation of power-to-methanol processes coupling electrolytic hydrogen production and catalytic CO_2 reduction," *Int. J. Hydrogen Energy,* vol. 41, pp. 4546-4559, 2016.

[239] D. Bellotti, M. Rivarolo, L. Magistri and A. F. Massardo, "Feasibility study of methanol production plant from hydrogen and captured carbon dioxide," *J.* CO_2 *Util.,* vol. 21, pp. 132-138, 2017.

[240] A. Varone and M. Ferrari, "Power to liquid and power to gas: An option for the German Energiewende," *Renewable Sustainable Energy Rev.,* vol. 45, pp. 207-218, 2015.

[241] Methanex Corporation, "Methanex Methanol Price Sheet," 27 March 2020. [Online]. Available: https://www.methanex.com/sites/default/files/methanol-price/Mx-Price-Sheet%20-%20Mar%2027%2C%202020.pdf. [Accessed 22 April 2020].

[242] M. Soltanieh, K. M. Azar and M. Saber, "Development of a zero emission integrated system for co-production of electricity and methanol through renewable hydrogen and CO_2 capture," *Int. J. Greenhouse Gas Control,* vol. 7, pp. 145-152, 2012.

[243] D. Mignard and C. Pritchard, "On the use of electrolytic hydrogen from variable renewable energies for the enhanced conversion of biomass to fuels," *Chem. Eng. Res. Des.,* vol. 86, pp. 473-487, 2008.

[244] Z. Liu, W. Tierney, Y. Shah and I. Wender, "Methanol synthesis via methylformate in a slurry reactor," *Fuel Process. Technol.,* vol. 23, pp. 149-167, 1989.

[245] V. M. Palekar, "Alkali compounds and copper chromite as low-temperature slurry phase methanol catalysts," *Appl. Catal., A,* vol. 103, pp. 105-122, 1993.

[246] Y. Zhao, L. Bai, Y. Hu, B. Zhong and S. Peng, "Catalytic performance of CuCr/CH3ONa used for low temperature methanol synthesis in slurry phase," *J. Nat. Gas Chem.,* vol. 8, pp. 181-187, 1999.

[247] W. Chu, T. Zhang, C. He and Y. Wu, “Low-temperature methanol synthesis (LTMS) in liquid phase on novel copper-based catalysts,” *Catal. Lett.,* vol. 79, pp. 129-132, 2002.

[248] M. Marchionna, L. Basini, A. L. M. Aragno and F. Ancillotti, “Mechanistic studies on the homogeneous nickel-catalyzed low temperature methanol synthesis,” *J. Mol. Catal.,* vol. 75, pp. 147-151, 1992.

[249] E. S. Lee and K. Aika, “Low-temperature methanol synthesis in liquid-phase with a Raney Nickel–alkoxide system: effect of Raney Nickel pretreatment and reaction conditions,” *J. Mol. Catal. A: Chem.,* vol. 141, pp. 241-248, 1999.

[250] S. Ohyama, “Low-temperature methanol synthesis in catalytic systems composed of nickel compounds and alkali alkoxides in liquid phases,” *Appl. Catal. A,* vol. 180, pp. 217-225, 1999.

[251] V. M. Palekar, H. Jung, J. W. Tierney and I. Wender, “Slurry phase synthesis of methanol with a potassium methoxide/copper chromite catalytic system,” *Appl. Catal. A,* vol. 102, pp. 13-34, 1993.

[252] R. S. Sapienza, W. A. Slegeir, T. E. O'Hare and D. Mahajn, “Low temperature catalysts for methanol production”. United States of America Patent US4614749A, 30 September 1986.

[253] W. R. Brown, D. P. Drown and F. S. Frenduto, “Commercial-scale Demonstration of the Liquid Phase Methanol (LPMEOH) Process. Public Design Report.,” 2000.

[254] E. C. Heydorn, B. W. Diamond and R. D. Lilly, “Commercial-scale Demonstration of the Liquid Phase Methanol (LPMEOH) Process,” 2003.

[255] U.S. Department of Energy, National Energy Technology Laboratory, “"Commercial-Scale Demonstration of the Liquid Phase Methanol (LPMEOH) Process. A DOE Assesment.,” 2003.

[256] L. Fan, Y. Sakaiya and K. Fujimoto, “Low-temperature methanol synthesis from carbon dioxide and hydrogen via formic ester,” *Appl. Catal. A,* vol. 180, pp. L11-L13, 1999.

[257] N. Tsubaki, M. Ito and K. Fujimoto, “ A New Method of Low-Temperature Methanol Synthesis,” *J. Catal.,* vol. 197, pp. 224-227, 2001.

[258] J. Zeng, K. Fujimoto and N. Tsubaki, "A New Low-Temperature Synthesis Route of Methanol: Catalytic Effect of the Alcoholic Solvent," *Energy Fuels,* vol. 16, pp. 83-86, 2002.

[259] R. Yang, Y. Fu, Y. Zhang and N. Tsubaki, "In situ DRIFT study of low-temperature methanol synthesis mechanism on Cu/ZnO catalysts from CO_2-containing syngas using ethanol promoter," *J. Catal.,* vol. 228, pp. 23-35, 2004.

[260] R. Yang, Y. Zhang and N. Tsubaki, "Rideal-type reaction of formate species with alcohol: A key step in new low-temperature methanol synthesis method," *Catal. Commun.,* vol. 8, pp. 1829-1833, 2007.

[261] R. Yang, Y. Zhang and N. Tsubaki, "Dual catalysis mechanism of alcohol solvent and Cu catalyst for a new methanol synthesis method," *Catal. Commun.,* vol. 6, pp. 275-279, 2005.

[262] Y. Zhang, R. Yang and N. Tsubaki, "A new low-temperature methanol synthesis method: Mechanistic and kinetics study of catalytic process," *Catal. Today,* vol. 132, pp. 93-100, 2008.

[263] P. Reubroycharoen, T. Yamagami, T. Vitidsant, Y. Yoneyama, M. Ito and N. Tsubaki, "Continuous Low-Temperature Methanol Synthesis from Syngas Using Alcohol Promoters," *Energy Fuels,* vol. 17, pp. 817-823, 2003.

[264] R. Yang, X. Yu, Y. Zhang, W. Li and N. Tsubaki, "A new method of low-temperature methanol synthesis on Cu/ZnO/Al2O3 catalysts from $CO/CO_2/H_2$," *Fuel,* vol. 87, pp. 443-450, 2008.

[265] J. Bao, Z. Liu, Y. Zhang and N. Tsubaki, "Preparation of mesoporous Cu/ZnO catalyst and its application in low-temperature methanol synthesis," *Catal. Commun.,* vol. 9, pp. 913-918, 2008.

[266] L. Shi, Y. Tan and N. Tsubaki, "A Solid-State Combustion Method towards Metallic Cu–ZnO Catalyst without Further Reduction and its Application to Low-Temperature Methanol Synthesis," *ChemCatChem,* vol. 4, pp. 863-871, 2012.

[267] L. Shi, W. Shen, G. Yang, X. Fan, Y. Jin, C. Zeng, K. Matsuda and N. Tsubaki, "Formic acid directly assisted solid-state synthesis of metallic catalysts without further reduction: As-prepared Cu/ZnO catalysts for low-temperature methanol synthesis," *J. Catal.,* vol. 302, pp. 83-90, 2013.

[268] L. Shi, K. Tao, R. Yang, F. Meng, C. Xing and N. Tsubaki, "Study on the preparation of Cu/ZnO catalyst by sol–gel auto-combustion method and its application for low-temperature methanol synthesis," *Appl. Catal., A,* vol. 401, pp. 46-55, 2011.

[269] T. Zhao, K. Zhang, X. Chen, Q. Ma and N. Tsubaki, "A novel low-temperature methanol synthesis method from $CO/H_2/CO_2$ based on the synergistic effect between solid catalyst and homogeneous catalyst," *Catal. Today.,* vol. 149, pp. 98-104, 2010.

[270] T. Zhao, Y. Yoneyama, K. Fujimoto, N. Yamane, K. Fujimoto and N. Tsubaki, "Promotional Effect of Potassium Salt in Low-temperature Formate and Methanol Synthesis from $CO/CO_2/H_2$ on Copper Catalyst," *Chem. Lett.,* vol. 36, pp. 734-735, 2007.

[271] B. Hu and K. Fujimoto, "High-performance Cu/MgO–Na catalyst for methanol synthesis via ethyl formate," *Appl. Catal. A,* vol. 346, pp. 174-178, 2008.

[272] B. Hu and K. Fujimoto, "Promoting behaviors of alkali compounds in low temperature methanol synthesis over copper-based catalyst," *Appl. Catal. B,* vol. 95, pp. 208-216, 2010.

[273] C. A. Huff and M. S. Sanford, "Cascade Catalysis for the Homogeneous Hydrogenation of CO_2 to Methanol," *J. Am. Chem. Soc.,* vol. 133, pp. 18122-18125, 2011.

[274] Y. Chen, S. Choi and L. T. Thompson, "Low-Temperature CO_2 Hydrogenation to Liquid Products via a Heterogeneous Cascade Catalytic System," *ACS Catal.,* vol. 5, pp. 1717-1725, 2015.

[275] S. Kar, R. Sen, A. Goeppert and G. K. Surya Prakash, "Integrative CO_2 Capture and Hydrogenation to Methanol with Reusable Catalyst and Amine: Toward a Carbon Neutral Methanol Economy," *J. Am. Chem. Soc.,* vol. 140, p. 1580−1583, 2018.

[276] F. M. Stuardi, F. MacPherson and J. Leclaire, "Integrated CO_2 capture and utilization: A priority research direction," *Current Opinion in Green and Sustainable Chemistry,* vol. 16, p. 71–76, 2019.

[277] J. Kothandaraman, A. Goeppert, M. Czaun, G. A. Olah and G. K. Surya Prakash, "Conversion of CO_2 from Air into Methanol Using a Polyamine and a Homogeneous Ruthenium Catalyst," *J. Am. Chem. Soc.,* vol. 138, pp. 778-781, 2016.

[278] C. Reller, M. Pöge, A. Lißner and O. R. L. Mertens, "Methanol from CO_2 by Organo-Cocatalysis: CO_2 Capture and Hydrogenation in One Process Step," *Environ. Sci. Technol.,* vol. 48, p. 14799−14804, 2014.

[279] J. Kothandaraman, R. A. Dagle, V. Labarbier Dagle, S. D. DAvidson, E. D. Walter, S. D. Burton, D. W. Hoyt and D. J. Heldebrant, "Condensed-phase low temperature heterogeneous hydrogenation of CO_2 to methanol," *Catal. Sci. Technol.,* vol. 8, p. 5098–5103, 2018.

[280] F. Hemmann, S. Frölich, A. Lißner and F. O. R. L. Mertens, "Formate Ester Is Not a Decisive Intermediate in the Low-Temperature Synthesis of Methanol from Carbon Dioxide Dissolved in Diethylaminoethanol," *Energy Fuels,* vol. 32, pp. 6200-6203, 2018.

[281] R. P. W. J. Struis, S. Stucki and M. Wiedorn, "A membrane reactor for methanol synthesis," *J. Membr. Sci.,* vol. 113, pp. 93-100 , 1996.

[282] F. Gallucci, L. Paturzo and A. Basile, "An experimental study of CO_2 hydrogenation into methanol involving a zeolite membrane reactor," *Chem. Eng. Process.,* vol. 43, pp. 1029-1036, 2004.

[283] S. Kumar, N. Singh and R. Prasad, "Anhydrous ethanol: A renewable source of energy," *Renewable Sustainable Energy Rev.,* vol. 14, p. 1830–1844, 2010.

[284] I. Illiuta, M. Illiuta and F. Larachi, "Sorption-enhanced dimethyl ether synthesis—Multiscale reactor modeling," *Chem. Eng. Sci.,* vol. 66, pp. 2241-2251, 2011.

[285] M. Bayat, Z. Dehghani, M. Hamidi and M. R. Rahimpour, "Methanol synthesis via sorption-enhanced reaction process: Modeling and multi-objective optimization," *J. Taiwan Inst. Chem. Eng.,* vol. 45, pp. 481-494, 2014.

[286] A. Zachopoulos and E. Heracleous, "Overcoming the equilibrium barriers of CO_2 hydrogenation to methanol via water sorption: A thermodynamic analysis," *J.* CO_2 *Util.,* vol. 21, pp. 360-367, 2017.

[287] Finnish Wind Power Association, "Wind power projects in Finland," March 2017. [Online]. Available: http://www.tuulivoimayhdistys.fi/filebank/969-968-STY_hankelista_2017_web_final.xls. [Accessed 28 February 2018].

[288] G. Towler and R. Sinnott, "Capital Cost Estimating," in *Chemical Engineering Design,* Oxford, Elsevier, 2013, pp. 307-354.

[289] G. Towler and R. Sinnott, “Estimating Revenues and Production Costs,” in *Chemical Engineering Design*, Oxford, Elsevier, 2013, pp. 355-387.

[290] J. Levene, B. Kroposki and G. Sverdrup, “Wind Energy and Production of Hydrogen and Electricity--Opportunities for Renewable Hydrogen: Preprint,” National Renewable Energy Laboratory (NREL), Golden, CO, 2006.

[291] M. Finkenrath, “Cost and performance of carbon dioxide capture from power generation,” IEA, 2011.

[292] Eurostat, “Electricity prices for non-household consumers - bi-annual data (from 2007 onwards),” 23 November 2017. [Online]. Available: http://appsso.eurostat.ec.europa.eu/nui/show.do?dataset=nrg_pc_205&lang=en. [Accessed 28 February 2018].

[293] J. N. Keuler, L. Lorenzen and S. Miachon, “The dehydrogenation of 2-butanol over copper-based catalysts: optimising catalyst composition and determining kinetic parameters,” *Appl. Catal., A,* vol. 218, pp. 171-180, 2001.

[294] S. R. Segal, K. A. Carrado, C. L. Marshall and K. B. Anderson, “Catalytic decomposition of alcohols, including ethanol, for in situ H_2 generation in a fuel stream using a layered double hydroxide-derived catalyst,” *Appl. Catal., A,* vol. 248, pp. 33-45, 2003.

[295] L. Fan, Y. Sakaiya and K. Fujimoto, “Low-temperature methanol synthesis from carbon dioxide and hydrogen via formic ester,” vol. 180, pp. L11-L13, 1999.

[296] J. Schumann, A. Tarasov, N. Thomas, R. Schlögl and M. Behrens, “Cu,Zn-based catalysts for methanol synthesis: On the effect ofcalcination conditions and the part of residual carbonates,” *Appl. Catal., A,* vol. 516, pp. 117-126, 2016.

[297] J. Sloczynski, R. Grabowski, A. Kozlowska, P. Olszewski and J. Stoch, “Reduction kinetics of CuO in CuO/ZnO/ZrO2 systems,” *Phys. Chem. Chem. Phys.,* vol. 5, pp. 4631-4640, 2003.

[298] T. Lunkenbein, F. Girgsdies, T. Kandemir, N. Thomas, M. Behrens, R. Schlögl and E. Frei, “Bridging the Time Gap: A Copper/Zinc Oxide/Aluminum Oxide Catalyst for Methanol Synthesis Studied under Industrially Relevant Conditions and Time Scales,” *Angew. Chem.,* vol. 128, pp. 12900-12904, 2016.

[299] Y. Jeong, I. Kim, J. Y. Kang, H. Jeong, J. K. Park, J. H. Park and J. C. Jung, "Alcohol-assisted low temperature methanol synthesis from syngas over Cu/ZnO catalysts: Effect of pH value in the co-precipitation step," *J. Mol. Catal. A: Chem.*, vol. 400, pp. 132-138, 2015.

Publication I

H. Nieminen, L. Järvinen, V. Ruuskanen, A. Laari, T. Koiranen and J. Ahola
Insights into a membrane contactor based demonstration unit for CO_2 capture

Reprinted with permission from
Separation and Purification Technology
Vol. 231, 115951, 2020

Separation and Purification Technology 231 (2020) 115951

Contents lists available at ScienceDirect

Separation and Purification Technology

journal homepage: www.elsevier.com/locate/seppur

Insights into a membrane contactor based demonstration unit for CO_2 capture

H. Nieminen[a,*], L. Järvinen[b], V. Ruuskanen[b], A. Laari[a], T. Koiranen[a], J. Ahola[b]

[a] Lappeenranta-Lahti University of Technology, Laboratory of Process Systems Engineering, P.O. Box 20, FI-53851 Lappeenranta, Finland
[b] Lappeenranta-Lahti University of Technology, Laboratory of Control Engineering and Digital Systems, P.O. Box 20, FI-53851 Lappeenranta, Finland

ARTICLE INFO

Keywords:
CO_2 capture
Membrane contactor
Vacuum
Stripping
Amino acid salt
Potassium glycinate

ABSTRACT

A continuously operated CO_2 capture unit, based on absorption in a membrane contactor and low-temperature vacuum desorption, is demonstrated. The major advantage of membrane contactors is their high specific interfacial area per unit volume. The unit is designed to be modular to allow different absorption membrane modules and stripping units to be tested, with the aim of capturing CO_2 from simulated flue gases at concentrations down to the ambient concentration. In addition, desorption can be performed under vacuum to improve the desorption efficiency. The experimental unit incorporates comprehensive measurements and a high level of automation, with heat integration and continuous measurement of electricity consumption providing real-time estimates of the energy consumed in the capture process.

In preliminary tests, the results of which are described herein, a 3 M Liqui-Cel™ polypropylene hollow-fiber membrane module and a glass vacuum chamber were used for absorption and desorption, respectively, along with a potassium glycinate amino acid salt absorbent solution. This solution has high surface tension and is fully compatible with the polypropylene membrane unit used. In preliminary tests, the highest observed CO_2 flux was 0.82 mol m^{-2} h^{-1}, with a CO_2 product purity of above 80%. The calculated overall mass transfer coefficient was comparable to reference systems. The performance of the unit in its current setup was found to be limited by the desorption efficiency. Due to the low desorption rates, the measured specific energy consumption was exceedingly high, at 4.6 MJ/mol CO_2 (29.0 MW h/t) and 0.8 MJ/mol CO_2 (5.0 MW h/t) of heat and electricity, respectively. Higher desorption temperatures and lower vacuum pressures enhanced the desorption efficiency and reduced the specific energy consumption. The energy efficiency could be improved via several methods in the future, e.g., by applying ultrasound radiation or by replacing the current vacuum chamber stripping unit with a membrane module or some other type of desorption unit.

1. Introduction

The development and implementation of carbon capture technologies is vital to mitigate the growing global CO_2 emissions, which have been linked to detrimental climatic effects, most notably global warming [1]. Carbon capture refers to the separation of carbon dioxide (CO_2) from point emission sources, or potentially directly from the atmosphere [2]. In the carbon capture and storage (CCS) approach, the captured CO_2 is stored underground in geological formations like aquifers or depleted oil or gas fields [3]. Alternatively, carbon capture and utilization (CCU) aims to convert the captured CO_2 into valuable products, such as fuels or chemicals [4].

The most established technology for the separation of CO_2 from flue gases or process streams involves the absorption of CO_2 into basic solutions such as aqueous amines, most commonly monoethanolamine (MEA) [5,6]. In the amine absorption process, CO_2 is chemically absorbed into the solution and then released by heating the CO_2-loaded solution [3]. The significant amount of heat required for the regeneration of the solvent constitutes one of the main costs of any CO_2 capture process [6]. Thus, reducing the energy consumption of CO_2 capture is a major motivation for the development of alternative processes.

One potential method to intensify CO_2 capture is the use of membrane gas-liquid contactors, in which CO_2 is absorbed into the liquid absorbent via mass transfer through a porous, non-selective membrane [7,8]. Compared to conventional absorption equipment, membrane contactors offer a significant increase in the interfacial area per unit volume [9,10]. In addition, the interfacial area remains constant

* Corresponding author. Tel.: +358 407451800.
E-mail address: harri.nieminen@lut.fi (H. Nieminen).

https://doi.org/10.1016/j.seppur.2019.115951
Received 13 June 2019; Received in revised form 14 August 2019; Accepted 14 August 2019
Available online 16 August 2019

Nomenclature

A	membrane surface area, m^2
C	concentration, mol m^{-3}
C^*	equilibrium concentration, mol m^{-3}
c_p	heat capacity, J kg^{-1} K^{-1}
E	enhancement factor, –
e	specific energy, J mol^{-1}
K	gas-side overall mass transfer coefficient, m s^{-1}
k	individual mass transfer coefficient, m s^{-1}
N	molar CO_2 flux, mol m^{-2} s^{-1}
$\dot{n}$	molar flow rate, mol s^{-1}
Q	duty, W
T	temperature, K
$\dot{V}$	volumetric flow rate, m^3 s^{-1}
ΔC_m	logarithmic mean driving force, –
η	CO_2 capture efficiency, %
ρ	density, kg m^{-3}

Subscripts

e	electricity
g	gas
h	heat
l	liquid
in	inlet to the membrane module
m	membrane
out	outlet from the membrane module

regardless of the operating conditions, allowing flexible operation and independent adjustment of the gas and liquid flow rates. The orientation of the module can also be freely selected, and its modular design allows for simple and linear scale-up by increasing the number of modules and total membrane area.

To maximize the interfacial area, membrane gas-liquid contactors are commonly fabricated using hollow fibers [7]. In hollow fiber modules, the membrane fibers are usually packed in parallel bundles inside a shell, with one fluid flowing inside the fibers (lumen-side) and the other outside the fibers (shell-side). However, the added mass transfer resistance caused by the membrane represents a disadvantage. In order to minimize this resistance, microporous polymeric membranes are commonly utilized, with polypropylene (PP) and polytetrafluoroethylene (PTFE) being particularly well studied [8]. The porous membranes are not selective to CO_2; instead, selectivity is facilitated by the chemical absorption of CO_2 into the absorbent solution. The membrane must be hydrophobic in order to resist wetting by the aqueous solution, as the mass transfer is severely limited when the membrane is operated in wetted mode [11]. Selection of the absorbent is also vital in preventing wetting. PP membranes have been found to be incompatible with common amine absorbents for longer contact times due to the low surface tension of the liquid and the chemical changes induced in the membrane surface structure [12–14].

Due to the wetting of PP membranes, which are more affordable than PTFE membranes, by aqueous amines, the use of alternative absorbents in membrane contactors is of interest. The use of aqueous amino acid salts has been proposed, as their CO_2 absorption rates and capacities are comparable to those of amine solutions [15] and their high surface tension results in low wetting tendency [16]. In addition, the low volatility and toxicity of amino acid salts compared to amines is advantageous. A variety of amino acid salts have been considered for CO_2 absorption [17,18]. One example is potassium glycinate

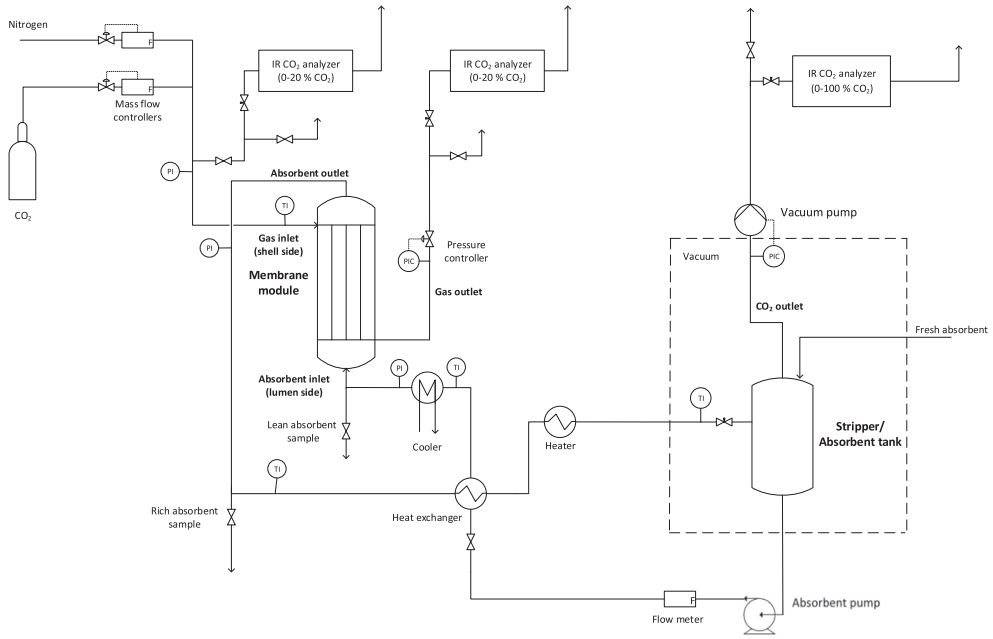

Fig. 1. Flowsheet of the experimental CO_2 capture unit.

[15,19–21], which is formed via the neutralization of the amino acid glycine with potassium hydroxide.

The application of a vacuum to lower the solvent regeneration temperature and the corresponding energy consumption has been suggested [22–25]. Lowering the regeneration temperature would also allow common membrane materials incapable of withstanding high operating temperatures to be utilized. The aim of the present study is to test and analyze the continuous absorption and desorption of CO_2 by a membrane contactor with potassium glycinate as the absorbent. Reports of such continuous processes are relatively scarce, as the majority of the previous literature has focused only on the absorption stage in non-steady-state operation. However, some reports of continuous processes at the laboratory and pilot scale are available [26–29,20].

Building on these developments, the present work demonstrates a continuously operated CO_2 capture unit based on absorption in a membrane contactor and low-temperature desorption under an applied vacuum. Here, the amino acid salt potassium glycinate is used as the absorbent, and a commercially available PP hollow fiber module is used as the membrane contactor. The aim of the present paper is to provide an overview of the equipment design, including its measurement and control capabilities, and to present and discuss the initial observations and results obtained using the unit. A more detailed characterization of the CO_2 absorption performance will be the subject of upcoming research.

2. Experimental

2.1. CO_2 capture unit

The continuously operated CO_2 capture unit consists of a hollow fiber membrane module as the absorber, a glass vessel that acts as a stripper, and a buffer tank for the absorbent solution. A flowsheet of the unit is presented in Fig. 1. The PP hollow fiber membrane contactor (Liqui-Cel 2.5 × 8 Extra-Flow) was supplied by 3 M. The membrane surface area of the module is 1.4 m^2. In the membrane module, the absorbent flows upwards inside the hollow fibers (lumen side, volume 0.15 l), while the inlet gas flows countercurrent on the shell side (volume 0.4 l). The inlet gas consists of a mixture of nitrogen (90% v/v, unless otherwise stated) and CO_2 (10% v/v) for simulated flue gas composition. The gas flows are controlled by mass flow controllers (Bronkhorst EL-FLOW Select, accuracy ± 0.5% reading, ± 0.1% full scale). The CO_2 concentration of the inlet gas is verified using an IR analyzer (GMP251 probe, ± 0.2% CO_2, and Indigo 201 transmitter, both supplied by Vaisala). The gas pressure is controlled using a back-pressure controller (Bronkhorst EL-PRESS, ± 0.1% reading, ± 0.5% full scale) located at the membrane gas outlet. The pressure at the gas outlet is maintained 0.1 bar below the liquid inlet pressure in order to avoid wetting of the membrane by the absorbent solution. The CO_2 concentration of the outlet gas is measured using a separate IR analyzer (Vaisala GMP251 probe and Indigo 201 transmitter).

Liquid is pumped through the system by a magnetic drive gear pump (Pulsafeeder Eclipse E12). The liquid flow rate is measured using a flow meter (Litre Meter LMX.48, ± 2% reading) located directly after the pump. The CO_2-lean absorbent pumped at the regeneration temperature (60–80 °C) is first cooled in a plate heat exchanger (Alfa Laval, heat transfer area 1.6 m^2) in which the heat is transferred to the cold absorbent exiting the membrane module. The liquid is then cooled to the absorption temperature (10–30 °C) in another plate heat exchanger (Alfa Laval, heat transfer area 0.2 m^2) with cooling water as the cold fluid. The temperature of the cooling water is controlled via a circulating cooler (Lauda Variocool VC5000, ± 0.05 °C). After flowing through the membrane module, the CO_2-rich absorbent is first heated in the heat exchanger and then heated to the regeneration temperature in a hot water heater. The heater consists of an electronic heating element and a coiled absorbent pipe inside a stainless-steel shell. The liquid pressure on the absorption side can be adjusted via a manual needle valve located before the stripper.

In the vacuum regeneration experiments, the gas outlet from the stripper vessel was connected to a vacuum pump (Vacuubrand MZ 2C NT) via an automatic vacuum control unit (Vacuubrand CVC-3000, ± 1 mbar, hysteresis 2%). The vacuum pump is equipped with a condenser to condense the solvent and water vapor. The outlet gas from the vacuum pump is routed to an IR CO_2-analyzer (CO2Meter CM-0052, ± 3% reading, ± 0.5% full scale) with a 0–100% v/v measuring

Fig. 2. Photograph of the CO_2 capture unit. 1. Membrane contactor, 2. vacuum desorption vessel.

range. In addition to CO_2, the analyzer measures the oxygen concentration with a 0–100% v/v measuring range. Fig. 2 presents a photograph of the unit.

2.2. Measurement and control

The control and data acquisition system is implemented using LabVIEW software. The data acquisition system (NI cDAQ-9189) is used for data gathering and analog control signal output. 4–20 mA analog input signals, measured with a NI 9208 module (accuracy ± 0.76% reading), are used for temperature measurements with Pt100 thermistors, pressure measurements, absorbent flow rate measurement, CO_2 analyzers, and mass flow controller feedback signals. A 4–20 mA analog output module (NI 9266, ± 0.76 reading, ± 1.4% full scale) is used to set the reference values for the mass flow controllers, the back-pressure controller, and the hot water heater. The internal temperature of the hot water heater is controlled via a PI control implemented in LabVIEW, and the 4–20 mA reference signal, which is equal to a power of 0–4.5 kW, is supplied to the REVO S three-phase thyristor power controller.

The analog input signals are sampled with a frequency of 2 kHz, and the mean value of 200 samples is then processed. Therefore, the control and data logging loop is executed with a frequency of 10 Hz. The circulating cooler and the vacuum pump are controlled over an RS232 serial bus with a loop time of around 1 s. The absorbent pump frequency converter is controlled and the electrical power measurement is read via Modbus/TCP with a loop time of roughly 1 s.

The electrical supply power is measured with a Sentron PAC3200 (± 0.5% reading) three-phase power analyzer equipped with MAK 62/W 25/1A current transformers. The circulating cooler and hot water heater are excluded from the electrical power measurement. Thus, the heating power of the absorbent is estimated based on the measured flow rate and temperature difference.

2.3. Procedure

The potassium glycinate absorbent was prepared by the neutralization of glycine (Sigma-Aldrich, > 99%) with an equimolar amount of potassium hydroxide (Sigma-Aldrich, > 85 wt%) in purified water. The solutions were prepared in a glass vessel equipped with a cooling water jacket. The concentrations of all the solutions were verified using potentiometric titration (Mettler-Toledo T50) using 1 M hydrochloric acid, and were within 1% of the nominal concentration. In the CO_2 capture experiments, the feed gas consisted of a mixture of nitrogen (> 99.5%) and CO_2 (> 99.99%).

The equipment was filled with 6 l of the absorbent solution; using this volume, the liquid level in the absorbent vessel was approximately half the vessel height. The system was started by flowing nitrogen through the membrane contactor, after which the liquid flow was started. The flows of CO_2 and nitrogen were then adjusted to reach the desired gas flow rate and composition. The CO_2 concentration (vol%) of the feed gas was verified by directing a portion of the flow to the IR-analyzer. Following this verification, the flow of feed gas to the analyzer was closed in order to measure the exact flow rate being delivered to the membrane contactor. The heater and cooler (Lauda) were turned on to adjust the liquid temperature during absorption and desorption. The pressure of the liquid entering the membrane module was adjusted using the manual needle valve located before the desorption vessel. In the vacuum desorption runs, the vacuum pump was switched on and the vacuum pressure was controlled by the vacuum control valve.

Unless otherwise stated, all experimental data were collected under steady-state conditions, as indicated by stable operating conditions (temperatures, flow rates, and pressures) together with a stable CO_2 concentration at the outlet of the membrane module (measured using the IR analyzer). The steady-state data were collected for periods of approximately 1 min in the LabView environment, and the final results were calculated as the average values during the sampling period. Liquid samples were also collected under steady-state conditions to analyze the CO_2 loading of the absorbent (mol CO_2 absorbed per mol of potassium glycinate). One rich solvent sample (collected after the membrane module) and one lean solvent sample (collected before the membrane module) were collected, and each sample was analyzed three times by titration with 1 M hydrochloric acid and measuring the volume of the released CO_2. This analysis was performed using a specifically designed Chittick-apparatus (Soham Scientific). The repeatability of the triplicate measurements was generally within 1.5% (relative standard deviation) with a maximum accepted deviation of 3.0%.

2.4. Calculation of the results

The CO_2 capture efficiency, i.e., the fraction of CO_2 absorbed from the feed gas, was calculated using the expression:

$$\eta = \frac{\dot{n}_{CO_2,in} - \dot{n}_{CO_2,out}}{\dot{n}_{CO_2,in}} \cdot 100\% \quad (1)$$

where η is the capture efficiency (%) and $\dot{n}_{CO_2,in}$ and $\dot{n}_{CO_2,out}$ are the molar flows of CO_2 (mol s^{-1}) in the inlet and outlet gas, respectively. The CO_2 molar flux from the gas phase to the liquid phase in the membrane contactor was calculated as:

$$N = \frac{\dot{n}_{CO_2,in} - \dot{n}_{CO_2,out}}{A} \quad (2)$$

where N is the flux (mol m^{-2} s^{-1}) and A is the membrane surface area (m^2) of the module, as specified by the supplier.

The overall mass transfer process in a membrane gas-liquid contactor consists of diffusion of CO_2 from the bulk gas phase to the gas-membrane interface, through the membrane pores to the membrane-liquid interface, and to the bulk liquid followed by chemical and/or physical absorption. The process can be described by the resistance-in-series model using the individual mass transfer coefficients for the gas, liquid, and membrane phases. The overall gas-phase mass transfer coefficient is given by the following expression [30]:

$$\frac{1}{K_g} = \frac{1}{k_g} + \frac{1}{k_m} + \frac{1}{mk_l E} \quad (3)$$

where k_g, k_m, and k_l are the gas, membrane, and liquid mass transfer coefficients, respectively, m is the distribution coefficient of CO_2 between the gas and liquid phases (Henry's constant in the case of physical absorption), and E is the enhancement factor caused by the chemical reaction, which is defined as the ratio of the absorption flux in the presence of the reaction and the flux with only physical absorption taking place.

To characterize the mass transfer performance of the present system, the gas-side overall mass transfer coefficient was calculated as:

$$K = \frac{N}{\Delta C_m} \quad (4)$$

where K is the overall mass transfer coefficient (m s^{-1}) and ΔC_m is the logarithmic mean driving force based on the gas-phase concentrations:

$$\Delta C_m = \frac{(C_{g,in} - C^*_{g,in}) - (C_{g,out} - C^*_{g,out})}{\ln[(C_{g,in} - C^*_{g,in})(C_{g,out} - C^*_{g,out})]} \quad (5)$$

here, $C_{g,in}$ and $C_{g,out}$ out are the measured CO_2 concentrations in the inlet and outlet gas (mol m^{-3}) and $C^*_{g,in}$ and $C^*_{g,out}$ are the inlet and outlet gas-phase CO_2 concentrations (mol m^{-3}) in equilibrium with the corresponding liquid-phase concentrations. The solubility data of Portugal et al. [31] for CO_2 in 1 M potassium glycinate were utilized to calculate the equilibrium concentrations. The gas-phase concentration was plotted against the liquid-phase concentration in the CO_2 partial pressure range relevant to the present experiments (100–1000 kPa), and an exponential curve was fitted to the data. As a result, the following

correlation was found:

$$C^*_{g,i} = 1.4 \cdot 10^{-4} e^{0.014 C_{l,i}} \quad (6)$$

where $C_{l,i}$ is the liquid-phase CO_2 concentration (mol m^{-3}).

The heat duty required for heating the absorbent from the absorption temperature to the desorption temperature was estimated as:

$$Q_h = \rho \dot{V} c_p \Delta T \quad (7)$$

where Q_h is the heat duty (W), $\dot{V}$ is the absorbent volume flow rate (m^3 s^{-1}), ΔT is the temperature difference (°C) between the desorption temperature and the temperature of the pre-heated absorbent leaving the plate heat exchanger, ρ is the absorbent density, approximated by the density of water (1000 kg m^{-3}), and c_p is the absorbent heat capacity, which was approximated using the heat capacity of pure water (4186 J kg^{-1} K^{-1}).

The specific heat consumption (J mol^{-1}) per mol of CO_2 captured was then calculated as:

$$e_{h,CO_2} = \frac{Q_h}{NA} \quad (8)$$

The specific electricity consumption (J mol^{-1}) was similarly calculated as:

$$e_{e,CO_2} = \frac{Q_e}{NA} \quad (9)$$

where Q_e is the total measured electrical power (W) of the absorbent pump and the vacuum pump.

2.5. Initial observations and challenges

Based on the initial experimental runs discussed here, it is apparent that the CO_2 absorption stage utilizing a membrane contactor can be run continuously with high degree of stability, providing consistent and reliable measurement data. The automatic gas-side pressure control is capable of maintaining the appropriate *trans*-membrane pressure under the dynamic conditions present during the start-up phase of the capture unit. The temperature of the absorbent solution entering the membrane module is effectively controlled by the heat exchanger and thermostat. Based on the limited operational time thus far, the PP membrane module appears to be compatible with the amino acid salt solution, and no indication of membrane wetting has been observed. At the start of the experiments, with unloaded absorbent, the mass transfer performance of the membrane contactor is excellent, with nearly 100% of the CO_2 being absorbed (Section 3).

However, from the initial results discussed below, it is clear that the overall CO_2 capture rate under steady-state conditions is limited by the performance of the current simple desorption unit. The glass vessel utilized as the desorber does not feature a distributor for the incoming absorbent and contains no packing to increase the gas/liquid contact area. As a result, the flow pattern of the liquid entering the vessel is not optimal, and the interfacial area is limited.

The desorption temperature is limited by the use of water as the heating medium in the absorbent heater. The temperature is limited to an absolute maximum of 80 °C, and even at that temperature, stable operation during longer periods was periodically disrupted by the overheating of the water bath. Higher temperatures could be achieved by using a different heat transfer fluid. However, operating the desorber at relatively low temperatures is preferred due to potential energy savings and to allow the utilization of low-grade heat or heat pumps, increased absorbent stability, and the possibility of utilizing membrane contactors at the desorption stage. The latter could significantly improve the mass transfer of CO_2 from the solution by increasing the interfacial area.

The rate at which water evaporated from the absorbent depended on the desorption temperature and vacuum pressure, and the vapor escaping the desorption vessel accumulated in the cold trap of the vacuum pump. In order to avoid excessive evaporation of water, the vacuum pressure was limited based on the boiling point of water at the desorption temperature. Operation at boiling conditions might have improved the desorption performance in the experiments due to the increased interfacial area created by the vapor bubbles and the sweeping effect of the vapor, resulting in a decreased partial pressure of CO_2 inside the vessel. Ideally, the condenser should be placed directly on top of the desorption vessel to allow the reflux of water.

3. Results and discussion

This section presents a summary of the preliminary results from the initial runs using the CO_2 capture unit. Fig. 3 presents an example of the evolution of the CO_2 concentration at the membrane outlet during start-up. In addition to the concentration, the corresponding CO_2 capture efficiency is also presented in the figure, and the profiles obtained using no vacuum and an 800-mbar vacuum at a desorption temperature of 60 °C are shown. During the first hour of operation, the unloaded

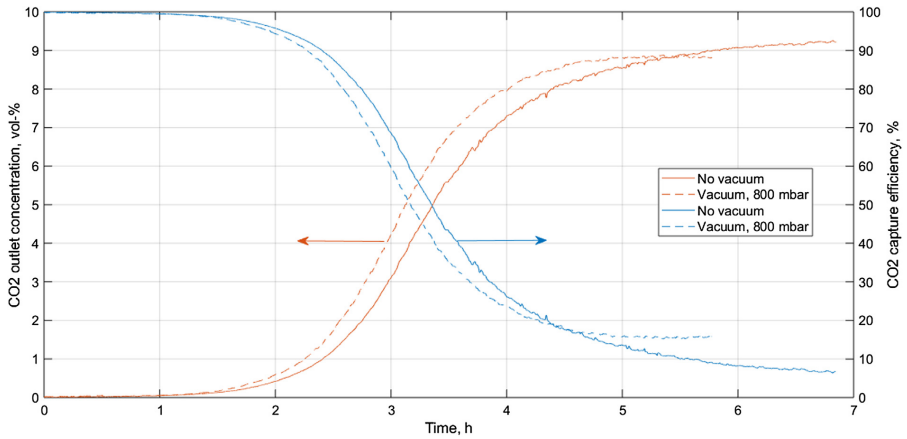

Fig. 3. CO_2 concentration and CO_2 capture efficiency during start-up: liquid: 1 l/min (3 M PG), gas: 5 l/min (10% CO_2), absorption: 20 °C, desorption: 60 °C.

absorbent was capable of near-complete absorption of the CO_2 fed to the membrane module, with a capture efficiency of approximately 100%. However, as the absorbed CO_2 was not completely desorbed from the solution, the CO_2 loading continually increased. The increased loading gradually led to a decrease in the CO_2 flux from the feed gas to the absorbent, and an increasing fraction of the CO_2 in the feed gas passed through the membrane module uncaptured. The steady state was reached when the absorption flux became equal to the flux of CO_2 desorbed from the solution.

When vacuum-assisted desorption was used, the steady state was achieved sooner, and the steady-state CO_2 concentration at the outlet was slightly lower (higher capture efficiency) compared to in desorption without vacuum. This indicates that the vacuum increased the CO_2 flux in the desorption stage. However, even using an 800-mbar vacuum, the desorption rate clearly limited the steady-state absorption performance, with the steady-state CO_2 capture efficiency of approximately 16%, compared to approximately 7% without the vacuum.

Fig. 4a presents the effect of the desorption temperature on the CO_2 flux for desorption without vacuum. Clearly, increasing the temperature had a favorable effect on the absorption performance. This can be explained by the more effective desorption of CO_2 from the loaded solution, leading to a lower CO_2 loading in the lean absorbent and increased driving force for absorption. The desorption temperature affects the solubility and resulting equilibrium CO_2 loading of the absorbent, the kinetics of the reactions involved in desorption, and the mass transfer of the desorbed CO_2. However, a detailed discussion of these effects is outside the scope of the present report. In summary, the overall effect of the desorption temperature was drastic in the studied temperature range, with the absorption flux increasing by 460% when the temperature was increased from 60 °C to 80 °C.

Fig. 4b presents the CO_2 flux during desorption under a 800–500 mbar vacuum at 60–80 °C. Compared to the non-vacuum results in Fig. 4a, the flux generally increased, and decreasing the pressure led to improved performance. The favorable effect of the vacuum can likely be explained by the decreased CO_2 partial pressure in the gas/vapor of the desorption vessel, leading to an increased driving force for desorption. In addition, the vacuum pump continuously swept the desorbed CO_2 out of the vessel, which also increased the driving force. However, the effect of temperature was more pronounced than that of the vacuum pressure. For example, at 60 °C, the flux increased by 115% when the vacuum pressure was lowered from 800 mbar to 500 mbar, while increasing the temperature from 60 °C to 80 °C at 800 mbar of vacuum resulted in a 500% increase in the flux.

Fig. 5 presents the overall mass transfer coefficients calculated from Eq. (3) for the different desorption pressures at a temperature of 80 °C. The overall mass transfer coefficient was found to increase with decreasing desorption pressure. This trend was consistent with the variation in the CO_2 flux (Fig. 4b) with vacuum pressure, and can be explained by the increased desorption efficiency and the resulting decrease in the CO_2 loading of the lean absorbent entering the membrane contactor. The lean adsorbent loading varied from 0.48 mol mol^{-1} at 800 mbar to 0.42 mol mol^{-1} at 500 mbar.

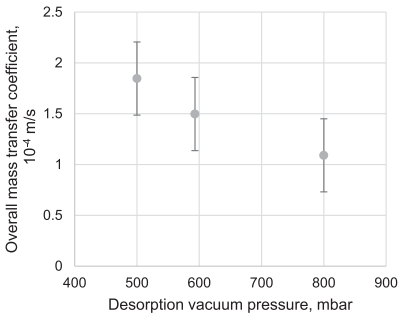

Fig. 5. Variation in the gas-side overall mass transfer coefficient with the desorption vacuum pressure at a desorption temperature of 80 °C. Absorbent flow rate: 1 l/min (1 M potassium glycinate), feed gas flow rate: 5 l/min (10% CO_2), absorption temperature: 20 °C. Error bars correspond to the 95% confidence interval as determined from repeat experiments.

As the driving force for the physical mass transfer from the gas to the liquid was included in the calculation of the overall mass transfer coefficient, the variation in the mass transfer coefficient likely corresponded to variation in the rate of chemical absorption. The higher lean loading under the less-favorable desorption conditions would result in a lower concentration of free amino acid salt in the solution, and a correspondingly lower reaction rate [16]. A similar explanation was given by Lu et al. [32], who also presented data on the overall mass transfer coefficient as a function of the lean solvent loading using N-methyldiethanolamine as the absorbent. Variation in the absorption flux with the CO_2 loading of the lean solution was also reported for various amino acid salt solutions in a screening study by He et al. [33].

The highest overall mass transfer coefficient was 1.9×10^{-4} m s^{-1}. Table 1 provides a comparison of this value to those in previous reports in the literature; all the listed references employed polypropylene hollow fiber membrane contactors with various absorbents. It should be noted that direct comparison of values determined under very different operating conditions, including different gas and liquid flow rates, temperatures, and solvent type and loadings, should be performed with caution. However, the value found here is well within the range of values found in the literature. Using amino acid salt solutions, Feron and Jansen [26] reported a value one order of magnitude higher utilizing a proprietary solution and custom-built transversal flow

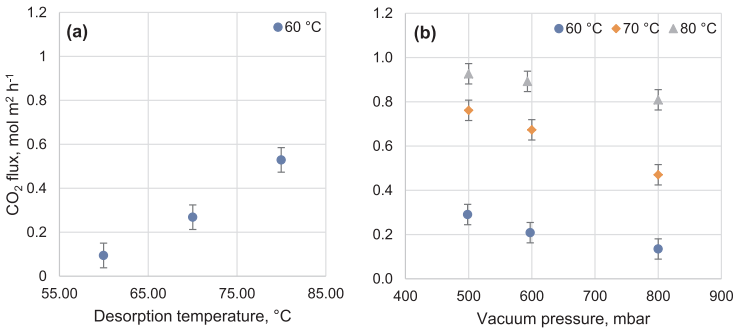

Fig. 4. (a) Dependence of the CO_2 absorption flux on the desorption temperature (no vacuum). (b) Dependence of CO_2 absorption flux on the vacuum pressure at desorption temperatures of 60, 70, and 80 °C. Absorbent flow rate: 1 l/min (1 M potassium glycinate), feed gas flow rate: 5 l/min (10% CO_2), absorption temperature: 20 °C. Error bars correspond to the 95% confidence interval as determined from repeat experiments.

Table 1
Comparison of experimental overall mass transfer coefficients in CO_2 absorption using polypropylene membrane contactors and various absorbents.

Reference	Absorbent	Overall mass transfer coefficient, $m\,s^{-1}$	Notes
This work	Potassium glycinate	1.9×10^{-4}	Continuous absorption-desorption, lean loading 0.42
Feron and Jansen (2002) [26]	CORAL (Proprietary amino acid salt based)	1.6×10^{-3}	Transversal flow module
Mavroudi et al. (2003) [35]	DEA	3.5×10^{-4}	Liqui-Cel module similar to this work
Dindore et al. (2004) [36]	Propylene carbonate	2.0×10^{-5}	Physical absorbent
Kosaraju et al. (2005) [28]	Polyamidoamine dendrimer	2.15×10^{-5}	Continuous absorption-stripping, lean loading not specified
Lu et al. (2005) [32]	MDEA	3.0×10^{-5} 0.8×10^{-5} (lean loading 0.3)	Variation of overall mass transfer coefficient with lean loading presented
Franco et al. (2008) [34]	MEA	4.3×10^{-4}	Simulated regenerated solution with lean loading of 0.27–0.30
Lu et al. (2009) [21]	Potassium glycinate	1.7×10^{-4}	
Lin et al. (2009) [37]	MDEA, AMP	3.3×10^{-4} (AMP) 7.7×10^{-5} (MDEA)	
Chabanon et al. (2011) [12]	MEA	3.3×10^{-4}	Wetting and performance monitored over long operating periods
Wang et al. (2013) [38]	Blended MEA, MDEA	6.8×10^{-4}	
Scholes et al. (2015) [39]	MEA	5.5×10^{-6}	Significant pore wetting observed
Scholes et al. (2015) [40]	BASF PuraTreat (Proprietary amino acid salt based)	7.0×10^{-6}	Pilot plant with real flue gas, significant pore wetting due to pressure fluctuations

membrane module. Lu et al. [21] obtained a value very similar to our result using a potassium glycinate solution. While most of the data were collected using fresh, unloaded solvent, some authors also have also presented results for CO_2-loaded solutions. Compared to these types of results [28,32,34] the performance of the present system is fairly competitive, especially considering its relatively high lean loading of 0.40 mol mol^{-1}.

The measurement of the CO_2 concentration of the outlet gas leaving the desorption unit allowed evaluation of the selectivity of the absorption process. As the feed gas in the present experiments consisted of only CO_2 and nitrogen, the analysis gave an indication of the CO_2/N_2 selectivity, as dictated by the chemical nature of the absorbent solution. Fig. 6 presents the CO_2 concentration of the outlet gas during vacuum desorption at 500–600 mbar and 60–80 °C. The CO_2 concentration ranged from 84 to 95 vol%, and no trends could be observed with respect to the desorption temperature and vacuum pressure. These values corresponded to CO_2/N_2 selectivities of 5–20. However, the reliability of these measurements was questionable, as oxygen concentrations of up to 3 vol% were also detected in the outlet gas. As oxygen was not present in the feed gas, the presence of oxygen can only be explained by air remaining in the system or by leaks in the vacuum system. As such, the measured CO_2 concentrations should be considered only as rough estimates, probably giving the lower limit of the actual concentration range.

The energy consumption of the capture unit consists of the heat required to heat the loaded absorbent to the desorption temperature and the electricity consumed by the absorbent and vacuum pumps. Fig. 7 presents the specific energy consumption obtained at a desorption temperature of 80 °C under 500–800 mbar vacuum. The electricity consumption was minor compared to the heat required: 4.1 MJ/mol of heat and 0.7 MJ/mol of electricity were consumed during desorption at 500 mbar. These conditions represented the lowest energy consumption among the preliminary runs, as the specific energy consumption was higher when lower desorption temperatures were used. The increased heating requirement at higher temperature was offset by the increased desorption efficiency. For the same reason, lowering the vacuum pressure led to lower heat consumption, while the specific electricity consumption remained essentially constant due to the increased power required by the vacuum pump.

The data available in the literature for the energy consumption of regeneration using membrane and/or vacuum technology are relatively limited, and the results vary significantly depending on the type of experimental system employed and the method used to estimate the energy consumption. Table 2 presents a summary of the specific energy consumption values found in the literature. Two types of approaches can be identified in the referenced works. In the first approach, the experiments and calculations are limited to the stripping stage in various configurations, and absorption and solvent circulation are not included [41,42,43]. Here, the energy consumption values range from 200 to 780 kJ kg CO_2^{-1}.

In the approach followed in this work, similar to Mulukutka et al. [44], the heat consumption is estimated based on the heating of the solvent in continuous absorption-stripping circulation. The energy consumption found in the current study is closely comparable to that reported by Mulukutka et al. This method seems to lead to energy consumption figures that are at least two orders of magnitude higher than those obtained using the first method. Part of the difference seems to arise from the experimental configuration: limiting the experiments to only the stripping stage allows the optimization of the operating conditions for effective and energy efficient desorption, while the operation in the continuous absorption-stripping mode requires also the consideration of the absorption performance when setting the operating parameters, such as the liquid flow rate. Compared to the work of Wang et al. [43], the liquid flow rate is higher in our case, leading to higher sensible heat requirement for heating the solvent. However, the major

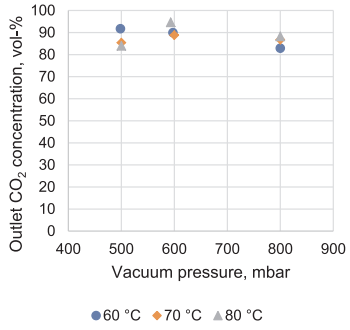

Fig. 6. Effect of vacuum pressure and desorption temperature on the CO_2 concentration of the outlet gas leaving the desorber. Absorbent flow rate: 1 l/min (1 M potassium glycinate), feed gas flow rate: 5 l/min (10% CO_2), absorption temperature: 20 °C.

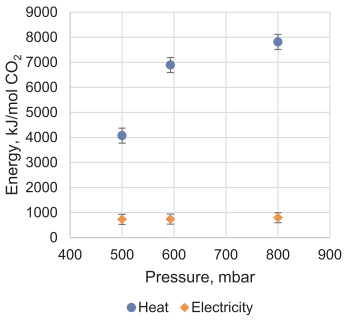

Fig. 7. Specific heat and electricity consumption per mole of CO_2 captured during desorption at 80 °C and 500–800 mbar vacuum. Absorbent flow rate: 1 l/min (1 M potassium glycinate), feed gas flow rate: 5 l/min (10% CO_2), absorption temperature: 20 °C.

difference is the much higher desorption efficiency of the membrane contactor stripping unit demonstrated by Wang et al. [43], indicating the potential for this type of technology.

The primary approach for improving the energy efficiency would be to increase the desorption efficiency. Increasing the temperature is not the preferred approach, as operation at relatively low regeneration temperatures is the explicit aim. However, applying lower vacuum pressures and employing intensified mass transfer equipment, including membrane contactors, is another potential approach. The use of membrane contactors in the desorption stage in conjunction with an applied vacuum to increase the driving force and gas sweep could significantly increase the desorption performance. It should be noted that membrane-based desorption is limited to lower regeneration temperatures due to the limited high-temperature stability of polymeric membranes. Intensification of the desorption stage could also be achieved by means of ultrasound radiation, which will also be explored in a future work.

In addition to modifications to the design of the experimental unit, the energy efficiency could also be improved by optimizing the operating parameters, such as the liquid and gas flow rates and the absorbent type and concentration. As the energy required for heating the solvent is linearly dependent on the liquid flow rate, minimizing the liquid flow rate relative to the gas flow rate would yield significant efficiency benefits. An optimum ratio could likely be found at which the liquid flow rate would be minimized without significant reduction in the CO_2 flux. At the optimum liquid/gas flow ratio, absorption would still be controlled by interphase mass transfer, while further decrease in the liquid flow rate would result the absorption being limited by the chemical reaction due to the depletion of free amino acid salt [16]. Increasing the absorbent concentration should also result in improved efficiency, as a greater concentration of CO_2 could be adsorbed while circulating and heating the same amount of liquid in the system, and accordingly, the CO_2 desorption flux would be higher at the same solvent heating duty.

4. Conclusion

A continuously operated CO_2 capture unit based on absorption in a membrane contactor and low-temperature desorption under an applied vacuum was demonstrated. The purpose of the unit is to capture CO_2 from simulated flue gas and process CO_2 stream concentrations down to ambient concentration. The experimental unit incorporates comprehensive measurements and a high level of automation, with heat integration and continuous measurement of electricity consumption potentially providing realistic estimates of the energy consumed in the capture process.

In preliminary runs using a potassium glycinate absorbent, the steady-state CO_2 absorption performance was found to be limited by the desorption stage. During start-up, the unloaded absorbent could achieve nearly complete absorption of the CO_2 fed to the membrane absorption module; the capture efficiency subsequently decreased as the CO_2 loading of the absorbent increased. Higher desorption temperatures and lower vacuum pressures were found to increase the desorption efficiency, resulting in a higher CO_2 absorption flux. The highest flux of 0.82 mol $m^{-2}h^{-1}$ (corresponding to 36 g CO_2 captured per hour) was found at a desorption temperature of 80 °C under a 500-mbar vacuum. The corresponding overall mass transfer coefficient (1.9×10^{-4} m s^{-1}) was comparable to previously published values for polypropylene contactors with various absorbents.

Increasing the desorption temperature and lowering the vacuum pressure also resulted in decreased specific energy consumption, as the increased heat and electricity consumption were offset by the increased desorption rate. The lowest specific heat and electricity consumption of 4.1 MJ/mol CO_2 (29.0 MW h/t) and 0.7 MJ/mol CO_2 (5.0 MW h/t) were achieved at 80 °C and 500 mbar vacuum. The observed purity of the desorbed CO_2 ranged from 84 to 95 vol%; however, the accuracy of these measurements was potentially compromised by the presence of air in the system.

Based on these initial findings, it is clear that the desorption efficiency of the unit must be improved via modification of the equipment setup and operational conditions. Optimization of the setup and conditions is facilitated by the modular nature of the unit, which allows it to operate with alternative membrane absorption modules and desorption configurations. The use of membrane contactors in the desorption stage could improve the performance via increased interfacial area. Lower vacuum pressures could be attained by eliminating the current operational limitations of the system. At present, the low desorption efficiency leads to very high values for the estimated specific

Table 2
Comparison of the specific energy consumption in vacuum- and membrane-based CO_2 stripping processes.

Reference	Method	Energy consumption, kJ $kg\ CO_2^{-1}$	Notes
This work	Potassium glycinate, 60–80 °C, 50–80 kPa	1.05×10^5 (heat) 1.82×10^4 (electricity)	Includes solvent heating and pumping, vacuum pump
Yan et al. (2009) [41]	MEA, 35 °C, 10–50 kPa	200	Includes vacuum pump but not solvent pumping or heating
Fang et al. (2012) [42]	MEA, PP membrane contactor as stripper, steam sweep, 70 °C, 10–48 kPa	200	Energy consumption increased at lower vacuum due to increased steam generation solvent pumping and heating not included
Wang et al. (2014) [43]	MEA, PP, and PVFD contactors, 75 °C, 5–80 kPa	780	Includes sensible and latent heat of solvent higher desorption flux with PVDF but improved stability with PP contactor
Mulukutka et al. (2014) [44]	Ionic liquid absorbent, PP module with fluorosiloxane coating, continuous absorption (50 °C) and stripping (85 °C, 98 kPa)	1.36×10^5	Considers heat of absorption and sensible heat of solvent, but not vacuum pump

energy consumption. In addition to improvements to the equipment setup, the specific energy consumption could be improved by optimization of the operating parameters, for example, by minimizing the liquid/gas flow ratio and increasing the absorbent concentration.

Declaration of Competing Interest

The authors declared that there is no conflict of interest.

Appendix A. Supplementary material

Supplementary data to this article can be found online at https://doi.org/10.1016/j.seppur.2019.115951.

References

[1] M. Mikkelsen, M. Jørgensen, F.C. Krebs, The teraton challenge. A review of fixation and transformation of carbon dioxide, Energ. Environ. Sci. 3 (2010) 43–81.
[2] J. Wilcox, Carbon Capture, Springer Science+Business Media, LLC, New York, 2012.
[3] M.E. Boot-Handford, J.C. Abanades, E.J. Anthony, M.J. Blunt, S. Brandani, N. Mac Dowell, J.R. Fernández, M.-C. Ferrari, R. Gross, J.P. Hallett, R.S. Haszeldine, P. Heptonstall, A. Lyngfelt, Z. Makuch, E. Mangano, R.T.J. Porter, Carbon capture and storage update, Energ Environ. Sci. 7 (2014) 130–189.
[4] M. Peters, B. Köhler, W. Kuckshinrichs, W. Leitner, P. Markewitz, T.E. Müller, Chemical technologies for exploiting and recycling carbon dioxide into the value chain, ChemSusChem 4 (2011) 1216–1240.
[5] N. MacDowell, N. Florin, A. Buchard, J. Hallett, A. Galindo, G. Jackson, C.S. Adjiman, C.K. Williams, N. Shah, P. Fennell, An overview of CO_2 capture technologies, Energ. Environ. Sci. 3 (2010) 1645–1669.
[6] E.S. Rubin, H. Mantripragada, A. Marks, P. Versteeg, J. Kitchin, The outlook for improved carbon capture technology, Prog. Energ. Combust. Sci. 38 (2012) 630–671.
[7] A. Gabelman, S.-T. Hwang, Hollow fiber membrane contactors, J. Membr. Sci. 159 (1–2) (1999) 61–106.
[8] S. Zhao, P.H.M. Feron, L. Deng, E. Favre, E. Chabanon, S. Yan, J. Hou, V. Chen, H. Qi, Status and progress of membrane contactors in post-combustion carbon capture: a state-of-the-art review of new developments, J. Membr. Sci. 511 (2016) 180–206.
[9] E. Cussler, Hollow fiber contactors, in: Membrane Processes in Separation and Purification, Kluwer Academic Publishers, Netherlands, 1994, pp. 375–394.
[10] E. Favre, H.F. Svendsen, Membrane contactors for intensified post-combustion carbon dioxide capture by gas–liquid absorption processes, J. Membr. Sci. 407–408 (2012) 1–7.
[11] S. Mosadegh-Sedghi, D. Rodrigue, J. Brisson, M.C. Iliuta, Wetting phenomenon in membrane contactors–causes and prevention, J. Membr. Sci. 452 (2014) 332–353.
[12] E. Chabanon, D. Roizard, E. Favre, Membrane contactors for postcombustion carbon dioxide capture: a comparative study of wetting resistance on long time scales, Ind. Eng. Chem. Res. 50 (13) (2011) 8237–8244.
[13] Y. Lv, X. Yu, S.-T. Tu, J. Yan, E. Dahlquist, Wetting of polypropylene hollow fiber membrane contactors, J. Membr. Sci. 362 (1–2) (2010) 444–452.
[14] D. deMontigny, P. Tontiwachwuthikul, A. Chakma, Using polypropylene and polytetrafluoroethylene membranes in a membrane contactor for CO_2 absorption, J. Membr. Sci. 277 (2006) 99–107.
[15] A.F. Portugal, P.W.J. Derks, G.F. Versteeg, F.D. Magalhães, A. Mendes, Characterization of potassium glycinate for carbon dioxide absorption purposes, Chem. Eng. Sci. 62 (2007) 6534–6547.
[16] P.S. Kumar, J.A. Hogendoorn, P.H.M. Feron, G.F. Versteeg, New absorption liquids for the removal of CO_2 from dilute gas streams using membrane contactors, Chem. Eng. Sci. 57 (9) (2002) 1639–1651.
[17] H.-J. Song, S. Park, H. Kim, A. Gaur, J.-W. Park, S.-J. Lee, Carbon dioxide absorption characteristics of aqueous amino acid salt solutions, Int. J. Greenhouse Gas Cont. 11 (2012) 64–72.
[18] B.M. Lerche, CO_2 Capture from Flue Gas Using Amino Acid Salt Solutions, Kgs. Lyngby: Technical University of Denmark (DTU), 2012.
[19] P.S. Kumar, J.A. Hogendoorn, G.F. Versteeg, Kinetics of the reaction of CO_2 with aqueous potassium salt of taurine and glycine, AIChE J. 49 (1) (2003) 203–213.
[20] S. Yan, M.-X. Fang, W.-F. Zhang, S.-Y. Wang, Z.-K. Xu, Z.-Y. Luo, K.-F. Cen, Experimental study on the separation of CO_2 from flue gas using hollow fiber membrane contactors without wetting, Fuel Process. Technol. 88 (2007) 501–511.
[21] J.-G. Lu, Y.-F. Zheng, M.-D. Cheng, Membrane contactor for CO_2 absorption applying amino-acid salt solutions, Desalination 249 (2009) 498–502.
[22] S. Nii, Y. Iwata, K. Takahashi, H. Takeuchi, Regeneration of CO_2-loaded carbonate solution by reducing pressure, J. Chem. Eng. Jpn. 28 (2) (1995) 148–153.
[23] M. Fang, S. Yan, Z. Luo, M. Ni, K. Cen, CO_2 chemical absorption by using membrane vacuum regeneration technology, Energ. Proc. 1 (2009) 815–822.
[24] Z. Wang, M. Fang, Y. Pan, S. Yan, Z. Luo, Amine-based absorbents selection for CO_2 membrane vacuum regeneration technology by combined absorption–desorption analysis, Chem. Eng. Sci. 93 (2013) 238–249.
[25] S. Yan, M. Fang, Z. Wang, Z. Luo, Regeneration performance of CO_2-rich solvents by using membrane vacuum regeneration technology: Relationships between absorbent structure and regeneration efficiency, Appl. Energ. 98 (2012) 357–367.
[26] P. Feron, A. Jansen, CO_2 separation with polyolefin membrane contactors and dedicated absorption liquids: performances and prospects, Sep. Purif. Technol. 27 (2002) 231–242.
[27] O. Falk-Pedersen, M. Grønvold, P. Nøkleby, F. Bjerve, CO_2 capture with membrane contactors, Int. J. Green Energ. 2 (2005) 157–165.
[28] P. Kosaraju, A.S. Kovvali, A. Korikov, K.K. Sirkar, Hollow fiber membrane contactor based CO_2 absorption-stripping using novel solvents and membranes, Ind. Eng. Chem. Res. 44 (2005) 1250–1258.
[29] S.-H. Yeon, K.-S. Lee, B. Sea, Y.-I. Park, K.-H. Lee, Application of pilot-scale membrane contactor hybrid system for removal of carbon dioxide from flue gas, J. Membr. Sci. 257 (2005) 156–160.
[30] J.-L. Li, B.-H. Chen, Review of CO_2 absorption using chemical solvents in hollow fiber membrane contactors, Sep. Purif. Technol. 41 (2) (2005) 109–122.
[31] A.F. Portugal, J.M. Souda, F.D. Magalhães, A. Mendes, Solubility of carbon dioxide in aqueous solutions of amino acid salts, Chem. Eng. Sci. 64 (2009) 1993–2002.
[32] J. Lu, L. Wang, X. Sun, J. Li, X. Liu, Absorption of CO_2 into aqueous solutions of methyldiethanolamine and activated methyldiethanolamine from a gas mixture in a hollow fiber contactor, Ind. Eng. Chem. Res. 44 (2005) 9230–9238.
[33] F. He, T. Wang, M. Fang, Z. Wang, H. Yu, Q. Ma, Screening test of amino acid salts for CO_2 absorption at flue gas temperature in a membrane contactor, Energ. Fuels 31 (2017) 770–777.
[34] J. Franco, D. deMontigny, S. Kentish, J. Perera, G. Stevens, A study of the mass transfer of CO_2 through different membrane materials in the membrane gas absorption process, Sep. Sci. Technol. 43 (2008) 225–244.
[35] M. Mavroudi, S.P. Kaldis, G.P. Sakellaropoulos, Reduction of CO_2 emissions by a membrane contacting process, Fuel 82 (2003) 2153–2159.
[36] V. Dindore, D. Brilman, F. Geuzebroek, G. Versteeg, Membrane–solvent selection for CO_2 removal using membrane gas–liquid contactors, Sep. Purif. Technol. 40 (2) (2004) 133–145.
[37] S.-H. Lin, C.-F. Hsieh, M.-H. Li, K.-L. Tung, Determination of mass transfer resistance during absorption of carbon dioxide by mixed absorbents in PVDF and PP membrane contactor, Desalination 249 (2009) 647–653.
[38] Z. Wang, M. Fang, S. Yan, H. Yu, C.-C. Wei, Z. Luo, Optimization of blended amines for CO_2 absorption in a hollow-fiber membrane contactor, Ind. Eng. Chem. Res. 52 (2013) 12170–12182.
[39] C. Scholes, S. Kentish, G. Stevens, D. deMontigny, Comparison of thin film composite and microporous membrane contactors for CO_2 absorption into monoethanolamine, Int. J. Greenhouse Gas Cont. 42 (2015) 66–74.
[40] C.A. Scholes, A. Qader, G.W. Stevens, S.E. Kentish, Membrane gas-solvent contactor pilot plant trials of CO_2 absorption from flue gas, Sep. Sci. Technol. 49 (2014) 2449–2458.
[41] S. Yan, M. Fang, Z. Luo, K. Cen, Regeneration of CO_2 from CO_2-rich alkanolamines solution by using reduced thickness and vacuum technology: regeneration feasibility and characteristic of thin-layer solvent, Chem. Eng. Process.: Proc. Intensif. 48 (2009) 515–523.
[42] M. Fang, Z. Wang, S. Yan, Q. Cen, Z. Luo, CO_2 desorption from rich alkanolamine solution by using membrane vacuum regeneration technology, Int. J. Greenhouse Gas Cont. 9 (2012) 507–521.
[43] Z. Wang, M. Fang, Q. Ma, Z. Zhao, T. Wang, Z. Luo, Membrane stripping technology for CO_2 desorption from CO_2-rich absorbents with low energy consumption, Energ. Proc. 63 (2014) 765–772.
[44] T. Mulukutla, G. Obuskovic, K.K. Sirkar, Novel scrubbing system for post-combustion CO_2 capture and recovery: experimental studies, J. Membr. Sci. 471 (2014) 16–26.

Publication II

H. Nieminen, L. Järvinen, V. Ruuskanen, A. Laari, T. Koiranen and J. Ahola
Mass transfer characteristics of a continuously operated hollow-fiber membrane contactor and stripper unit for CO_2 capture

Reprinted with permission from
International Journal of Greenhouse Gas Control
Vol. 98, 103063, 2020

International Journal of Greenhouse Gas Control 98 (2020) 103063

Contents lists available at ScienceDirect

International Journal of Greenhouse Gas Control

journal homepage: www.elsevier.com/locate/ijggc

Mass transfer characteristics of a continuously operated hollow-fiber membrane contactor and stripper unit for CO_2 capture

H. Nieminen[a,*], L. Järvinen[b], V. Ruuskanen[b], A. Laari[a], T. Koiranen[a], J. Ahola[b]

[a] Lappeenranta-Lahti University of Technology, Laboratory of Process Systems Engineering, P.O. Box 20, FI-53851 Lappeenranta, Finland
[b] Lappeenranta-Lahti University of Technology, Laboratory of Control Engineering and Digital Systems, P.O. Box 20, FI-53851 Lappeenranta, Finland

ARTICLE INFO

Keywords:
CO_2 capture
Membrane contactor
Vacuum
Stripping
Desorption
Amino acid salt
Potassium glycinate

ABSTRACT

Mass transfer performance of a polypropylene hollow-fiber membrane contactor as part of a continuously operated CO_2 capture unit with amino acid salt (potassium glycinate) absorbent and vacuum solvent regeneration was studied. The effects of key operating parameters on the absorption mass transfer characteristics were explored. Without vacuum stripping, absorption rate was found to be limited by low CO_2 desorption efficiency from the loaded absorbent solution in the stripping unit, resulting in high solvent CO_2 loadings and limited chemical absorption rates. Introduction of vacuum stripping greatly improved desorption performance, resulting in improved steady-state absorption performance. The overall mass transfer coefficient increased at higher stripping temperatures and lower vacuum pressures in the range of 60 – 80 °C and 300 – 800 mbar (abs). The overall mass transfer coefficient increased with increasing liquid flow rate, and the highest value reached was $1.8 \cdot 10^{-4}$ m s^{-1}. The individual mass transfer coefficients in absorption were calculated based on mass transfer correlations and experimental data, including estimation of the enhancement factor for chemical absorption. The overall mass transfer resistance was found to be dominated by the liquid-side resistance, at almost 90 % of the total resistance. The estimated membrane mass transfer coefficient was low compared to a theoretical value assuming non-wetted operation, suggesting potential partial wetting of the membrane. Stable performance of the unit and the membrane contactor was demonstrated during a stability test with over 30 h of operation.

1. Introduction

The continuously increasing atmospheric carbon dioxide (CO_2) concentration resulting from growing global CO_2 emissions has been linked to detrimental climatic effects (Mikkelsen et al., 2010). Development of carbon capture technologies for the separation of carbon dioxide both from point emission sources and directly from the atmosphere could provide a partial solution for the mitigation of CO_2 emissions (Wilcox, 2012). Furthermore, the utilization of captured CO_2 by chemical conversion could provide a fossil-free route to various valuable fuel or chemical products (Peters et al., 2011).

The established technology for the capture of CO_2 from flue gases or process streams is based on chemical absorption in columns using basic solutions such as aqueous amines, most commonly monoethanolamine (MEA) (MacDowell et al., 2010; Rubin et al., 2012). The process consists of absorption of CO_2 into the solution followed by solvent regeneration and release of CO_2 by heating of the CO_2-loaded solution (Boot-Handford et al., 2014). The solvent regeneration stage requires a significant amount of heat, which constitutes the main operating cost of the overall capture process (Rubin et al., 2012). Thus, reduction of the energy consumption is a major motivation for the development of alternative CO_2 capture processes. Another objective is to decrease the desorption temperature level, which would enable the usage of waste heat streams, solar thermal and heat pumps for the generation of required heat energy. Such alternatives include the utilization of alternative absorbents (Dutcher et al., 2015; Mumford et al., 2015; Ramdin et al., 2012), or alternative processes based on absorption (D'Alessandro et al., 2010) or membrane separation (Brunetti et al., 2010).

Alternative for columns is the use of membrane gas-liquid contactors, where CO_2 is absorbed to the chemical absorbent via mass transfer through a porous, non-selective membrane (Gabelman and Hwang, 1999; Zhao et al., 2016). A major advantage of membrane contactors compared to conventional absorption equipment is the significantly higher interfacial area per unit volume offered by the membrane hollow fiber configuration (Cussler, 1994; Favre and Svendsen, 2012). The interfacial area remains constant regardless of the operating conditions which allows highly flexible operation and independent

* Corresponding author.
E-mail address: harri.nieminen@lut.fi (H. Nieminen).

https://doi.org/10.1016/j.ijggc.2020.103063
Received 3 February 2020; Received in revised form 24 April 2020; Accepted 1 May 2020

Nomenclature

A	membrane surface area, m^2
C	concentration, mol^{-3}
C^*	equilibrium concentration, mol^{-3}
D	diffusivity, $m^2 s^{-1}$
d	diameter, m
E	enhancement factor
Ha	Hatta number
K	gas-side overall mass transfer coefficient, m s^{-1}
k	individual mass transfer coefficient, m s^{-1}
k	reaction rate constant, $m^3 mol^{-1} s^{-1}$
l	membrane length
m	dimensionless Henry's constant
N	molar CO_2 flux, $mol^{-2} s^{-1}$
n	number of membrane fibers
$\dot{n}$	molar flow rate, mol/s
Re	Reynolds number
Sc	Schmidt number
Sh	Sherwood number
$\dot{V}$	volumetric flow rate, $m^3 s^{-1}$
v	superficial velocity, $m^{-1} s^{-1}$
α	CO_2 loading in absorbent, mol mo^{-1}
ΔC_m	logarithmic mean driving force
δ	membrane thickness, m
ε	membrane porosity
η	efficiency
ν	kinematic viscosityy, $m^2 s^{-1}$
τ	membrane tortuosity

Subscripts

1	forward reaction
− 1	reverse reaction
abs	absorption
B	base
c	contactor
chem	chemical
des	desorption
eff	effective (diffusivity)
G	gas
i	inside (membrane fiber)
in	inlet to the membrane module
L	liquid
LM	liquid-membrane interface
M	membrane
o	outside (membrane fiber)
out	outlet from the membrane module
phys	physical
PG	potassium glycinate
R	reaction
∞	limiting (enhancement factor)

adjustment of the gas and liquid flow rates. In addition, the module orientation can be freely selected, and simple linear scale-up is facilitated by increasing the number of modules and the total membrane area.

A disadvantage of membrane contactors is the added mass transfer resistance caused by the membrane. In order to minimize this resistance, microporous polymeric materials such as polypropylene (PP) and polytetrafluoroethylene (PTFE) are commonly employed (Zhao et al., 2016). The membrane has to be hydrophobic in order to resist wetting by the aqueous absorbent, as mass transfer is severely limited if the membrane operates in wetted mode (Mosadegh-Sedghi et al., 2014). Compatibility of the membrane material and the absorbent is vital for preventing membrane wetting. As cost-effective PP membranes have been found to be wetted by common amine absorbents during longer contact times (Chabanon et al., 2011; Lv et al., 2010; deMontigny et al., 2006), the use of alternative absorbents in membrane contactors has found interest. Aqueous amino acid salts offer comparable CO_2 absorption rates and capacities compared to amine solutions combined with a high surface tension and low wetting tendency (Kumar et al., 2002; Portugal et al., 2007a; Feron and Jansen, 2002). In addition, the ionic absorbents possess low volatility and toxicity. An example of an amino acid salt considered for membrane contactors is potassium glycinate (Portugal et al., 2007a; Kumar et al., 2003a; Yan et al., 2007; Lu et al., 2009), formed by neutralization of the amino acid glycine with potassium hydroxide.

The present study analyses the continuous absorption and desorption of CO_2 utilizing a membrane contactor with the potassium glycinate absorbent. Reports on such complete, continuous processes are relatively scarce as the majority of previous literature has focused primarily on the absorption stage. However, some reports of complete capture processes based on membrane contactors in the laboratory and pilot scale are available (Falk-Pedersen and Dannström, 1997; Falk-Pedersen et al., 2005; Feron and Jansen, 2002; Yeon et al., 2005; Kosaraju et al., 2005; Scholes et al., 2014; Li et al., 2017). These processes are generally based on the combination of a membrane contactor for absorption with a conventional stripper for desorption. The use of membrane contactors for CO_2 stripping would be interesting as the same advantages found in the absorption stage could be realized also at the solvent regeneration stage. However, a major challenge is the requirement for membrane stability at elevated temperatures. Instead of low-cost polymeric membranes, membranes with a more limited availability and higher cost are generally required for stable performance under desorption conditions (Nii et al., 1995; Fang et al., 2009; Wang et al., 2013a; Yan et al., 2012).

The application of vacuum for CO_2 stripping has been suggested for lowering the solvent regeneration temperature and the corresponding energy consumption (Nieminen et al., 2020). Decreasing the regeneration temperature would also serve to increase the applicability of common membrane materials incapable of withstanding higher operating temperatures. Vacuum desorption of CO_2 from various amine solutions using PP hollow fiber contactors has been demonstrated (Kumar et al., 2003b; Li and Chen, 2005). For reference, Fang et al. (Kumar et al., 2003b) performed desorption at pressures of 10 − 35 kPa and temperatures of 40 − 70 °C, showing the potential for significant decreases in the regeneration temperature. The vacuum regeneration performance of potassium glycinate has been found comparable to amines (Portugal et al., 2007b), suggesting potential for utilizing amino acid salts in such a process.

This work characterises the CO_2 capture performance of a continuously operated unit combining absorption in a membrane contactor and solvent regeneration utilizing vacuum. It is in continuation of a previous report which focused on the design and operation of the unit and presented initial findings concerning the absorption/desorption performance and energy consumption (Lerche, 2012). The present report provides a more detailed mass transfer analysis of the membrane contactor in a CO_2 absorption/desorption process during steady-state operation. The aim is to assess the effect of key process parameters on the mass transfer performance of the membrane module, as primarily measured by the gas-side overall mass transfer coefficient. In addition, the gas, membrane and liquid individual mass transfer resistances are evaluated from mass transfer correlations and measured absorption data. In addition, stable performance is demonstrated during a stability test with over 30 h of operation. A number of data points, as referenced, are reproduced from the previous publication.

2. Experimental

2.1. CO_2 capture unit

The continuously operated CO_2 capture unit consists of a hollow fiber membrane module as the absorber, a reaction vessel acting as a stripper and a buffer tank for the absorbent solution, and pumping and temperature control equipment for maintaining absorbent liquid circulation at controlled temperatures. A flowsheet of the unit is presented in Fig. 1. The same unit was first described in a previous publication (Lerche, 2012). The membrane surface area of the PP hollow fiber membrane module (Liqui-Cel™ 2.5 × 8 Extra-Flow, supplied by 3 M) is 1.4 m^2. In the membrane module, the absorbent flows upwards inside the hollow fibers (lumen side) while the inlet gas flows countercurrent on the shell side.

The inlet gas consists of nitrogen or air mixed with CO_2 (10 % v/v unless stated otherwise) for a simulated flue gas composition, with gas flows controlled by mass flow controllers (Bronkhorst EL-FLOW Select, accuracy ± 0.5 % reading, ± 0.1 % full scale). The CO_2 concentration of the inlet gas is verified by an IR-analyzer analyzer (GMP251 probe, ± 0.2 % CO_2, and Indigo 201 transmitter, both supplied by Vaisala). The gas pressure is controlled by a back-pressure controller (Bronkhorst EL-PRESS, ± 0.1 % reading, ± 0.5 % full scale) located at the membrane gas outlet. The pressure at the gas outlet is maintained at 0.1 bar below the liquid inlet pressure in order to avoid wetting of the membrane by the absorbent solution. The CO_2 concentration of the outlet gas is measured by a separate IR-analyzer (Vaisala GMP251 probe and Indigo 201 transmitter).

Liquid is pumped through the system by a magnetic drive gear pump (Pulsafeeder Eclipse E12) and the liquid flow rate is measured by a flow meter (Litre Meter LMX.48, ± 2 % reading) located directly after the pump. The CO_2-lean absorbent pumped at the regeneration temperature (60 − 80 °C) is first cooled in a plate heat exchanger (Alfa Laval, 1.6 m^2) in which heat is transferred to the cold absorbent exiting the membrane module. The liquid is then cooled to the absorption temperature (10 − 30 °C) in another plate heat exchanger (Alfa Laval, 0.2 m^2) with cooling water as the cold fluid. The temperature of the cooling water is controlled by a circulating cooler (Lauda Variocool VC5000, ± 0.05 °C). After flowing through the membrane module, the CO_2-rich absorbent is first heated in the heat exchanger and then heated to the regeneration temperature in a hot water heater. The liquid pressure on the absorption side is adjusted by a manual needle valve located before the stripper.

For use of vacuum in solvent regeneration, the gas outlet from the stripper vessel is connected to a vacuum pump (Vacuubrand MZ 2C NT) via an automatic vacuum control unit (Vacuubrand CVC-3000, ± 1 mbar). The outlet gas from the vacuum pump flows to an IR CO_2-analyzer (CO2Meter CM-0052, ± 3 % reading, ± 0.5 % full scale) with a 0–100 % v/v measuring range. In addition to CO_2, the analyzer measures the oxygen concentration with a 0–100 % v/v measuring range.

The control and data acquisition system is implemented with LabVIEW software. Data acquisition system (NI cDAQ-9189) is used for data gathering and analog control signals output. 4 − 20 mA analog input signals are measured with NI 9208 module (accuracy ± 0.76 % reading), and 4 − 20 mA analog output module (NI 9266, ± 0.76 % reading, ± 1.4 % full scale) is used to set reference values for the process units. The system includes online measurement of the electricity consumed by the liquid and vacuum pumps, and calculation of the heat energy consumed in heating of the absorbent to the regeneration temperature, based on the measured flow rate and temperature difference. The electrical supply power is measured with a Sentron PAC3200 (± 0.5 % reading) three-phase power analyzer equipped with MAK 62/W 25/1A current transformers.

2.2. Chemicals

The potassium glycinate absorbent was prepared by neutralization of glycine (Sigma-Aldrich, > 99 %) with an equimolar amount of potassium hydroxide (Sigma-Aldrich, > 85 w-%) in purified water. The solutions were prepared in a glass vessel equipped with a cooling water jacket. The concentration of all solutions was verified by potentiometric titration (Mettler-Toledo T50) using 1 M hydrochloric acid. The concentration of all solutions was within 1% of the nominal concentration. In the CO_2 capture experiments, the feed gas consisted of technical grade nitrogen (> 99.5 %) or ambient air mixed with CO_2 from a gas cylinder (> 99.99 %). 1 M hydrochloric acid and methyl red (5% solution in ethanol) were used in the titrimetric CO_2-loading analysis of

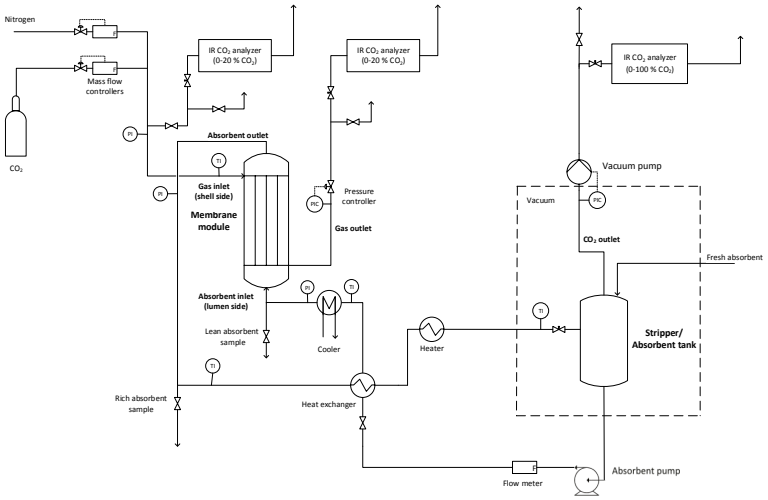

Fig. 1. Flowsheet of the experimental CO_2 capture unit (Nieminen et al., 2020).

the liquid absorbent samples.

2.3. Procedure

The equipment was filled with 6 L of the absorbent solution; using this volume, the liquid level in the absorbent vessel was approximately half the vessel height. The system was started by flowing nitrogen through the membrane contactor, after which the liquid flow was started. The flows of CO_2 and nitrogen were then adjusted to reach the desired gas flow rate and composition. The CO_2 concentration (vol%) of the feed gas was verified by directing a portion of the flow to the IR-analyzer. Following this verification, the flow of feed gas to the analyzer was closed in order to measure the exact flow rate being delivered to the membrane contactor. The heater and cooler were turned on to adjust the liquid temperature during absorption and desorption. The pressure of the liquid entering the membrane module was adjusted using the manual needle valve located before the desorption vessel. In the vacuum desorption runs, the vacuum pump was switched on and the vacuum pressure was controlled by the vacuum control valve.

Unless otherwise stated, all experimental data was collected under steady-state conditions, as indicated by stable operating conditions (temperatures, flow rates, pressures) together with a stable CO_2 concentration at the outlet of the membrane module (measured by the IR-analyzer). Depending on the process parameters, the time required to achieve steady-state was above 8 h after fresh absorbent was introduced, due to the slow increase in the CO_2-loading of the circulating liquid. Following a change in the experimental conditions without absorbent replacement, the new steady-state was generally reached within 2 h.

The steady-state data were collected for periods of approximately 1 min in the LabView environment, and the final results were calculated as the average values during the sampling period. Liquid samples were also collected under steady-state conditions to analyze the CO_2 loading of the absorbent (mol CO_2 absorbed per mol of potassium glycinate). One rich solvent sample (collected after the membrane module) and one lean solvent sample (collected before the membrane module) were collected. Each sample was analyzed three times by titration with 1 M hydrochloric acid with methyl red indicator with the volume of released CO_2 measured. This analysis was performed using a specifically designed Chittick-apparatus (Soham Scientific). The repeatability of the triplicate measurements was generally within 1.5 % (relative standard deviation) with a maximum accepted deviation of 3.0 %.

A summary of the main operating parameters is presented in Table 1. The experimental plan consisted of varying the absorbent flow rate, the CO_2 concentration in the feed gas, and the absorption and desorption temperatures. In the vacuum desorption experiments, the vacuum pressure was also varied. The repeatability of the experiments was checked by performing a series of repeat runs at one operating point. The standard error of the mean was calculated for each measured or calculated result observed in these repeat runs and multiplied by a factor of 2 for a 95 % confidence interval. The same confidence interval is assumed to hold for all data points. These confidence intervals are presented as error bars in the relevant figures.

2.4. Theory and calculations

The overall mass transfer process in a membrane gas-liquid contactor consists of diffusion of CO_2 from the bulk gas phase to the gas-membrane interface, through the membrane pores to the membrane-liquid interface, and to the bulk liquid followed by chemical and/or physical absorption. The process can be described by the resistance-in-series model using the individual mass transfer coefficients for the gas, liquid and membrane phases. The gas-side overall gas-phase mass transfer coefficient is given by the following expression (Portugal et al., 2009; Kumar et al., 2003c):

$$\frac{1}{K_G} = \frac{1}{k_G} + \frac{1}{k_M} + \frac{1}{mk_L E} \quad (1)$$

Where k_G, k_M, and k_L are the gas, membrane and liquid mass transfer coefficients, respectively, m is the distribution coefficient of CO_2 between gas and liquid phases (dimensionless Henry's constant), and E is the enhancement factor caused by chemical reaction defined as the ratio of the absorption flux in the presence of reaction and the flux with only physical absorption taking place:

$$E = \frac{N_{chem}}{N_{phy}} \quad (2)$$

Where N refers to the CO_2 flux through the membrane.

In aqueous solution, amino acid salts formed by the neutralization of amino acids by a strong base are present in the amine form. The amino acid salts are weakly basic, e.g. the pK_a of potassium glycinate is 9.67 (Kumar et al., 2003a). Similarly to aqueous alkanolamines, chemical absorption of CO_2 by aqueous amino acid salts is considered to take place by the zwitterion mechanism, where dissolved CO_2 and the amino acid salt form a zwitterion intermediate (Eq. 3), which is then deprotonated by a base present in solution (Eq. 4) to form carbamate (Kreulen et al., 1993). CO_2 may also react with hydroxide ions present in solution, forming bicarbonate (Eq. 5). The kinetics of CO_2 absorption is controlled by the carbamate formation reaction. The ratio of carbamate and bicarbonate formed varies with the type of amino acid salt, the reaction conditions, and the CO_2 loading of the solution (Dindore et al., 2005; Yang and Cussler, 1986).

$$H_2NCH_2COOK^+ + CO_2 \rightleftharpoons {}^-OOC^+H_2NCH_2COO^-K^+ \quad (3)$$

$${}^-OOC^+H_2NCH_2COO^-K^+ + B_i \rightleftharpoons {}^-OOCHNCH_2COO^-K^+ + B_iH^+ \quad (4)$$

$$CO_2 + OH^- \rightarrow HCO_3^- \quad (5)$$

Where B_i refers to H_2O, OH^-, or the amino acid salt, all capable of deprotonating the zwitterion. The overall forward rate for the chemical absorption of CO_2 can be given by (Scholes et al., 2015)

$$R_{CO_2} = \frac{k_1[CO_2][A]}{1 + \frac{k_{-1}}{\sum k_{B,i}[B_i]}} \quad (6)$$

Where [A] is the amino acid salt concentration, and the kinetic constants k_1 and k_{-1} refer to the forward and reverse reactions described by Eq. 3. $\sum k_{B,i}[B_i]$ includes the contribution of bases B_i in the removal of protons (Eq. 4), with $k_{B,i}$ referring to the deprotonation rate constant for the corresponding bases B_i.

The CO_2 flux was calculated from the experimental data using the following expression:

$$N = \frac{\dot{n}_{CO_2,in} - \dot{n}_{CO_2,out}}{A} \quad (7)$$

Where N is the flux, $\dot{n}_{CO_2,in}$ and $\dot{n}_{CO_2,out}$ are the CO_2 molar flows in the inlet and outlet gas, respectively, and A is the membrane outer surface area in the module. The molar CO_2 flows were calculated from the mass balance over the membrane module, assuming nitrogen and oxygen as inert gases with no absorption.

The CO_2 capture efficiency, i.e. the fraction of CO_2 absorbed from the feed gas, was calculated from

Table 1
Main operating parameters in the experiments.

Membrane surface area: 1.4 m^2
Absorbent concentration: 1 M
Absorbent flow rate: 0.75 – 1.5 l min^{-1} (superficial velocity 0.03 – 0.06 m s^{-1})
Feed gas CO_2 concentration: 5 – 15 vol-% (CO_2 partial pressure 5.75 – 17.25 kPa)
Feed gas flow rate: 5 L min^{-1} (superficial velocity 0.05 m s^{-1})
Absorption temperature: 10 – 30 °C
Desorption temperature: 60 – 80 °C
Desorption vacuum pressure: 300 – 800 mbar (abs)

$$\eta_{abs} = \frac{\dot{n}_{CO_2,in} - \dot{n}_{CO_2,out}}{\dot{n}_{CO_2,in}} \times 100\,\% \quad (8)$$

The gas-side overall mass transfer coefficient was calculated as

$$K_G = \frac{N}{\Delta C_m} \quad (9)$$

Where ΔC_m is the logarithmic mean driving force based on the gas-phase concentrations:

$$\Delta C_m = \frac{(C_{g,in} - C^*_{g,in}) - (C_{g,out} - C^*_{g,out})}{\ln[(C_{g,in} - C^*_{g,in})((C_{g,out} - C^*_{g,out})]} \quad (10)$$

Here, $C_{g,in}$ and $C_{g,out}$ out are the measured CO_2 concentrations in the inlet and outlet gas and $C^*_{g,in}$ and $C^*_{g,out}$ are the inlet and outlet gas-phase CO_2 concentrations in equilibrium with the corresponding liquid-phase concentrations. The solubility data of Portugal et al. (Yang and Cussler, 1986) for CO_2 in 1 M potassium glycinate were utilized to calculate the equilibrium concentrations. The gas-phase concentration was plotted against the liquid-phase concentration in the CO_2 partial pressure range relevant to the present experiments (100–1000 kPa), and an exponential curve was fitted to the data (R^2 equal to 97.8 %). As a result, the following correlation was found:

$$C^*_g = 1.4 \times 10^{-4} e^{0.014 C_L} \quad (11)$$

Where C_L is the liquid-phase CO_2 concentration.

The desorption efficiency was calculated from the measured CO_2 loading in the rich and lean absorbent:

$$\eta_{des} = \frac{\alpha_{rich} - \alpha_{lean}}{\alpha_{rich}} \times 100\,\% \quad (12)$$

Where η_{des} is the desorption efficiency, α_{rich} and α_{lean} are the CO_2 loadings of the rich absorbent leaving the membrane module and the lean absorbent leaving the stripper, respectively.

2.4.1. Evaluation of individual mass transfer coefficients

The individual mass transfer coefficients can be predicted by various experimental correlations based on the hydrodynamics and configuration of the membrane contactor (Gabelman and Hwang, 1999). For laminar (Re < 2100) flow of liquid inside the hollow fiber, the liquid mass transfer coefficient can be estimated from (Khaisri et al., 2009; Rode et al., 2012)

$$Sh = \sqrt[3]{3.67^3 + 1.62^3 Gz} \quad (13)$$

Where Sh is the Sherwood number and Gz is the Graetz number, described by

$$Sh = \frac{k_L d_i}{D_{CO_2,L}} \quad (14)$$

$$Gz = \frac{v_L d_i^2}{D_{CO_2,L} l} \quad (15)$$

Where d_i is the inner diameter of the hollow fiber, $D_{CO_2,L}$ is the diffusivity of CO_2 in the absorbent solution, v_L is the liquid superficial velocity inside the fiber, and l is the membrane fiber length.

For parallel flow of gas in a randomly packed module, the gas mass transfer coefficient can be estimated by the following correlation (van Swaaij and Versteeg, 1992; Zhang et al., 2008)

$$Sh = \frac{k_G d_h}{D_{CO_2,G}} = 1.25\left(\frac{Re\, d_h}{l}\right)^{0.93} Sc^{0.33} \quad (16)$$

Where Re is the Reynolds number, d_h is the shell-side hydraulic diameter (Eq. 18), $D_{CO_2,G}$ is the diffusivity of CO_2 in the feed gas, and Sc is the Schmidt number (Eq. 19):

$$d_h = \frac{d_{c,i}^2 - n d_o^2}{d_{c,i} + n d_o} \quad (17)$$

Here, $d_{c,i}$ is the inner diameter of the membrane contactor (shell), d_o is the outer diameter of the membrane fiber, and n is the number of fibers. The Reynolds number can be calculated as

$$Re = \frac{4\dot{V}_G}{n d_o \nu_G} \quad (18)$$

Where $\dot{V}_G$ is the gas volumetric flow rate and ν_G is the gas kinematic viscosity ($m^2\ s^{-1}$). The Schmidt number is defined by

$$Sc = \frac{\nu_G}{D_{CO_2,G}} \quad (19)$$

The value of the membrane mass transfer coefficient was estimated by calculation from Eq. 1, with the liquid and gas mass transfer coefficients calculated by the correlations presented above, and the overall mass transfer coefficient set equal to the experimentally found values (Eq. 9). A constant value of the membrane mass transfer coefficient was assumed, with the average value over the liquid flow rate data points taken as the estimate. For comparison, a theoretical estimate for the membrane mass transfer coefficient assuming completely non-wetted operation, was calculating using the following equation (Rumble, 2019):

$$k_M = \frac{\varepsilon D_{CO_2,M}}{\tau \delta} \quad (20)$$

Where ε is the membrane porosity, $D_{CO_2,M}$ is the effective diffusivity of CO_2 in the membrane, τ is the membrane tortuosity, and δ is the membrane thickness. The value of the enhancement factor can be estimated based on the calculation of the Hatta number and the infinite enhancement factor (Kumar et al., 2002; Portugal et al., 2009; Kim and Yang, 2000). The Hatta number describes the ratio of reaction kinetics to the mass transfer flux at the gas-liquid interface:

$$Ha = \frac{\sqrt{D_{CO_2,L} k_1 C_{PG,L}}}{k_L} \quad (21)$$

Where Ha is the Hatta number, k_1 is the forward reaction rate constant for chemical absorption (Eq. 6), and $C_{PG,L}$ is the concentration of potassium glycinate in the solution. The infinite enhancement factor corresponds to the situation where diffusion of the absorbent in the liquid phase is rate-limiting:

$$E_\infty = \left(\frac{D_{CO_2,L}}{D_{PG,L}}\right)^{1/3} + \frac{C_{PG,L}}{2C_{CO_2,LM}}\left(\frac{D_{CO_2,L}}{D_{PG,L}}\right)^{-2/3} \quad (22)$$

Where $C_{CO_2,LM}$ is the CO_2 concentration at the liquid-membrane interface and $D_{PG,L}$ is the diffusivity of potassium glycinate in the solution. The value of the enhancement factor can then be estimated by the DeCoursey solution (He et al., 2017):

$$E = \frac{-(Ha)^2}{2(E_\infty - 1)} + \sqrt{\frac{(Ha)^4}{4(E_\infty - 1)^2} + \frac{E_\infty (Ha)^2}{(E_\infty - 1)} + 1} \quad (23)$$

Table 2 presents the values for the parameters used in the calculations.

3. Results and discussion

The main experimental results comprise of the mass transfer performance, as measured by the capture efficiency, CO_2 flux and overall mass transfer coefficient, and the specific energy consumption. In this section, the effect of the main varied operating parameters on the steady-state absorption and desorption performance is discussed. Section 3.1 presents results from the experiments without vacuum employed in the solvent regeneration, with the primary aim of assessing the absorption performance of the membrane contactor. Section 3.2

Table 2
Parameter values used in the estimation of individual mass transfer coefficients. The values are valid at a temperature of 20 °C, at which the values of the mass transfer coefficients were estimated.

1 M potassium glycinate (Portugal et al., 2007a)	
Density, kg m^{-3}	1056.6
Viscosity, kg m^{-1} s^{-1}	1.26×10^{-3}
CO_2 diffusivity, m^2 s^{-1}	1.42×10^{-9}
CO_2 dimensionless Henry's constant	0.73
PG diffusivity, m^2 s^{-1}	3.89×10^{-10}
Forward reaction rate constant k_1, m^3 mol^{-1} s^{-1}	49.68 (Kumar et al., 2003a)
Membrane module	
Membrane outer surface area, m^2	1.4
Fiber length, mm	160
Fiber outer diameter, μm	300
Fiber inner diameter, μm	220
Number of fibers	10,200
Shell diameter, mm	67
Porosity, -	0.4 (Franco et al., 2008)
Tortuosity, -	2.5 (Zhang et al., 2008)
Thickness, m	4.0×10^{-5} (Franco et al., 2008)
Effective CO_2 diffusivity, m^2 s^{-1}	3.87×10^{-6} (Franco et al., 2008)
Feed gas	
CO_2 diffusivity, m^2 s^{-1} (in air)	1.60×10^{-5} (Yeon et al., 2003)

presents a more comprehensive set of results from the vacuum solvent regeneration for assessment of the CO_2 desorption efficiency and the resulting mass transfer performance of the membrane contactor. Section 3.3 presents the calculated individual mass transfer coefficients. Finally, Section 3.4 presents data from a 6-day stability test which was performed to assess the long-term stability and performance of the unit.

3.1. Non-vacuum desorption

Fig. 2 presents the effect of the liquid flow rate on the CO_2 capture efficiency and the overall mass transfer coefficient. Desorption was carried out at 80 °C. The liquid flow rate was varied from 0.75 L/min (velocity 0.03 m/s) to 1.5 L/min (velocity 0.06 m/s). The capture efficiency was found to increase from 54 % at the flow rate of 0.75 L/min to 72 % at 1.5 L/min, with the corresponding overall mass transfer coefficients ranging from $4.7 \cdot 10^{-5}$ m s^{-1} to $7.9 \cdot 10^{-5}$ m s^{-1}. The observed trend is similar to previous studies with potassium glycinate absorbent (Yan et al., 2007; Lu et al., 2009). The mass transfer coefficients are also similar in magnitude to those reported by Lu et al. (2009) for a similar membrane absorption system. With increasing liquid velocity, the liquid-side mass transfer resistance is decreased due to decreased thickness of the boundary layer (Kumar et al., 2003c), increasing the overall mass transfer rate.

With sufficiently high flow rates and low CO_2 loadings over the membrane length, there is an excess in free amino acid salt present at the liquid interface, and the absorption is controlled by the kinetics of chemical reaction (Kumar et al., 2002; Scholes et al., 2015). In this fast reaction regime, the CO_2 flux and overall mass transfer coefficient are not significantly increased with increasing liquid flow rate. At lower liquid flow rates and/or higher loadings, the free amino acid salt at the liquid interface is depleted, and the absorption is controlled by the diffusion of the reacting species. Here, a roughly linear increase can be found in the overall mass transfer coefficient with increasing liquid flow rate. Based on the relatively low liquid velocities combined with high lean CO_2 loadings of the absorbent solution (ranging from 0.49 at the flow rate of 0.75 L min^{-1} to 0.51 at 1.5 L min^{-1}), some degree of amino acid salt depletion could be expected (Kumar et al., 2002) under the present conditions. The high lean loadings are caused by the ineffective desorption without utilization of vacuum in the stripper, as discussed below.

Fig. 3 presents the effect of the absorption temperature on the CO_2 capture efficiency and the overall mass transfer coefficient calculated from experimental data using Eqs. (8) and (9). The capture efficiency was found to decrease from 70 % to 56 % with the temperature increased from 10 °C to 30 °C. The mass transfer coefficient correspondingly decreased from $7.4 \cdot 10^{-5}$ m s^{-1} to $5.0 \cdot 10^{-5}$ m s^{-1}. An opposite effect is usually found with amine absorbents (Lin et al., 2009). However, Yan et al. (2007) also found a decreasing absorption rate with increasing temperature using potassium glycinate. In contrast, Lu et al. (2009) found that increasing the temperature from 20 °C to 40 °C resulted in an increased overall mass transfer coefficient with the same solvent.

Generally, increased mass transfer at higher temperatures would be expected both due to the increased rate of chemical reaction and increased diffusivity of CO_2 in the liquid. Thus, the observed decrease is likely due to reduced CO_2 solubility at higher temperature (Yang and Cussler, 1986). Under the present conditions, the CO_2 loading in the liquid is high, resulting in a high equilibrium concentration in the gas-phase (following Eq. 11). The lean loading values at the absorption temperatures of 10, 20 and 30 °C were measured at 0.52, 0.50, and 0.52 mol mol^{-1}, respectively. There is no trend observed and the lower value at 20 °C can likely be explained by experimental error. The loadings at all temperatures are essentially the same but the equilibrium loading (corresponding to the CO_2 partial pressure in the membrane module) is decreased with increasing temperature. As a result, the mass transfer driving force is decreased, offsetting the favorable effects of increased temperature on the mass transfer rate.

Fig. 4 shows the effect of the feed gas CO_2 concentration on the CO_2 capture efficiency and the overall mass transfer coefficient. The capture efficiency decreased from 66 % to 56 % with the increasing feed concentration. At otherwise identical conditions, the higher CO_2 concentration in the feed resulted in a larger fraction of CO_2 exiting the module uncaptured, as is expected.

Increasing the feed CO_2 concentration should result in an increased absorption rate due to the increasing mass transfer driving force and increased rate of chemical absorption. This was observed also here, as the CO_2 flux (not shown) was increased with the increasing CO_2 concentration. However, the value of the mass transfer coefficient decreased from $6.8 \cdot 10^{-5}$ m s^{-1} to $4.8 \cdot 10^{-5}$ m s^{-1} with the feed concentration increased from 5 vol-% to 15 vol-%. The decreasing mass transfer coefficient is most likely caused by changes in the rate of chemical absorption. Again, with high CO_2 loadings (approximately 0.5), the concentration of free amine in the absorbent is relatively low, and depletion at the reactive interface may have taken place. Possibly, this depletion was more significant as the CO_2 concentration was increased and the reaction rate correspondingly increased. This would

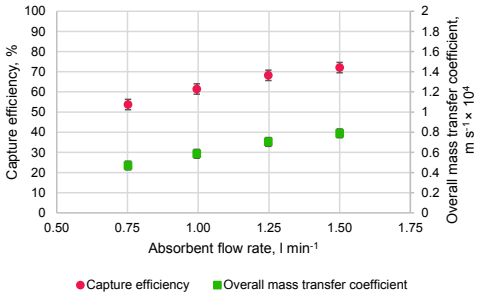

Fig. 2. Effect of absorbent flow rate on the CO_2 capture efficiency and the overall mass transfer coefficient. Absorbent 1 M potassium glycinate, absorption temperature 20 °C, regeneration temperature 80 °C, feed gas 10 % CO_2 (balance N_2), gas flow rate 5.0 L min^{-1}.

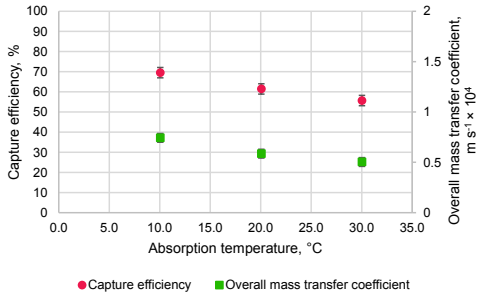

Fig. 3. Effect of absorption temperature on the CO_2 capture efficiency and the overall mass transfer coefficient. Absorbent 1 M potassium glycinate, liquid flow rate 1.0 L min^{-1}, regeneration temperature 80 °C, feed gas 10 % CO_2 (balance N_2), gas flow rate 5.0 L min^{-1}.

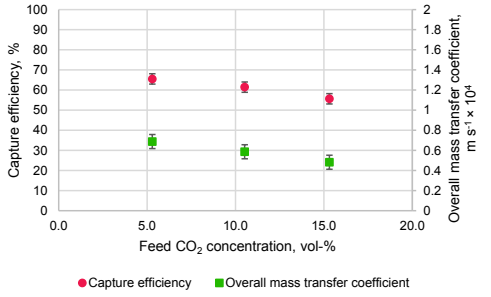

Fig. 4. Effect of feed gas CO_2 concentration (balance N_2) on the CO_2 capture efficiency and the overall mass transfer coefficient. Absorbent 1 M potassium glycinate, liquid flow rate 1.0 L min^{-1}, absorption temperature 20 °C, regeneration temperature 80 °C, gas flow rate 5.0 L min^{-1}.

result in a lower value of the enhancement factor, and thus a lower value of the overall mass transfer coefficient, as described by Eq. 1.

Fig. 5 presents the variation in CO_2 capture efficiency and the overall mass transfer coefficient with the solvent regeneration temperature varied from 60 °C to 80 °C. The capture efficiency was found to range from only 10 % at the regeneration temperature of 60 °C to 61 % at 80 °C. The corresponding overall mass transfer coefficients ranged from $0.7 \cdot 10^{-5}$ m s^{-1} to $4.9 \cdot 10^{-5}$ m s^{-1}. At relatively low regeneration temperatures, and with no vacuum employed, the steady-state CO_2 absorption rate is strongly limited by the efficiency of CO_2 desorption from the solution, especially at regeneration temperatures below 80 °C. Increasing the temperature results in a significant increase in the desorption rate due to the lower equilibrium loading (Yang and Cussler, 1986) as dictated by the chemical equilibrium (Eq. 3–5) and the increased rate of the reverse reactions leading to release of CO_2 from solution. In addition, mass transfer rate of CO_2 from the solution to the gas phase in the stripper increases as a result of higher CO_2 diffusivity and lower solution viscosity at higher temperature (Kreulen et al., 1993).

Regardless of the desorption temperature, the absorption rate is limited by the high CO_2-loading in the lean absorbent, which ranges from 0.55 mol mol^{-1} at 60 °C to 0.50 mol mol^{-1} at 80 °C. He et al. showed that the CO_2 absorption rate of amino acid salt solutions is strongly dependent on the CO_2 loading (Wang et al., 2013b). With various amino acid salts including potassium glycinate, the absorption rate was found to decrease by more than 80 % with the loading changing from zero to 0.4 mol mol^{-1}. The effect of the CO_2 loading on the absorption rate could be explained by the influence of both physical and chemical absorption. The higher loading results in a decreased driving force for mass transfer through the membrane from the gas to the liquid phase. At the same time, according to Eq. 6, the rate of chemical absorption is decreased due to the lowered concentrations of free amino acid at the membrane-liquid interface, which results in a lower value for the enhancement factor and lower overall absorption rate.

3.2. Vacuum desorption

The main objective of the non-vacuum results discussed above was to characterize the membrane mass transfer performance, as measured by the overall mass transfer coefficient, with variation of key operating parameters. In the vacuum desorption experiments described in this section, the focus is shifted on to the performance of the whole unit consisting of the absorption and desorption stages. The key issue here is the effect of the desorption performance, and the resulting CO_2 loading of the lean absorbent, on the mass transfer performance of the membrane contactor.

3.2.1. Desorption temperature and vacuum pressure

Desorption of CO_2 from the rich solution takes place by shifting the equilibrium of the absorption reactions (Eq. 3–5) to the reverse side, followed by diffusion of the released CO_2 from the bulk liquid to the gas-liquid interface, and finally to the gas phase. The shift in the chemical equilibrium leads to decreasing solubility of CO_2 in the absorbent solution at elevated temperatures. In conventional amine-based CO_2 capture processes, desorption is performed at temperatures above 100 °C to facilitate effective release of CO_2 from solution (MacDowell et al., 2010). However, operating at lower desorption temperatures would be preferable to minimize heat energy consumption, to allow utilization of low-grade heat, and to avoid solvent losses and environmental concerns related to degradation of the absorbent.

To decrease the desorption temperature, vacuum was employed in the experiments described here. By utilizing vacuum, the partial pressure of CO_2 in the gas phase can be reduced, leading to decreased CO_2 solubility in the liquid and increased driving force for the transfer of CO_2 from the liquid phase. In addition, the vacuum pump continuously removes the released CO_2 from the desorption vessel, providing a sweeping effect which is conventionally achieved by evaporating water from the solution. Minimizing the evaporation of water while maintaining a high CO_2 desorption flux would minimize the energy input required for regeneration of the solvent (Nieminen et al., 2020).

Fig. 6 presents the CO_2 capture efficiency and the overall mass

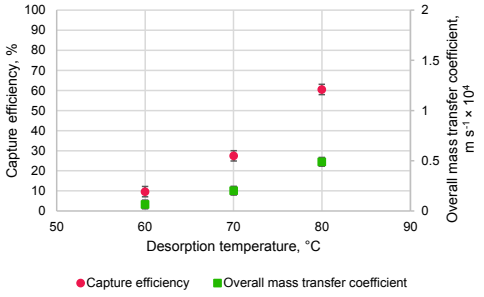

Fig. 5. Effect of regeneration temperature on CO_2 capture efficiency and the overall mass transfer coefficient. Absorbent 1 M potassium glycinate, liquid flow rate 1.0 L min^{-1}, absorption temperature 20 °C, feed gas 10 % CO_2 (balance N_2), gas flow rate 5.0 L min^{-1}.

transfer coefficient at the membrane contactor with the desorption temperature varied at 60 – 80 °C and vacuum pressure at 300 – 800 mbar. The maximum temperature of 80 °C was dictated by the operating limits of the experimental unit, while the low limit of the vacuum pressure was set by the water vapor pressure at each temperature. Clearly, the absorption performance is favored both by higher temperature and lower pressure at desorption. At 60 °C, lowering the pressure from 800 mbar to 300 mbar results in a 4.7-fold increase in the value of the overall mass transfer coefficient. As another example, at the vacuum pressure of 500 mbar the overall mass transfer coefficient at 80 °C is higher by a factor of 7.4 compared to that at 60 °C. Correspondingly, the capture efficiency is significantly increased at higher temperature and lower vacuum pressure, with efficiency above 90 % reached at 80 °C and 500 – 600 mbar.

The improved absorption performance at more favorable desorption conditions is explained by changes in the lean loading, as depicted in Fig. 7. With more efficient desorption of CO_2 from the solution at increased temperature and reduced pressure, the lean liquid entering the membrane contactor is able to absorb CO_2 at higher rate. At 60 °C, the measured lean loading was reduced from 0.57 mol mol^{-1} to 0.48 mol mol^{-1} with the vacuum pressure lowered from 800 to 300 mbar. At 80 °C, the loading varied from 0.48 mol mol^{-1} at 800 mbar to 0.42 mol mol^{-1} at 500 mbar. However, even at the optimal conditions of 80 °C and 500 mbar, the desorption efficiency remained low, at 5.5 ± 1.42 %. This also resulted in a cyclic CO_2 capacity (the difference between rich and lean solvent loading) of only 0.02 ± 0.006 mol. In benchmark amine capture processes, the cyclic capacity is above 0.2 mol (Favre and Svendsen, 2012). As such, the overall CO_2 capture rate here remains strongly limited by the desorption performance.

To improve the performance, lower vacuum pressures and/or higher temperatures should be tested, and the configuration of the desorption unit improved. The latter could be achieved e.g. by introducing packings to the desorption vessel, installing a reboiler, or by replacing the vessel with alternative equipment such as a membrane contactor (Li and Chen, 2005).

The limiting effect of the desorption performance and the resulting

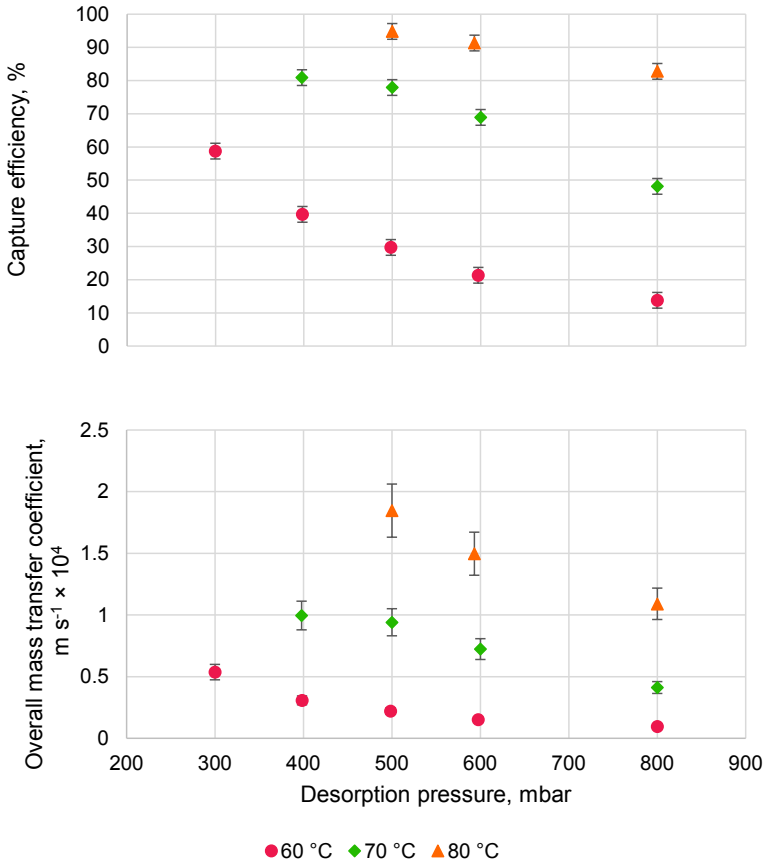

Fig. 6. CO_2 capture efficiency and absorption overall mass transfer coefficient with the temperature and vacuum pressure varied in solvent regeneration. Absorbent 1 M potassium glycinate, liquid flow rate 1.0 L min^{-1}, absorption temperature 20 °C, feed gas 10 % CO_2 (balance N_2), gas flow rate 5.0 L min^{-1}. The 95 % confidence interval of the overall mass transfer coefficient was determined at the temperature of 80 °C. At the lower temperatures, a similar relative deviation is assumed. All measurements at vacuum pressures 500-800 mbar were previously presented as the corresponding CO_2 fluxes in a previous publication (Lerche, 2012).

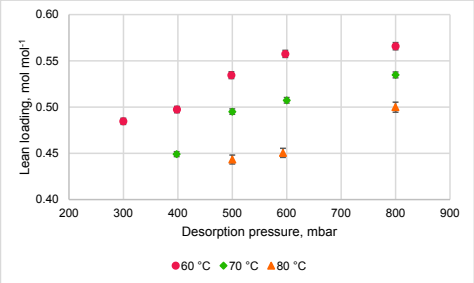

Fig. 7. CO_2 loading of the lean absorbent solution with the temperature and vacuum pressure varied in solvent regeneration. Absorbent 1 M potassium glycinate, liquid flow rate 1.0 L min^{-1}, absorption temperature 20 °C, feed gas 10 % CO_2 (balance N_2), gas flow rate 5.0 L min^{-1}. Error bars represent the standard deviation from three repeated titrimetric analyses. All measurements at vacuum pressures 500-800 mbar were previously reported as the corresponding CO_2 fluxes in a previous publication (Lerche, 2012).

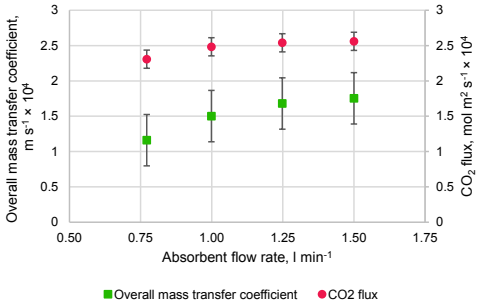

Fig. 9. Effect of absorbent flow rate on the overall mass transfer coefficient and the CO_2 flux. Absorbent 1 M potassium glycinate, absorption temperature 20 °C, regeneration temperature 80 °C and pressure 600 mbar, feed gas 10 % CO_2 (balance N_2), gas flow rate 5.0 L min^{-1}.

high lean CO_2 loading was studied by collecting data from a start-up period during which a fresh, unloaded absorbent was circulated and the CO_2 loading was continuously increased during CO_2 absorption. By collecting a series of liquid samples during the start-up, the variation of the absorption rate with the lean loading could be followed, with results shown in Fig. 8a. The absorption rate is decreased by approximately 35 % with the lean loading increasing from 0.02 mol mol^{-1} to 0.45 mol mol^{-1}. This decrease is consistent with the data from He et al. (Wang et al., 2013b), who measured the CO_2 absorption rates in a membrane contactor at various CO_2 loadings and temperatures using potassium glycinate and other amino acid salt absorbents.

The lean loadings depicted in Fig. 8a are based on lean solvent samples collected once per hour, with the first sample collected one hour after initiating CO_2 absorption. Rich solvent samples were collected simultaneously to the lean samples. Based on the difference in lean and rich loadings, the cyclic capacity at the sampling points was determined, with results shown in Fig. 8b. Following one hour of absorption, a higher cyclic capacity (0.028 mol mol^{-1}) is found compared to the later data points where the cyclic capacity values are in a similar range (0.012 − 0.017 mol mol^{-1}) to those found during steady-state experiments. Accordingly, the desorption efficiency is much higher (14.8 %) at the initial data point compared to 2.7 % to 4.2 % at the later points.

Generally, desorption is expected to be more effective at higher solvent CO_2 loading due to increased driving force. The higher efficiency found after one hour of operation is likely explained by changes in the gas atmosphere present in the desorption vessel. Prior to starting the operation and initiating the absorption/desorption cycle, the vessel is filled with air and the partial pressure of CO_2 is very low. As more CO_2 is absorbed into the circulating solution and then released in the desorption vessel, the partial pressure of CO_2 is gradually increased. This explanation is supported by CO_2 concentration measured at the outlet gas from the desorption vessel. After one hour, the CO_2 concentration is nearly 0 % but the concentration gradually increases, reaching the final steady-state value of almost 90 % after 3.5 h of operation. This finding also suggests that the CO_2 partial pressure in the desorption vessel may be a limiting factor for the desorption performance in the current setup.

3.2.2. Liquid flow rate

Fig. 9 presents the effect of the liquid flow rate on the CO_2 flux and the overall mass transfer coefficient with desorption performed under 600 mbar vacuum. The CO_2 fluxes found here are in the order of 50 % lower compared to the values from Yan et al. (2007) at similar liquid velocities. This difference can be explained by the higher CO_2 feed concentration in that study (14 %) and more importantly, the use of unloaded potassium glycinate absorbent, compared to the circulated, CO_2-loaded solvent used here. The effect of the flow rate on the CO_2 flux is not very significant, with the flux ranging from 2.3×10^{-4} mol m^{-2} s^{-1} at 0.75 L min^{-1} to 2.6×10^{-4} mol m^{-2} s^{-1} at 1.5 L min^{-1}. The liquid-side physical mass transfer coefficient generally increases at increasing liquid velocity, which should increase the absorption rate. This implies that under these conditions, significant depletion of free amine at the interface does not take place, and absorption takes place in a

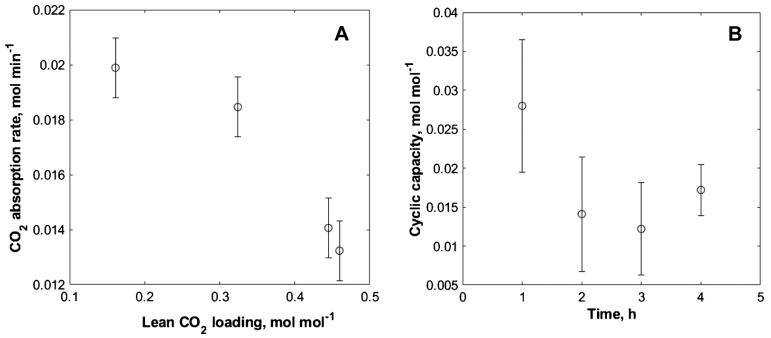

Fig. 8. A) Variation of CO_2 absorption rate with the lean solvent CO_2 loading and B) variation of cyclic CO_2 capacity during a start-up period of five hours. Absorbent 1 M potassium glycinate, liquid flow rate 1 L min^{-1}. Absorption temperature 20 °C, regeneration temperature 70 °C and pressure 500 mbar. Feed gas 10 % CO_2 (balance air), gas flow rate 5.0 L min^{-1}.

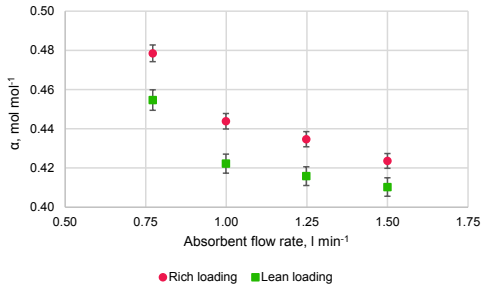

Fig. 10. CO_2 loading of the rich and lean absorbent with absorbent flow rate varied. Absorbent 1 M potassium glycinate, absorption temperature 20 °C, regeneration temperature 80 °C and pressure 600 mbar, feed gas 10 % CO_2 (balance N_2), gas flow rate 5.0 L min^{-1}.

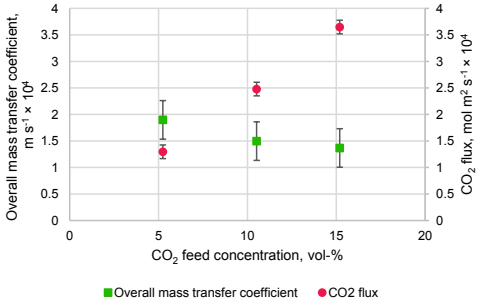

Fig. 11. Effect of feed CO_2 concentration (balance N_2) on the overall mass transfer coefficient and the CO_2 flux. Absorbent 1 M potassium glycinate, liquid flow rate 1.0 L min^{-1}, absorption temperature 20 °C, regeneration temperature 80 °C and pressure 600 mbar, gas flow rate 5.0 L min^{-1}.

regime significantly controlled by reaction kinetics (Kumar et al., 2002).

A slightly more significant change is observed in the values of the overall mass transfer coefficient, ranging from 1.2×10^{-4} m s^{-1} at 0.75 L min^{-1} to 1.8×10^{-4} m s^{-1} at 1.5 L min^{-1}. The magnitude of these values is consistent with those presented by Lu et al. (2009) for potassium glycinate absorbent used in a PP membrane contactor. The increase in the overall mass transfer coefficient is primarily due to the decreasing liquid-side mass transfer resistance with increasing liquid velocity. The calculated values of the overall mass transfer coefficient are also affected by the solvent CO_2-loading due to the variation in the logarithmic mean driving force (Eq. 10). As such, the values of the overall mass transfer coefficient are sensitive to the equilibrium relationship used in the calculation of the gas-side equilibrium CO_2 concentrations.

The variation in the CO_2-loading of the lean and rich absorbent with the liquid flow rate is presented in Fig. 10. The lean loading decreases with increasing liquid flow rate. However, as is evident from the CO_2 fluxes in Fig. 9, the decreased CO_2-loading in the absorbent entering the membrane module does not have a significant impact on the CO_2 absorption rate. Such an impact would be expected based on the higher physical mass transfer driving force (i.e. lower gas-side equilibrium concentration), and the increased availability of free amine for reaction. This again points to the significance of the intrinsic chemical reaction rate (as measured by the kinetic constant k_1 in Eq. 6) as a significant limiting factor for the absorption rate under the present conditions.

As the increase in the absorption rate is not very significant, the relative increase in the CO_2-loading over the membrane module is decreased at increasing liquid flow rate, as the residence time is correspondingly decreased. This is observed from the differences between the rich and lean loadings in Fig. 10. The relative differences range from 5 % at 0.75 L min^{-1} to 3 % at 1.5 L min^{-1}. In absolute terms, the amount of CO_2 accumulated in the absorbent over the module is decreased from 0.024 mol to 0.013 mol, respectively. From the discussion above, it appears that the absorbent is more effectively utilized at the lower range of the flow rates studied, and the higher flow rates would result in unnecessary increases in operating costs from circulation and heating of the solvent.

3.2.3. CO_2 concentration

Fig. 11 presents the variation in CO_2 flux and overall mass transfer coefficient with the feed CO_2 concentration varied from 5 to 15 vol-%. A linear increase in the CO_2 flux was found with the increasing feed concentration as a result of the increased driving force for mass transfer and chemical absorption. At the same time, a slightly decreasing overall mass transfer was found with the increasing feed concentration. The change in the overall mass transfer coefficient could be a result of decreasing amino acid concentration at the reaction interface, resulting in decreasing enhancement factor and higher overall mass transfer resistance. Due to these limitations, the increasing mass transfer driving force is not completely utilized. The corresponding capture efficiencies (not shown) range from 94.6 % at 5 % CO_2 feed to 90.2 % at 15 % CO_2 feed, showing that the efficiency can be maintained at a high level over a wide range of feed concentrations under the present conditions.

3.3. Individual mass transfer coefficients in absorption

The magnitude of the individual mass transfer coefficients with the liquid flow rate varied was evaluated based on the procedure described in Section 3.4.1. The values of the corresponding individual mass transfer coefficients are presented in Table 3, together with the values of the Reynolds number and enhancement factor. The liquid-side resistance constitutes the major fraction (88–89 %) of the overall mass transfer resistance, while the membrane resistance is also significant (11–12 %). The gas-side resistance is negligible. The differences in the enhancement factor are due to variation in the lean absorbent loading (Fig. 10) and small deviations in the feed gas CO_2 partial pressure.

Compared to the data from Feron and Jansen (2002) for a transversal-flow PP membrane module and proprietary amino-acid salt absorbent, both the liquid and membrane mass transfer coefficients are almost two orders of magnitude lower here. The difference in the liquid mass transfer coefficient could be explained by the different flow configuration, but the difference in the membrane mass transfer coefficient is significant and cannot be explained by differences in the membrane properties. Both the liquid and membrane mass transfer coefficients are of the same order of magnitude to the values reported by Franco et al. (Wang et al., 2005) for PP module and MEA absorbent (7.8×10^{-4} m s^{-1} and 7.0×10^{-4} m s^{-1} for liquid and membrane, respectively). Compared to these values, the membrane mass transfer coefficient is 67 % lower in our case. The membrane resistance here is comparable to other studies with PP membranes and amine absorbents (Chabanon et al., 2013; Lin et al., 2009; Wang et al., 2013b).

As PP membranes are commonly partially wetted by MEA, a lower membrane resistance (higher mass transfer coefficient) would be expected with potassium glycinate as the wetting tendency is lower. Even a minor degree of membrane wetting results in a sharp increase in the membrane mass transfer resistance (Wang et al., 2005). It appears that some degree of degradation in the membrane performance due to wetting or other effects (e.g. fouling) may have taken place in the present work, which is plausible as the same module had been used for an extended period of time prior to the experiments discussed in this

Table 3
Values of the Reynolds number, enhancement factor, and individual mass transfer coefficients with the liquid velocity varied. Absorbent 1 M potassium glycinate, absorption temperature 20 °C, regeneration temperature 80 °C and pressure 600 mbar, feed gas 10 % CO_2 (balance N_2), gas flow rate 5.0 L min^{-1}.

Liquid velocity, m s^{-1}	Re, -	E, -	$k_L \times 10^5$, m s^{-1}	$k_G \times 10^3$, m s^{-1}	$k_m \times 10^4$, m s^{-1} (calculated from experiments)	$k_m \times 10^2$, m s^{-1} (theoretical)
0.033	6.1	12.9	2.78	1.14	2.92 ± 0.40	1.55
0.043	7.9	24.9	2.87			
0.054	9.9	22.3	2.98			
0.064	11.9	26.2	3.07			

section. This possibility is also reflected by the fact that the theoretical membrane mass transfer coefficient, which assumes completely non-wetted operation, is higher than the calculated value by a factor of almost 50. It should be noted that the theoretical value is itself subject to uncertainties in the membrane properties used in the calculation (e.g. the values of porosity and tortuosity). Generally, any uncertainties involved in the mass transfer analysis are likely lumped into the membrane mass transfer coefficient as the single adjusted parameter (Chabanon et al., 2013). A likely source of such uncertainty is the estimation of the enhancement factor at the high liquid CO_2 loadings under present conditions.

3.4. Long-term stability and CO_2 selectivity

To check for potential membrane wetting or other stability issues, a stability test was performed over a period of six days. The test was run at the desorption conditions of 70 °C and 500 mbar, with the system running continuously during the day and shut off for the night. Instead of nitrogen, CO_2 was mixed with air in the feed gas in order to include the potential effects of oxygen on the solvent or membrane stability. The same batch of absorbent liquid was used throughout the test, and the liquid was not drained in-between the runs, maintaining constant contact between the absorbent and the membrane contactor. Water evaporated from the solution in the desorption vessel and condensed in the vacuum pump condenser was replaced to the solution after each day to maintain the liquid volume and concentration.

Fig. 12 presents the continuous variation in the CO_2 concentration at the membrane outlet over the testing period. The concentration remains stable over the period, with no decline in performance found. This suggests that no significant membrane wetting took place over a total of approximately 33 h, which is of course a very limited time period concerning long-term operation. A similar results was found by Yan et al. (2007) over 40 h of operation with potassium glycinate and PP membrane contactor. Here, the membrane module had been used for months of experiments prior to the stability test. It is possible that some performance decline during the initial operating period had taken place, as has been observed in the case of amine absorbents (Wang et al., 2005). However, significant changes in the performance over the entire period of use for the membrane module were ruled out by repeated experiments.

Based on lean and rich solvent samples collected once per day, the cyclic capacity during the stability test ranged from 0.016 ± 0.007 mol mol^{-1} to 0.037 ± 0.011 mol mol^{-1} with no trend observed during the operating period. Considering the experimental uncertainty, the values seem to be in a similar range to those found at the later data points collected during start-up (Fig. 8b). The start-up data was collected prior to beginning the stability test, using the same batch of solvent and identical operating conditions. This suggest that the cyclic capacity found at the end of the start-up period and subsequent long-term operation correspond the steady-state value at the corresponding operating conditions.

The CO_2 and oxygen concentrations in the product gas leaving the desorption stage were also monitored during the stability test. The CO_2 concentration varied in the range of 84.4–89.4 vol-%, and the oxygen concentration in the range of 6.1–8.5 vol-%. This implies that co-absorption of oxygen from the feed air takes place despite the high selectivity of the absorbent solution towards CO_2. Also, any oxygen absorbed is expected to desorb effectively under heating and vacuum, resulting in a relatively high cyclic capacity for oxygen. As a result, the apparent CO_2/O_2 selectivity is in the range of only 10.5–14.4 during the continuous runs discussed here. It should be noted that minor air leaks in the vacuum system could not be completely ruled out, and the oxygen concentration could be affected by air intrusion. However, the point could be made that in the operation of membrane contactor systems under low cyclic capacity and high lean loading conditions, the absorption of oxygen may not be negligible, as is commonly assumed in modelling approaches (Chabanon et al., 2013).

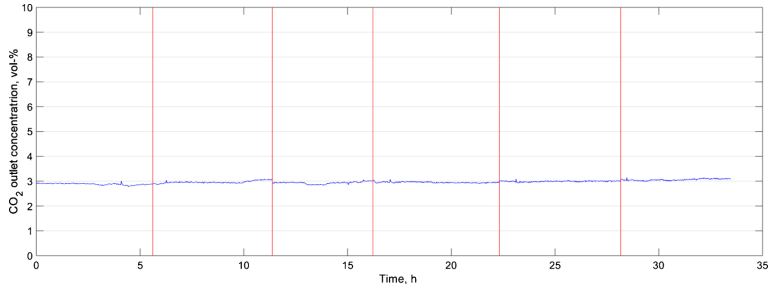

Fig. 12. CO_2 concentration of the membrane outlet gas over six days of continuous operation. Absorbent 1 M potassium glycinate, liquid flow rate 1 L min^{-1}. Absorption temperature 20 °C, regeneration temperature 70 °C and pressure 500 mbar. Feed gas: 10 % CO_2, balance air. Gas flow rate 5.0 L min^{-1}.

3.5. Summary of results

The effect of key operating parameters on the CO_2 absorption performance of the membrane contactor was assessed. In a series of experiments without vacuum employed, the overall mass transfer coefficient was found to be favored by higher liquid flow rates, higher CO_2 concentration in the feed gas, and interestingly, by lower absorption temperatures. Desorption efficiency was improved by increasing the temperature at the solvent regeneration stage from 60 °C to 80 °C, which resulted in higher CO_2 capture efficiency and higher overall mass transfer coefficient at the absorption stage due to the reduced CO_2 loading in the lean absorbent entering the membrane module.

The introduction of vacuum improved the desorption performance, which in turn resulted in higher capture efficiencies and overall mass transfer coefficients. Both were increased at higher temperatures and lower vacuum pressures in the range of $60-80$ °C and $300-800$ mbar. The low limit of the vacuum pressure was set by the water boiling point at the corresponding temperature. However, the desorption efficiency was still low due to mass transfer limitations in the stripper with only 5.5 % of the CO_2 released from the amount absorbed in the solution. As a result, the lean CO_2 loading remained as high as 0.42 mol mol^{-1}, limiting the CO_2 absorption rate in the membrane contactor.

With vacuum desorption employed, the CO_2 flux increased with increasing liquid flow rate, but the effect was relatively small. This suggests that absorption took place under a regime significantly controlled by the kinetics of the reactive absorption. A more significant increase with liquid flow rate was found in the overall mass transfer coefficient, as the liquid-side mass transfer resistance was decreased at increasing liquid velocity. The highest value of the overall mass transfer coefficient reached 1.8×10^{-4} m s^{-1}, which is comparable to values presented in literature for similar systems.

The liquid and gas mass transfer resistances were predicted using correlations available in literature, including estimation of the enhancement factor for chemical absorption. The membrane resistance was estimated based on the experimentally obtained overall mass transfer coefficients and measured absorption data. This value was significantly lower compared to a theoretical estimate assuming non-wetted operation, which suggests possibility of partial wetting of the membrane. The values of the individual mass transfer coefficients are reasonably comparable to literature data on amine and amino acid salt absorbents and PP membrane contactors. The overall mass transfer resistance was found to be dominated by the liquid-side resistance, constituting almost 90 % of the overall resistance.

4. Conclusions

The mass transfer performance of a continuously operated CO_2 capture unit based on a membrane contactor and vacuum solvent regeneration was characterized. The system utilized a polypropylene membrane contactor with aqueous potassium glycinate as absorbent. The present results provide an overview on the effects of key operating parameters on the absorption performance, as measured by the gas-side overall mass transfer coefficient.

In the current experimental set-up, steady-state performance is limited by inefficient desorption resulting in high CO_2 loading in the lean absorbent entering the membrane contactor, decreasing the CO_2 absorption rate. Desorption performance was improved by introduction of vacuum and by increasing the desorption temperature. The highest value of the overall mass transfer coefficient was found with desorption performed at 80 °C and 500 mbar. The overall mass transfer coefficient increased with increasing liquid flow rate. The highest value of the overall mass transfer coefficient was 1.8×10^{-4} m s^{-1}. The individual mass transfer resistances were evaluated, and the overall mass transfer resistance was found to be dominated by the liquid-side resistance at almost 90 % of the total resistance. The membrane mass transfer resistance calculated from experimental data is high compared to a theoretical value which assumes completely non-wetted operation of the membrane contactor, suggesting partial wetting of the membrane under present conditions.

Operation under desorption-limited conditions allows the characterization of the membrane mass transfer performance at high lean CO_2 loadings, as opposed to unloaded absorbent solutions used in the majority of previous studies. Stable performance of the unit and the membrane contactor was also demonstrated during a stability test with over 30 h of operation.

Declaration of conflicting interests

The authors declare that they have no known competing financial interests or personal relationships that could have appeared to influence the work reported in this paper.

CRediT authorship contribution statement

H. Nieminen: Conceptualization, Data curation, Investigation, Methodology, Writing - original draft. **L. Järvinen:** Methodology, Software, Writing - review & editing. **V. Ruuskanen:** Methodology, Software, Writing - review & editing. **A. Laari:** Conceptualization, Methodology, Supervision, Writing - review & editing. **T. Koiranen:** Project administration, Supervision, Writing - review & editing. **J. Ahola:** Project administration, Resources, Funding acquisition, Writing - review & editing.

Appendix A. Supplementary data

Supplementary material related to this article can be found, in the online version, at doi:https://doi.org/10.1016/j.ijggc.2020.103063.

References

Boot-Handford, M.E., Abanades, J.C., Anthony, E.J., Blunt, M.J., Brandani, S., Mac Dowell, N., Fernández, J.R., Ferrari, M.-C., Gross, R., Hallett, J.P., Haszeldine, R.S., Heptonstall, P., Lyngfelt, A., Makuch, Z., Mangano, E., Porter, R.T.J., 2014. Carbon capture and storage update. Energy Environ. Sci. 7, 130–189.

Brunetti, A., Scura, F., Barbieri, G., Drioli, E., 2010. Membrane technologies for CO2 separation. J. Membr. Sci. 359, 115–125.

Chabanon, E., Roizard, D., Favre, E., 2011. Membrane contactors for postcombustion carbon dioxide capture: a comparative study of wetting resistance on long time scales. Ind. Eng. Chem. Res. 50 (13), 8237–8244.

Chabanon, E., Roizard, E., Favre, D., 2013. Modeling strategies of membrane contactors for post-combustion carbon capture: a critical comparative study. Chem. Eng. Sci. 87, 393–407.

Cussler, E., 1994. Hollow fiber contactors. Membrane Processes in Separation and Purification. Kluwer Academic Publishers, Netherlands, pp. 375–394.

D'Alessandro, D.M., Smit, B., Long, J.R., 2010. Carbon dioxide capture: prospects for new materials. Angew. Chem. Int. Ed. 49, 6058–6082.

deMontigny, D., Tontiwachwuthikul, P., Chakma, A., 2006. Using polypropylene and polytetrafluoroethylene membranes in a membrane contactor for CO2 absorption. J. Membr. Sci. 277, 99–107.

Dindore, V., Brilman, D., Versteeg, G., 2005. Hollow fiber membrane contactor as a gas–liquid model contactor. Chem.Eng.Sci. 60 (2), 467–479.

Dutcher, B., Fan, M., Russell, A.G., 2015. Amine-based CO2 capture technology development from the beginning of 2013 - a review. ACS Appl. Mater. Interfaces 7, 2137–2148.

Falk-Pedersen, O., Dannström, H., 1997. Separation of carbon dioxide from offshore gas turbine exhaust. Energy Convers. Mgmt 38, S81–S86.

Falk-Pedersen, O., Grønvold, M., Nøkleby, P., Bjerve, F., 2005. CO2 capture with membrane contactors. Int. J. Green Energy 2, 157–165.

Fang, M., Yan, S., Luo, Z., Ni, M., Cen, K., 2009. CO2 chemical absorption by using membrane vacuum regeneration technology. Energy Procedia 1, 815–822.

Favre, E., Svendsen, H.F., 2012. Membrane contactors for intensified post-combustion carbon dioxide capture by gas–liquid absorption processes. J. Membr. Sci. 407-408, 1–7.

Feron, P.H.M., Jansen, A.E., 2002. CO2 separation with polyolefin membrane contactors and dedicated absorption liquids: performances and prospects. Sep. Purif. Technol. 27, 231–242.

Franco, J., deMontigny, D., Kentish, S., Perera, J., Stevens, G., 2008. A study of the mass transfer of CO2 through different membrane materials in the membrane gas absorption process. Sep. Sci. Technol. 43, 225–244.

Gabelman, A., Hwang, S.-T., 1999. Hollow fiber membrane contactors. J. Membr. Sci. 159 (1-2), 61–106.

He, F., Wang, T., Fang, M., Wang, Z., Yu, H., Ma, Q., 2017. Screening test of amino acid salts for CO2 absorption at flue gas temperature in a membrane contactor. Energy Fuels 31, 770–777.
Khaisri, S., deMontigny, D., Tontiwachwuthikul, P., Jiraratananon, R., 2009. Comparing membrane resistance and absorption performance of three different membranes in a gas absorption membrane contactor. Sep. Purif. Technol. 65, 290–297.
Kim, Y.-S., Yang, S.-M., 2000. Absorption of carbon dioxide through hollow fiber membranes using various aqueous absorbents. Sep. Purif. Technol. 21, 101–109.
Kosaraju, P., Kovvali, A.S., Korikov, A., Sirkar, K.K., 2005. Hollow Fiber membrane contactor based CO2 absorption-stripping using novel solvents and membranes. Ind. Eng. Chem. Res. 44, 1250–1258.
Kreulen, H., Smolders, C., Versteeg, G., van Swaaij, W., 1993. Microporous hollow fibre membrane modules as gas-liquid contactors. Part 1. Physical mass transfer processes - A specific application: mass transfer in highly viscous liquids. J. Membr. Sci. 78 (3), 197–216.
Kumar, P.S., Hogendoorn, J.A., Feron, P.H.M., Versteeg, G.F., 2002. New absorption liquids for the removal of CO2 from dilute gas streams using membrane contactors. Chem. Eng. Sci. 57 (9), 1639–1651.
Kumar, P.S., Hogendoorn, J.A., Versteeg, G.F., 2003a. Kinetics of the reaction of CO2 with aqueous potassium salt of taurine and glycine. AIChE J. 49 (1), 203–213.
Kumar, P., Hogendoorn, J., Feron, P., Versteeg, G., 2003b. Approximate solution to predict the enhancement factor for the reactive absorption of a gas in a liquid flowing through a microporous membrane hollow fiber. J. Membr. Sci 213 (1-2), 231–245.
Kumar, P., Hogendoorn, J., Versteeg, G., 2003c. Kinetics of the reaction of CO2 with aqueous potassium salt of taurine and glycine. AIChE J. 49 (1), 203–213.
Lerche, B.M., 2012. CO2 Capture From Flue Gas Using Amino Acid Salt Solutions. Kgs. Lyngby: Technical University of Denmark (DTU).
Li, J.-L., Chen, B.-H., 2005. Review of CO2 absorption using chemical solvents in hollow fiber membrane contactors. Sep. Purif. Technol. 41 (2), 109–122.
Li, S., Pyrzynski, T.J., Klinghoffer, N.B., Tamale, T., Zhong, Y., Aderhold, J.L., Zhou, S.J., Meyer, H.S., Ding, Y., Bikson, B., 2017. Scale-up of PEEK hollow fiber membrane contactor for post-combustion CO2 capture. J. Membr. Sci. 527, 92–101.
Lin, S.-H., Hsieh, C.-F., Li, M.-H., Tung, K.-L., 2009. Determination of mass transfer resistance during absorption of carbon dioxide by mixed absorbents in PVDF and PP membrane contactor. Desalination 249, 647–653.
Lu, J.-G., Zheng, Y.-F., Cheng, M.-D., 2009. Membrane contactor for CO2 absorption applying amino-acid salt solutions. Desalination 249, 498–502.
Lv, Y., Yu, X., Tu, S.-T., Yan, J., Dahlquist, E., 2010. Wetting of polypropylene hollow fiber membrane contactors. J. Membr. Sci. 362 (1-2), 444–452.
MacDowell, N., Florin, N., Buchard, A., Hallett, J., Galindo, A., Jackson, G., Adjiman, C.S., WIlliams, C.K., Shah, N., Fennell, P., 2010. An overview of CO2 capture technologies. Energy Environ. Sci. 3, 1645–1669.
Mikkelsen, M., Jørgensen, M., Krebs, F.C., 2010. The teraton challenge. A review of fixation and transformation of carbon dioxide. Energy Environ. Sci. 3, 43–81.
Mosadegh-Sedghi, S., Rodrigue, D., Brisson, J., Iliuta, M.C., 2014. Wetting phenomenon in membrane contactors – causes and prevention. J. Membr. Sci. 452, 332–353.
Mumford, K.A., Wu, Y., Smith, K.H., Stevens, G.W., 2015. Review of solvent based carbon-dioxide capture technologies. Front. Chem. Sci. Eng. 9 (2), 125–141.
Nieminen, H., Järvinen, L., Ruuskanen, V., Laari, A., Koiranen, T., Ahola, J., 2020. Insights into a membrane contactor based demonstration unit for CO2 capture. Sep. Purif. Technol. 231.
Nii, S., Iwata, Y., Takahashi, K., Takeuchi, H., 1995. Regeneration of CO2-loaded carbonate solution by reducing pressure. J. Chem. Eng. Jpn. 28 (2), 148–153.
Peters, M., Köhler, B., Kuckshinrichs, W., Leitner, W., Markewitz, P., Müller, T.E., 2011. Chemical technologies for exploiting and recycling carbon dioxide into the value chain. ChemSusChem 4, 1216–1240.
Portugal, A.F., Derks, P.W.J., Versteeg, G.F., Magalhães, F.D., Mendes, A., 2007a. Characterization of potassium glycinate for carbon dioxide absorption purposes. Chem. Eng. Sci. 62, 6534–6547.
Portugal, A., Derks, P., Versteeg, G., Magalhães, F., Mendes, A., 2007b. Characterization of potassium glycinate for carbon dioxide absorption purposes. Chem. Eng. Sci. 62, 6534–6547.
Portugal, A.F., Souda, J.M., Magalhães, F.D., Mendes, A., 2009. Solubility of carbon dioxide in aqueous solutions of amino acid salts. Chem. Eng. Sci. 64, 1993–2002.
Ramdin, M., de Loos, T.W., Vlugt, T.J.H., 2012. State-of-the-Art of CO2 capture with ionic liquids. Ind. Eng. Chem. Res. 51, 8149–8177.
Rode, S., Nguyen, P.T., Roizard, D., Bounaceur, R., Castel, C., Favre, E., 2012. Evaluating the intensification potential of membrane contactors for gas absorption in a chemical solvent: a generic one-dimensional methodology and its application to CO2 absorption in monoethanolamine. J. Membr. Sci. 389, 1–16.
Rubin, E.S., Mantripragada, H., Marks, A., Versteeg, P., Kitchin, J., 2012. The outlook for improved carbon capture technology. Prog. Energy Combust. Sci. 38, 630–671.
Rumble, J.Re., 2019. Physical constants of organic compounds. CRC Handbook of Chemistry and Physics, 100th Edition (Internet Version 2019). Boca Raton, CRC Press/Taylor & Francis.
Scholes, C.A., Qader, A., Stevens, G.W., Kentish, S.E., 2014. Membrane gas-solvent contactor pilot plant trials of CO2 absorption from flue gas. Sep. Sci. Technol. 49, 2449–2458.
Scholes, C.A., Kentish, S.E., Stevens, G.W., deMontigny, D., 2015. Comparison of thin film composite and microporous membrane contactors for CO2 absorption into monoethanolamine. Int. J. Greenhouse Gas Control 42, 66–74.
van Swaaij, W.P.M., Versteeg, G.F., 1992. Mass transfer accompanied with complex reversible chemical reactions in gas-liquid systems: an overview. Chem. Eng. Sci. 47, 3181–3195.
Wang, R., Zhang, H., Feron, P., Liang, D., 2005. Influence of membrane wetting on CO2 capture in microporous hollow fiber membrane contactors. Sep. Purif. Technol. 46 (1-2), 33–40.
Wang, Z., Fang, M., Pan, Y., Yan, S., Luo, Z., 2013a. Amine-based absorbents selection for CO2 membrane vacuum regeneration technology by combined absorption–desorption analysis. Chem. Eng. Sci. 93, 238–249.
Wang, L., Zhang, Z., Zhao, B., Zhang, H., Lu, X., Yang, Q., 2013b. Effect of long-term operation on the performance of polypropylene and polyvinylidene fluoride membrane contactors for CO2 absorption. Sep. Purif. Technol. 116, 300–306.
Wilcox, J., 2012. Carbon Capture. Springer Science + Business Media, LLC, New York.
Yan, S., Fang, M.-X., Zhang, W.-F., Wang, S.-Y., Xu, Z.-K., Luo, Z.-Y., Cen, K.-F., 2007. Experimental study on the separation of CO2 from flue gas using hollow fiber membrane contactors without wetting. Fuel Process. Technol. 88, 501–511.
Yan, S., Fang, M., Wang, Z., Luo, Z., 2012. Regeneration performance of CO2-rich solvents by using membrane vacuum regeneration technology: relationships between absorbent structure and regeneration efficiency. Appl. Energy 98, 357–367.
Yang, M., Cussler, E.L., 1986. Designing hollow-fiber contactors. AIChE J. 32, 1910–1916.
Yeon, S.-H., Sea, B., Park, Y.I., Lee, K.-H., 2003. Determination of mass transfer rates in PVDF and PTFE hollow Fiber membranes for CO2 absorption. Sep. Sci. Technol. 38 (2), 271–293.
Yeon, S.-H., Lee, K.-S., Sea, B., Park, Y.-I., Lee, K.-H., 2005. Application of pilot-scale membrane contactor hybrid system for removal of carbon dioxide from flue gas. J. Membr. Sci. 257, 156–160.
Zhang, H.-Y., Wang, R., Liang, D., Tay, J., 2008. Theoretical and experimental studies of membrane wetting in the membrane gas–liquid contacting process for CO2 absorption. J. Membr. Sci. 308, 162–170.
Zhao, S., Feron, P.H.M., Deng, L., Favre, E., Chabanon, E., Yan, S., Hou, J., Chen, V., Qi, H., 2016. Status and progress of membrane contactors in post-combustion carbon capture: a state-of-the-art review of new developments. J. Membr. Sci. 511, 180–206.

Publication III

H. Nieminen, G. Givirovskiy, A. Laari and T. Koiranen

Alcohol promoted methanol synthesis enhanced by adsorption of water and dual catalysts

Reprinted with permission from
Journal of CO_2 Utilization
Vol. 24, pp. 180-189, 2018

Journal of CO_2 Utilization 24 (2018) 180–189

Contents lists available at ScienceDirect

Journal of CO_2 Utilization

journal homepage: www.elsevier.com/locate/jcou

Alcohol promoted methanol synthesis enhanced by adsorption of water and dual catalysts

Harri Nieminen*, Georgy Givirovskiy, Arto Laari, Tuomas Koiranen

Lappeenranta University of Technology, Laboratory of Process and Product Development, P.O. Box 20, FI-53851 Lappeenranta, Finland

ARTICLE INFO

Keywords:
CO_2 hydrogenation
Methanol synthesis
Cu/ZnO
Liquid-phase
Alcohol promoted
Dual catalysis
Copper chromite
Molecular sieve

ABSTRACT

Alcohol-promoted methanol synthesis uses heterogeneous methanol synthesis catalysts in alcoholic solvents where the alcohols act as a co-catalyst. In the presence of alcohol, the reaction proceeds through alcohol formate ester as an intermediate, allowing methanol synthesis at lower temperatures than conventional gas-phase synthesis. In the present work, alcohol-promoted CO_2 hydrogenation to methanol was studied experimentally using a Cu/ZnO catalyst with 1-butanol and 2-butanol as solvents. As water is known to inhibit methanol synthesis on Cu/ZnO catalysts, the alcohol-promoted process was further developed by in-situ adsorption of water using a 3 Å molecular sieve. The methanol productivity significantly improved as a result of the lowered concentration of water. The concentration of water was thus identified as a key factor affecting the overall methanol productivity. As the alcohol-promoted methanol synthesis process is characterized by two separate reaction steps, the use of separate catalysts optimized for each step offers an interesting approach for the development of this process. Such a dual-catalysis concept was tested using a copper chromite catalyst together with Cu/ZnO. Promising results were obtained, as methanol productivity increased with the addition of copper chromite. Catalyst characterization was carried out using XRD and SEM-EDS and potential effects of observed changes in catalyst structure during reaction are discussed.

1. Introduction

Development of efficient and flexible energy storage methods is critical for a global shift from a fossil fuels based economy to a renewable energy based economy [1]. The use of surplus peak electricity generated from fluctuating renewable energy sources, such as wind and solar energy, for the production of chemical compounds would enable energy storage in a highly transportable form at high energy density. Generation of hydrogen by electrolysis of water is the common starting point in chemical energy storage strategies [2]. However, due to the difficulties and hazards associated with large-scale storage and transportation of gaseous hydrogen, further utilization of hydrogen for production of carbon-containing liquid fuels and chemical compounds might be preferable.

Methanol is an example of such a potential liquid-phase chemical energy carrier [3]. Methanol is an important and versatile industrial chemical that can also be used as a fuel in power generation and in internal combustion engines and fuel cells [4]. Additionally, methanol is a versatile raw material for synthesis of a variety of chemical products. For instance, methanol can be transformed into gasoline in the methanol-to-gasoline process (MTG) [5] or into olefins in the methanol-to-olefins process (MTO) [6].

Current production of methanol is based on catalytic conversion of synthesis gas generated from fossil sources, commonly natural gas. The syngas is mainly composed of mixtures of hydrogen, carbon monoxide and carbon dioxide. In conventional methanol synthesis, copper and zinc oxide (Cu/ZnO) catalysts are generally employed at reaction temperatures of 200–300 °C and pressures of 50–100 bar [7].

The methanol synthesis process can be described by the following three equilibrium reactions:

$$CO_2 + 3\,H_2 \rightleftharpoons CH_3OH + H_2O\;\Delta H^0 = -49.8\,\text{kJ/mol} \quad (1)$$

$$CO + 2\,H_2 \rightleftharpoons CH_3OH\;\Delta H^0 = -91.0\,\text{kJ/mol} \quad (2)$$

$$CO + H_2O \rightleftharpoons CO_2 + H_2\;\Delta H^0 = 41.2\,\text{kJ/mol} \quad (3)$$

The exothermic reactions (1) and (2) represent, respectively, the hydrogenation of CO_2 and CO to methanol. Reaction (3), the water-gas shift (WGS) reaction, is relevant to methanol synthesis as the reaction is also activated by the copper-based methanol synthesis catalysts [8]. As methanol synthesis is exothermic and results in a reduction of molar volume, methanol synthesis is favored by low temperatures and high pressures. However, temperatures above 200 °C are required for sufficiently high reaction rates, and thus the thermodynamic equilibrium

* Corresponding author.
E-mail address: harri.nieminen@lut.fi (H. Nieminen).

https://doi.org/10.1016/j.jcou.2018.01.002
Received 23 October 2017; Received in revised form 15 December 2017; Accepted 2 January 2018
Available online 06 January 2018

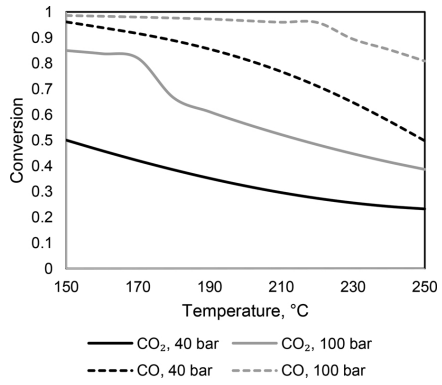

Fig. 1. Effect of temperature and pressure on the equilibrium carbon conversion from stoichiometric CO_2:H_2 (1:3) and CO:H_2 (1:2) mixtures. Calculated with the predictive Soave-Redlich-Kwong (PSRK) [58] equation of state in Aspen Plus.

limits the methanol synthesis to low conversion levels. Hydrogenation of pure CO_2 to methanol is also possible but the equilibrium conversions are even lower than for CO. Fig. 1 shows the calculated equilibrium conversion of stoichiometric CO and CO_2 feeds at different temperatures and pressure. The conversions are modelled by Soave-Redlich-Kwong equations of state, which have been shown to accurately predict experimental results in methanol synthesis [9]. However, the hydrogenation of CO_2 on Cu/ZnO catalysts is highly selective to methanol, with other thermodynamically more favorable products such as methane, ethers and ketones formed only in negligible amounts [10].

To overcome the thermodynamic limitations in the gas-phase methanol process, liquid-phase synthesis processes have been proposed as an alternative approach to enable lower reaction temperatures in syngas reactions. Early developments utilized highly basic catalyst systems such as alkali alkoxides in combination with copper chromite [11,12,13] or nickel-based catalysts [14,15,16]. Methanol synthesis from CO/H_2 at temperatures as low as 100 °C and pressures between 30 and 65 bar were reported [17]. However, the basic catalysts are incompatible with CO_2 or water, the presence of which, even at trace amounts, leads to rapid catalyst deactivation [16]. A method proposed by the Brookhaven National Laboratory (BNL) also utilized a highly basic system for the conversion of CO to methanol at significantly low temperature and pressure [18]. Furthermore, liquid-phase methanol synthesis from CO_2-containing synthesis gas in inert hydrocarbon solvent has been demonstrated in the LPMeOH process [19].

CO_2 has been identified as the main carbon source in methanol synthesis from syngas [20]. Hence, it may be expected that methanol can also be produced by hydrogenation of pure CO_2. Hydrogenation of CO_2, captured from point sources or even directly from the atmosphere, would then provide a sustainable source of carbon-based fuels and chemicals while helping to reduce the atmospheric concentration of CO_2 [21]. Some pilot-scale methanol processes that can use CO_2 as the starting material have been developed. These include the CAMERE process [22], which combines the reverse water-gas-shift reaction and methanol synthesis from syngas, and the Matsui Chemicals process [23], which directly converts CO_2 to methanol. Additionally, Carbon Recycling International established commercial methanol production from CO_2 in 2011, and the Svartsengi plant is presently operating at a capacity of above 5 million liters per year [24]. The process utilizes geothermal energy readily available in Iceland.

One possible way to influence the reaction kinetics and conditions is to change the reaction route that leads to the formation of methanol. A novel alcohol-promoted liquid-phase methanol synthesis process first proposed by Fan et al. [25] is based on the combination of a conventional Cu/ZnO catalyst and alcohol as a catalytic solvent. The alcohol promotes methanol synthesis by altering the reaction route, allowing operation at lower temperatures. In the presence of the alcohol, the reaction proceeds through the formate ester of the corresponding alcohol as an intermediate. As a result, methanol can be produced from syngas at temperatures starting from 170 °C and pressures in the range of 30 to 50 bar [26]. Importantly, the process does not employ basic catalysts sensitive to deactivation by CO_2, allowing direct conversion of CO_2. The following reaction steps have been proposed for this process [27], supported by subsequent *in-situ* IR observations [28]:

1 Hydrogenation of carbon dioxide into formic acid

$$CO_2 + H_2 \rightleftarrows HCOOH \quad (4)$$

2 Reaction of formic acid with ethanol, forming ethyl formate

$$HCOOH + C_2H_5OH \rightleftarrows HCOOC_2H_5 + H_2O \quad (5)$$

3 Hydrogenation of ethyl formate, forming methanol and ethanol

$$HCOOC_2H_5 + 2\,H_2 \rightleftarrows CH_3OH + C_2H_5OH \quad (6)$$

The net reaction is the hydrogenation of carbon dioxide to methanol (Eq. (1)) with a standard reaction enthalpy of -49.8 kJ/mol. Different alcohols have been shown to possess different promoting effect for methanol synthesis. Tsubaki et al. [29] found linear alcohols to be more effective compared to their branched counterparts, with n-butanol showing the best results. Zeng et al. [30] reported that the yield of both methanol and the corresponding ester decreased with increasing carbon number of the 1-alcohols from ethanol to 1-hexanol. For alcohols with the same carbon number but different structure, 2-alcohols were found to have higher activity, which was explained by a combination of spatial and electronic effects. As a result, 2-propanol showed the highest promotional effect. Later, 2-butanol was reported as the most effective solvent for the continuous methanol synthesis in a semibatch reactor [31].

As the alcohol-promoted methanol synthesis process is characterized by two separate reaction steps, the utilization of separate catalysts optimized for each reaction could be beneficial. Such dual- or cascade catalytic systems have been considered previously for methanol synthesis. Huff and Sanford [32] reported effective CO_2 conversion to methanol at 135 °C using a combination of homogeneous catalysts. Chen et al. [33] used heterogeneous catalysts in 1,4-dioxane solvent: copper chromite for the hydrogenation of CO_2 to formate and Cu/Mo_2C for the formate hydrogenolysis to methanol. This system was capable of methanol production at rates comparable to conventional gas-phase synthesis at 135 °C and exhibited methanol selectivity above 75%. The methanol synthesis was promoted by the addition of ethanol, with the reaction proceeding through ethyl formate, as reported in the alcohol-promoted process. On the other hand, copper chromite is known to catalyze the hydrogenolysis of esters to alcohols, i.e. the latter stage in the alcohol-promoted reaction route [34]. As such, copper chromite appears an interesting component of a dual catalytic system for alcohol-promoted methanol synthesis.

In comparison to CO-containing syngas feed, CO_2 hydrogenation to methanol is further complicated by the increased formation rate of water. Water is formed as a byproduct in methanol synthesis, and in the absence of CO, the water-gas shift reaction proceeds in the reverse direction, producing more water. The negative effect of water on methanol synthesis on Cu/ZnO-based catalysts has been well documented [35]. This effect has been explained as a combination of kinetic inhibition effects and structural catalyst deactivation. Water-derived hydroxyl species can block the active sites on the catalyst, resulting in

kinetic inhibition. The presence of water can also accelerate the sintering of copper particles [36], resulting in decreased copper dispersion and catalyst deactivation. Removal of methanol and water using membrane reactors [37,38] and by condensation at high pressures [39] or low temperatures [40] has been previously described for gas-phase methanol synthesis. Reactive distillation [41] provides a further possible approach for continuous product removal, particularly in liquid-phase processes, and has been proposed in literature for the methanol synthesis process [42] and for the Fischer-Tropsch process [43] operating at similar conditions. In addition, selective removal of water by adsorption on zeolite molecular sieves has also been suggested in sorption-enhanced methanol [44] and related dimethyl ether [45] synthesis operated in the gas-phase.

In the present work, alcohol-promoted methanol synthesis was investigated experimentally using a commercial Cu/ZnO-based methanol synthesis catalyst with 1-butanol and 2-butanol as the solvents. 2-butanol was selected because of the previously reported high activity for methanol synthesis, and 1-butanol was considered interesting because of the potentially simplified product separation due to the higher boiling point of the alcohol. As novel developments, enhancement of the alcohol-promoted methanol synthesis by *in-situ* adsorption of water and by the use of dual catalysts were studied. Water adsorption was carried out using a molecular sieve. Methanol synthesis combined with water removal has previously been modelled based on 4Å molecular sieves [44], and the use of 4Å molecular sieves has been modelled for a related dimethyl ether (DME) synthesis [45]. However, experimental work of methanol synthesis promoted by water adsorption has not been published earlier to our knowledge. A dual catalyst system comprising of a combination of Cu/ZnO and copper chromite catalysts was tested with the aim of improving methanol productivity by influencing separately the formate formation and hydrogenolysis reaction steps.

2. Materials and methods

A Parr 4520 autoclave reactor with an inner volume of 450 ml was used for the reaction experiments. The reactor was connected to a Parr 4848 control unit used to control the reaction temperature and mixing speed. A mixing speed of 600 rpm was used in all experiments. Liquid samples from the reaction mixture were collected using a water-cooled sample collection vessel, in which any vapors present in the sample were condensed prior to collecting the sample.

Analysis grade 1-butanol and 2-butanol, were used as solvents. A commercial Cu/ZnO-based methanol synthesis catalyst (Alfa Aesar, 65.5% CuO, 24.7% ZnO, 10.1% Al_2O_3, 1.3% MgO) was used. The catalyst was ground and sieved to 150–500 µm for each experiment. The 3Å molecular sieve (UOP, beads with diameter of 2 mm), was also ground and sieved to 150–500 µm. An initial experiment with the unground molecular sieve was also performed. The molecular sieve was activated by heating to 250 °C for at least 8 h under air and subsequent cooling to ambient temperature inside a desiccator prior to use. Powdered copper chromite (Sigma-Aldrich) was used in the dual catalyst experiments. A mixed gas containing 75% hydrogen and 25% carbon dioxide was used as the reaction feed gas, and a mixed gas containing 5% hydrogen in nitrogen was used for activation of the catalysts. A diagram of the experimental setup is presented in Fig. 2.

The ground Cu/ZnO catalyst and the copper chromite catalyst were activated *in-situ* in the reactor vessel. Catalyst activation was performed under 5 bar of the 5% H_2/N_2 mixed gas, with the gas inside the reactor replaced every 30 min. The temperature was 200 °C during the activation. Following catalyst activation, the reactor was cooled and the catalysts were kept under the activation gas until the reaction experiment was executed. 200 ml of the alcohol was quickly poured into the reactor, minimizing the contact time of the catalysts with air. The reactor was purged with nitrogen and heated to the reaction temperature under N_2. At the reaction temperature, an initial liquid sample was collected and the reactor was pressurized with the feed gas (CO_2:H_2 = 1:3) to the set reaction pressure, which was 60 bar unless otherwise noted. Constant pressure was maintained during the experiments by replacing the consumed reaction gas with fresh gas. The total reaction time was 6 h and liquid samples were collected every 2 h.

An Agilent Technologies 6890N gas chromatograph with a thermal conductivity detector was used for analysis of the liquid samples. A polar Zebron ZB-WAXplus column was used for the 2-butanol samples. An isothermal method with the column temperature at 70 °C and helium (1.1 ml/min) as a carrier gas was used. For the 1-butanol samples, a non-polar HP-1ms column was used due to insufficient separation of butanal and methanol in the ZB-WAXplus column. A temperature program with an initial temperature of 50 °C (3 min hold) followed by a 25 °C/min ramp to 100 °C (3 min hold) was used. Helium (0.7 ml/min) was used as the carrier gas. In the ZB-WAXplus column, the retention times were 2.9 min for methanol, 3.0 min for 2-butanone, 3.8 min for 2-butanol, and 3.9 min for water. In the HP-1ms column, the retention times were 2.7 min for water, 2.9 min for methanol, 4.7 min for butanal, and 5.8 min for 1-butanol. Sample concentrations were calculated by the external standard method.

Analysis uncertainty was estimated by repeated measurements and by estimation of the uncertainty related to the preparation and analysis of the calibration standards. The total uncertainty is expressed as the relative standard deviation for each product compound in 1-butanol and 2-butanol, which is presented as error bars in the relevant figures. In 1-butanol, the relative standard uncertainty is 8% for methanol, 11% for water and 12% for butanal. In 2-butanol, the relative standard uncertainty is 8% for methanol and 11% for water. The uncertainty related to the experimental procedure was estimated as relatively insignificant.

Characterization of the Cu/ZnO catalyst by XRD and SEM-EDS was performed in order to observe any structural changes in the catalyst during the reaction. The catalyst used in methanol synthesis in 1-butanol at 180 °C was analyzed before the reaction (in calcined form) following grinding, and also after the experiment. A separate batch of ground catalyst was characterized by XRD following reduction by the method described above.

XRD analysis was performed on a Bruker D8 Advance system with Cu-Kα radiation at 2θ of 20° to 90° at 0.02° increment, with fixed sample illumination and LYNXEYE 1D detector. For analysis, a layer of the ground catalyst in the 150–500 µm particle size range was placed on the plastic powder specimen holder, which was rotated at 10 rpm during analysis. Phase analysis was performed in DIFFRAC.SUITE EVA software based on the PDF 4 + 2018 database. SEM micrographs and EDS element analyses were obtained using a Hitachi SU3500 Scanning Electron Microscope with SE detector and Thermo Fisher Scientific UltraDry SDD EDS. The acceleration voltage was varied between 10 and 20 kV. The samples were introduced as 150–500 µm particles on a two-sided carbon tape, without coating.

3. Results and discussion

3.1. Detected reaction products

In addition to methanol and water, significant quantities of alcohol dehydrogenation products were found in the reaction mixture. Alcohol dehydrogenation is known to be catalyzed by copper catalysts [46] with the reaction yielding corresponding aldehydes or ketones and hydrogen as products [47]. For instance, the dehydrogenation of 1-butanol yields butanal, while 2-butanol is dehydrogenated to 2-butanone. These reactions have also been identified in other published studies on alcohol-promoted methanol synthesis [48].

Fig. 3 depicts a typical concentration profile of the observed reaction products in 1-butanol during 6 h of reaction time. The temperature was 180 °C and pressure 60 bar for the experiment depicted. Similar concentration curves were observed for all reaction conditions and alcohols used.

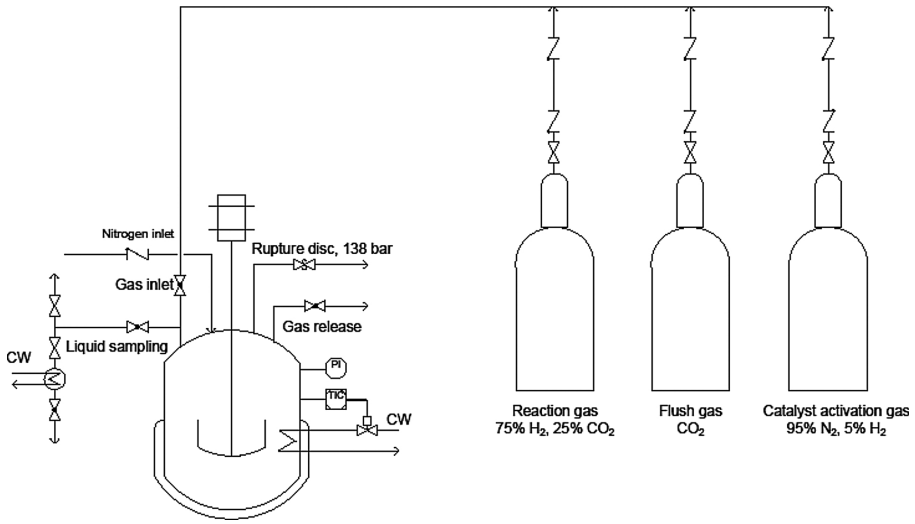

Fig. 2. Experimental setup used in the reaction experiments.

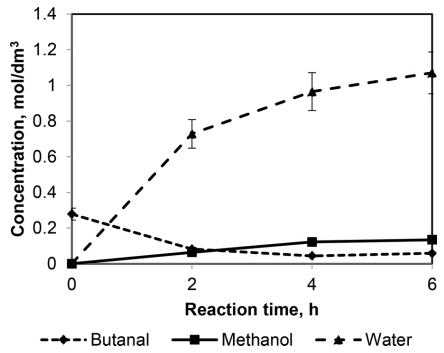

Fig. 3. Typical concentration profile of the detected reaction products in 1-butanol. 20 g of Cu/ZnO catalyst in 200 ml of alcohol, temperature 180 °C, feed gas CO_2:H_2 = 1:3, total pressure 60 bar.

The highest concentration of dehydrogenation products was found after heating of the reaction mixture prior to introducing the reaction feed gas. A corresponding increase in the reactor pressure was noticed during the heating process. The pressure increase was presumably caused by the hydrogen formed in the alcohol dehydrogenation reaction. The peak concentration of the dehydrogenation products varied depending on the temperature and the alcohol used but always remained below 10% of the total solution on a mass fraction basis. However, the concentration of the aldehyde or ketone significantly decreased under the reaction gas atmosphere with increasing reaction time. The dehydrogenation reactions appear to reverse direction under increased hydrogen pressure, returning the original alcohols to the solution. Due to the relatively minor conversion of the alcohols and the apparent reversibility of these reactions, alcohol dehydrogenation is not considered harmful for the overall process.

The concentration of methanol continuously increases over the 6 h of reaction time. Thus, equilibrium conversion is not reached during this time, and more methanol would likely form if the reaction time were increased. The higher total concentrations of methanol and water found in the molecular sieve experiments (Section 3.3) are further evidence that the equilibrium product concentration is not reached. However, in many of the experiments, the methanol production rate decreases after 4 h of reaction time, as evidenced by the declining slope of the methanol concentration curve in Fig. 3. As the thermodynamic equilibrium is not reached at this point, the methanol synthesis rate appears to be limited by kinetic effects, most likely by inhibition caused by the by-product water.

The concentration of water also increases during the reaction as water is formed both as the by-product of CO_2 hydrogenation to methanol and also in the RWGS reaction. The amount of water formed is significantly higher than the amount of methanol. In 1-butanol at 180 °C, the end concentration of water is almost 7 times the end concentration of methanol (Fig. 3). A similar result is found at higher reaction temperatures. Fig. 4 presents the concentrations of methanol and water in 1-butanol at reaction temperatures of 180, 200 and 220 °C.

If water is only formed as the by-product of methanol synthesis, the molar amounts of methanol and water formed should be equal. The much higher concentrations of water compared to methanol suggest that a significant majority of the water is formed in reactions other than methanol synthesis. On the Cu/ZnO catalyst, the RWGS reaction is most likely the source of the excess water. The high molar ratios of water to methanol formed would suggest that the RWGS reaction is the main reaction in this system and the total selectivity to methanol is rather low. In 1-butanol (Fig. 4), the molar ratio of water to methanol ranges approximately from 7 to 10, which implies methanol selectivity in the range of 10–20 %. Some water is also present at the start of the reaction, most likely formed during the reduction of the catalyst. This amount of water is significant in some of the experiments, for example, in 1-butanol at 220 °C (Fig. 4), constituting a potential disadvantage of the *in-situ* catalyst activation method.

Although hydrogenation of the esters is considered to be the rate-determining step in this process [25], alkyl formates, the intermediate products of alcohol-promoted methanol synthesis, were not detected in the reaction mixture, neither in 1-butanol nor in 2-butanol. The formate esters appear to be rapidly hydrogenated into methanol and alcohol

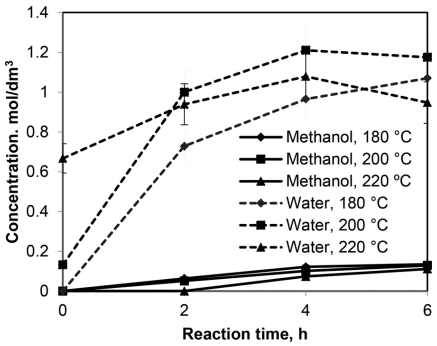

Fig. 4. Overall effect of temperature on the formation of methanol and water in alcohol promoted methanol synthesis with 1-butanol as solvent. 20 g of Cu/ZnO catalyst. Feed gas CO_2:H_2 = 1:3. Total pressure 60 bar. Error bars for the concentration of water at 180 and 200 °C are omitted for clarity.

(reaction 9) and their concentrations remain below the detection limit of the analysis method. As the intermediates were not detected, it was not possible to confirm that the reactions proceed through the suggested reaction route. However, the overall promoting effect of the alcohols was convincingly confirmed by a blank experiment in hexane at 180 °C, in which no methanol was formed.

3.2. Effect of reaction temperature and pressure

Reactions in 1-butanol were carried out using a constant overall pressure at different temperatures. Fig. 5 shows the combined effect of the reaction temperature and the partial pressure of the reaction gas on methanol productivity with constant total pressure at 180, 200 and 220 °C. The methanol productivity is measured as grams of methanol produced per kg of catalyst per hour. The concentrations of the reaction products in these experiments are shown in Fig. 4. Methanol productivity is found to decrease with increasing temperature at the temperature range studied. This result can be explained by the decreased partial pressure of the reaction gas due to increased vapor pressure of 1-butanol at constant total pressure. The partial pressures, shown also in Fig. 5, are calculated by subtracting the alcohol vapor pressure from the total reaction pressure.

As the concentration of water did not markedly change when the reaction temperature was varied (Fig. 4), it can be concluded that the

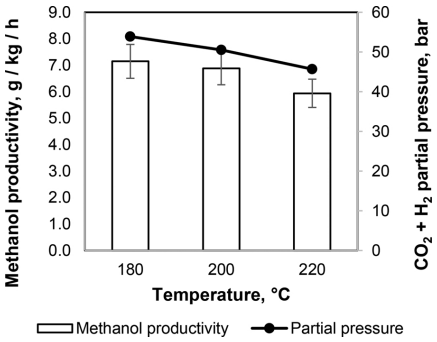

Fig. 5. Effect of temperature on methanol productivity with 20 g of Cu/ZnO catalyst in 200 ml of 1-butanol. Reaction time 6 h, feed gas CO_2:H_2 = 1:3, total pressure 60 bar.

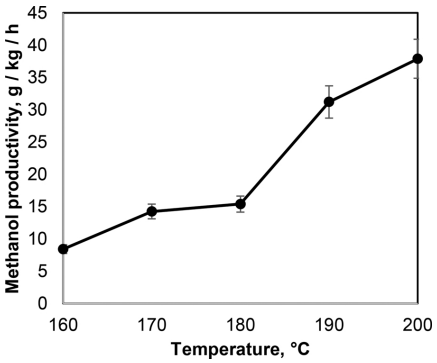

Fig. 6. Effect of temperature on methanol productivity with 10 g of Cu/ZnO catalyst in 200 ml of 2-butanol. Feed gas (CO_2:H_2 = 1:3), partial pressure 40 bar, reaction time 6 h.

effect of the RWGS reaction does not explain the lowered methanol productivity at increased temperature.

In theory, the reduced methanol synthesis rate at increased temperatures could also be explained by increased selectivity to CO. Increased CO formation by the RWGS reaction should also lead to increased production of water, as water is also formed in the RWGS reaction. The increased concentrations of water would further inhibit the rate of methanol synthesis. However, the concentration of water did not markedly change when the reaction temperature was varied (Fig. 4). Thus, it is concluded that the RWGS reaction does not explain the lowered methanol productivity at increased temperature.

The reactions in 2-butanol were carried out using a constant reaction gas partial pressure at different temperatures and a constant temperature at different reaction gas partial pressures. The effect of the feed gas partial pressure on methanol productivity can be clearly seen in Fig. 6, which presents methanol productivity at different reaction temperatures with $CO_2 + H_2$ partial pressure fixed to 40 bar by varying the total reaction pressure. A significant increase in the methanol production rate with increasing reaction temperature is observed.

Fig. 7 presents the methanol productivity at a fixed reaction temperature of 180 °C with the feed gas partial pressure varied from 30 to 50 bar. The productivity clearly increases with the increased partial pressure. The obtained productivities in 2-butanol seem to be higher than in 1-butanol. It should however be noted that the higher productivity values in 2-butanol might be explained by the lower amount

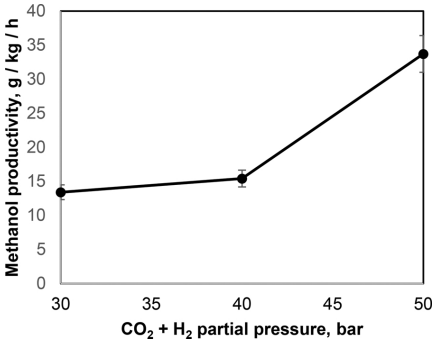

Fig. 7. Effect of reaction gas partial pressure on methanol productivity with 10 g of Cu/ZnO catalyst in 2-butanol at 180 °C. Feed gas (CO_2:H_2 = 1:3), reaction time 6 h.

(10 g) of catalyst used. The specific productivity of the catalyst appears to decrease as a result of increased water formation due to the RWGS reaction when larger amounts of catalysts are used. This effect is discussed further in Section 3.3.

3.3. Water removal by molecular sieve

Continuous removal of water from the reaction mixture was tested by addition of a zeolite molecular sieve. Molecular sieves with a pore diameter of 3 Å can be used for the dehydration of alcohols because of their selective adsorption of water [49]. The selective adsorption is based on size exclusion of molecules larger than water in the inner microporous structure of the zeolite.

The limiting effect of water on the alcohol-promoted methanol synthesis process was first confirmed by performing an experiment with approximately 1.4 mol/dm^3 of water added to 2-butanol. This concentration is slightly above the maximum concentration range of water found in the experiments (Fig. 4). At 180 °C and 60 bar of total pressure, the methanol production rate was approximately 74% lower than in the base experiment with no water added. The concentration of water did not significantly increase during this experiment but rather remained relatively constant at the apparent equilibrium level.

Next, the effect of *in-situ* adsorption of water by the addition of a 3Å molecular sieve was tested. The relative amounts of the catalyst and the molecular sieve were varied, maintaining a total solids mass of 50 g. The results of these experiments are presented in Fig. 8. A base experiment with 20 g of catalyst and no molecular sieve is also presented for comparison.

Compared to the base case with 20 g of Cu/ZnO catalyst and no molecular sieve, the addition of the unground molecular sieve increased the methanol productivity from 8.2 g/kg/h to 11.2 g/kg/h. A more significant improvement was found with the molecular sieve ground into 150–300 µm particle size range. Due to the clear effect of the particle size, the adsorption of water appears to be significantly diffusion-limited for the unground molecular sieve. With 20 g of catalyst, the addition of 30 g of the ground molecular sieve increases the methanol productivity to 33.6 g/kg/h, an increase of over 300% over the Cu/ZnO catalyst used without a molecular sieve. Keeping the total amount of solids (catalyst + molecular sieve) at 50 g, the methanol productivity increased with increasing amounts of molecular sieve. For instance, the productivity increased to 54.4 g/kg/h using 10 g of the catalyst and 40 g of the molecular sieve. These results clearly show that the catalyst is most effectively utilized for methanol synthesis when larger relative amounts of the molecular sieve to the catalyst are used. This observation can be explained by the increased water adsorption capacity of the larger amount of the molecular sieve, leading to decreased concentrations of water, as shown in Fig. 8.

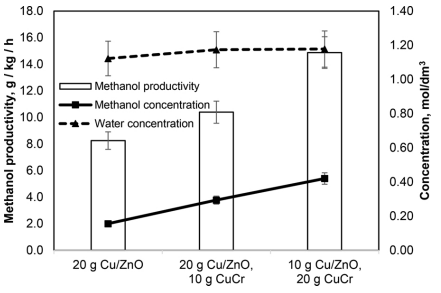

Fig. 9. Effect of different amounts of Cu/ZnO and copper chromite (CuCr) catalysts on the formation of methanol and water in 2-butanol. Reaction time 6 h. Temperature 180 °C, feed gas CO_2:H_2 = 1:3, total pressure 60. An experiment with 20 g of Cu/ZnO catalyst and no copper chromite is included for comparison.

3.4. Dual catalysts

To test the dual catalysis concept for alcohol-promoted methanol synthesis, copper chromite (CuCr) was used in combination with the Cu/ZnO catalyst. The ratios of the two catalysts were varied: 20 g of the Cu/ZnO catalyst was used with 10 g of CuCr, and vice versa. The experiments were carried out in 2-butanol at 180 °C and 60 bar of total pressure, corresponding to a CO_2 + H_2 partial pressure of 50.1 bar. The results of these experiments are presented in Fig. 9. A base experiment with 20 g of Cu/ZnO catalyst and no copper chromite is also presented for comparison.

The addition of the copper chromite catalyst clearly increases the methanol productivity. Both the absolute methanol production rate, as measured by the methanol end concentration, and the specific productivity of the catalyst increase with addition of copper chromite. The increased productivity can be explained either by a synergistic effect between the two catalysts or by higher methanol synthesis activity of CuCr compared to Cu/ZnO. However, a higher intrinsic activity of copper chromite appears unlikely, as the activity of Cu/ZnO for methanol synthesis is well-known and industrially applied. Fan et al. [25] also reported higher methanol yield and selectivity of Cu/ZnO compared to CuCr in alcohol promoted methanol synthesis. Fan et al. also found similar CO selectivity, or RWGS activity, for both of the catalysts. This is supported by the present results, as the concentration of water was not significantly affected by the changed ratio of Cu/ZnO and CuCr (Fig. 9, columns 2 and 3), supporting similar RWGS activity of the two catalysts. The overall methanol selectivity appears to be higher with the combined catalysts, as the ratio of methanol to water produced is increased compared to Cu/ZnO used alone.

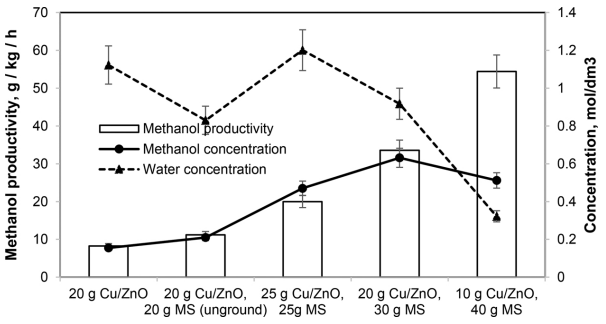

Fig. 8. Effect of catalyst and molecular sieve mass on methanol and water formation in 2-butanol. Temperature 180 °C, feed gas CO_2:H_2 = 1:3, total pressure 60 bar.

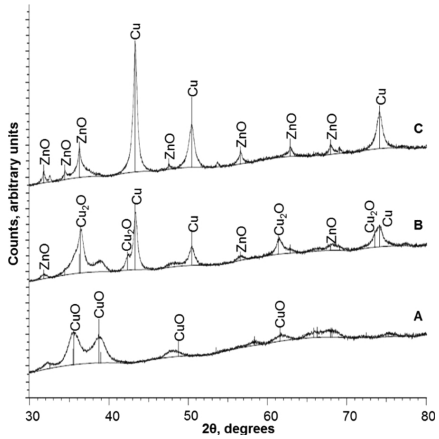

Fig. 10. X-ray diffractograms of the unused Cu/ZnO catalyst (A), the reduced catalyst (B), and the catalyst following methanol synthesis from CO_2 and H_2 (1:3) in 1-butanol at 180 °C (C).

3.5. Characterization of Cu/ZnO catalyst before and after reaction

The structural features of the Cu/ZnO catalyst before and after reaction were investigated by the means of XRD and SEM-EDS in order to assess the catalyst stability. Fig. 10 presents the X-ray diffractograms of the catalyst as supplied in the calcined form, following reduction in 5% hydrogen, and following use in alcohol-promoted methanol synthesis in 1-butanol at 180 °C. It is noted that the same batch of catalyst was analyzed prior to reduction and following the reaction, while the reduced catalyst was prepared and analyzed separately.

The calcined catalyst is largely amorphous, showing a minor pattern corresponding to copper(II)oxide (CuO) typical to Cu/ZnO catalysts [50]. The patterns are identified based on the PDF 4 + 2018 crystallography database. The reduced catalyst presents with a clearly defined pattern consistent with crystalline, copper(I)oxide (Cu_2O), and metallic copper. Weak crystalline features of zinc oxide are also evident, consistent with previous studies [51]. As the reduction of copper proceeds stepwise from CuO to Cu via Cu_2O [52], the presence of Cu_2O may imply incomplete reduction, possibly due to insufficient reduction time or temperature. However, as the reduced catalyst sample was transferred and analyzed in contact with air, re-oxidation of copper crystallites during this process cannot be ruled out.

Only metallic copper and zinc oxide is found present in the used catalyst. Cu/ZnO catalysts are known to show dynamic structural changes depending on the oxidation potential of the gas phase [53,54] and ongoing reduction of the catalyst at the reaction conditions is possible. As the reduced and used catalyst analyzed here are not from the same batch of ground and prepared catalyst, batch-to-batch variation cannot be eliminated as a cause of the observed structural differences.

The peaks corresponding to zinc oxide are more clearly defined compared to the reduced catalyst, potentially indicating continuing crystallization of ZnO at the reaction conditions. Lunkenbein et al. [55] identified zinc oxide as the more dynamic phase compared to metallic copper under reaction conditions, and found that crystallization of ZnO and the resulting loss of reactive Cu-ZnO interfaces is the main mechanism of initial catalyst deactivation. The SEM-EDS elemental maps of copper and zinc presented in Fig. 11 indicate that such a process may have initiated in the catalyst used here. The unused (calcined) catalyst shows a relatively homogeneous distribution of both copper and zinc. However, a degree of segregation of these elements can be observed in the used catalyst, with the elemental map showing distinct areas with high content of zinc (oxide) that are relatively poor in copper.

Further insight is provided by the SEM images presented in Fig. 12. Distinct crystals in the micrometer dimension can be observed, identified as zinc oxide by the EDS analysis. No such features were found in the unused catalyst. It is concluded that agglomeration and crystallization of zinc oxide during reaction has occurred, acting as a potential deactivation mechanism for the catalyst. However, as long-term stability tests were not performed here, the actual effect of these structural changes on the activity of the catalyst cannot be discussed.

These observations can be compared to other findings discussed in literature. Previously, the stability of Cu/ZnO catalyst in alcohol promoted methanol synthesis has been explored by Reubroycharoen et al. [31] who found the performance stable during 40 h of continuous methanol synthesis (at 170 °C), and by Jeong et al. [56] who found no decline in activity during 60 h of reaction (150 °C). In contrast to our results, Jeong et al. found no changes in the XRD profile of the catalyst before and after reaction. Other than the lower reaction temperature, the differing findings might be explained by different feed gas composition, as a CO-rich syngas was used in these studies opposed to the CO_2:H_2 mixture used here. Therefore, it is possible that the detected differences might be caused by the large amount of water present in the reaction system in the present study.

4. Conclusions

Methanol synthesis from CO_2 was studied in an alcohol-promoted liquid-phase process using conventional Cu/ZnO and copper chromite as catalysts. 1-butanol and 2-butanol were found to act as catalytic solvents, allowing methanol synthesis at lower temperatures than conventional gas-phase processes. Although it was not possible to determine the exact reaction route, it is expected that the promoting effect of the alcohols is based on a reaction route proceeding through the intermediate of formate ester of the alcohol.

The effect of continuous water removal using molecular sieve adsorption was explored. The addition of a 3Å molecular sieve significantly enhanced methanol productivity. Grinding of the molecular sieve resulted in improved results due to the shorter diffusion path compared to the granular material. The maximum methanol productivity of 54.4 g/kg/h was found when the maximum relative amount of the molecular sieve (40 g) to the catalyst (10 g) was used. The final methanol concentration after 6 h of reaction time reached 0.5 mol/dm^3. The catalyst was most effectively used for methanol synthesis when the amount of molecular sieve was maximized, which minimized the concentration of water. The water concentration was found to significantly affect the rate of methanol synthesis. The overall methanol production rate in this process appears to be limited by the concentration of water and its effects on the catalyst surface. To prevent the negative effects of water, continuous water removal or development of more water resistant catalysts is vital for further development of this process. Based on the results, the use of a 3Å molecular sieve for water removal appears a promising approach.

The methanol productivity obtained in the current research can be compared to results reported in other studies. Yang et al. [48] found an even higher methanol productivity of up to 167 g/kg/h for alcohol-promoted methanol synthesis at 170 °C and 50 bar using an optimized Cu/ZnO catalyst composition. The difference to the results presented here can be explained mainly by the different feed gas composition in their experiments ($CO/CO_2/H_2/Ar$ = 32.4/5.1/59.5/3.9). For gas-phase CO_2 hydrogenation to methanol, productivity values even up to 1200 g/kg/h have been achieved [57]. However, these results were obtained at a relatively high temperature of 240 °C and at high space velocities giving relatively low CO_2 conversions.

Dual catalysis by the combination of Cu/ZnO with copper chromite was also studied in this work. A remarkable increase in catalytic

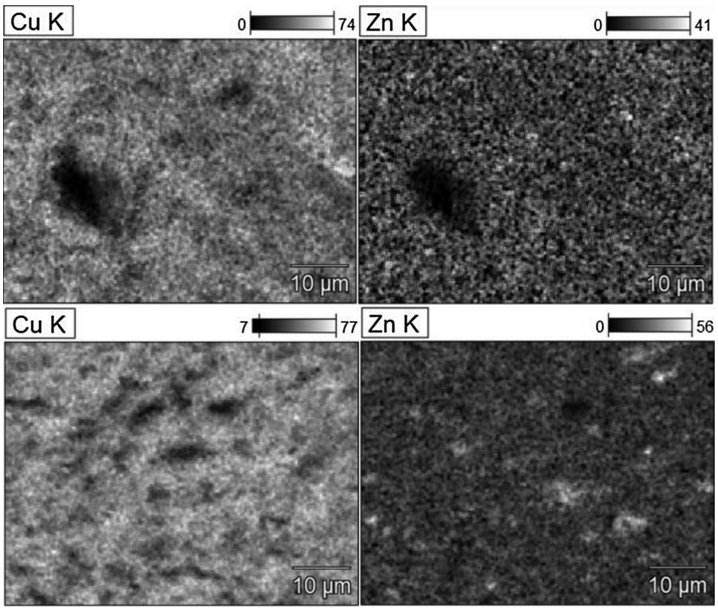

Fig. 11. SEM-EDS elemental maps of copper and zinc in the unused Cu/ZnO catalyst (upper), and the catalyst following methanol synthesis from CO_2 and H_2 (1:3) in 1-butanol at 180 °C (lower). Composition scales in weight percent.

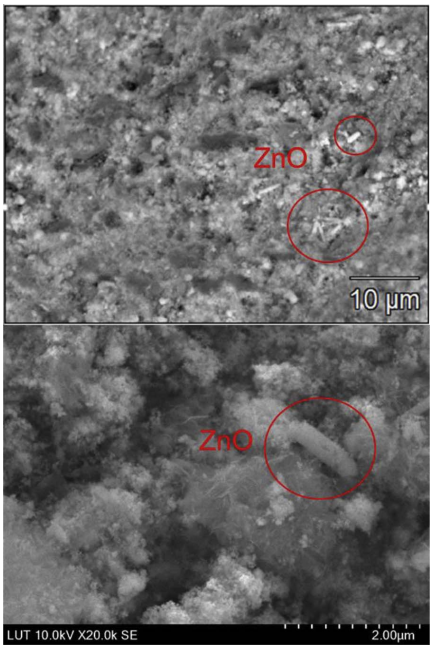

Fig. 12. SEM micrographs of the Cu/ZnO catalyst following methanol synthesis from CO_2 and H_2 (1:3) in 1-butanol at 180 °C. Zinc oxide crystals are highlighted.

activity was found for the dual catalyst. When 20 g of copper chromite and 10 g of Cu/ZnO was used, the productivity increased by 80% compared to the use of 20 g of the Cu/ZnO catalyst alone. A synergistic effect between the two catalysts is suggested, which is possibly based on an increased formation rate of the formate ester intermediate by the copper chromite catalyst. The two catalysts appeared to have similar reverse water-gas shift activity, as the concentration of water did not change when the relative amounts of Cu/ZnO and copper chromite were varied.

Structural changes in the catalyst during alcohol-promoted methanol synthesis were found by the means of XRD and SEM-EDS investigations. EDS elemental analysis showed that segregation of copper and zinc oxide had taken place, and both XRD analysis and SEM imaging provided evidence that crystallization of zinc oxide occurred. Such phenomena has previously been identified as cause of catalyst deactivation due to the loss of reactive Cu-ZnO interfaces [55]. However, comprehensive catalyst stability tests were not performed in the current study, and thus the effect of the observed changes on catalytic activity cannot be determined conclusively. It is clear that stability tests at different reaction temperatures and, importantly, at different feed gas compositions are necessary to further characterize the alcohol-promoted methanol synthesis process.

Conflicts of interest

None.

Acknowledgements

The Authors are grateful for Finnish Academy of Science for “Micro- and millistructured reactors for catalytic oxidation reactions” MICATOX project funding, number: 269896. Funding provided by the Lappeenranta University of Technology Doctoral School is also gratefully acknowledged.

References

[1] R. Schlögl, The solar refinery, Chemical Energy Storage, Walter de Gruyter GmbH, Berlin/Boston, 2013, pp. 1–34.
[2] F. Schüth, Energy storage strategies, Chemical Enery Storage, Walter de Gruyter GmbH, Berlin/Boston, 2013, pp. 35–48.
[3] G. Olah, Beyond oil and gas: the methanol economy, Angew. Chem. Int. Ed. 44 (2005) 2636–2639, http://dx.doi.org/10.1002/anie.200462121.
[4] H. Offermanns, L. Plass, M. Bertau, From raw materials to methanol, chemicals, and fuels, Methanol: The Basic Chemical and Energy Feedstock of the Future, Springer-Verlag, Berlin Heidelberg, 2014, pp. 1–7, http://dx.doi.org/10.1007/978-3-642-39709-7.
[5] L. Reichelt, F. Schmidt, Methanol-to-gasoline process, Methanol: The Basic Chemical and Energy Feedstock of the Future, Springer-Verlag, Berlin Heidelberg, 2015, pp. 440–453, http://dx.doi.org/10.1007/978-3-642-39709-7.
[6] F. Schmidt, C. Pätzold, Methanol-to-olefins processes, Methanol: The Basic Chemical and Energy Feedstock of the Future, Springer-Verlag, Berlin Heidelberg, 2015, pp. 454–472, http://dx.doi.org/10.1007/978-3-642-39709-7.
[7] J. Ott, V. Gronemann, F. Pontzen, E. Fiedler, G. Grossmann, D.B. Kersebohm, G. Weiss, C. Witte, Methanol, Ullmann's Encyclopedia of Industrial Chemistry, Wiley-VCH Verlag GmbH & Co. KGaA, Weinheim, 2012, pp. 1–27, http://dx.doi.org/10.1002/14356007.
[8] S. Lee, Methanol synthesis from syngas, Handbook of Alternative Fuel Technology, Taylor & Francis Group, LLC, 2007, pp. 297–321.
[9] J. Skrzypek, M. Lachowska, M. Grzesik, J. Sloczynski, P. Nowak, Thermodynamics and kinetics of low pressure methanol synthesis, Chem. Eng. J. 58 (1995) 101–108, http://dx.doi.org/10.1016/0923-0467(94)02955-5.
[10] E. Kunkes, M. Behrens, Introduction to methanol synthesis and steam reforming, Chemical Energy Storage, Walter de Gruyter GmbH, Berlin, 2013, pp. 415–417.
[11] T. Holderbaum, J. Gmehling, PSRK: A group contribution equation of state based on UNIFAC, Fluid. Phase Equilib. 70 (1991) 251–265, http://dx.doi.org/10.1016/0378-3812(91)85038-V.
[12] V. Palekar, Alkali compounds and copper chromite as low-temperature slurry phase methanol catalysts, Appl. Catal. A 103 (no. 1) (1993) 105–122, http://dx.doi.org/10.1016/0926-860X(93)85177-Q.
[13] Y. Zhao, L. Bai, Y. Hu, B. Zhong, S. Peng, Catalytic performance of CuCr/CH_3ONa used for low temperature methanol synthesis in slurry phase, J. Nat. Gas Chem. 8 (no. 3) (1999) 181–187.
[14] W. Chu, T. Zhang, C. He, Y. Wu, Low-temperature methanol synthesis (LTMS) in liquid phase on novel copper-based catalysts, Catal. Lett. 79 (2002) 129–132, http://dx.doi.org/10.1023/A:1015384015528.
[15] M. Marchionna, L. Basini, A.L.M. Aragno, F. Ancillotti, Mechanistic studies on the homogeneous nickel-catalyzed low temperature methanol synthesis, J. Mol. Catal. 75 (no. 2) (1992) 147–151, http://dx.doi.org/10.1016/0304-5102(92)80116-X.
[16] E. Lee, K. Aika, Low-temperature methanol synthesis in liquid-phase with a Raney nickel–alkoxide system: effect of Raney nickel pretreatment and reaction conditions, J. Mol. Catal. A: Chem. 141 (1999) 241–248, http://dx.doi.org/10.1016/S1381-1169(98)00267-2.
[17] S. Ohyama, Low-temperature methanol synthesis in catalytic systems composed of nickel compounds and alkali alkoxides in liquid phases, Appl. Catal. A 180 (1999) 217–225, http://dx.doi.org/10.1016/S0926-860X(98)00338-X.
[18] V. Palekar, H. Jung, J. Tierney, I. Wender, Slurry phase synthesis of methanol with a potassium methoxide/copper chromite catalytic system, Appl. Catal. A 102 (no. 1) (1993) 13–34, http://dx.doi.org/10.1016/0926-860X(93)85152-F.
[19] R. Sapienza, W. Slegeir, T. O'Hare, D. Mahajn, "Low temperature catalysts for methanol production". United States of America Patent US4614749A, 30 September 1986.
[20] S. Lee, A. Sardesai, Liquid phase methanol and dimethyl ether synthesis from syngas, Top. Catal. 32 (2005) 197–207, http://dx.doi.org/10.1007/s11244-005-2891-8.
[21] G. Chinchen, P. Denny, D. Parker, M. Spencer, D. Whan, Mechanism of methanol synthesis from CO_2/CO/H_2 mixtures over copper/zinc oxide/alumina catalysts: use of 14C-labelled reactants, Appl. Catal. 30 (no. 2) (1987) 333–338, http://dx.doi.org/10.1016/S0166-9834(00)84123-8.
[22] G. Olah, A. Goeppert, G. Surya Prakash, Chemical recycling of carbon dioxide to methanol and dimethyl ether: from greenhouse gas to renewable, environmentally carbon neutral fuels and synthetic hydrocarbons, J. Org. Chem. 74 (2009) 487–498, http://dx.doi.org/10.1021/jo801260f.
[23] O. Joo, K. Jung, I. Moon, A. Rozovskii, G. Lin, S. Han, S. Uhm, Carbon dioxide hydrogenation to form methanol via a reverse-water-gas-shift reaction (the CAMERE process), Ind. Eng. Chem. Res. 38 (1999) 1808–1812, http://dx.doi.org/10.1021/ie9806848.
[24] J. Tremblay, CO_2 as feedstock, Chem. Eng. News 86 (2008) 13.
[25] Carbon Recycling International, World's Largest CO_2 Methanol Plant, [Accessed 16 August 2017]. Available: (2017) http://carbonrecycling.is/george-olah/.
[26] L. Fan, Y. Sakaiya, K. Fujimoto, Low-temperature methanol synthesis from carbon dioxide and hydrogen via formic ester, Appl. Catal. A 180 (1999) L11–L13, http://dx.doi.org/10.1016/S0926-860X(98)00345-7.
[27] B. Xu, R. Yang, F. Meng, P. Reubroucharoen, T. Vitidsant, Y. Zhang, Y. Yoneyama, N. Tsubaki, A new method of low temperature methanol synthesis, Catal. Surv. Asia 13 (2009) 147–163, http://dx.doi.org/10.1007/s10563-009-9075-7.
[28] R. Yang, Y. Fu, Y. Zhang, N. Tsubaki, In situ DRIFT study of low-temperature methanol synthesis mechanism on Cu/ZnO catalysts from CO_2-containing syngas using ethanol promoter, J. Catal. 228 (no. 1) (2004) 23–35, http://dx.doi.org/10.1016/j.jcat.2004.08.017.
[29] R. Yang, Y. Zhang, N. Tsubaki, Dual catalysis mechanism of alcohol solvent and Cu catalyst for a new methanol synthesis method, Catal. Commun. 6 (no. 4) (2005) 275–279, http://dx.doi.org/10.1016/j.catcom.2005.01.008.
[30] N. Tsubaki, M. Ito, K. Fujimoto, A new method of low-temperature methanol synthesis, J. Catal. 197 (2001) 224–227, http://dx.doi.org/10.1006/jcat.2000.3077.
[31] J. Zeng, K. Fujimoto, N. Tsubaki, A new low-temperature synthesis route of methanol: catalytic effect of the alcoholic solvent, Energy Fuels 16 (2002) 83–86, http://dx.doi.org/10.1021/ef0100395.
[32] P. Reubroycharoen, T. Yamagami, T. Vitidsant, Y. Yoneyama, M. Ito, N. Tsubaki, Continuous low-temperature methanol synthesis from syngas using alcohol promoters, Energy Fuels 17 (2003) 817–823, http://dx.doi.org/10.1021/ef020240v.
[33] C. Huff, M. Sanford, Cascade catalysis for the homogeneous hydrogenation of CO_2 to methanol, J. Am. Chem. Soc. 133 (2011) 18122–18125, http://dx.doi.org/10.1021/ja208760j.
[34] Y. Chen, S. Choi, L. Thompson, Low-temperature CO_2 hydrogenation to liquid products via a heterogeneous cascade catalytic system, ACS Catal. 5 (2015) 1717–1725, http://dx.doi.org/10.1021/cs501656x.
[35] T. Turek, D. Trimm, The catalytic hydrogenolysis of esters to alcohols, Catal. Rev.: Sci. Eng. 36 (1994) 645–683, http://dx.doi.org/10.1080/01614949408013931.
[36] M. Sahibzada, I.S. Metcalfe, D. Chadwick, Methanol synthesis from CO/CO_2/H_2 over Cu/ZnO/Al2O3 at differential and finite conversions, J. Catal. 174 (1998) 111–118, http://dx.doi.org/10.1006/jcat.1998.1964.
[37] O. Martin, J. Pérez-Ramírez, New and revisited insights into the promotion of methanol synthesis catalysts by CO_2, Catal. Sci. Technol. 3 (2013) 3343–3352, http://dx.doi.org/10.1039/C3CY00573A.
[38] R. Struis, S. Stucki, M. Wiedorn, A membrane reactor for methanol synthesis, J. Membr. Sci. 113 (1996) 93–100, http://dx.doi.org/10.1016/0376-7388(95)00222-7.
[39] F. Gallucci, L. Paturzo, A. Basile, An experimental study of CO_2 hydrogenation into methanol involving a zeolite membrane reactor, Chem. Eng. Process. 43 (2004) 1029–1036, http://dx.doi.org/10.1016/j.cep.2003.10.005.
[40] J. van Bennekom, R. Venderbosch, J. Winkelman, E. Wilbers, D. Assink, K. Lemmens, H. Heeres, Methanol synthesis beyond chemical equilibrium, Chem. Eng. Sci. 87 (2013) 204–208, http://dx.doi.org/10.1016/j.ces.2012.10.013.
[41] M. Bos And, D. Brilman, A novel condensation reactor for efficient CO2 to methanol conversion for storage of renewable electric energy, Chem. Eng. J. 278 (2015), http://dx.doi.org/10.1016/j.cej.2014.10.059 pp. 572–532.
[42] M. Malone, M. Doherty, Reactive distillation, Ind. Eng. Chem. Res. 39 (2000) 3953–3957, http://dx.doi.org/10.1021/ie000633m.
[43] J. Allison, H. Wright, T. Harkins, D. Jack, "Use of catalytic distillation reactor for methanol synthesis". United States of America Patent US 6,723, 886 B2, 20 April 2004.
[44] S. Srinivas, R. Malik, S. Mahajani, Feasibility of reactive distillation for Fischer–Tropsch synthesis, Ind. Eng. Chem. Res. 47 (2008) 889–899, http://dx.doi.org/10.1021/ie071094p.
[45] M. Bayat, Z. Dehghani, M. Hamidi, M. Rahimpour, Methanol synthesis via sorption-enhanced reaction process: modeling and multi-objective optimization, J. Taiwan Inst. Chem. Eng. 45 (no. 2) (2014) 481–494, http://dx.doi.org/10.1016/j.jtice.2013.06.013.
[46] I. Illiuta, M. Illiuta, F. Larachi, Sorption-enhanced dimethyl ether synthesis—Multiscale reactor modeling, Chem. Eng. Sci. 66 (no. 10) (2011) 2241–2251, http://dx.doi.org/10.1016/j.ces.2011.02.047.
[47] J. Keuler, L. Lorenzen, S. Miachon, The dehydrogenation of 2-butanol over copper-based catalysts: optimising catalyst composition and determining kinetic parameters, Appl. Catal. A 218 (2001) 171–180, http://dx.doi.org/10.1016/S0926-860X(01)00639-1.
[48] S. Mostafa, J. Croy, H. Heinrich, B. Roldan Cuenya, Catalytic decomposition of alcohols over size-selected Pt nanoparticles supported on ZrO_2: A study of activity, selectivity, and stability, Appl. Catal., A 366 (2009) 353–362, http://dx.doi.org/10.1016/j.apcata.2009.07.028.
[49] R. Yang, X. Yu, Y. Zhang, W. Li, N. Tsubaki, A new method of low-temperature methanol synthesis on Cu/ZnO/Al_2O_3 catalysts from CO/CO_2/H_2, Fuel 87 (2008) 443–450, http://dx.doi.org/10.1016/j.fuel.2007.06.020.
[50] N. Tsubaki, J. Zeng, Y. Yoneyama, K. Fujimoto, Continuous synthesis process of methanol at low temperature from syngas using alcohol promoters, Catal. Commun. 2 (2001) 213–217, http://dx.doi.org/10.1016/S1566-7367(01)00039-5.
[51] W. Teo, D. Ruthven, Adsorption of water from aqueous ethanol using 3-Å molecular sieves, Ind. Eng: Chem. Process. Des. Dev. 25 (no. 1) (1986) 17–21, http://dx.doi.org/10.1021/i200032a003.
[52] T. Kandemir, F. Girgsdies, T. Hansen, K. Liss, I. Kasatkin, E. Kunkes, G. Wowsnick, N. Jacobsen, R. Sclögl, M. Behrens, In situ study of catalytic processes: neutron diffraction of a methanol synthesis catalyst at industrially relevant pressure, Angew. Chem. Int. Ed. 52 (2013) 5166–5170.
[53] J. Sloczynski, R. Grabowski, A. Kozłowska, P.K. Olszewski, J. Stoch, Reduction kinetics of CuO in CuO/ZnO/ZrO_2 systems, Phys. Chem. Chem. Phys. 5 (2003) 4631–4640, http://dx.doi.org/10.1039/b306132a.
[54] J. Grunwaldt, A. Molenbroek, N. Topsøe, H. Topsøe, B. Clausen, In situ investigations of structural changes in Cu/ZnO catalysts, J. Catal. 194 (2000) 452–460, http://dx.doi.org/10.1006/jcat.2000.2930.
[55] P. Hansen, J. Wagner, S. Helveg, J. Rostrup-Nielsen, B. Clausen, H. Topsøe, Atom-resolved imaging of dynamic shape changes in supported copper nanocrystals, Science 295 (2002) 2053–2055, http://dx.doi.org/10.1126/science.1069325.
[56] T. Lunkenbein, F. Girgsdies, T. Kandemir, N. Thomas, M. Behrens, R. Schlögl, E. Frei, Bridging the time Gap: a copper/zinc oxide/aluminum oxide catalyst for methanol synthesis studied under industrially relevant conditions and time scales,

Angew. Chem. 128 (2016) 12900–12904, http://dx.doi.org/10.1002/anie.201603368.
[57] Y. Jeong, I. Kim, J. Kang, H. Jeong, J. Park, J. Park, J. Jung, Alcohol-assisted low temperature methanol synthesis from syngas over Cu/ZnO catalysts: effect of pH value in the co-precipitation step, J. Mol. Catal. A: Chem. 400 (2015) 132–138, http://dx.doi.org/10.1016/j.molcata.2015.01.008.
[58] F. Arena, G. Mezzatesta, G. Zafarana, G. Trunfio, F. Frusteri, L. Spadaro, Effects of oxide carriers on surface functionality and process performance of the Cu–ZnO system in the synthesis of methanol via CO_2 hydrogenation, J. Catal. 300 (2013) 141–151, http://dx.doi.org/10.1016/j.jcat.2012.12.019.

Publication IV

H. Nieminen, A. Laari and T. Koiranen
CO_2 Hydrogenation to Methanol by a Liquid-Phase Process with Alcoholic Solvents: A Techno-Economic Analysis

Reprinted with permission from
Processes
Vol. 7, 405, 2019

processes

MDPI

Article

CO_2 Hydrogenation to Methanol by a Liquid-Phase Process with Alcoholic Solvents: A Techno-Economic Analysis

Harri Nieminen *, Arto Laari and Tuomas Koiranen

Laboratory of Process Systems Engineering, Lappeenranta-Lahti University of Technology, P.O. Box 20 FI-53851 Lappeenranta, Finland

* Correspondence: harri.nieminen@lut.fi; Tel.: +358-40-7451800

Received: 31 May 2019; Accepted: 24 June 2019; Published: 1 July 2019

Abstract: Synthesis of methanol from recirculated CO_2 and H_2 produced by water electrolysis allows sustainable production of fuels and chemical storage of energy. Production of renewable methanol has, however, not achieved commercial breakthrough, and novel methods to improve economic feasibility are needed. One possibility is to alter the reaction route to methanol using catalytic alcoholic solvents, which makes the process possible at lower reaction temperatures. To estimate the techno-economic potential of this approach, the feasibilities of the conventional gas-phase process and an alternative liquid-phase process employing 2-butanol or 1-butanol solvents were compared by means of flowsheet modelling and economic analysis. As a result, it was found that despite improved methanol yield, the presence of solvent adds complexity to the process and increases separation costs due to the high volatility of the alcohols and formation of azeotropes. Hydrogen, produced from wind electricity, was the major cost in all processes. The higher cost of the present, non-optimized liquid-phase process is largely explained by the heat required in separation. If this heat could be provided by heat integration, the resulting production costs approach the costs of the gas-phase process. It is concluded that the novel reaction route provides promising possibilities, but new breakthroughs in process synthesis, integration, optimization, and catalysis are needed before the alcoholic solvent approach surpasses the traditional gas-phase process.

Keywords: CO_2 hydrogenation; methanol synthesis; liquid-phase process; alcohol promoted; process simulation; techno-economic analysis

1. Introduction

The synthesis of liquid fuels from hydrogen using captured CO_2 as the carbon source would allow sustainable fuel production with the potential to reduce CO_2 emissions in the energy and transportation sectors [1], while simultaneously providing an option for the chemical storage of intermittent renewable electricity [2]. Such an approach could potentially make a significant contribution to decarbonization of the energy system [3]. Methanol provides an example of such a liquid energy carrier [4].

Methanol is both an important industrial chemical and a useful multi-purpose fuel [5]. It can also be readily converted into products such as gasoline in the methanol-to-gasoline process (MTG) [6] or olefins in the methanol-to-olefins process (MTO) [7]. At present, most methanol comes from the catalytic conversion of synthesis gas (syngas) that is usually generated by steam reforming of natural gas [8]. The syngas, a mixture of hydrogen, CO, and CO_2, is converted into methanol on copper and zinc oxide (Cu/ZnO)-based catalysts at temperatures of 200–300 °C and pressures of 50–100 bar. The methanol synthesis process can be described by three equilibrium reactions:

$$CO_2 + 3H_2 \rightleftharpoons CH_3OH + H_2O \qquad \Delta H^0 = -49.8 \text{ kJ/mol} \tag{1}$$

$$CO_2 + 2H_2 \rightleftharpoons CH_3OH \qquad \Delta H^0 = -91.0 \text{ kJ/mol} \tag{2}$$

$$CO + H_2O \rightleftharpoons CO_2 + H_2 \qquad \Delta H^0 = -41.2 \text{ kJ/mol} \tag{3}$$

Equations (1) and (2) represent the exothermic hydrogenation of CO_2 and CO to methanol, and Equation (3) represents the water-gas shift (WGS) reaction that is activated by the copper-based methanol synthesis catalysts [8]. As Reactions (1) and (2) are exothermic and result in a reduction of molar volume, methanol synthesis is favored at low temperatures and high pressures. However, sufficiently fast reaction kinetics requires temperatures above 200 °C, and methanol conversion is thus limited by the thermodynamic equilibrium.

Alternative to syngas, methanol can be produced by directly hydrogenating pure CO_2 with H_2 with high selectivity on conventional Cu/ZnO-based catalysts. However, the reaction rates are lower than with syngas feeds [9]. The equilibrium conversions are also lower compared to CO hydrogenation [10]. In addition to the thermodynamic limitation, methanol synthesis from pure CO_2 is complicated because of the increased water formation. In the absence of CO, water is produced both as the by-product of CO_2 hydrogenation (Equation (1)) and by the reverse-water gas shift reaction (reverse of Equation (3)). The increased formation of water leads to kinetic inhibition [11] and accelerated deactivation [12] of the Cu/ZnO catalysts.

The economic feasibility of CO_2 hydrogenation to methanol has been explored in a number of studies. While some studies paid close attention to the design and modelling of the methanol synthesis process [13–16], others focused on the electrolysis technology [17], electricity sources [18,19], or grid-scale implementation in a future renewable-based energy system [20]. Some studies have considered sustainability and environmental metrics in more detail [21,22]. Comparisons of methanol against other alternative energy carrier compounds have also been made [23]. Concerning the economics of the process, however, these studies draw significantly different conclusions. For example, Mignard et al. [13] and Anicic et al. [15] found the methanol production costs from CO_2 to be potentially competitive with fossil-based methanol production. In contrast, Pérez-Fortes [16] and Tremel et al. [23] found the production costs to be substantially higher than current methanol market prices. The overall costs have generally been found to be dominated by the hydrogen production costs, which consist of the electrolyzer capital costs and the cost of electricity.

There have been attempts to lower methanol processing costs by replacing the conventional gas-phase process with alternative liquid-phase processes. In the LPMeOH (liquid-phase methanol) process, the reaction is carried out in inert hydrocarbon solvent, allowing effective heat control of the exothermic reaction [24]. A demonstration-scale process has shown stable performance in conversion of coal-derived syngas with varying composition. Alternatively, methanol synthesis in co-catalytic alcoholic solvents has also been presented [25,26]. In the alcoholic solvent, methanol synthesis proceeds by an altered reaction mechanism via the formate ester of the alcohol, allowing lowered reaction temperatures. The lower temperature in turn allows higher equilibrium conversion in methanol synthesis.

The kinetics of the alcohol-promoted methanol synthesis process has been widely studied at the laboratory scale [25,26]. However, the techno-economic potential of this novel process has not been thoroughly examined. The aim of the present study is to assess the techno-economic feasibility of the liquid-phase alcohol-based process of CO_2 hydrogenation to methanol. For this purpose, the alcohol-promoted process with two alternative solvents is compared to the gas-phase process by means of process flowsheet simulation and subsequent economic analysis. 2-Butanol was selected as the primary solvent due to the good catalytic performance shown in experimental studies [27,28]. However, 1-butanol was also considered to assess whether a higher solvent boiling point would be favorable for the overall process efficiency and economics. It should be noted that published experimental details on the alcohol-promoted process are relatively limited, and the thermodynamics and kinetics have not been established in detail. Thus, the present work aims to provide a preliminary feasibility analysis rather than a rigorous optimization of the process alternatives. The key objectives

are to provide useful information for further development of the alcohol-promoted methanol synthesis process and to clarify its potential at the industrial scale.

2. Materials and Methods

Steady-state models of the processes for CO_2 hydrogenation to methanol were created in Aspen Plus (V9, AspenTech, Bedford, MA, USA). The processes studied included a gas-phase process and liquid-phase processes in alternative alcoholic solvents 2-butanol and 1-butanol. Mass and energy balances were generated and used to evaluate the technical performance of each process. The capital and operating costs of each process were estimated and compared and used to calculate the net present value (NPV) over the project lifetime. The boundaries of the present work are summarized in Figure 1. The design and costing of the CO_2 capture and water electrolysis units are outside the scope of the analysis, and the economic analysis was based on the referenced costs of CO_2 and hydrogen.

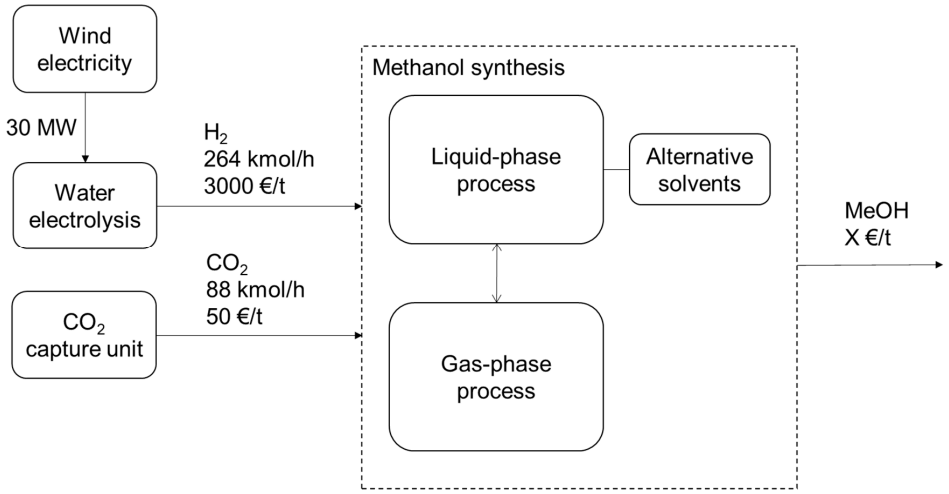

Figure 1. Scope and boundaries of the techno-economic analysis of CO_2 hydrogenation to methanol and the plant design capacity based on renewable electricity input.

2.1. Modelling Details

The capacity of the methanol synthesis unit is based on the amount of hydrogen available from the electrolysis unit powered by wind electricity at a 30-MW capacity. This capacity was selected as being representative of current wind energy projects in Finland [29].

The high-pressure sections (>10 bar) of each process were modelled in Aspen Plus using the RKSMHV2 (Redlich-Kwong-Soave with modified Huron-Vidal mixing rules) property method and the low-pressure sections using the NRTL-RK (Non-random two-liquid-Redlich-Kwong) property method. The property methods were selected following the guidelines given in Aspen Plus and taking into account the temperature, pressure, and polarity of the reaction system. All compressors were modelled with polytropic efficiency of 0.85 and mechanical efficiency of 0.95. Pumps were modelled at 0.85 pump efficiency and 0.95 driver efficiency. Heat exchangers were modelled by the shortcut method. The minimum temperature approach was set to 10 °C for liquid-liquid, 15 °C for gas-liquid, and 30 °C for gas-gas exchangers, and the pressure drop in each exchanger was set to 2% [30]. Distillation columns were modelled using the rigorous RADFRAC model in equilibrium mode.

The reactor in the gas-phase process was modelled using the RPLUG block model with an adiabatic setting. A relatively low inlet pressure of 50 bar was selected in order to facilitate comparison to the liquid-phase processes. The kinetics of the CO_2 hydrogenation to methanol and the water-gas shift reaction were estimated according to the model by Vanden Bussche and Froment [31] with readjusted

parameters by Mignard and Pritchard [32] and implemented in Aspen Plus as described by Van-Dal and Bouallou [14]. The reactor consisted of 1000 tubes with a length of 2 m and diameter of 0.05 m. The catalyst bed voidage was set at 0.4, particle density at 1775 kg/m^3, and particle diameter at 0.0055 m [14]. The pressure drop was calculated by the Ergun equation.

A bubble column reactor similar to the one utilized in the LPMeOH liquid-phase methanol synthesis process [24,33] was proposed for the liquid-phase process. The feed gases were bubbled through the solvent, and the product vapors together with unreacted gases were removed from the reactor. In the process with alcohol solvents, significant evaporation of the solvent took place, and the solvent vapors were removed together with the product vapors and gases. The solvent was then separated in downstream processing and returned to the reactor. Due to the lack of any detailed kinetic model for the alcohol promoted reaction route, the reactor in all liquid-phase processes was modelled with the RCSTR block based on the thermodynamic equilibrium by Gibbs energy minimization. In the model, CO_2 hydrogenation to methanol and the reverse-water gas shift were assumed as equilibrium reactions with the 0 °C approach to equilibrium. The reactor was operated isothermally at 180 °C and 50 bar, with reactions taking place in the liquid phase.

The sizing of the reactor for capital cost estimation was based on the specific methanol formation rate of 0.17 kg/(l h) reported by Tsubaki et al. for Cu/ZnO catalyst in ethanol solvent [34]. This rate was achieved in laboratory experiments under kinetics-controlled conditions with an approximate catalyst volume fraction of 1% in the slurry. In the present design, the same rate was assumed with a catalyst volume fraction of 10%, as limitations by mass and heat transfer are likely in a large-scale bubble column reactor. The same rate was also assumed regardless of the alcohol used as the solvent. The results of the reactor sizing are presented in Section 3.1.

2.2. Environmental Impact Analysis

The environmental impact of the alternative processes was assessed in terms of the CO_2 balance, electricity consumption, and water balance. In the calculation of the CO_2 balance, the amount of CO_2 fed to the process was subtracted from the sum of direct and indirect CO_2 emissions related to the process. These emissions consisted of CO_2 present in outlet streams, the CO_2 emitted in steam generation, and the indirect emissions of grid electricity. The specific electricity consumption (per t MeOH) of the processes was calculated, and the corresponding CO_2 emission was estimated from the carbon intensity of the Finnish electricity grid at the time of writing (170 g CO_2/kWh) [35]. For steam generation, emissions from both the combustion of externally-supplied fuel (natural gas) and the combustion of process waste streams were considered. Cooling water input and waste water output were considered in the water balance. The mass flow rate and composition of the waste water streams, consisting of water/alcohol mixtures, were assessed.

2.3. Cost Estimation

The following section describes the methods used and the assumptions made in the evaluation of the capital and operating costs of the CO_2 hydrogenation to methanol processes.

2.3.1. Capital Costs

The capital costs were estimated by the factorial method according to Towler and Sinnott [36]. The installed equipment costs for the estimation were obtained from the cost functions integrated into the Aspen Plus software. The installed costs in USD were converted to Euros at the exchange rate of 0.89 €/USD (2018). The installed costs were further corrected for construction from SS304 stainless steel by a material factor of 1.3 [36] and by a location factor of 1.043 corresponding to Western Europe [16]. The reactor's cost in the liquid-phase process was based on the sizing procedure described above. A 50% contingency was added on top of the cost of the pressure vessel in order to account for auxiliary equipment such as heat transfer equipment, slurry handling, and catalyst activation. The reactor cost

was identical in all the liquid-phase processes, as the effect of different solvents on the reaction rate and the resulting reactor volume was not considered.

The corrected installed equipment costs corresponded to the inside battery limits (ISBL) capital costs comprising the purchase and installation of all the main and auxiliary process equipment. The offsite (OSBL) capital costs, including the infrastructure and site improvements, were calculated as 25% of the ISBL capital costs. The plant would be preferably located on an existing fuel production site with readily-available infrastructure. Engineering costs were estimated as 20% of the sum of the ISBL and OSBL costs. Finally, a contingency of 30% of the sum of ISBL and OSBL costs was added to obtain the total fixed capital cost (TFCC). The working capital was estimated as 15% of the sum of the ISBL and OSBL costs. The factorial method of capital cost estimation is summarized in Table 1.

Table 1. Factorial method of capital cost estimation [16,36]. ISBL, inside battery limits; OSBL, offsite battery limits.

Item	Basis
ISBL capital cost	Installed equipment cost from the Aspen Plus Exchange rate of 0.89 €/USD Material factor 1.3 (304 stainless steel) Location factor 1.043 (Western Europe)
OSBL capital cost	25% of ISBL
Engineering cost	20% of ISBL and OSBL
Contingency	30% of ISBL and OSBL

To calculate its contribution to the total methanol production cost, the total fixed capital cost was annualized based on an assumed plant lifetime of 20 years and an interest rate of 5%.

2.3.2. Variable and Fixed Operating Costs

The overall cost of hydrogen production, including capital and operating costs of both the 30-MW wind farm and the alkaline electrolysis unit and the hydrogen storage costs, was assumed to be 3000 €/t of hydrogen. This value was based on a 2006 report by Levene et al. [37], which estimated that the production cost of wind-based hydrogen was in the range of $2.90–3.40/kg, including hydrogen storage. The production cost of wind electricity in the Finnish scenario has been recently estimated at 41.4 €/MWh [38]. This value is fairly consistent with the wind electricity cost ($0.038/kWh) used by Levene et al. [37]. The hydrogen cost is also consistent with Smolinka et al. [39], who estimated a value of 3.17 €/kg for large-scale alkaline electrolysis with intermittent operation (average capacity factor 35%). All the electricity available from the wind farm was utilized in the electrolysis unit. In order to maintain constant operation, the methanol synthesis unit was powered by grid electricity, available at an assumed market cost of 60 €/MWh [40]. Electricity consumption of the synthesis unit was calculated in the Aspen Plus process models.

The cost of CO_2 consisted of the capital and operational costs of an amine absorption unit. A cost of 50 €/t was assumed based on the International Energy Agency report [41]. If the CO_2 capture unit is located at a distance from the electrolysis and synthesis units, CO_2 transportation cost should also be included. However, this was not considered as the transport cost was small compared to the CO_2 capture costs [42].

The cost of steam was calculated based on a fuel (natural gas) cost of 30 €/MWh [43] and boiler efficiency of 80%, including heat losses. The fuel cost was calculated for the generation of medium-pressure (MP) steam at 20 bar (saturation temperature 212 °C). The overall cost was corrected by a factor of 1.3 taking non-fuel costs into account [44]. As a result, a cost of 35 €/t was obtained for the MP steam, and an identical cost was assumed for the low-pressure (LP) steam at 6 bar (saturation temperature 159 °C). Shaft work or condensate credits were not considered. In process modelling, MP and LP steam were included as utilities in the Aspen Plus model for calculation of the steam

consumption rate. Full condensation of steam in exchangers was assumed, and the outlet temperatures of MP and LP steam were set at 211 °C and 158 °C, respectively.

Steam generation by waste heat available from the combustion of process waste and purge streams was also considered. Both gas/vapor and liquid streams suitable for combustion were included in waste heat generation. Lower heating values of 10.1 MJ/kg for CO, 121 MJ/kg for H_2, 19.9 MJ/kg for methanol, and 34.4 MJ/kg for both 2-butanol and 1-butanol were used in the calculation of the heat produced [45]. A boiler efficiency of 80% was assumed for the waste heat boilers. The steam generated by the waste heat was utilized in the processes by subtraction of the amount of steam generated from the process MP steam consumption. In cases where the process produced a net heat output, the steam generated was considered a by-product with a selling price of 35 €/t.

The consumption rate of cooling water was also calculated in the Aspen Plus process models. The cost of cooling water was 0.26 €/m^3 [42], with an inlet temperature of 20 °C and outlet temperature of 25 °C. The cost of waste water was 0.32 €/m^3 [42] regardless of the composition of the waste water streams. Consumables included the methanol synthesis catalyst (assumed cost of 95 €/kg [16] and lifetime of 4 years) and the solvent make-up. The amount of catalyst used in the gas-phase process (3.49 t) was calculated based on the volume of the reactor tubes (1000 tubes, length 2 m, diameter 0.05 m), catalyst density (1775 kg/m^3 [14]), and bed porosity (0.5). Assuming a 4-year catalyst lifetime, 0.87 t of the catalyst needs to be replaced each year, giving a per year cost of approximately 83,000 €, which was not discounted. The amount and cost of catalyst used in the liquid-phase methanol synthesis processes was calculated by the reactor sizing procedure described in Section 2.1. The cost of make-up solvent was assumed to be 500 €/t in the liquid-phase processes, regardless of the alcohol used. A summary of the variable costs considered is given in Table 2.

Table 2. Variable costs considered in the analysis. MP, medium-pressure; LP, low-pressure.

Item	Cost and Details
Hydrogen	3000 €/t, based on alkaline electrolysis powered by 30 MW of wind electricity (cost includes electricity production and hydrogen storage) [37,39]
Grid electricity	60 €/MWh [40]
CO_2	50 €/t [41]
Steam	35 €/t for MP (20 bar) and LP (6 bar) steam, based on natural gas cost of 30 €/MWh [43]
Cooling water	0.26 €/m^3 [42]
Waste water	0.32 €/m^3 [42]
Catalyst	95.24 €/kg [16], assumed lifetime 4 years
Solvent make-up	500 €/t for all alcohols

Fixed operating costs were calculated according to the factorial method from Towler and Sinnott [46]. A labor requirement of 4 shift positions with 4 operators per position with a salary of 40,000 €/a was assumed. Supervision was estimated as 25% of labor cost. Labor overheads were assumed as 45% of the sum of labor and supervision. Maintenance costs were assumed as 3% of the ISBL capital cost. Plant and company overheads constituted 65% of the labor and maintenance costs, while taxes and insurance constituted 2% of the total fixed capital cost.

2.3.3. Revenues

A methanol price of 400 €/t [47] was assumed in the economic analysis. Additional revenues from the sales of oxygen by-product generated in the electrolysis unit were also considered. A conservative price of 70 €/t [15,18] was assumed for oxygen, and the costs of oxygen compression and liquefaction were omitted.

2.4. Economic Analysis

The net present value (NPV) of each process was calculated based on the following assumptions. Plant lifetime was set at 20 years. Thirty percent, 60%, and 10% of the capital costs were distributed to Years 1, 2, and 3, respectively. Thirty percent and 70% of revenues and operating costs were considered during Year 3 and Year 4, and 100% thereafter. One hundred percent of working capital was deployed during the first year. A discount rate of 8% was assumed, and taxes and depreciation were not considered [16].

2.5. Process Descriptions

The overall process discussed here consisted of the electrolysis unit powered by wind electricity and the methanol synthesis unit. Options for the methanol synthesis unit included the gas-phase synthesis process and the liquid-phase synthesis process with alternative solvents (2-butanol and 1-butanol).

2.5.1. Electrolysis and Wind Electricity

The present analysis considered wind electricity in the Finnish scenario [38] for the electrolysis process. The plant consisting of the electrolysis unit, the methanol synthesis unit, and possibly the CO_2 capture unit was assumed to be located near a land-based wind turbine farm. Transportation of CO_2 was not ruled out, as this location assumption might prove unrealistic. Potential sources of CO_2 would consist of fossil power plants and various industrial sources (especially bioprocessing plants in the Finnish scenario).

Based on available data on current and upcoming wind energy projects in Finland [29], the electricity generation capacity of the wind farm was set at 30 MW. Due to the significant temporal variation inherent in wind-based electricity generation, the full capacity was not constantly available for the electrolysis unit. However, a constant supply of hydrogen to the methanol synthesis unit is required to allow steady-state operation at design capacity. Thus, a sufficient capacity for hydrogen storage for the methanol synthesis unit should be assumed.

Hydrogen was generated by pressurized alkaline electrolysis operating at 30 bar. The capacity of the electrolysis unit was 30 MW, and the system efficiency was 70% [39]. Based on the heat of formation of water (285.8 MJ/kmol), 264.5 kmol/h of water was split to form an equal amount of hydrogen in moles. At the 30-bar operating pressure, this corresponds to 533.2 kg/h of hydrogen fed to the methanol synthesis unit.

2.5.2. Gas-Phase Methanol Synthesis

The flowsheet of the gas-phase methanol synthesis process is presented in Figure 2. At the feed compression stage, hydrogen was compressed from 30.0 bar (outlet pressure of the alkaline electrolyzer) to 51 bar in a single stage (COMP5), and CO_2 was compressed from 1.0 bar–51.0 bar in four stages (COMP1–4) with intercooling (COOLER1–3). The pressure ratio of Stages 1–3 equaled 3.0, while the final stage was specified to the outlet pressure of 51.0 bar. The molar ratio of the fresh feed was three moles hydrogen per one mole CO_2, with mass flows of 533.2 and 3881.7 kg/h, respectively. The feed gases were mixed with the recycle gas (MIX1), and the mixed feed was preheated to 215.0 °C by heat exchange with the reactor outlet in the heat exchanger HX1. The feed was then converted in the adiabatic reactor.

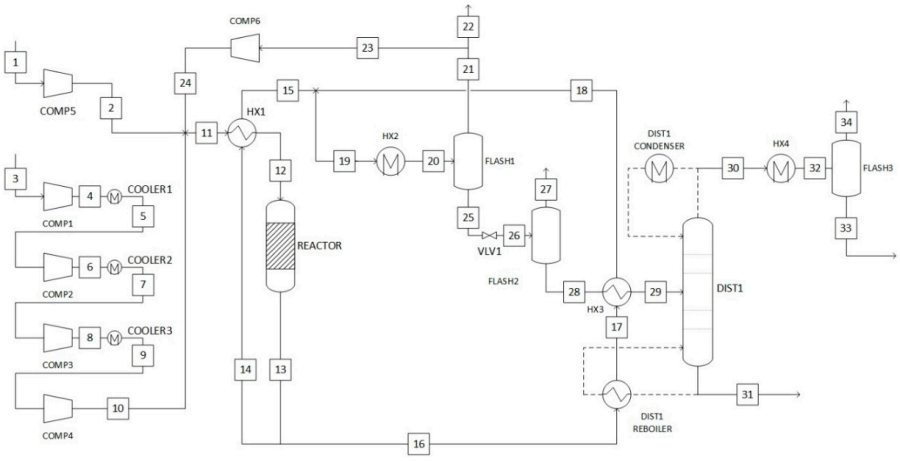

Figure 2. Flowsheet of the gas-phase CO_2 hydrogenation to methanol process. The corresponding stream table is presented in Table S1 (Supplementary Material). Inlet and outlet streams: 1. Hydrogen inlet, 3. CO_2 inlet, 22. purge from gas recycle, 27. gas purge from second flash tank, 31. waste water outlet, 33. methanol product outlet, 34. gas purge from final flash tank. COMP, compression stage; HX, heat exchanger; DIST, distillation column.

The temperature at the reactor outlet was 274.4 °C. The outlet gas was split into two fractions in SPLIT1, with 68% of the gas (Stream 14) used to preheat the feed in HX1. The remaining 32% was heat integrated with the reboiler of the distillation column and preheated the column feed (HX3). The two streams were recombined (MIX2) and cooled to 35.0 °C in the cooler HX2. The unreacted gases were separated in the flash drum (FLASH1). For the recycled gas, 1% was purged in order to avoid accumulation of by-products and inert components [14]. Such components were however not included in the process model. The remaining recycled gas was recompressed to 51.0 bar in COMP6 and mixed with the fresh feed.

The liquid separated in FLASH1 consisted of methanol and water at a molar ratio of approximately one, together with a small fraction of dissolved gases. The pressure of this stream was reduced to 1.2 bar, and the majority of the dissolved gases were separated and purged in FLASH2. The liquid stream was heated to 81.0 °C in HX3 and fed to the distillation column (DIST1) operated at 1.2 bar. The column consisted of 30 ideal equilibrium stages, and the reflux ratio equaled 1.1. The top product, consisting mainly of methanol and dissolved CO_2, was cooled to 35.0 °C in HX4, and most of the CO_2 was separated in FLASH3. The final purity of the methanol product was 99.3 wt%. Water (99.0 wt%) was removed from the bottom of the distillation column.

2.5.3. Liquid-Phase Methanol Synthesis

The liquid-phase methanol synthesis process was based on the combination of a conventional Cu/ZnO catalyst and alcohol as a catalytic solvent. In the presence of the alcoholic solvent, the reaction proceeded through the formate ester of the corresponding alcohol as an intermediate [25]. This reaction mechanism allowed methanol synthesis at lower reaction temperatures compared to the gas-phase process.

The flowsheet of the liquid-phase methanol synthesis process using 1-butanol solvent is presented in Figure 3. The liquid-phase process was also modelled with 2-butanol using identical process design. In the following description, the stream conditions and compositions of the 1-butanol process are used as examples. The major differences between the two solvents were found in the design and performance of the separation stage, as summarized in Table 3 at the end of this section.

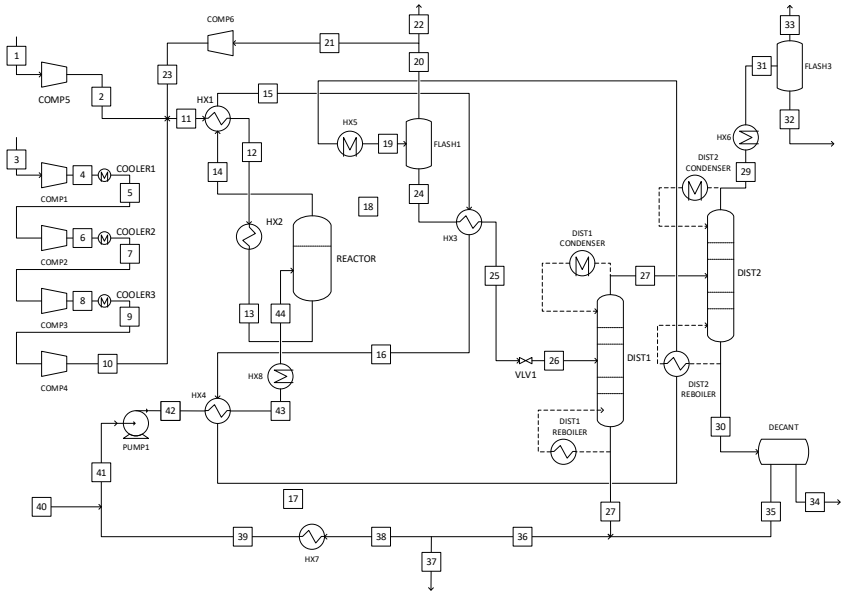

Figure 3. Flowsheet of the liquid-phase CO_2 hydrogenation to methanol process with 1-butanol solvent. The corresponding stream table is presented in Table S2. 1. Hydrogen inlet, 3. CO_2 inlet, 22. purge from gas recycle, 32. methanol product outlet, 33. gas purge from final flash tank. 34. waste water outlet, 37. purge from solvent recycle, 40. solvent make-up.

Table 3. Distillation specifications and performance in the alternative methanol synthesis processes.

	Gas-Phase	2-Butanol	1-Butanol
Distillation feed flow rate, kg/h	3660	26,641.1	14,650
Column #1			
Number of ideal stages	30	15	10
Reflux ratio (molar)	1.1	1.0	1.0
Reboiler duty, kW	940	7282	5445
Column #2			
Number of stages	-	50	30
Reflux ratio	-	6.5	4.0
Reboiler duty, kW	-	4210	2265
Methanol purity * (wt%)	99.3%	99.2%	99.2%

* Following FLASH3 (35 °C, 1 bar).

Identical to the gas-phase process, 533.2 kg/h of hydrogen and 3881.7 kg/h CO_2 were fed to the liquid-phase process. The hydrogen feed was compressed to 52.0 bar in a single stage (COMP5), and the CO_2 feed was compressed to 52.0 bar in four stages (COMP1–4) with intercooling (COOLER1–3). The pressure ratio of Stages 1–3 equaled 3.0, while the final stage was specified to the outlet pressure of 52.0 bar. The feed gases were mixed with the recycled gas (MIX1), and the mixed feed was preheated to 138.1 °C by heat exchange with the reactor vapor outlet (HX1). The feed was further heated to 180.0 °C in the heater HX2. The feed gas was fed to the isothermal bubble column reactor operated at

180.0 °C and 50.0 bar. Details on the design and modelling of the liquid-phase reactor are discussed in Section 2.1.

The unreacted gases together with product and solvent vapors were removed from the reactor, while the liquid level was maintained by the solvent recycled. The heat from the gas/vapor outlet (Stream 14) was used to preheat the reactor feed in HX1. The heat available in the outlet stream was utilized to pre-heat the distillation feed (HX3), to pre-heat the solvent recycle (HX4), and in the reboiler of the second distillation column (DIST2). The product stream was then further cooled to 35 °C in HX5, and the majority of the unreacted gases were then separated from the condensed solvent and products in FLASH1. In SPLIT1, 1% of the recycled gases was purged and the remainder recompressed to 52.0 bar (COMP6) and mixed with the fresh feed gases.

The condensed liquid stream leaving FLASH1 was pre-heated in HX3; the pressure was reduced to 1.4 bar, and the stream entered the first distillation column (DIST1) at 75.4 °C. Methanol and water were removed as the top product. A fraction of the solvent was also distilled due to the alcohol-water azeotrope. The majority of the solvent was removed from the bottom stage and recycled.

The vapor product from DIST1 was fed to the second distillation column (DIST2), operated at 1.2 bar. Methanol was removed from the top of the column, while water and the remaining solvent were removed from the bottom. The methanol stream was cooled to 35.0 °C in the exchanger HX6, and most of the dissolved CO_2 remaining was removed in FLASH3. The purity of the methanol product was 99.2% by weight. The mixture of water and solvent from the bottom stage was fed to a decanter at 95.8 °C and 1.2 bar. In the decanter, the heterogeneous alcohol-water azeotrope was split into a removed water-rich (89% by mass) waste stream and a solvent-rich (81% 1-butanol) recycled stream (2-butanol process: 90% water and 82% 2-butanol, respectively). The recycled gas was mixed with the solvent removed in DIST1, resulting in a final composition of 96 wt% 1-butanol and 4 wt% water in the solvent recycled. One percent of the solvent recycled was purged, and the stream was cooled in HX7 for vapor condensation. The recycled gas was then mixed with the solvent make-up, and the pressure of the mixed stream was then increased to the reactor pressure by the solvent pump (PUMP1). The solvent was pre-heated to 136.7 °C in HX4 and finally heated to 180 °C in HX8.

Details of the specifications and performance of the distillation columns in the gas-phase and liquid-phase processes are given in Table 3. The data allowed us to compare the simplicity of separating methanol from each product-solvent mixture. In the gas-phase process, only a single column with low energy input was required to separate methanol from the water by-product. In the liquid-phase processes, two columns were necessary to separate both methanol and water from the solvent. In 2-butanol, this separation was significantly capital and energy intensive due to the similar volatility of the components (2-butanol has a boiling point of approximately 99 °C). The separation was less costly with 1-butanol, which has a boiling point of 117.7 °C. The formation of azeotropes between water and the solvent was also a complicating factor in the separation processes. The azeotropic mixtures with water consisted of 40% of 2-butanol (at 87.2 °C) and 25% of 1-butanol (92.5 °C) on a molar basis [48].

The energy consumed in distillation could be reduced by more rigorous heat integration in the processes. In all of the processes, the heat from the hot reactor outlet was exchanged to preheat the distillation feed, based on the implementation of the gas-phase process by Van-Dal and Bouallou [14]. In the liquid-phase processes, alternative heat integration schemes could lead to energy savings, but this was not explored in detail in the present work.

3. Results and Discussion

The various methanol synthesis processes were compared in terms of the mass balances, energy and electricity consumption, and the overall methanol production cost. The performance of the reactor in the gas-phase and liquid-phase processes was also compared. Additional results with more details are included in the Supplementary Material, as referenced in the text.

3.1. Reactor Sizing and Performance

Figure 4 presents the temperature and composition profile of the adiabatic reactor in the gas-phase process. The composition is given in terms of the mole fractions of CO_2, CO, and methanol. The mole fraction of water over the reactor length was essentially identical to that of methanol. The reactions modelled here, i.e., CO_2 hydrogenation to methanol (Equation (1)) and the reverse-water gas shift (RWGS, Equation (3)), reached equilibrium after one meter of reactor length. Due to the low contribution of the reactor capital cost to the overall production cost (Section 3.4), this was considered satisfactory, and further reactor optimization was omitted. At this point, the peak temperature inside the reactor (274.5 °C) was reached, and 20.3% of the CO_2 entering the reactor was converted. Thus, a significant amount of unreacted gases was recycled, and the recycle ratio equaled 5.3 in the reactor loop. CO_2 was converted to methanol at a selectivity of 96.1%. The mole fraction of CO remained low throughout the reactor length, and the constant concentration of CO after approximately 0.5 m corresponded to the equilibrium level of the RWGS.

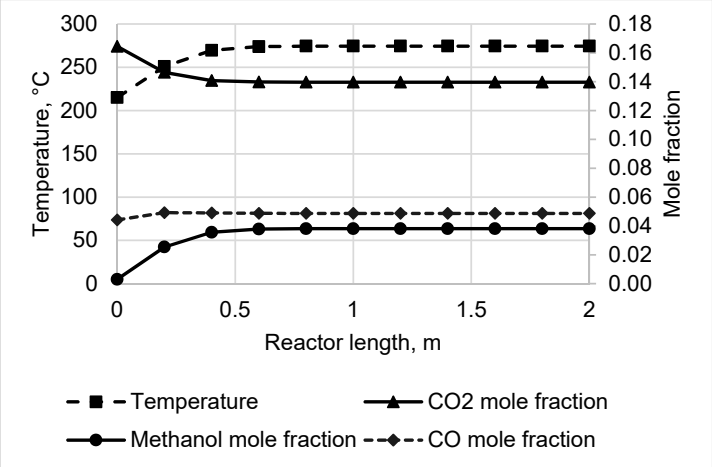

Figure 4. Reactor temperature and composition profile in the gas-phase CO_2 hydrogenation to methanol process. Adiabatic reactor, inlet temperature 215.0 °C, and pressure 52.0 bar.

The lack of a detailed kinetic model for the alcohol-promoted process prevented detailed reactor modelling in the liquid-phase processes. Therefore, the reactor was approximated as an ideal continually-stirred tank reactor (CSTR) with full equilibrium conversion of the CO_2 hydrogenation to methanol and RWGS reactions. This method gave a "best-case scenario" view of this process, as the reaction kinetics was ignored.

In the 1-butanol process, approximately 2.7 t/h of methanol was produced in the reactor based on the reactor mass balance. Based on the specific methanol formation rate of 0.17 kg/(l h), the slurry (liquid + catalyst) volume required was thus 15.8 m^3. At a 5% catalyst volume fraction, the volume of the catalyst was 0.8 m^3. At a catalyst density of 1775 kg/m^3 [14], the mass of the catalyst was 1.4 t. Assuming a 25 vol% provision for gas/vapor space, the total reactor volume was 17.8 m^3. To determine the aspect ratio, a superficial gas velocity of 0.1 m/s [49] was assumed, resulting in a reactor diameter of 1.7 m and a height of 8.8 m. The average residence time of the gas in the reactor was 67 s and the hourly space velocity per catalyst weight was 576.3 L/kg h and per slurry volume 51.1 L/h. The same reactor sizing was assumed for the 2-butanol process.

Table 4 presents the composition of the inlet and outlet streams to the reactor in the 1-butanol process. A similar distribution of reactants and products in the liquid and gas/vapor phases was found in other solvents. The gas-phase inlet consisted of the feed gas mixture, and the recycled and make-up

solvent constituted the liquid phase inlet. The gas/vapor outlet consisted of the product and solvent vapors together with unreacted gases.

Table 4. Composition of the gas/vapor and liquid phases in the reactor inlet and outlet streams of the liquid-phase process with 1-butanol solvent. Reaction conditions are 180.0 °C and 50.0 bar, and the reactor is modelled as a continually-stirred tank reactor (CSTR) with the full equilibrium approach of the CO_2 hydrogenation to methanol and the reverse-water gas shift reactions.

Reactor Inlet				**Reactor Outlet**	
Gas/Vapor Phase		**Liquid Phase**		**Gas/Vapor Phase**	
Component	**Flow, kmol/h**	**Component**	**Flow, kmol/h**	**Component**	**Flow, kmol/h**
CO_2	118.6	CO_2	0.0	CO_2	36.2
CO	0.8	CO	0.0	CO	0.8
Methanol	1.4	Methanol	0.4	Methanol	84.2
Hydrogen	934.9	Hydrogen	1.4	Hydrogen	689.0
Water	0.7	Water	23.1	Water	106.2
1-butanol	0.2	1-butanol	132.7	1-butanol	132.8
Total	1056.5	Total	157.6	Total	1049.3

The lower reaction temperature (180.0 °C) compared to the gas-phase process led to a relatively higher CO_2 conversion. The per-pass conversion was 81% with 1-butanol and 79% with 2-butanol as the solvent. The phase distribution of the reactants and the products appeared to have a favorable effect on the conversion, as the single-phase equilibrium conversion was in the region of 40% at the present reaction conditions [10]. The evaporation of methanol and water from the liquid phase seemed to drive the conversion of the reactants. The slightly different phase distribution due to the higher volatility of 2-butanol was also suggested to lead to the different conversion value in the 2-butanol and 1-butanol processes.

3.2. Mass and Energy Balances

Table 5 gives a summary of the mass balances of the alternative methanol synthesis processes. More detailed balances with the individual inlet and outlet streams can be found in Tables S4–S6 in the Supplementary Material. The overall methanol yield was calculated as the mass flow of methanol in the product stream divided by the stoichiometric methanol output based on the CO_2 and hydrogen inlet. The yield was decreased by losses of reactants or methanol from the process. In Table 5, the methanol yield is 81% in the gas-phase process, 82% in the 2-butanol process, and 88% in the 1-butanol process.

Table 5. Mass balance of the alternative methanol synthesis processes. Methanol yield is the ratio of the mass flow of methanol product to the mass flow corresponding to 100% yield based on the stoichiometric CO_2 and hydrogen inlets. Fractional solvent loss is calculated as the ratio of solvent flow removed from the process to the solvent flow (make-up + recycle) fed to the reactor.

Flow, kg/h	**Gas-Phase**	**2-Butanol**	**1-Butanol**
Hydrogen in	533	533	533
CO_2 in	3882	3882	3882
Methanol out	2275	2311	2474
Methanol losses	44	248	167
CO_2 losses	560	369	255
Hydrogen losses	89	51	35
CO_2 conversion per pass	20%	79%	81%
Methanol yield	81%	82%	88%
Solvent loss, kg/h	-	352	249
Fractional solvent loss	-	2%	3%

Losses of CO_2, hydrogen, and methanol are also seen in Table 5. Components were lost with the purge and waste streams removed from the processes. In the gas-phase process, these streams consisted of the purge from the gas recycle, the bottoms from the distillation column, and the purged gases from the separators FLASH2 and FLASH3 (see the flowsheet in Figure 2). The majority of the methanol loss occurred in the purge from FLASH2. Due to the large amount of unreacted CO_2 and the hydrogen present in the recycle stream, the loss of reactants with the purge was significantly higher compared to the liquid-phase processes, leading to the lower overall methanol yield.

In the liquid-phase processes, components were lost with the gas and solvent recycle purges, the water-rich stream from the decanter, and also the purge stream from FLASH3 (Figure 3). The purge from FLASH3 constituted most of the methanol and gas losses, while the solvent was mainly lost from the decanter. This loss is explained by the alcohol-water azeotrope. A significant amount was also lost with the liquid purge stream, which could only be minimized based on detailed information on the formation and accumulation of by-products. Overall, the fraction of solvent lost was 2% for 2-butanol and 3% for 1-butanol. However, the absolute amount of solvent lost was higher in the 2-butanol process, as a larger amount of solvent was circulated in order to maintain the liquid/gas volume ratio in the reactor.

The presence of a large quantity of solvent in the product streams significantly increased the distillation energy requirement in the liquid phase process, especially as a second column was required. For each process, the overall heat and electricity consumption per ton of methanol produced are presented in Table 6. It should be noted that the electricity required in the electrolysis unit was included in the cost of hydrogen, and hence was not included here. Electricity consumption in Table 6 only includes that used in compression of the gaseous feed and recycle streams and in pumping the recycled solvent in the liquid-phase processes. The waste heat generated by combustion of the process purge and waste streams was also included in the energy balance. The hot utility requirement corresponded to the amount of external heat required after integration of the waste heat.

Table 6. Thermal electrical energy consumption (in kWh per t of methanol produced) of the alternative CO_2 hydrogenation to methanol processes.

Energy, kWh/t MeOH	Gas-Phase	2-Butanol	1-Butanol
Hot utility	0	6668	3912
Cold utility	2960	15,313	9604
Heat integrated within process	5104	5376	4047
Waste heat generated	2697	4048	2366
Electricity	624	683	625

The gas-phase process did not require hot utility as the reaction heat was sufficient to supply all process heating. Due to the combustion of purge streams for waste heat, the process produced a net heat output of 2.7 MW. In contrast, the liquid-phase process required external heat due to the more energy-intensive separation stage. In addition, less heat was available from the reactor due to the energy consumed in solvent evaporation, which is a downside to the efficient heat control provided by the liquid. Due to the less energy-intensive distillation stage, the use of the less volatile solvent 1-butanol was found to improve the energy efficiency of the liquid-phase process compared to 2-butanol significantly. The net heating duty in the 1-butanol process was 41% and the cooling duty 37% lower compared to the 2-butanol process. The utilization of waste heat significantly reduced the amount of external hot utility required: waste heat provided 38% of the process heat in each of the liquid-phase processes.

The electricity consumption of the liquid-phase processes was slightly higher compared to the gas-phase process. The increased per-pass conversion in the liquid-phase processes led to lower flow rate of the gas recycle, resulting in a reduction in electricity consumption by the recycle compressor. These reductions were, however, offset by the requirement of the solvent recycle pump in the liquid

phase processes. Energy requirements of the individual process equipment can be found in Table S9 in the Supplementary Material.

3.3. Environmental Analysis

The CO_2 and water balances of the alternative processes are presented in Table 7. A negative CO_2 balance signifies that the amount of CO_2 consumed in methanol synthesis was higher than the sum of the direct and indirect CO_2 emissions of the process. The lowest net emissions (−3046 kg/h) were found with the gas-phase process, in which all process heat was supplied by the exothermic reaction and fuel combustion was not required. In the liquid-phase process, generation of process heat lead to significant CO_2 emissions. In the 1-butanol process, the net emission was −1239 kg/h, or 59% higher compared to the gas-phase process. In the 2-butanol process, the net emission was positive (216 kg/h), as the amount of CO_2 emitted in heat generation was significantly higher compared to the 1-butanol process. In each process, waste heat generation led to additional emissions. However, in the liquid-phase processes, these emissions were offset by the reduced amount of natural gas burned for process heating.

Table 7. CO_2 and water balance of the alternative CO_2 hydrogenation to methanol processes.

	Gas-Phase	2-Butanol	1-Butanol
CO_2 balance, kg/h			
Inlet streams	−3882	−3882	−3882
Outlet streams	560	369	255
Hot utility (natural gas)	0.0	2777	1837
Waste heat combustion	170	836	448
Electricity (grid)	106	116	106
Net emissions	−3046	216	−1239
Water balance			
Cooling water input, t/h	379	516	516
Solvent/water waste, kg/h	1371	1574	1644
Alcohol in waste, wt% *	1%	9%	9%

* Methanol in the gas-phase process, solvent in the liquid-phase processes.

Although large amounts of cooling water were required in the processes, the environmental impact of the cooling water input was not particularly significant, assuming that the used water (at 25 °C) can be released without treatment and that a sufficient amount of water is readily available. Waste water treatment was simplified by minimizing the amount of mixed water/alcohol waste and by minimizing the alcohol content in the waste stream. The gas-phase process appeared the most favorable in terms of waste water treatment as the amount of waste produced was the lowest and the alcohol content (methanol) was only 1.1%. The waste water flow rate and alcohol content were similar in both the 2-butanol and 1-butanol processes.

As grid electricity was assumed to be used in the methanol synthesis processes, the environmental impact of electricity consumption was dependent on the sources of electricity supporting the grid at the particular location and time. The electricity consumption of the processes is compared in Table 6, and discussed in Section 3.2. The electricity consumption did not significantly differ between the alternative processes. At the CO_2 intensity of 170 g CO_2/kWh, the corresponding CO_2 emissions were 106 kg/h, 116 kg/h, and 106 kg/h for the gas-phase, 1-butanol, and 2-butanol processes, respectively. These emissions were not significant for the overall CO_2 balance, as seen in Table 7.

3.4. Methanol Production Cost and Net Present Value

The overall methanol production cost consisted of the variable and fixed operating costs and the annualized capital investment. A comparison of the production costs of the different processes is presented in Figure 5, while a detailed overview of the capital and operating costs is given in

the Supplementary Material (Tables S10 and S11). The gas-phase process was found to be the most competitive with a methanol production cost of 963 €/t. The overall production costs were higher with the liquid-phase processes due to the energy-intensive separation stage and the added cost of solvent make-up. The cost of 1205 €/t with the 1-butanol process was 25% higher compared to the gas-phase process, while the cost of 1349 €/t with the 2-butanol process was 40% higher compared to the gas-phase process.

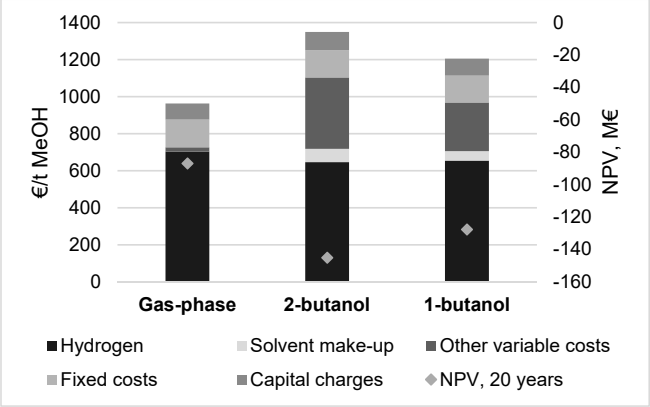

Figure 5. Methanol production cost and net present value (NPV) of the different CO_2 hydrogenation processes. Capital costs are annualized at an interest rate of 5% to obtain the annual capital charges. NPV is calculated assuming plant lifetime of 20 years and discount rate of 8%. Other variable costs: carbon dioxide, by-products and waste, and utilities.

The net present value (NPV) of each process over the assumed plant lifetime of 20 years is presented in Figure 5. The NPV was negative for all of the processes; thus, no process was financially feasible under the presented conditions and assumptions. In accordance with the lowest methanol production cost, the highest NPV (−87.0 M€) was found with the gas-phase process, whereas the NPV was −127.7 M€ for the 1-butanol process and −145 M€ for the 2-butanol process.

Figure 6 presents the contribution of individual variable cost components in the gas-phase and liquid phase processes. In all three processes, hydrogen was the main cost component, constituting 97%, 59%, and 68% of the variable costs, and 73%, 48%, and 54% of the total methanol production cost in the gas-phase, 2-butanol, and 1-butanol processes, respectively. In the gas-phase process, the cost of CO_2 was the second largest variable cost, while in the liquid-phase processes, the cost of utility steam was more significant due to the increased distillation energy requirement compared to the gas-phase process. The cost of heating in the 1-butanol process corresponded to 174 €/t MeOH, and if the heat requirement could be eliminated by process or site heat integration, the resulting methanol production cost would equal 1031 €/t. As the gas-phase process produced an output of heat that was available for steam generation, the variable costs were decreased by the steam credit. The steam credit also offset the electricity and cold utility costs of the process. In the 1-butanol process, the cost of solvent make-up constituted 5% of the variable costs and 4% of the overall cost. In the 2-butanol process, solvent make-up corresponded to 6% of the variable costs and 5% of the overall cost.

Compressors constituted the largest fraction of installed equipment costs, as seen in Figure 7. The total capital investment, calculated from the installed equipment costs by the factorial method, was lowest in the gas-phase process at 10.5 M€. The 2-butanol and 1-butanol processes required a capital investment of 12.9 M€ and 11.6 M€, respectively. The share of the separation section (flash vessels and distillation columns) was larger in the liquid-phase process compared to the gas-phase process. The higher capital costs of the 2-butanol process compared to the 1-butanol process were explained by the more costly distillation columns.

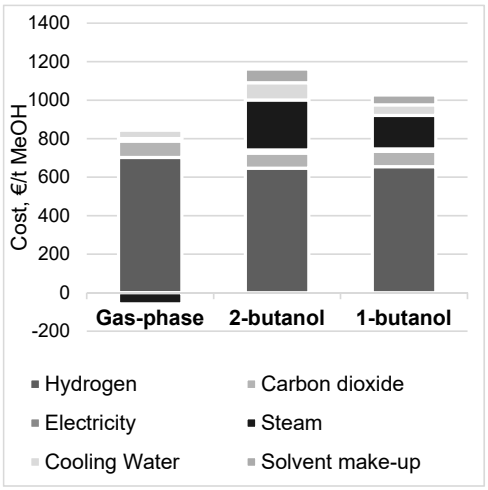

Figure 6. Distribution of the variable production costs in three CO_2 hydrogenation to methanol processes: the gas-phase process, the liquid-phase process with 2-butanol solvent, and the liquid-phase process with 1-butanol solvent.

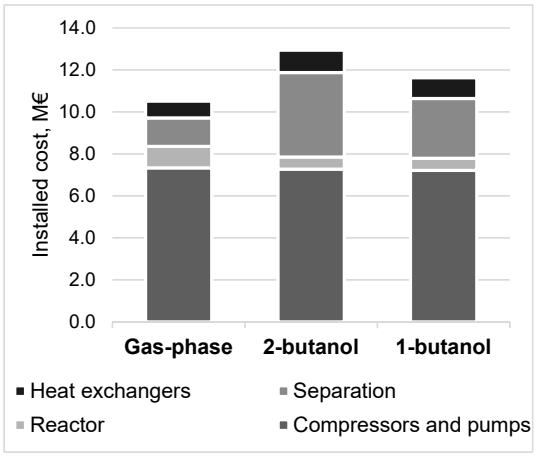

Figure 7. Installed equipment costs by type in three CO_2 hydrogenation to methanol processes: the gas-phase process, the liquid-phase process with 1-pentanol solvent, and the liquid-phase process with 1-pentanol solvent and solvent recovery by decantation. Separation included distillation, flash, and decanter vessels.

3.5. Sensitivity Analysis

A sensitivity analysis was performed in order to measure the effect of key variables on the economics of the various methanol synthesis processes. The sensitivity analysis was performed in terms of the methanol production cost, and NPV was not considered in the analysis. The cost of hydrogen, constituting a major fraction of the overall cost, was included in the sensitivity analysis. In addition, the effects of the costs of oxygen, CO_2, and the total capital investment were also analyzed. The gas-phase process and the 1-butanol process were selected for the sensitivity analysis. The cost of solvent was also included as a variable for the 1-butanol process. The results for the gas-phase process are shown in Figure 8, and those for the 1-butanol process are shown in Figure 9.

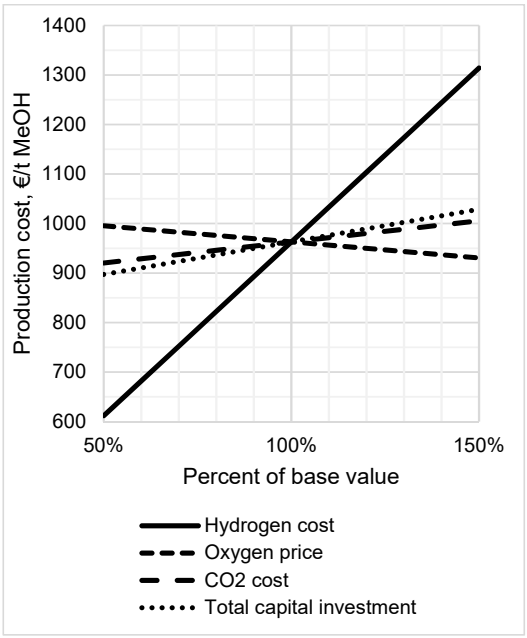

Figure 8. Sensitivity of methanol production cost to variations in selected parameters in the gas-phase methanol synthesis process. Base values: hydrogen cost 3000 €/t, oxygen price 70 €/t, CO_2 cost 50 €/t, total capital investment 17.9 M€.

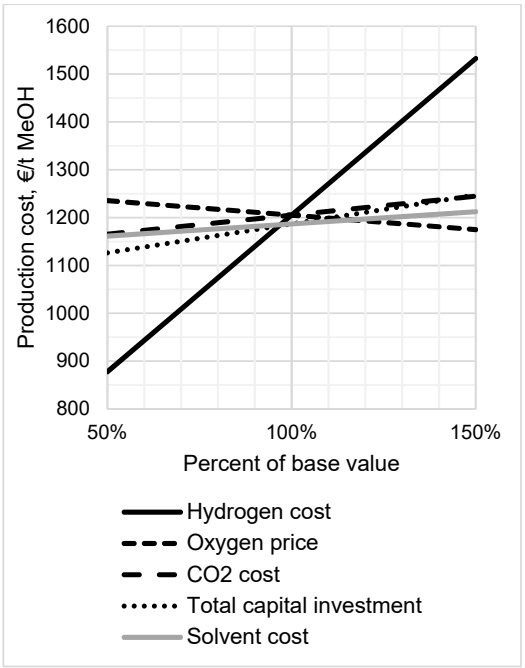

Figure 9. Sensitivity of methanol production cost to variations in selected parameters in the liquid-phase methanol synthesis process with 1-butanol solvent. Base values: hydrogen cost 3000 €/t, oxygen price 70 €/t, CO_2 cost 50 €/t, total capital investment 19.4 M€, solvent cost 500 €/t.

As expected from Figure 6, the cost of hydrogen was found to have the highest impact on the overall cost. In the gas-phase process, the overall production cost was 612 €/t at a hydrogen cost 50% of the base value, corresponding to a hydrogen cost of 1500 €/t. In the 1-butanol process, the production cost was 878 €/t at the hydrogen cost of 1500 €/t. The cost of hydrogen generated by water electrolysis was expected to decrease with the development of electrolyzer technology and the decreasing cost of renewable electricity. The decline in the cost of photovoltaic electricity has been particularly quick [50], potentially providing a more competitive route to renewable methanol compared to wind electricity in the near future. At the same time, the electrolyzer capital costs are expected to decrease, particularly in the case of more advanced proton exchange membrane (PEM) and solid oxide (SOEC) electrolyzers [51]. Clearly, a significant reduction in the hydrogen cost would be required to make these processes competitive at present methanol prices. The hydrogen cost required to reach a methanol cost of 400 €/t was approximately 600 €/t for the gas-phase process. For the 1-butanol process, this threshold was not reached even at zero hydrogen cost.

Due to the high contribution of operating costs to the overall production cost, the economics of CO_2 hydrogenation to methanol were not particularly sensitive to the capital investment. The economic impact of oxygen sales was apparent. If oxygen was not sold at all, the methanol production cost increased to 1028 €/t in the gas-phase process and 1266 €/t in the 1-pentanol process. The impact of oxygen sales was found to be higher than that of the CO_2 cost. Similar to the hydrogen cost, the cost of CO_2 capture is expected to decrease with technological development. However, the economics of the CO_2 hydrogenation to methanol process do not seem to be heavily affected by these developments.

3.6. Summary

The benefits and challenges of the liquid-phase CO_2 hydrogenation to methanol process compared to the gas-phase process are qualitatively summarized in Table 8. The advantage of the liquid-phase process was the increased per pass conversion due to the lower reaction temperature and the apparent favorable distribution of products between the gas and liquid phases in the reactor. At the same reaction pressure of 50 bar, the per pass CO_2 conversion was increased from 20% in the gas-phase process to 79% in the 2-butanol process and 81% in the 1-butanol phase process. The conversion in the liquid-phase processes was higher than the single-phase equilibrium conversion at the reaction conditions. This is presumably due to the beneficial phase equilibrium, i.e., the evaporation of products from the reacting liquid phase. However, uncertainties in the prediction of the phase distribution were present due to a lack of experimental data at the reaction conditions. In addition, whereas the gas-phase reaction could be modelled in detail using an available kinetic model, the liquid-phase reactions were modelled as equilibrium reactions without considering the reaction kinetics. In practice, the reaction rates in the liquid-phase process should be similar in magnitude to the gas-phase process in order to avoid excessively large reactor volumes.

In the gas-phase process, large amounts of gases are recycled in the reactor loop and purged from the process. As a result, the overall methanol yield was only 81%. In the liquid-phase processes, the overall methanol yield was 82% with 2-butanol and 88% with 1-butanol. However, the introduction of the solvent led to a more complicated overall process due to the complex phase equilibrium and mutual solubility of the reactants, products, and solvent, as well as increased demands on the separation stage. The large amounts of solvent present led to increased capital and energy intensity of the separation stage. The difference was manifested in the overall energy balance of the gas-phase and liquid-phase processes. While the gas-phase process produced a net heat output, the liquid phase processes required a significant net heat input, together with increased cooling duties. However, the energy consumption of the liquid-phase processes could be improved by more rigorous heat integration.

The different alcohols used as solvents had a significant effect on the energy consumption and overall methanol production cost. Compared to 2-butanol, whose boiling point is similar to that of water, the heat efficiency of the process was significantly improved by using 1-butanol, which possesses a higher boiling point. Ideally, even higher boiling point solvents would be used to simplify

the separation, potentially allowing selective evaporation of methanol and water from the reactor. However, the solvent should also be sufficiently active in the alcohol-promoted reaction to obtain reasonable reaction rates at low reaction temperatures. Development of increasingly active catalyst systems could allow even lower reaction temperatures, further increasing the equilibrium conversion. For example, Chen et al. [52] demonstrated a heterogeneous cascade catalytic system for liquid-phase CO_2 hydrogenation to methanol at 135 °C, with the reaction promoted by ethanol. The beneficial effect of the phase distribution in the liquid-phase reactor to the equilibrium conversion level, found in the present process modelling work, should also be experimentally verified and further investigated. Another approach to increase the equilibrium conversion and reaction rate could be provided by the adsorption of water from the reaction mixture [53] or by in situ condensation of water and methanol [54].

Table 8. Summary of the potential benefits and challenges of the liquid-phase CO_2 hydrogenation to methanol process with alcoholic solvents compared to the gas-phase process.

Benefits	Challenges	Comments and Outlook
Lower reaction temperature leads to higher equilibrium conversion and lower reactant recycle and losses	-	Reaction temperature could be further lowered with catalyst development (e.g., Chen et al. [52])
-	Complicated and energy-intensive separation leads to higher overall production cost and less favorable energy and CO_2 balances	The amount of solvent recycle should be minimized by utilizing high-boiling alcohols and improved reactor design (e.g., reactive distillation?); energy consumption could be minimized by improved heat integration
-	Formation of azeotropic alcohol-water mixtures further complicates solvent separation and recovery	Solvent recovery improved by phase separation of water and higher alcohols
Liquid-phase reaction potentially allows improved reactor temperature control and catalyst stability	-	Previously demonstrated in liquid-phase methanol synthesis using inert solvents [24]

Additional costs to the liquid-phase process were caused by the loss of solvent. Two percent of 2-butanol and 3% of 1-butanol and 2-butanol entering the reactor were lost in downstream processing in the present processes. The loss was explained by the alcohol forming azeotropic mixtures with water. Without the introduction of an additional, complicated separation sequence to break the azeotropes, a fraction of the solvent was necessarily lost with the waste water removed from the process.

Environmental analysis was performed in terms of the CO_2 and water balances and the electricity consumption of the studied processes. The net CO_2 balance of the gas-phase and 1-butanol processes was found to be negative, i.e., the processes consumed more CO_2 than was released. However, the CO_2 balance was positive for the 2-butanol processes. The lowest net CO_2 emission, −3.0 t/h, was found with the gas-phase process, which did not require fuel combustion for heat generation. The hot utility requirement of the liquid-phase processes led to increased emissions. The net emission was −1.2 t/h with the 1-butanol process and 216 t/h with the 2-butanol process. The impact of the CO_2 emitted in electricity generation was insignificant as regards the process CO_2 balances. The gas-phase process produced the lowest flow rate of waste water (1371 kg/h), with a methanol content of 1.11 wt%. The 2-butanol process produced 1573 kg/h, and the 1-butanol process produced 1644 kg/h of waste water, both streams with an alcohol content of 9 wt%.

In terms of overall methanol production costs, the gas-phase process appeared more competitive than the liquid-phase processes, having a production cost of 963 €/t. This value appears to be consistent with previous studies. For example, Atsonios et al. [18], Rivera-Tinoco et al. [17], and Tremel et al. [23] estimated costs between 800 and 1000 €/t at production scales comparable to the present study. Pérez-Fortes et al. [16] estimated a break-even methanol price of 724 €/t for large industrial-scale production at a hydrogen cost of 3090 €/t (compared to 3000 €/t in the present study). However,

significantly lower costs have been reported by other authors [15,32,55,56]. For instance, Anicic et al. [15] found the cost of methanol produced from captured CO_2 and hydrogen from electrolysis (below 400 €/t) to be competitive with fossil fuel-based methanol production. It appears that this variation was a result of the different assumptions and methods employed in the analyses.

In the liquid-phase process, the production cost was 1205 €/t with 1-butanol and 1349 €/t with 2-butanol. The costs were 25% and 40% higher compared to the gas-phase process. The higher costs compared to the gas-phase process were explained by the more complex and energy-intensive separation stage and the added cost of the solvent make-up. The variation in the production cost for different liquid solvents was explained by the different capital costs and especially the energy costs of the distillation stage.

In all the processes considered here, the overall production cost was dominated by variable operating costs, especially the cost of hydrogen (73%, 48%, and 54% of the total production cost in the gas-phase, 2-butanol, and 1-butanol processes, respectively). As a result, the overall methanol production cost was highly sensitive to the cost of hydrogen. In the gas-phase process, a hydrogen cost of 600 €/t would be required to lower the methanol production cost to 400 €/t, representing the present methanol price. The liquid-phase processes did not meet this threshold value even at zero hydrogen cost. The heating costs in the 1-butanol process corresponded to 174 €/t MeOH. At present, none of the processes appeared economically feasible, with the 20-year net present values of −87 M€ for the gas-phase process, −128 M€ for the 1-butanol process, and −145 M€ for the 2-butanol process.

4. Conclusions

The feasibility of alternative CO_2 hydrogenation to methanol processes was compared by means of flowsheet modelling and economic analysis. The processes compared included a conventional gas-phase process and a liquid-phase process with 2-butanol and 1-butanol as alternative solvents. The potential benefit of the liquid-phase processes was that lower reaction temperatures were allowed by the co-catalytic activity of the alcoholic solvent. At the same reaction pressure of 50 bar, the per pass conversion of CO_2 in the reactor was increased from 20% in the gas-phase process to approximately 80% in the liquid-phase processes. The conversion in the liquid-phase processes was higher than the single-phase equilibrium conversion at the reaction conditions, apparently due to the evaporation of reaction products from the reacting liquid phase. As a result of the decreased amount of recycled gases, the overall conversion of CO_2 to methanol of 81% in the gas-phase process was increased to 82% and 88% in the 2-butanol and 1-butanol processes, respectively.

The benefits of the increased equilibrium conversion were found to be limited to slightly lower capital and operating costs in the reactor loop. However, the presence of large quantities of solvent in the reactor effluent led to a capital- and energy-intensive separation stage, which required two distillation columns compared to one in the gas-phase process. In addition, the formation of azeotropes between the alcohols and the water by-product complicated the separation and led to losses of solvent. Due to the increased energy consumption and the cost of solvent make-up, the methanol production cost of the most competitive liquid-phase process (1-butanol) was 1205 €/t, compared to the production cost of 963 €/t for the gas-phase process. The cost of heating in the 1-butanol process corresponded to 174 €/t MeOH, and if the heat requirement could be eliminated by process or site heat integration, the resulting methanol production cost would equal 1031 €/t.

None of the processes, in gas or liquid phases, were competitive at the present methanol price of approximately 400 €/t. The 20-year net present values of the gas-phase process and the 1-butanol and 2-butanol processes were estimated at −87 M€, −128 M€, and −145 M€, respectively. Hydrogen constituted the largest fraction of the overall cost in all processes, at 73%, 48%, and 54% in the above processes, respectively. In terms of CO_2 emissions, the most favorable CO_2 balance was found with the gas-phase process, with a net consumption of 3.0 t/h of CO_2. The 1-butanol process also showed a negative CO_2 balance, with a net CO_2 consumption of 1.2 t/h. Due to the higher amount of utility heat required, the 2-butanol process showed positive net emission of 0.2 t/h of CO_2. The water balance of

the gas-phase was also the most favorable, with the smallest amount of waste water released at the lowest alcohol content. The amount of and composition of waste water produced was similar in each of the liquid-phase processes.

To conclude, a feasible preliminary process design for the liquid-phase methanol synthesis process was developed. However, further optimization and improved heat integration are required to improve the process economics. Due to the greater complexity and less favorable energy balance of the liquid-phase process, the estimated methanol production cost was found to be 25% and 40% higher with the 1-butanol and 2-butanol processes compared to the baseline gas-phase process. It should be noted that significant assumptions and simplifications were made in modelling of the liquid-phase processes. In particular, reaction kinetics were not considered, and the equilibrium reactor model used presented a "best-case scenario" of the reactor performance. More detailed experimental information on reaction kinetics, yields, and thermodynamics is required to allow more in-depth modelling of the liquid-phase reaction system.

Regardless of these limitations, it is concluded that the liquid-phase CO_2 hydrogenation to methanol process shows potential, and the present findings provide valuable information for further development. The main advantage of the alcohol-promoted liquid-phase process is the higher equilibrium conversion allowed by operation at lower temperatures, and future development should aim to further increase the conversion levels to approach ideally full single-pass conversion. Possibilities include increasingly active catalyst/solvent systems allowing even lower reaction temperatures, removal of water from the reactor by means of adsorption, or in situ condensation of water and methanol from a gaseous reaction mixture. The apparent beneficial effect of the phase distribution in the liquid-phase reactor should also be investigated further, and both the co-catalytic effect and ease of separation should be considered in the selection of alcoholic solvents. More advanced reactor designs (e.g., reactive distillation) and separation methods (e.g., dividing wall columns) should also be considered, together with energy provision by heat pumps to decrease the cost and CO_2 intensity of the processes.

Supplementary Materials: The following are available online at http://www.mdpi.com/2227-9717/7/7/405/s1: Table S1: Stream table for the gas-phase CO_2 hydrogenation to methanol process. Table S2: Stream table for the liquid-phase CO_2 hydrogenation to methanol process with 2-butanol solvent. Table S3: Stream table for the liquid-phase CO_2 hydrogenation to methanol process with 1-butanol solvent. Table S4: Component mass balance of the gas-phase CO_2 hydrogenation to methanol process. Table S5: Component mass balance of the liquid-phase CO_2 hydrogenation to methanol process in 1-butanol solvent. Table S6: Component mass balance of the liquid-phase CO_2 hydrogenation to methanol process in 2-butanol solvent. Table S7: Thermal duties (kW) in the gas-phase CO_2 hydrogenation to methanol process. Table S8: Thermal duties (kW) in the liquid-phase CO_2 hydrogenation to methanol processes. Table S9: Electric duties (kW) in the alternative CO_2 hydrogenation to methanol processes. Table S10: Installed equipment costs of the alternative CO_2 hydrogenation to methanol processes (M€). Table S11: Operating and total methanol production costs of the alternative CO_2 hydrogenation to methanol processes (k€/t MeOH)

Author Contributions: Conceptualization, H.N. and A.L.; data curation, H.N.; methodology, H.N.; supervision, A.L. and T.K.; writing, original draft, H.N.; writing, review and editing, H.N., A.L., and T.K.

Acknowledgments: Funding provided by the LUT REFLEX platform and the Lappeenranta-Lahti University of Technology Doctoral School is gratefully acknowledged.

Conflicts of Interest: The authors declare no conflicts of interest.

References

1. Mikkelsen, M.; Jørgensen, M.; Krebs, F.C. The teraton challenge. A review of fixation and transformation of carbon dioxide. *Energy Environ. Sci.* **2010**, *3*, 43–81. [CrossRef]
2. Schlögl, R. The Solar Refinery. In *Chemical Energy Storage*; Walter de Gruyter GmbH: Berlin, Germany; Boston, MA, USA, 2013; pp. 1–34.
3. Olah, G.; Goeppert, A.; Prakash, G. *Beyond Oil and Gas: The Methanol Economy*, 2nd ed.; Wiley-VCH: Weinheim, Germany, 2009.
4. Goeppert, A.; Czaun, M.; Jones, J.P.; Prakash, G.K.S.; Olah, G.A. Recycling of carbon dioxide to methanol and derived products—Closing the loop. *Chem. Soc. Rev.* **2014**, *43*, 7995–8048. [CrossRef] [PubMed]

5. Offermanns, H.; Plass, L.; Bertau, M. From Raw Materials to Methanol, Chemicals and Fuels. In *Methanol: The Basic Chemical and Energy Feedstock of the Future*; Springer: Heidelberg/Berlin, Germany, 2014; pp. 1–7.
6. Reichelt, L.; Schmidt, F. Methanol-to-Gasoline Process. In *Methanol: The Basic Chemical and Energy Feedstock of the Future*; Springer: Heidelberg/Berlin, Germany, 2015; pp. 440–453.
7. Schmidt, F.; Pätzold, C. 6.4.2 Methanol-to-Olefins Processes. In *Methanol: The Basic Chemical and Energy Feedstock of the Future*; Springer: Heidelberg/Berlin, Germany, 2015; pp. 454–472.
8. Ott, J.; Gronemann, V.; Pontzen, F.; Fiedler, E.; Grossmann, G.; Kersebohm, D.B.; Weiss, G.; Witte, C. Methanol. In *Ullmann's Encyclopedia of Industrial Chemistry*; Wiley-VCH Verlag GmbH & Co. KGaA: Weinheim, Germany, 2012; pp. 1–27.
9. Pontzen, F.; Liebner, W.; Gronemann, V.; Rothaemel, M. BAhlers, CO_2-based methanol and DME—Efficient technologies for industrial scale production. *Catal. Today* **2011**, *171*, 242–250. [CrossRef]
10. Kunkes, E.; Behrens, M. Methanol Chemistry. In *Chemical Energy Storage*; Walter de Gruyter GmbH: Berlin, Germany, 2013; pp. 413–435.
11. Sahibzada, M.; Metcalfe, I.S.; Chadwick, D. Methanol Synthesis from $CO/CO_2/H_2$ over $Cu/ZnO/Al_2O_3$ at Differential and Finite Conversions. *J. Catal.* **1998**, *174*, 111–118. [CrossRef]
12. Martin, O.; Pérez-Ramírez, J. New and revisited insights into the promotion of methanol synthesis catalysts by CO_2. *Catal. Sci. Technol.* **2013**, *3*, 3343–3352. [CrossRef]
13. Mignard, D.; Sahibzada, M.; Duthie, J.M.; Whittington, H.W. Methanol synthesis from flue-gas CO_2 and renewable electricity: A feasibility study. *Int. J. Hydrog. Energy* **2003**, *28*, 455–464. [CrossRef]
14. Van-Dal, È.; Bouallou, C. Design and simulation of a methanol production plant from CO_2 hydrogenation. *J. Clean. Prod.* **2013**, *57*, 38–45. [CrossRef]
15. Anicic, B.; Trop, P.; Goricanec, D. Comparison between two methods of methanol production from carbon dioxide. *Energy* **2014**, *77*, 279–289. [CrossRef]
16. Pérez-Fortes, M.; Schöneberger, J.C.; Boulamanti, A.; Tzimas, E. Methanol synthesis using captured CO_2 as raw material: Techno-economic and environmental assessment. *Appl. Energy* **2016**, *161*, 718–732. [CrossRef]
17. Rivera-Tinoco, R.; Farran, M.; Bouallou, C.; Auprêrte, F.; Valentin, S.; Millet, P.; Ngameni, J.R. Investigation of power-to-methanol processes coupling electrolytic hydrogen production and catalytic CO_2 reduction. *Int. J. Hydrogen Energy* **2016**, *41*, 4546–4559. [CrossRef]
18. Atsonios, K.; Panopoulos, K.D.; Kakaras, E. Investigation of technical and economic aspects for methanol production through CO_2 hydrogenation. *Int. J. Hydrogen. Energy* **2016**, *41*, 2202–2214. [CrossRef]
19. Rivarolo, M.; Bellotti, D.; Magistri, L.; Massardo, A.F. Feasibility study of methanol production from different renewable sources and thermo-economic analysis. *Int. J. Hydrogen Energy* **2016**, *41*, 2105–2116. [CrossRef]
20. Varone, A.; Ferrari, M. Power to liquid and power to gas: An option for the German Energiewende. *Renew. Sustain. Energy Rev.* **2015**, *45*, 207–218. [CrossRef]
21. Matzen, M.; Alhajji, M.; Demirel, Y. Chemical storage of wind energy by renewable methanol production: Feasibility analysis using a multi-criteria decision matrix. *Energy* **2015**, *93*, 343–353. [CrossRef]
22. Matzen, M.; Demirel, Y. Methanol and dimethyl ether from renewable hydrogen and carbon dioxide: Alternative fuels production and life-cycle assessment. *J. Clean. Prod.* **2016**, *139*, 1068–1077. [CrossRef]
23. Tremel, A.; Wasserscheid, P.; Baldauf, M.; Hammer, T. Techno-economic analysis for the synthesis of liquid and gaseous fuels based on hydrogen production via electrolysis. *Int. J. Hydrogen Energy* **2015**, *40*, 11457–11464. [CrossRef]
24. Lee, S.; Sardesai, A. Liquid phase methanol and dimethyl ether synthesis from syngas. *Top. Catal.* **2005**, *32*, 197–207. [CrossRef]
25. Fan, L.; Sakaiya, Y.; Fujimoto, K. Low-temperature methanol synthesis from carbon dioxide and hydrogen via formic ester. *Appl. Catal. A* **1999**, *180*, L11–L13. [CrossRef]
26. Xu, B.; Yang, R.; Meng, F.; Reubroycharoen, P.; Vitidsant, T.; Zhang, Y.; Yoneyama, Y.; Tsubaki, N. A New Method of Low Temperature Methanol Synthesis. *Catal. Surv. Asia* **2009**, *13*, 147–163. [CrossRef]
27. Tsubaki, N.; Zeng, J.; Yoneyama, Y.; Fujimoto, K. Continuous synthesis process of methanol at low temperature from syngas using alcohol promoters. *Catal. Commun.* **2001**, *2*, 213–217. [CrossRef]
28. Reubroycharoen, P.; Yamagami, T.; Vitidsant, T.; Yoneyama, Y.; Ito, M.; Tsubaki, N. Continuous Low-Temperature Methanol Synthesis from Syngas Using Alcohol Promoters. *Energy Fuels* **2003**, *17*, 817–823. [CrossRef]

29. Finnish Wind Power Association. Wind Power Projects in Finland, March 2017. Available online: http://www.tuulivoimayhdistys.fi/filebank/969--968-STY_hankelista_2017_web_final.xls (accessed on 28 February 2018).
30. Liu, G.; Larson, E.D.; Williams, R.H.; Kreutz, T.G.; Guo, X. Online Supporting Material, Making Fischer-Tropsch Fuels and Electricity from Coal and Biomass: Performance and Cost Analysis. *Energy Fuels* **2011**, *25*, 415–437. [CrossRef]
31. Bussche, K.M.V.; Froment, G.F. A Steady-State Kinetic Model for Methanol Synthesis and the Water Gas Shift Reaction on a Commercial $Cu/ZnO/Al_2O_3$ Catalyst. *J. Catal.* **1996**, *161*, 1–10. [CrossRef]
32. Mignard, D.; Pritchard, C. On the use of electrolytic hydrogen from variable renewable energies for the enhanced conversion of biomass to fuels. *Chem. Eng. Res. Des.* **2008**, *86*, 473–487. [CrossRef]
33. Brown, W.R.; Drown, D.P.; Frenduto, F.S. *Commercial-Scale Demonstration of the Liquid Phase Methanol (LPMeOH) Process—Public Design Report*; Air Products, Chemicals, Inc., Eastman Chemical Company: Kingsport, TN, USA, 2000.
34. Tsubaki, N.; Ito, M.; Fujimoto, K. A New Method of Low-Temperature Methanol Synthesis. *J. Catal.* **2001**, *197*, 224–227. [CrossRef]
35. Tomorrow Electricity Map. Available online: https://www.electricitymap.org/?page=country&solar=false&remote=true&wind=false&countryCode=FI (accessed on 6 July 2018).
36. Towler, G.; Sinnott, R. Capital Cost Estimating. In *Chemical Engineering Design*; Elsevier: Oxford, UK, 2013; pp. 307–354.
37. Levene, J.; Kroposki, B.; Sverdrup, G. *Wind Energy and Production of Hydrogen and Electricity—Opportunities for Renewable Hydrogen*; Preprint; National Renewable Energy Laboratory (NREL): Golden, CO, USA, 2006.
38. Vakkilainen, E.; Kivistö, A. *Comparison of Electricity Generation Costs*; Lappeenranta University of Technology: Lappeenranta, Finland, 2017.
39. Smolinka, T.; Günther, M.; Garche, J. *Stand und Entwicklungspotenzial der Wasserelektrolyse zur Herstellung von Wasserst off aus Regenerativen Energien*; NOW-Studie: Freiburg im Breisgau, Germany, 2011.
40. Eurostat. Electricity Prices for Non-Household Consumers-bi-Annual Data 23 November 2017. Available online: http://appsso.eurostat.ec.europa.eu/nui/show.do?dataset=nrg_pc_205&lang=en (accessed on 28 February 2018).
41. Finkenrath, M. *Cost and Performance of Carbon Dioxide Capture from Power Generation*; IEA: Paris, France, 2011.
42. Trippe, F.; Fröhling, M.; Schultmann, F.; Stahl, R.; Henrich, E.; Dalai, A. Comprehensive techno-economic assessment of dimethyl ether (DME) synthesis. *Fuel Process. Technol.* **2013**, *106*, 577–586. [CrossRef]
43. Statistics Finland, Energy Prices Grew in the Third Quarter, 7 December 2017. Available online: https://tilastokeskus.fi/til/ehi/2017/03/ehi_2017_03_2017--12-07_tie_001_en.html (accessed on 28 February 2018).
44. Hall, S. Energy Conservation. In *Rules of Thumb for Chemical Engineers*; Elsevier: Oxford, UK, 2012; pp. 375–385.
45. The Engineering ToolBox, Fuels—Higher and Lower Calorific Values, 2003. Available online: https://www.engineeringtoolbox.com/fuels-higher-calorific-values-d_169.html (accessed on 10 April 2019).
46. Towler, G.; Sinnott, R. Estimating Revenues and Production Costs. In *Chemical Engineering Design*; Elsevier: Oxford, UK, 2013; pp. 355–387.
47. Methanex Corporation, Methanex Monthly Average Regional Posted Contract Price History, February 2018. Available online: https://www.methanex.com/sites/default/files/methanol-price/MxAvgPrice_Feb%2028%2C%202018.pdf (accessed on 12 March 2018).
48. VLE—Calc, Azeotrope Database for Organic Solvent Mixtures. Available online: http://vle-calc.com/azeotrope.html (accessed on 12 March 2018).
49. Kaneko, T.; Derbyshire, F.; Makino, E.; Gray, D.; Tamura, M.; Li, K. Coal Liquefaction. In *Ullmann's Encyclopedia of Industrial Chemistry*; Wiley-VCH Verlag GmbH & Co. KGaA: Weinheim, Germany, 2012; p. 32.
50. IREN. *Renewable Power Generation Costs in 2017*; International Renewable Energy Agency: Abu Dhabi, UAE, 2018.
51. Schmidt, O.; Gambhir, A.; Staffell, I.; Hawkes, A.; Nelson, J.; Few, S. Future cost and performance of water electrolysis:An expert elicitation study. *Int. J. Hydrogen Energy* **2017**, *42*, 30470–30492. [CrossRef]
52. Chen, Y.; Choi, S.; Thompson, L.T. Low-Temperature CO_2 Hydrogenation to Liquid Products via a Heterogeneous Cascade Catalytic System. *ACS Catal.* **2015**, *5*, 1717–1725. [CrossRef]
53. Bayat, M.; Dehghani, Z.; Hamidi, M.; Rahimpour, M. Methanol synthesis via sorption-enhanced reaction process: Modeling, multi-objective optimization. *J. Taiwan Inst. Chem. Eng.* **2014**, *45*, 481–494. [CrossRef]

54. Wu, W.; Xie, K.; Sun, D.; Li, X.; Fang, F. CuO/ZnO/Al_2O_3 Catalyst Prepared by Mechanical-Force-Driven Solid-State Ion Exchange and Its Excellent Catalytic Activity under Internal Cooling Condition. *Ind. Eng. Chem. Res.* **2017**, *56*, 8216–8223. [CrossRef]
55. Kourkoumpas, D.S.; Papadimou, E.; Atsonios, K.; Karellas, S.; Grammelis, P.; Kakaras, E. Implementation of the Power to Methanol concept by using CO_2 from lignite power plants: Techno-economic investigation. *Int. J. Hydrogen Energy* **2016**, *41*, 16674–16687. [CrossRef]
56. Bellotti, D.; Rivarolo, M.; Magistri, L.; Massardo, A.F. Feasibility study of methanol production plant from hydrogen and captured carbon dioxide. *J. CO_2 Util.* **2017**, *21*, 132–138. [CrossRef]

ACTA UNIVERSITATIS LAPPEENRANTAENSIS

892. PÖLLÄNEN, ILKKA. The efficiency and damage control of a recovery boiler. 2019. Diss.

893. HEKMATMANESH, AMIN. Investigation of EEG signal processing for rehabilitation robot control. 2019. Diss.

894. HARMOKIVI-SALORANTA, PAULA. Käyttäjät liikuntapalvelujen kehittäjinä - Käyttäjälähtöisessä palveluinnovaatioprosessissa käyttäjien tuottama tieto tutkimuksen kohteena. 2020. Diss.

895. BERGMAN, JUKKA-PEKKA. Managerial cognitive structures, strategy frames, collective strategy frame and their implications for the firms. 2020. Diss.

896. POLUEKTOV, ANTON. Application of software-defined radio for power-line-communication-based monitoring. 2020. Diss.

897. JÄRVISALO, HEIKKI. Applicability of GaN high electron mobility transistors in a high-speed drive system. 2020. Diss.

898. KOPONEN, JOONAS. Energy efficient hydrogen production by water electrolysis. 2020. Diss.

899. MAMELKINA, MARIA. Treatment of mining waters by electrocoagulation. 2020. Diss.

900. AMBAT, INDU. Application of diverse feedstocks for biodiesel production using catalytic technology. 2020. Diss.

901. LAAPIO-RAPI, EMILIA. Sairaanhoitajien rajatun lääkkeenmääräämistoiminnan tuottavuuden, tehokkuuden ja kustannusvaikuttavuuden arviointi perusterveydenhuollon avohoidon palveluprosessissa. 2020. Diss.

902. DI, CHONG. Modeling and analysis of a high-speed solid-rotor induction machine. 2020. Diss.

903. AROLA, KIMMO. Enhanced micropollutant removal and nutrient recovery in municipal wastewater treatment. 2020. Diss.

904. RAHIMPOUR GOLROUDBARY, SAEED. Sustainable recycling of critical materials. 2020. Diss.

905. BURGOS CASTILLO, RUTELY CONCEPCION. Fenton chemistry beyond remediating wastewater and producing cleaner water. 2020. Diss.

906. JOHN, MIIA. Separation efficiencies of freeze crystallization in wastewater purification. 2020. Diss.

907. VUOJOLAINEN, JOUNI. Identification of magnetically levitated machines. 2020. Diss.

908. KC, RAGHU. The role of efficient forest biomass logistics on optimisation of environmental sustainability of bioenergy. 2020. Diss.

909. NEISI, NEDA. Dynamic and thermal modeling of touch-down bearings considering bearing non-idealities. 2020. Diss.

910. YAN, FANGPING. The deposition and light absorption property of carbonaceous matter in the Himalayas and Tibetan Plateau. 2020. Diss.

911. NJOCK BAYOCK, FRANCOIS MITERAND. Thermal analysis of dissimilar weld joints of high-strength and ultra-high-strength steels. 2020. Diss.

912. KINNUNEN, SINI-KAISU. Modelling the value of fleet data in the ecosystems of asset management. 2020. Diss.

913. MUSIKKA, TATU. Usability and limitations of behavioural component models in IGBT short-circuit modelling. 2020. Diss.

914. SHNAI, IULIIA. The technology of flipped classroom: assessments, resources and systematic design. 2020. Diss.

915. SAFAEI, ZAHRA. Application of differential ion mobility spectrometry for detection of water pollutants. 2020. Diss.

916. FILIMONOV, ROMAN. Computational fluid dynamics as a tool for process engineering. 2020. Diss.

917. VIRTANEN, TIINA. Real-time monitoring of membrane fouling caused by phenolic compounds. 2020. Diss.

918. AZZUNI, ABDELRAHMAN. Energy security evaluation for the present and the future on a global level. 2020. Diss.

919. NOKELAINEN, JOHANNES. Interplay of local moments and itinerant electrons. 2020. Diss.

920. HONKANEN, JARI. Control design issues in grid-connected single-phase converters, with the focus on power factor correction. 2020. Diss.

921. KEMPPINEN, JUHA. The development and implementation of the clinical decision support system for integrated mental and addiction care. 2020. Diss.

922. KORHONEN, SATU. The journeys of becoming ang being an international entrepreneur: A narrative inquiry of the "I" in international entrepreneurship. 2020. Diss.

923. SIRKIÄ, JUKKA. Leveraging digitalization opportunities to improve the business model. 2020. Diss.

924. SHEMYAKIN, VLADIMIR. Parameter estimation of large-scale chaotic systems. 2020. Diss.

925. AALTONEN, PÄIVI. Exploring novelty in the internationalization process - understanding disruptive events. 2020. Diss.

926. VADANA, IUSTIN. Internationalization of born-digital companies. 2020. Diss.

927. FARFAN OROZCO, FRANCISCO JAVIER. In-depth analysis of the global power infrastructure - Opportunities for sustainable evolution of the power sector. 2020. Diss.

928. KRAINOV, IGOR. Properties of exchange interactions in magnetic semiconductors. 2020. Diss.

929. KARPPANEN, JANNE. Assessing the applicability of low voltage direct current in electricity distribution - Key factors and design aspects. 2020. Diss.

ISBN 978-952-335-578-1
ISBN 978-952-335-579-8 (PDF)
ISSN-L 1456-4491
ISSN 1456-4491
Lappeenranta 2020